AN EXPERIMENTAL STUDY OF THIN FOIL POSITRON MODERATORS AND POSITRONIUM INTERACTIONS IN GASES

A thesis submitted to the University of London
for the degree of Doctor of Philosophy

Nazrene Zafar
Department of Physics and Astronomy
University College London

February 1990

ABSTRACT

The use of thin single crystal tungsten, W(100), and nickel, Ni(100), foils as slow positron moderators in the transmission mode has been investigated. A simple annealing technique has been developed, employing resistive heating in low vacuum conditions of $6x10^{-2}$ Torr, to treat the foils of thicknesses in the range 1000-18000Å. The maximum efficiencies obtained were $(8.8\pm1.2)x10^{-4}$ from a 2000Å W(100) foil and $(6.5\pm1.0)10^{-4}$ from a 5000Å Ni(100) film in a system with a base pressure of 10^{-7} Torr. The considerations required to determine the efficiency, defined as the ratio of the slow positrons emitted to the number of fast positrons striking the foil, have been discussed in the context of the present arrangement. Comparisons show that the results obtained are a factor of 2.5-4.5 lower than calculated yields, however are in good agreement with values from experimental studies using more complex annealing procedures in higher vacuum conditions ($\geq10^{-8}$ Torr). The full width at half maximum of the energy distribution of the emitted positrons were found to be 1.7eV from W and 0.3eV from Ni compared to 2.8eV from W mesh.

The timed positronium beam system developed by Laricchia *et al* (1988b) has been modified to allow the observation of n=2 state Ps formed in helium and argon gases. The excited state component of the positronium flux was quantified at incident positron energies of 16-52.5eV and found to compose, at maximum, 33% (He) and 42% (Ar) of the total positronium beam without correction for in-flight decay. Comparisons made with theoretical studies indicate that metastable S state positronium may constitute a large proportion of the excited state flux (≈70%). Total positronium scattering cross-sections were extracted and the results obtained ranged from (4.5±0.8) to (7.6±0.8) $x10^{-20}m^2$ in Ar for positronium energies of 17-41eV and fluctuated about $\approx3x10^{-20}m^2$ in He in the regime 7-35eV from a minimum of (2.4±0.8) to a maximum of (3.5±1.3) $x10^{-20}m^2$. The assumptions and corrections required to determine these values have been detailed and comparisons have been made with theory and with cross-sections for hydrogen scattering from helium and argon. Possible extensions of both the slow positron moderator and the positronium scattering investigations have been discussed.

CONTENTS

FIGURE CAPTIONS

TABLE CAPTIONS

ACKNOWLEDGEMENTS

I would like to express my gratitude to the many people who have helped and encouraged, in particular (though not exclusively) those named below:

My supervisor, Professor Ceiri Griffith, Nella Laricchia and Mike Charlton for invaluable help and discussion.
Past and present members of the positron group and the department for their support and steadfast encouragement.
Ivan Rangué, Ted Oldfield, Tony Walker, Derek Attree and members of the workshop for their excellent technical assistance.
The SERC for financial support.
Vishal Nayar and Richard Simpson for much helpful advice and discussion.

Lastly, I would like to thank my family and friends for their ceaseless encouragement, understanding and moral support during the last few years. In particular, I am deeply grateful to Wyndham Johnstone, Nicholas James especially for the preparation of the diagrams in this thesis, my sister -Yasmeen Zafar and my parents - Hisako Nakajima and A.Z. Muslim. And to Jahn and Obāchan.

to my family

CHAPTER 1
BACKGROUND

1.1 Introduction

The existence of the antiparticle was originally predicted in the "hole" theory formulated by Dirac in 1930. Dirac's development of the relativistic wave equation to describe the motion of free electrons in an electromagnetic field led to solutions corresponding to negative total relativistic energies. In interpretating these results, he proposed that all negative energy states were normally totally occupied, thus according to the Pauli exclusion principle, free electrons were prevented from making the transition from positive to negative levels. However, electrons from the "negative sea" could be excited to positive states, leaving a "hole" in the negative level which would appear to behave as a positive electron. Confirmation of this prediction followed from the experimental work of Anderson in 1932 and, in 1933, the conclusive identification was made by Blackett and Occhialini of an electron-like antiparticle - the positron. Interest soon arose in this new fundamental particle and some of the first studies in positron physics are summarised in Table 1.1.

Since the early cloud chamber investigations, positrons were found to be emitted from radioactive isotopes and these have provided a convenient source for experimentation. Extensive studies on positron interactions began in the late 1940s when techniques were developed which are still widely used today. These concentrated mainly on swarm-type experiments where the energy distribution of the positrons was large, extending from eV to keV-MeV levels. A new method of investigation was successfully pioneered in the late 1950s - the slow positron beam technique - which allowed control of the positron energy prior to interaction. Studies have shown that, on implantation of fast positrons, certain solids were found to emit positrons with characteristic energies of a few eV. Following the early work, considerable effort has been placed on the investigation of materials for use as "slow positron moderators".

Year	Event	Reference
1930	Hole theory–prediction of antiparticle	Dirac
1931	Prediction of e^-–like antiparticle	Weyl
1932	Discovery of e^+	Anderson
1933	Identification of e^+ from cloud chamber tracks	Blackett and Occhialini
1934	Observation of 2γ annihilation	Klemperer
1934	Prediction of $(e^+–e^-)$ bound state	Mohorovic
1945	$(e^+–e^-)$ named positronium	Ruark
1946	Lifetime calculations of $(e^+e^-e^-)$, $(e^+e^+e^-)$ and 1S positronium	Wheeler
1946 1947	Calculations of 1S positronium lifetime and fine structure separation of 1^1S_0 and 1^3S_1 states	Pirenne
1949	Lifetime of 1S state positronium, cross-section of $3–\gamma$ annihilation	Ore and Powell
1949	Non co-linearity observed in 2γ annihilation	DeBenedetti et al
1949	Lifetime measurement of e^+ in gases	Shearer and Deutsch
1949	Calculation of positronium yield - Ore model	Ore
1951	Discovery of Ps in gases, measurement of decay rate	Deutsch
1951	Stability of PsH	Ore
1953	Observation of two lifetimes in quartz	Bell and Graham
1954	Calculations of fine structure levels of n=2 state positronium	Fulton and Martin

Table 1.1 Chronological summary of some of the early events in positron physics

The availability of this antimatter counterpart of the electron has stimulated many investigations into the behaviour of positrons in all media, yielding information on the nature of its interactions and the structure of its environment. The positron has the same mass and spin as the electron but its charge, although identical in magnitude, is opposite in sign. This important difference can manifest itself with interesting consequences, for example in collisions of positrons (e^+) and electrons (e^-) with atomic and molecular gases. Variations in the size of cross-sections and the distribution with energy arise from differences in the static and polarisation interactions of the two particles with the target (discussed in Section 1.5). Additionally, exchange effects are not present in e^+ scattering, however, positronium (Ps) formation may occur.

In the condensed matter field, advances have been made in the deduction of material structure using positrons to probe the bulk and surface. Developments have been made of techniques which, in future, may become standard tools of analysis, complementing the well-established methods such as that of low energy electron diffraction (LEED).

In astronomy, the annihilation radiation of positrons has been detected in solar flares (*e.g.* Share *et al*, 1983), gamma-ray bursts (*e.g.* Yoshimori *et al*, 1979), and from the centre of the galaxy (*e.g.* Riegler *et al*, 1983). Gravitational, magnetic, rotational and nuclear effects have been proposed to account for the concentration of energy required to create positron-electron pairs in these environments. Hypotheses such as neutron starquakes and galactic black hole accretion have been suggested (Ellison and Kazanas, 1983, Lovelace and Ruchti, 1983) and comparison of the observations to such theoretical models may aid in elucidating the conditions of the annihilation region.

Positronium, too, is of great interest. Like the electron and the positron, positronium interactions with matter can yield information on basic processes. Its hydrogen-like states are being used to test the accuracy of quantum electrodynamics and compares well with the H atom as a fundamental marker. Further afield in the realms of cosmology, the decay of positronium has been used in refuting the existence of an antimatter universe, previously proposed as the missing "dark matter" in this universe (Glashow, 1986).

In the sections below, some basic features of the positron and positronium are

discussed, followed by a general review of some of the methods most widely used in positron physics. The work documented in this thesis has involved investigations into positron moderators for the generation of slow beams and the subsequent use of the beam technique in a study of positronium formation and interaction in atomic gases. Emphasis is therefore placed on the development of this technique and the properties of some of the materials used as moderators. In the remainder of the chapter, some examples of recent e^+–gas scattering investigations employing slow e^+ beams are reported.

1.2 Basic Properties of the Positron and Positronium

The annihilation of low energy positrons on interaction with electrons almost inevitably results in the emission of a number γ-ray photons with a total energy of 1.022MeV, the combined rest mass energies of the two particles. The number of photons, n, is determined by the conservation of charge parity, P_c, which for single photons is -1. Thus, for a system of n photons

$$P_c = (-1)^n \qquad 1.1$$

For annihilation of the e^+–e^- system, Yang (1950) has demonstrated, by symmetry arguments, that n is determined by

$$(-1)^n = (-1)^{L+S} \qquad 1.2$$

where L is the total orbital angular momentum and S is the total spin of the system. Equation 1.2 shows that the annihilation photons can reveal information about the relative states of the e^+–e^- pair, however, it imposes no restrictions other than that of odd or even photon production.

The relative likelihood of annihilation via any number of photons can be ascertained on inspection of the Feynman representation of e^+–e^- interaction. The cross-section of decay into a particular number of photons is proportional to α^m, where α is the fine structure constant and m is the number of vertices corresponding to absorption or emission of photons. The fine structure constant is given by $e^2/4\pi\varepsilon_0\hbar c$ ($\approx 1/137$), where e, ε_0 and $\hbar$ are the electronic charge, the vacuum permittivity and Planck's constant, respectively. The Feynman diagrams for annihilation into one, two and three

photons, illustrated in Figure 1.1, show that 2–γ decay, with two vertices, has the largest probability of occurrence.

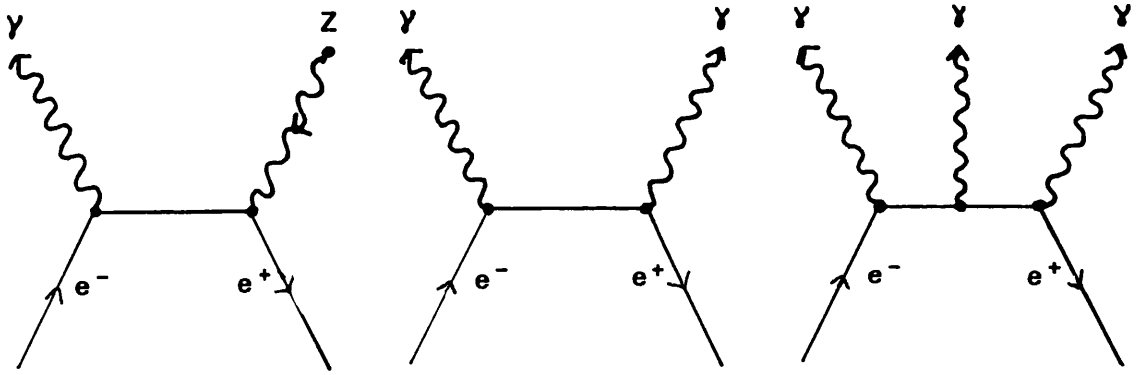

Figure 1.1 Feynman diagrams of annihilation into one, two and three photons

Modes (a) and (b) both have three vertices, however, mode (a) is additionally constrained by the requirement of the presence of a third body for momentum conservation. A resultant correction to the cross-section of the order of α^m makes this process much less likely to occur than 3–γ annihilation.

The cross-section for 2–γ annihilation, $\sigma_{2\gamma}$, of a positron at non-relativistic velocity, v, with a free electron was calculated by Dirac (1930b) to be

$$\sigma_{2\gamma} = \pi r_o^2 c/v \qquad 1.3$$

where $r_o=e^2/4\pi\varepsilon_o m_o c^2$ is the classical electron radius and m_o and c are the electronic mass and the speed of light *in vacuo*, respectively.

Equation 1.3 can be modified, for positrons moving in gaseous media, to

$$\sigma_{2\gamma}(v) = \pi r_o^2 c Z_{eff}(v)/v \qquad 1.4$$

where $Z_{eff}(v)$ is the effective number of electrons per atom seen by the positron at velocity, v. The difference between Z, the atomic number, and $Z_{eff}(v)$ arises from the polarisation effect of the e^+ as it approaches the atom. As this is long range interaction is most effective at low velocities, Z_{eff} tends to Z at energies commonly used in e^+ beam studies and Bransden (1969) has shown that $\sigma_{2\gamma}$ is of the order of $10^{-26}m^2$ at these typical energies (≥0.2eV). Furthermore, Ore and Powell (1949) have calculated the ratio of the cross-section of 2–γ to 3–γ annihilation to be 1/372 for free positrons. Thus, direct annihilation of e^+ is negligible when compared to most other atomic processes investigated in e^+ beam studies in gases.

Positronium (Ps), the bound leptonic state, is structurally comparable to the hydrogen atom. With half the reduced mass of H, it has twice the Bohr radius (1.05Å) and thus half the binding energy, 6.8eV. Formation of the ground state can occur in two modes: with parallel spin axes (ortho-positronium) or with anti-parallel spin axes (para-positronium). The total angular momentum, J=L+S, of o–Ps is 1, giving rise to three substates with magnetic quantum numbers, m=0, +1, −1, whereas for p–Ps, J=m=O. Hence statistically, the ratio of formation of the triplet to the singlet state is 3:1.

Ps decay is also governed by Equation 1.2. The singlet state, para-positronium (p–Ps), spectroscopically denoted by 1^1S_0, annihilates with the emission of an even number of photons, predominantly two. For momentum conservation, these are emitted with equal energies at 180° to each other, as viewed from the centre of mass system. The triplet state, ortho-positronium (o–Ps), 1^3S_1, decays mainly via three co-planar photon emission with a distribution of energies from zero to 511keV. This distribution has been calculated by Ore and Powell (1949) and measured by Chang *et al* (1982, 1985); the results from these studies are illustrated in Figure 1.2.

The self-annihilation rates of the singlet ($_0\lambda_{p-Ps}$) and triplet ($_0\lambda_{o-Ps}$) states in vacuum have been calculated by Harris and Brown (1957) and Caswell and Lepage (1979), respectively, to be $_0\lambda_{p-Ps} = 7.9852ns^{-1}$ and $_0\lambda_{o-Ps} = (7.0386\pm0.0002)\mu s^{-1}$.

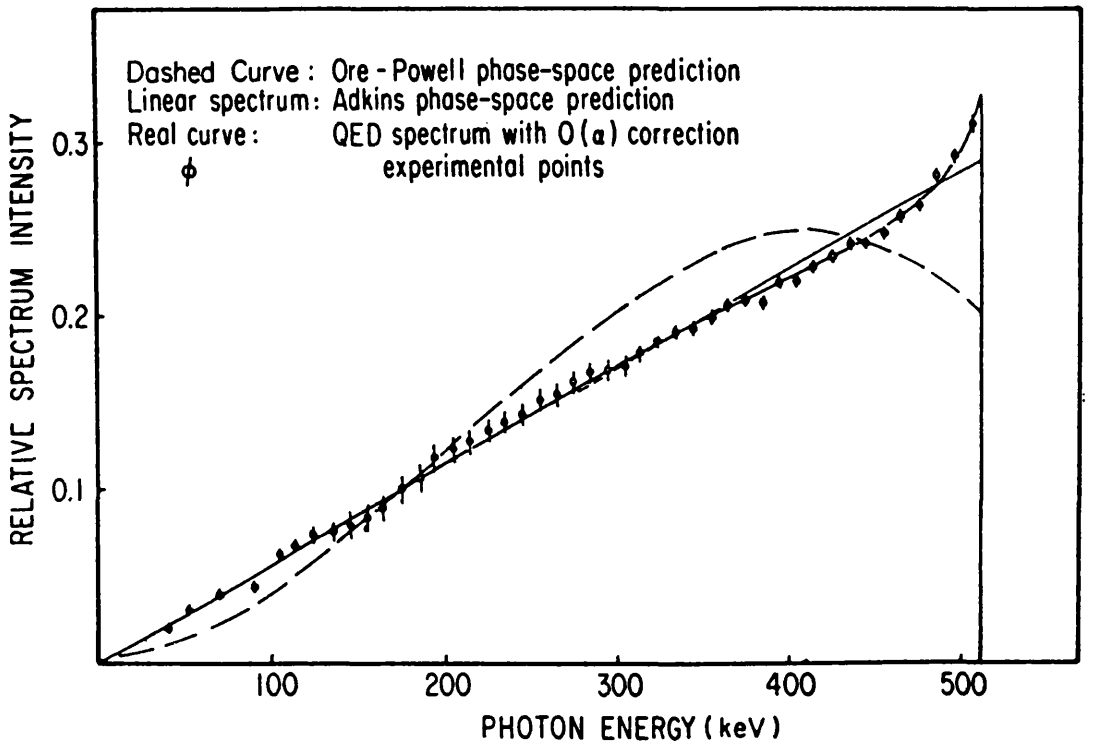

Figure 1.2 Energy distribution of γ–ray emission from o–Ps decay (Ore and Powell, 1949, Chang *et al*, 1982, 1985)

The singlet state decay rate is experimentally difficult to measure because of its short lifetime of 125ps. However, Gidley *et al* (1982), using Zeeman mixing of the two m=0 substates, have determined ${}_0\lambda_{p\text{-}Ps}$ to be (7.994 ± 0.011)ns–1. Measurements of the vacuum decay rate of the triplet state have been made by several workers (Griffith *et al*, 1978, Gidley *et al*, 1978, Gidley and Zitzewitz, 1978, Gidley *et al*, 1982). The most accurate result to date, obtained by Westbrook *et al* (1987), is (7.0516 ± 0.0013)μs^{-1}. This latest measurement is in accord with the previously obtained experimental results but is significantly different from the theoretically calculated value. Westbrook *et al* (1987) can find no systematic reason for this and suggest several factors that may account for the difference such as exotic decay of o–Ps, mixing of Ps into mirror-universe states and consideration of higher order terms in the calculation of the decay rate.

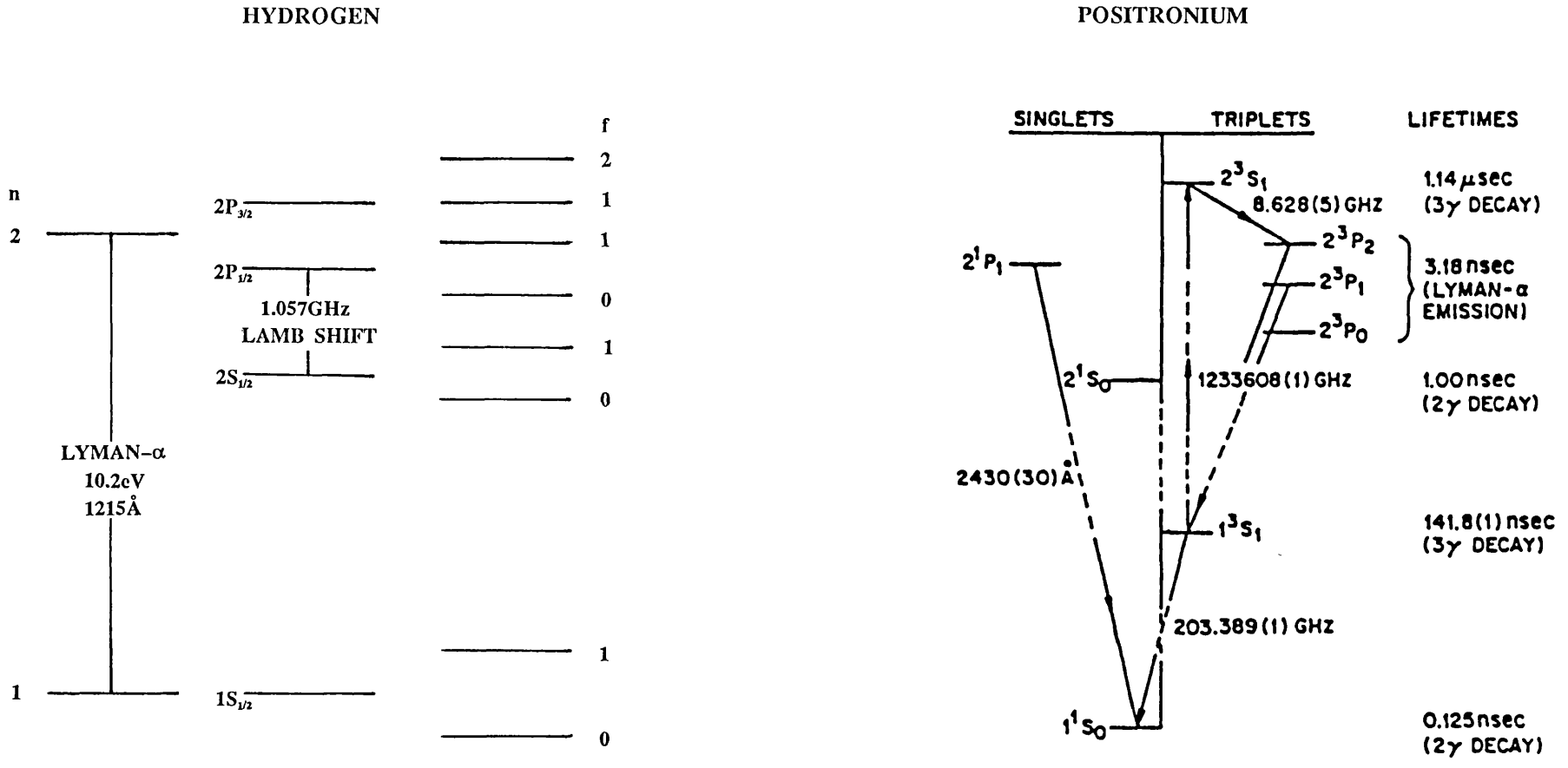

Figure 1.3 Energy level diagrams of hydrogen and positronium

Positronium formation in the first excited state can occur in two singlet and four triplet states. Fulton and Martin (1954) have computed the fine structure levels for n=1 and n=2 Ps and these are illustrated in Figure 1.3 in relation to the energy levels of H. The absence of the hyperfine structure in Ps is due to the large magnetic moment of the positron, 657 times that of the proton, making the sizes of the spin-spin and spin-orbit interactions comparable. Measurements of allowed transitions have been made by several workers and these results provide a stringent test to the bound state calculations of quantum electrodynamics.

1.3 Positron Swarm Experiments

The first investigations of positron interactions with solid and gaseous media were pioneered by workers such as DeBenedetti *et al* (1949) and Shearer and Deutsch (1949). The former authors observed a deviation from co-linearity of the 2-γ annihilation radiation and the latter were the first to determine positron lifetimes in gases. These studies employed sources of positrons with large energy distributions extending to high energies (O[keV-MeV]) and relied on the media under investigation to slow down the particles.

Though principally unchanged, the measurement of positron lifetimes and the angular correlation of the annihilation radiation (ACAR) have been refined into sophisticated techniques. These, along with other methods such as Doppler broadening of the detected annihilation radiation, play a leading role in elucidating the behaviour of the positron, augmenting the findings from e^+ beam studies. To give an overview on methods used in swarm-type experiments, the three techniques mentioned above are briefly discussed in the following section.

1.3.1 Lifetime technique

The principle of this method relies, as the name implies, on measuring the lifetime of the positron by monitoring the time difference between its creation and its eventual annihilation in the media. From this, information on the formation of Ps and the slowing down and thermalisation processes of e^+ and Ps can be discerned. To this end, ^{22}Na is ideally suited as the positron source for the creation of a β^+ particle is signalled by the emission of a 1.27(45)MeV photon within 10ps from the de-excitation

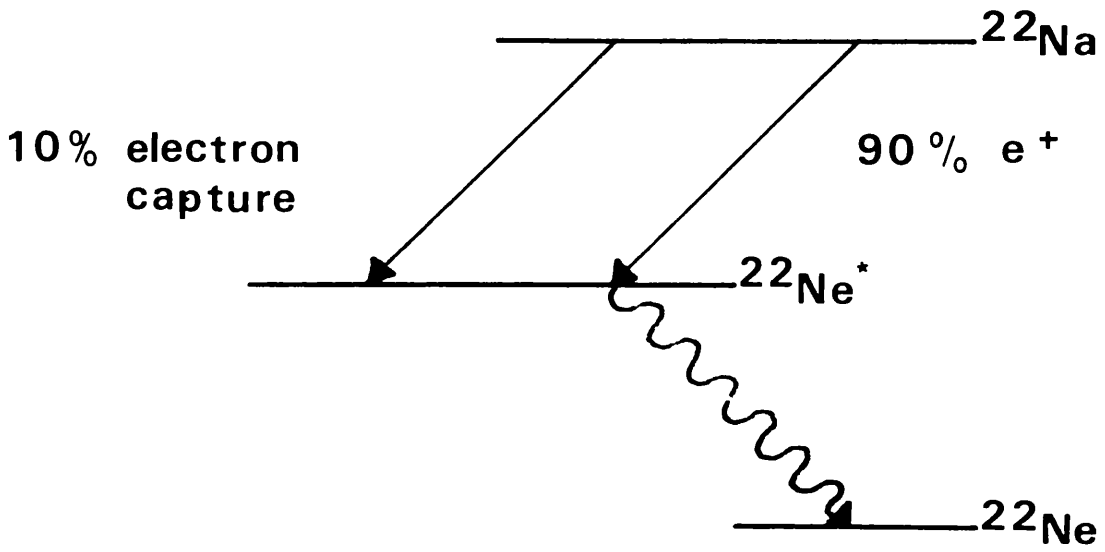

Figure 1.4 Decay process of ^{22}Na

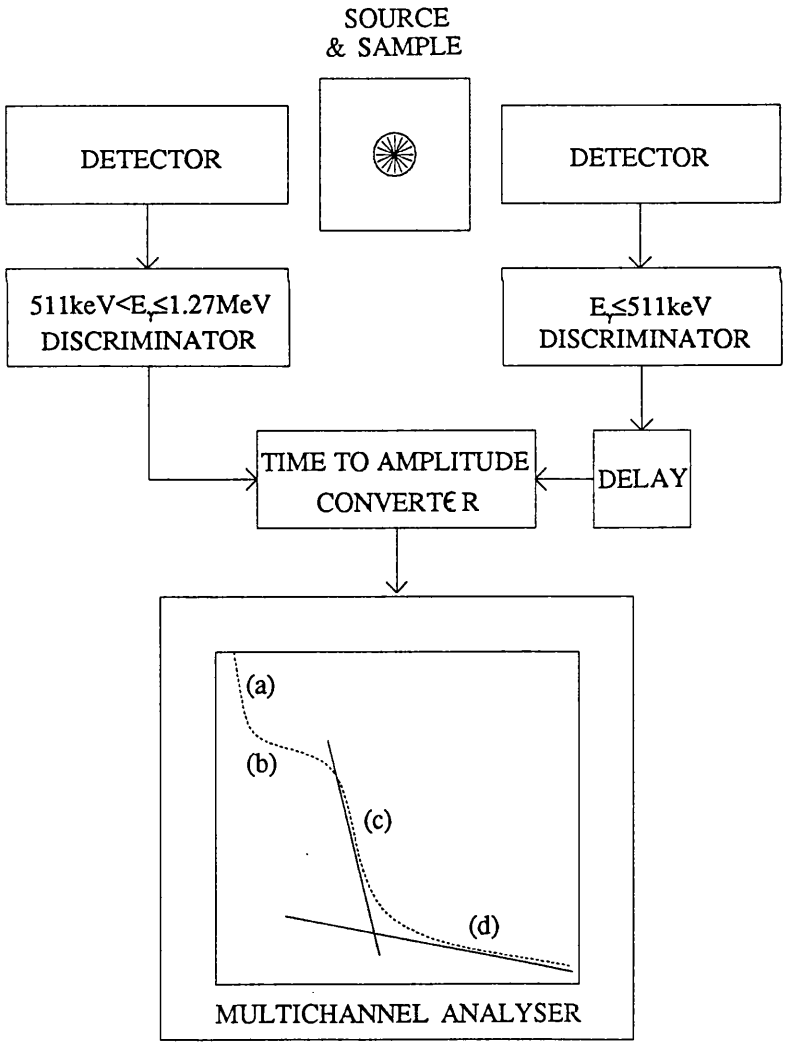

Figure 1.5 Schematic diagram of a typical lifetime system and Ar gas lifetime spectrum

of the decay product, $^{22}Ne^*$. Furthermore, the decay process of ^{22}Na to $^{22}Ne^*$ with positron emission has a high branching ratio, 90.6%, compared to the alternative path of this reaction via e^- capture (Figure 1.4). The term β^+ henceforth refers to positrons emitted from sources prior to energy loss.

A schematic diagram of a typical lifetime apparatus together with a spectrum is shown in Figure 1.5. The γ-rays from the β^+ creation and the subsequent annihilation are detected by scintillators (for example: NaI(Tl); plastic; BaF_2) coupled to photomultiplier tubes placed in close proximity to the chamber. The resulting pulses are fed as start and stop signals into a Time-to-Amplitude Converter (TAC) with an appropriate delay on the stop line. The time difference between the registration of the two signals emanate as pulses of correspondingly varying amplitudes which are monitored by a Multi-Channel Analyser (MCA). Over a period of time, the spectrum accumulated is the distribution of the e^+ lifetimes in a certain gas at a particular density.

The lifetime spectrum shown in Figure 1.5 is representative of those typically obtained with a ^{22}Na source in a few amagats of Ar gas at room temperature (1 amagat = 2.69×10^{25} atoms/molecules m^{-3}). The spectrum can be divided into four regions, labelled (a), (b), (c) and (d). The sharp (prompt) peak on the left of the spectrum, indicated by (a), corresponds to p-Ps decay and e^+ annihilation in the source and on the chamber walls. This is followed by a non-exponential shoulder region due to annihilation events of free e^+, with energies below E_{Ps}, before thermalisation. E_{Ps} is the minimum energy required to form positronium from the charge transfer process (discussed below). The shoulder is a feature common to spectra taken with most noble gases where energy loss rates are slow compared to annihilation rates, in particular below E_{Ps}. In this range, energy loss via elastic interactions is the only available channel and the mean fractional loss per collision, $\Delta E/E$, is given by

$$\Delta E/E = 2m_o/M \qquad 1.5$$

where m_o and M are the masses of the positron and the atom.

The last part of the spectrum is the convolution of two overlapping exponentials, caused by the decay of the free positrons and of the o-Ps. The two regions are separated by fitting the slower o-Ps component (d) and subtracting from the curve to

obtain the faster thermalised free e^+ component (c).

Decay rates of the two exponentially varying components may be extracted and used to determine Z_{eff} for free e^+, the weighted mean of the energy dependent parameter $Z_{eff}(v)$ (see section 1.2) and ${}_1Z_{eff}$ for o–Ps. The decay rate of o–Ps can be expressed as the sum of its decay rate in vacuum and the quenching rate in the gas. From this ${}_1Z_{eff}$, the effective number of electrons per atom available to the o–Ps for quenching, may be deduced.

Lifetime measurements can be used to study the quenching mechanisms involved in various gases such as spin-exchange of the electron to form p-Ps or chemical binding to the atom or molecule. Both result in high values of ${}_1Z_{eff}$ and, therefore, a faster annihilation rate. Extrapolation of the lifetime to zero density can yield values of ${}_0\lambda_{o-Ps}$ to compare with theory. Griffith *et al* (1978), Gidley *et al* (1982) and Westbrook *et al* (1987) have employed this method to determine the vacuum annihilation rate of o-Ps (see previous section).

The fraction of e^+ forming Ps, F, can be deduced from lifetime spectra and a number of models have been proposed to account for the observed yields in various media. The Ore model (1949) predicts that e^+ with energies, E_{e+}, in the range $E'_{Ps} \leq E_{e+} \leq E_I$ can form Ps, where E'_{Ps} is the minimum positron energy required to form Ps and E_I is the ionisation energy of the target. The formation of ground state Ps occurs via the charge transfer process, described in Section 4.2, where the incident e^+ removes an e^- leaving behind a positive ion. If E'_{Ps} is lower than the first excitation level, E_{ex}, as in the case of all atomic gases, the fraction of Ps formed, F, is given by

$$F = \{(E_{ex} - E'_{Ps}) + \int_{Ei}^{Eex} (\sigma_{ps}(E)/[\sigma_{ps}(E)+\sigma_{ex}(E)])dE\}/E_I \qquad 1.6$$

where σ_{Ps} and σ_{ex} are the Ps formation and excitation cross-sections, respectively. This assumes that all e^+ with energies in the range from E'_{Ps} to E_{ex}, the "Ore gap", form Ps. However, density-independent values of F, a requirement of the Ore model, have only been observed in He, Ar and Ne gases. Discrepancies between the measured fraction of Ps and those calculated using the Ore model have been reported for gases such as H_2, CH_4 and N_2, where density and/or temperature variations have been noted.

The spur model, an alternative hypothesis formulated by Mogensen (1974), has been demonstrated to successfully predict the Ps yields in liquid phase media. Together, the Ore and the spur models have been used by Jacobsen (1986) to account for the observed yields in dense gases: CO_2 and SF_6 (Heyland *et al*, 1985), C_2H_6 (Sharma *et al*, 1982) and N_2 (Griffith *et al*, 1982). In the latter model, the positrons, as they slow down, become "localised" in "spurs" at the end of their trajectories. Essentially a concentration of free e^-, positive ions and other radical species, the spur allows the combination of the e^+ with a free e^- to form Ps, if their separation is small enough. The probability of reaction becomes significant when the magnitude of this distance is of the order of the Onsanger radius, that is the separation at which the Coulomb energy of the e^+ and the e^- is equal to the thermal energy. Unlike the Ore model, a lower energy limit does not apply.

Since the early work of Shearer and Deutsch (1949) the lifetime technique has been extensively used to study e^+ interactions in numerous gases and further developed to investigate the influence of electric and magnetic constraints. Its application to condensed matter is technically more difficult since characteristic lifetimes in metals and semiconductors are typically of the order of 10^{-10}s. Simpson *et al* (1989) have recently employed this technique with silicon to measure the lifetime of e^+ drifted to an interface under the influence of an electric field and hence extract the e^+ mobility in the material. Values obtained are in accord with those using Doppler broadening and e^+ beam techniques.

1.3.2 Two photon angular correlation technique

The technique of angular correlation of the annihilation radiation, ACAR, is based upon the measurement of the angular deviation, θ, from co-linearity of the two γ–rays emitted on decay. Figure 1.6 shows a schematic diagram of an ACAR system where the positron source, for example ^{22}Na, is placed close to the sample under investigation. The photons are monitored by scintillators coupled to photomultiplier tubes, sited at a distance of a few metres with detector 1 in a fixed position and detector 2 rotated to vary θ.

The positrons, once implanted, thermalise rapidly and eventually annihilate with an e^-. The momentum contribution from the e^+ to the centre of mass of the pair is minimal. This is due to the presence, on average, of only one e^+ in the solid at any

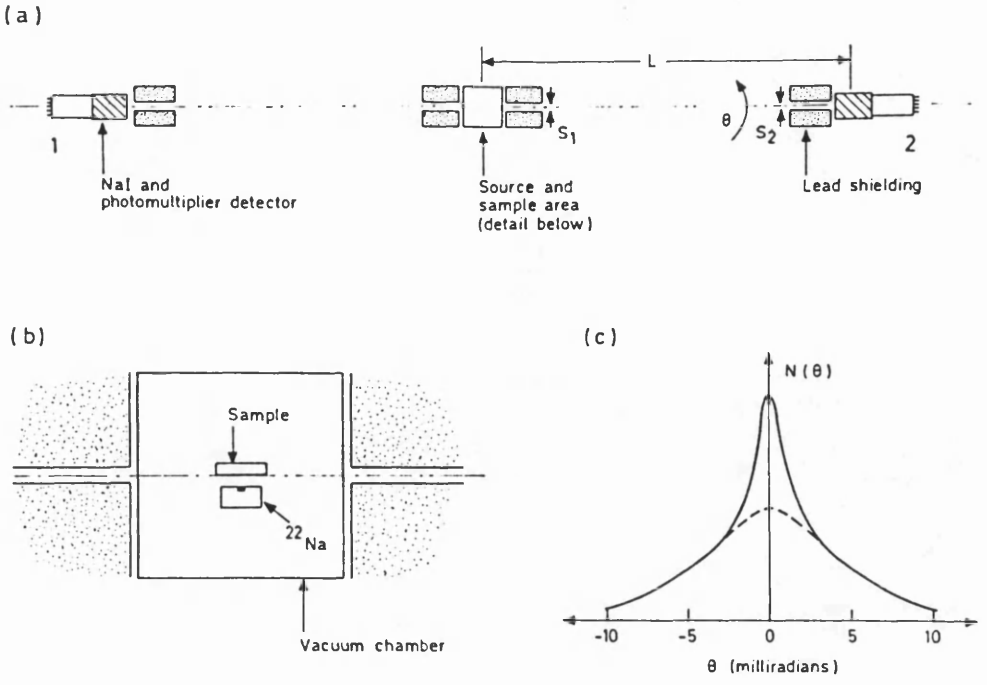

Figure 1.6 Schematic diagram of typical ACAR system (a, b) and spectrum (c)

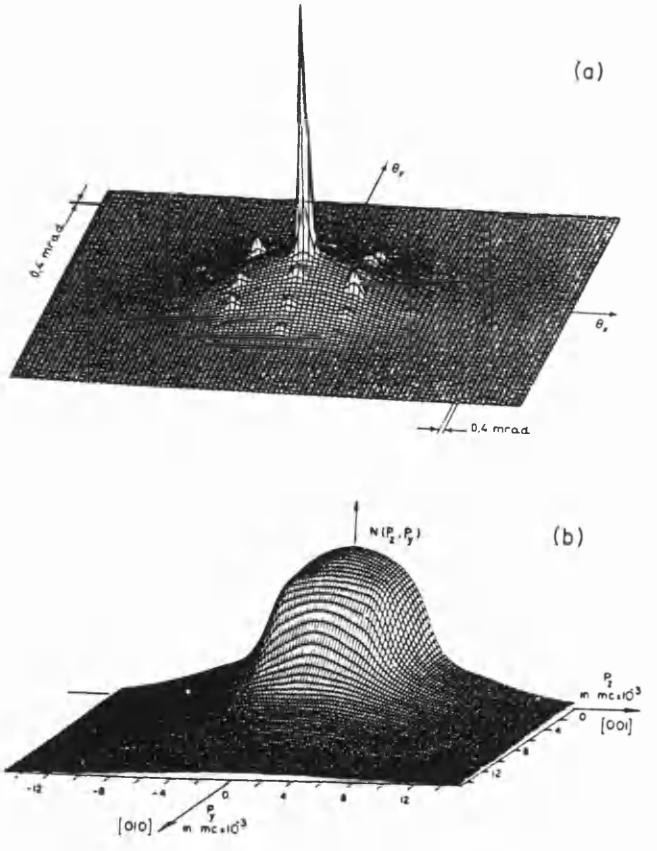

Figure 1.7 Two dimensional e^- momentum distribution in:
(a) single crystal quartz (Manuel, 1981)
(b) single crystal Cu (Haghgooie *et al*, 1978)

time, so allowing the occupation of the lowest e^+ level. The e^-, however, can possess significant momentum by virtue of the Pauli exclusion principle on the sea of $\approx 10^{22}$ e^- cm^{-3}, hence resulting in the angular deviation of the photon emission as observed in the laboratory frame. The momentum distribution of the e^- can thus be deduced from the count rate variation with θ as $\theta \approx v/c$ for small angles where v is the centre of mass speed of the pair in the laboratory frame and c is the speed of light *in vacuo*.

Annihilations in metals and semiconductors arise from the interaction of delocalised e^+ with the e^-. Ps has not been detected in the bulk of these solids due to the screening effect of e^+–e^- interactions by the polarisation of the medium. Furthermore, stable Ps formation cannot occur in metals as the binding energy approaches 0eV at electron densities greater than those found in the most dilute elements (Kahana, 1960, Lowy and Jackson, 1975). Some molecular and ionic solids, however, have been observed to support bulk Ps formation. An example is quartz, the ACAR spectrum of which is illustrated in Figure 1.7a (Manuel, 1981). The spectrum shows a sharp peak associated with a virtually momentum free system of p–Ps. In contrast, Figure 1.7b shows the momentum distribution of the e^- from the annihilation of delocalised e^+ in single crystal Cu (Haghgooie *et al*, 1978). The high sensitivity of this technique in the investigation of the positron's environment has resulted in its extensive employment in bulk studies of solids such as the mapping of the Fermi surface of metals and alloys and investigations of lattice defects (West, 1985).

1.3.3 Doppler broadening technique

The Doppler broadening method, although not exclusive to swarm experiments, can supplement the information from angular correlation measurements on e^- momentum. Figure 1.8 shows, schematically, a typical system employed in this technique. The red/blue-shifted annihilation radiation is monitored by a semiconductor Ge or Ge(Li) detector and, following amplification of the signal, the annihilation line shape may be viewed on an MCA as shown in Figure 1.8. The e^- momentum can be extracted from the deconvolution of the Doppler broadened distribution, however, it is more frequently quantified by a parameter S, which is the ratio of the counts in the central portion of the peak, A, to the total peak count, B. The trapping of e^+ in vacancies, as mentioned above, is well illustrated by this method as the e^+ can become localised in minimum potential regions created by the absence of ions, dislocations or defects in the lattice structure. As the e^+ wavefunction collapses into the vacancy, its

interaction with the less energetic conduction e^- increases compared to the core e^-, thereby resulting in a narrower line shape from a reduction in the range of the e^- momentum distribution.

The localisation of e^+, first investigated by Mackenzie *et al* (1967), has been widely studied, both experimentally and theoretically. The primary reason for this is to gain information on the behaviour of the e^+ and the electronic structure of matter but secondly for the development of a non-destructive method of defect profiling. Details of these techniques can be found in reviews such as Schultz and Lynn (1988).

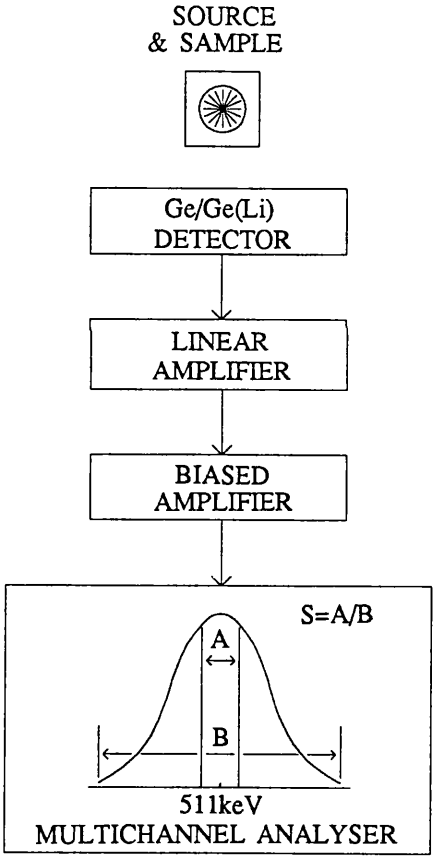

Figure 1.8 Schematic diagram of system for measuring the Doppler broadening of annihilation radiation

1.4 Slow Positron Beam Technique

1.4.1 Outline of technique

In the methods discussed above, fast positrons are emitted from radioactive sources, with mean energies of the order of 100's of keV and moderated (that is, lose energy) in the material under study. Information is then extracted from the detection of the radiation emitted upon annihilation in the sample. The application of these techniques, however, is limited in the study of low density gas targets and solid surface structure because of the requirement of a high density moderating material and the lack of control over the positron energy.

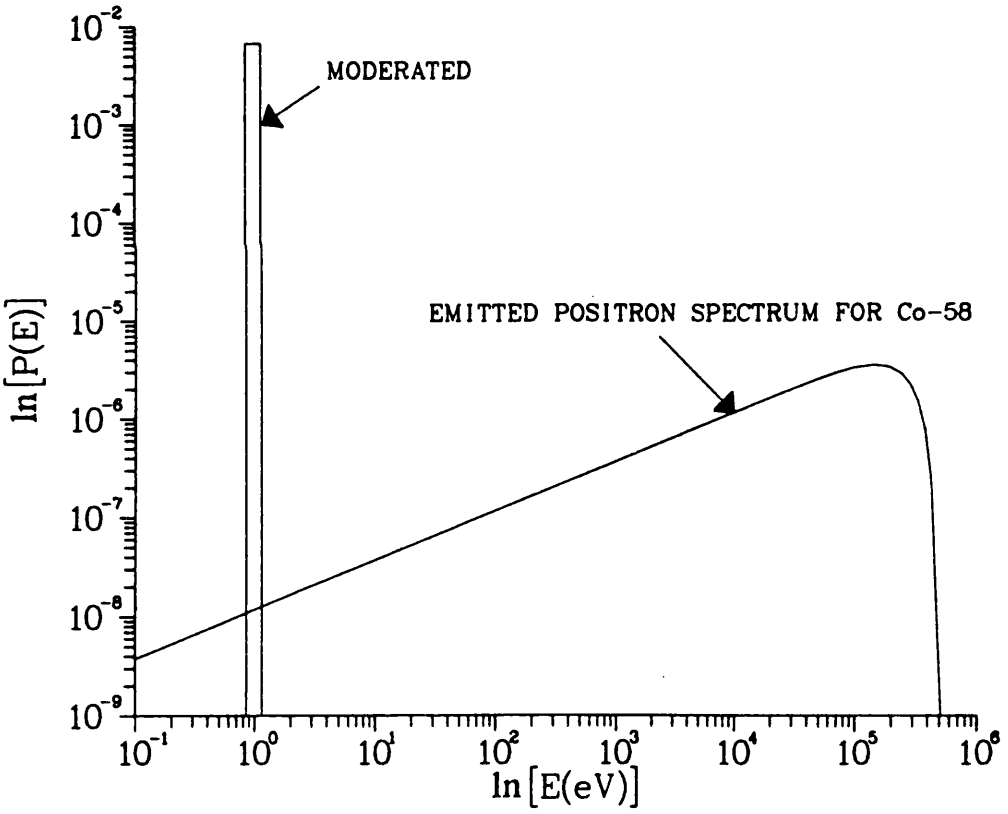

Figure 1.9 Comparison of positron yield from a W(110) moderator with the ß⁺ spectrum from a ^{58}Co source (Schultz and Lynn, 1988)

The development of the slow beam technique has resulted in the production of nearly monoenergetic, energy-variable positrons. The fast β^+ particles are slowed down in a target different from that being investigated and the resulting slow e^+ are transported to an interaction region away from the point of origin. Measurements can thus be made free from contributions of γ–rays and fast particles from the source area. The method of energy moderation, rather than that of energy selection, of the β^+ particles is more commonly employed to obtain slow e^+ because it results in much higher efficiencies, as graphically represented in Figure 1.9. This illustration shows the comparison in yield versus energy for the β^+ spectrum emitted from a ^{58}Co source with that moderated by a W(110) single crystal. At energies of a few eV , moderation is six orders of magnitude more efficient than selection. Conversion into slow e^+, however, is limited to materials possessing certain properties. These are described briefly in the following section and to greater depth in Chapter 2. In the sections below, the development of slow e^+ moderators is traced, detailing landmarks in the e^+ beam technique and methods and materials used in beam generation are described.

1.4.2 Moderator Development

Following the work of DeBenedetti *et al* in 1950 on positron diffusion in solids, Madansky and Rasetti (1950) made the first attempt to detect thermal energy positrons that had "diffused through and out of various materials". In this study, a ^{64}Cu source (10-30mCi) was employed to irradiate samples of Pt, K, Ga, glass, mica, celluloid and octoil placed in an evacuated tube in an axial magnetic field of 100 Gauss. A thin Al foil,at a distance of 80cm from the samples,was used as the positron collector about which a pair of scintillation counters were placed to monitor the 2-γ annihilation photons. Madansky and Rasetti (1950) were unsuccessful in detecting any low energy e^+ due to low sensitivity of their system, however, the reasons cited for the negative results (e^+ trapping in the lattice and at the surface and Ps formation) were predictions of processes observed many years later. Moreover, they correctly estimated their expected efficiency to be, approximately, the ratio of the positron "diffusion length" to the mean implantation depth of the fast β^+, thus stating two factors which determine the yield from a moderator. The diffusion length, L_+, is the characteristic path length of a positron in the solid before localisation in a potential well or annihilation and the mean implantation depth essentially scales with the

reciprocal of the material density, ρ. Therefore, the efficiency of a moderator, ε, according to Madansky and Rasetti (1950) can be expressed as

$$\varepsilon \propto L_+ \rho \qquad 1.7$$

The first successful detection of slow e^+ emission came in 1958 when Cherry irradiated a chromium-plated mica sample with a ^{64}Cu source. The ratio of slow e^+ (<10eV) to fast β^+ emission was found to be $3x10^{-8}$ and using this yield he investigated the secondary electron emission properties of surfaces subjected to e^+ and e^- bombardment.

Interest in the slow e^+ beam technique somewhat diminished until 1969 when Madey observed e^+ emission from polyethelene and Groce *et al*, with the aim of performing gas scattering cross-section measurements, discovered a slow e^+ yield from the surface of gold.

In 1972, Costello *et al* observed the emission of e^+ from gold-coated samples with a particular energy and made the first documented link between the e^+ emission energy and the surface property known as the positron workfunction. Their experiment deployed 55MeV electrons from a linear accelerator (LINAC) to create positrons by pair production from the bremsstrahlung radiation. The electrons were impacted onto a 0.004" water-cooled tantalum (Ta) target and the ensuing β^+ particles were moderated in samples placed in direct contact with the Ta (the term β^+ is extended to include high energy positrons from pair production). Samples of mica and CsBr crystal, both with 150Å Au coatings and Al with a 200Å Au layer were tested. A potential was applied to these materials with respect to an earthed Au plated Cu grid placed in front. The positrons were guided by a weak magnetic solenoid field to an Al foil in a vacuum of $2x10^{-7}$ Torr, where they were further accelerated onto the surface of the foil. Two fast liquid scintillators coupled to photomultiplier tubes placed about the Al plate detected the 2-γ annihilation photons. The energies of the e^+ were determined using a time-of-flight method; the electron beam was pulsed at a rate of 500Hz with 20ns long bursts and the coincidental annihilation signal was detected at the end of the 3m flight path.

After unsuccessful attempts to observe e^+ in the 10-100eV energy interval, they focused on the range (1.0 - 10)eV and detected positrons in a peak centred about 1eV

with an efficiency of 10^{-7} to 10^{-6}. Using this system, the first measurements of the e^+–He total scattering cross-sections were made by Costello *et al* (1972b).

Complementary to the experimental work, a model was developed by Tong (1972) to account for the emission of positrons from metals. In analogy to the electron workfunction, he postulated that a positron workfunction could also be defined and if the value was negative, positrons would essentially be ejected from the surface with this energy. Thus, metals which do not possess a negative positron work function will not directly emit free e^+. The estimation described by Equation 1.7 is, therefore, only applicable if the surface conditions permits e^+ emission. However, a point of note is that the e^+ workfunction of Au has since been determined to be positive (Nieminen and Hodges, 1976, Lynn, 1980 [unpublished]). Although the results of Costello *et al* (1972a) cannot now be attributed to this mechanism, many other metals have been observed to emit e^+ with workfunction dependent energies. The e^+ detected in the above experiment may have been epithermal, that is non-thermalised.

The next major improvement in the field of moderator development came when Canter *et al* (1972) discovered copious emission of positrons from magnesium oxide-coated Au. Using a venetian blind arrangement of Au strips, the vanes were coated with "smoked" MgO powder produced by burning Mg ribbon in a flame and an efficiency of $3x10^{-5}$ was obtained with an energy spread of 2–3eV.

The model of Tong (1972) relating to workfunction energy in metals could not be applied to this new type of moderator. The process of e^+ emission was initially thought to be indirect and Griffith *et al*, in 1978 suggested that field-ionisation of Ps may be a possible mechanism. Reports of enhanced secondary e^- emission from oxide layers upon e^- bombardment (Malter, 1936) led Jacobs (1951) to hypothesise that the formation of a charge layer due to the liberation of electrons in a non-conductive material may be responsible for this effect. The charge layer idea was substantiated with evidence from many workers who noted a persistence in the emission after removal of the incident e^- beam; Griffith *et al* (1978) also observed time-lags upon changing the moderator bias on a MgO coated W sample. They noted that slow e^+ yields from such a moderator were no higher than the yields of excited state positronium observed from metal surface (Canter *et al* 1975) and suggested that e^+ were produced via field-ionisation of the n=2 state. However, the recent work on rare gas moderators (Gullikson and Mills, 1986) has provided evidence contrary to

this, showing the Ps^* break-up model to be inconsistent in the interpretation of their results. The authors found indications that the e^+ detected were those that had been emitted prior to complete thermalisation. These studies and the "hot positron" model are discussed below.

In 1974, another method of positron production was developed by Stein *et al* using a self-moderating source. Employing a Van de Graff accelerator, 4.75 MeV protons were fired into a boron target and positrons were produced via the reaction

$$^{11}_{5}B + p \rightarrow {}^{11}_{6}C + n \rightarrow {}^{11}_{5}B + \beta^+ + \nu \qquad 1.8$$

This reaction has a threshold of 3.0MeV and the maximum energy of the β^+ particles produced is 0.9MeV with a $^{11}_{6}C$ decay ratio of 0.99. The boron itself acts as the moderator, producing slow e^+ with a very narrow energy width, $\approx$0.25eV, and with 10^{-7} efficiency. Further improvement of the yield to 10^{-6} was noted after 60 operational hours and this was attributed to a coverage of cracked polyphenyl ether pump oil on the boron target (Stein *et al*, 1974). Figure 1.10 shows a later version of this apparatus (Kauppila *et al*, 1981); electrostatic fields were used initially for extraction and guidance, then a curved solenoid was incorporated to differentiate the slow beam from the fast particles. Detection was made using a channeltron electron multiplier (channeltron), and the energy distribution was measured by the application of a potential on the retarding element. The target, of polycrystalline boron (99.8% pure), was approximately 0.2 x 0.5 x 0.015 cm and water cooled to avoid evaporation upon proton bombardment. Although an increase in flux was possible, this was limited by the ability to remove the excess heat from the target. Advantages of this system, in addition to the narrow energy width, were the short half life of the radioactive C after switching off the beam (20.3minutes), and the absence of an intense background from bremsstrahlung radiation. This technique was used to make the first experimental observation of the Ramsauer-Townsend minimum in e^+–Ar total scattering cross-section (Kauppila *et al*, 1976) and to measure the e^+ total cross-sections in gaseous potassium (Stein *et al*, 1985).

Since the study of Groce *et al* in 1969, several workers have observed slow e^+ emission from metal surfaces such as Al, Au and Cu when irradiated with a radioactive source (Pendyala *et al*, 1973, 1974, Coleman *et al*, 1973, Keever *et al*, 1972). Pendyala *et al* (1976) performed an extensive survey of various polycrystalline

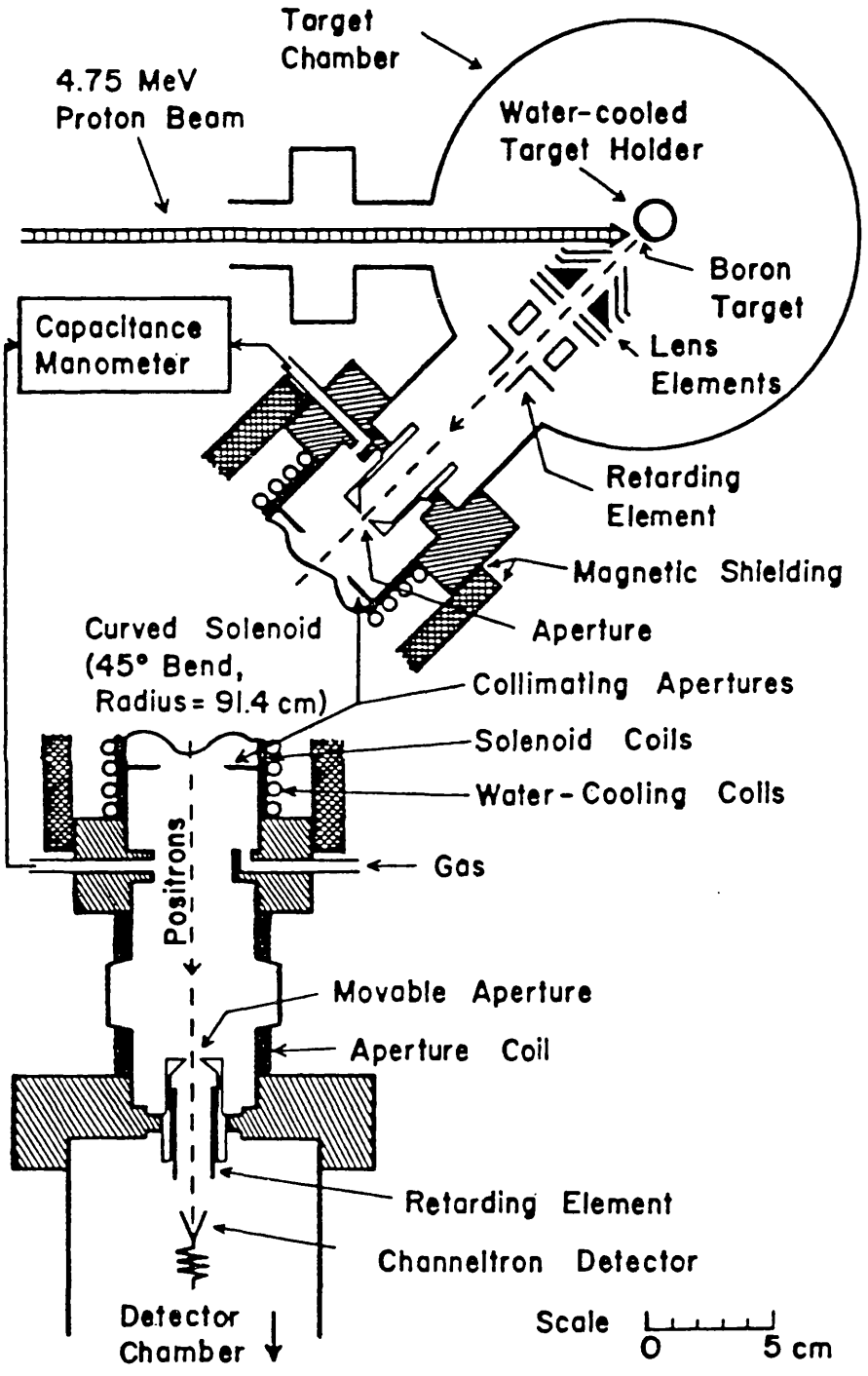

Figure 1.10 Schematic diagram of positron beam apparatus using a boron self-moderator (Kauppila *et al*, 1981)

solid moderators; they found that only Cu yielded values higher than MgO which they used as their standard. However, the structure, surface conditions and purity of these materials was unknown.

It was not until the work of Mills *et al*, in 1978, that well-characterised, high-purity samples were investigated and the factors relating to their moderation property were better understood. In this study, a 100mCi ^{58}Co source was used to produce slow e^+ from a Pt moderator biased positively up to 3keV. The magnetically confined flux was deflected through two sets of **ExB** plates, first off axis, then returned to axis to remove the fast $ß^+$ particles from the beam, and subsequently guided into an ultra high vacuum (UHV) chamber (10^{-10} Torr) containing the target. The samples were mounted on a heating element which could be moved to different positions for cleaning and analysis. The longitudinal energy spread of the re-emitted slow e^+ was deduced by measuring the annihilation rate behind the target with a NaI(Tl) detector whilst varying the target bias. Single crystal samples of Al(100), Cr and Si(100) were investigated - the number in brackets are the Miller indices denoting the crystal face orientation.

For the study of yield variation in relation to the incident beam energy and to the temperature, the properties of the Al(100) sample were investigated after surface cleaning by Ar ion bombardment and heating to 600°C for 10 minutes. Conditions on the surface, both before and after the studies, were checked by low energy electron diffraction (LEED) and Auger spectroscopy methods and found to have less than 0.2% oxygen coverage.

The results showed that slow e^+ were emitted from Al(100) with an efficiency of approximately 20% at 1keV incident beam energy and that the re-emitted e^+ energy distribution was narrow, peaking at (0.2 ± 0.1)eV. When used with a $ß^+$ source, yields of $(3\pm1)x10^{-5}$ were obtained with a 10-90% energy width of (0.16±0.02)eV at an emitted e^+ energy of 19.4eV. Furthermore, the yield of emitted e^+ also showed variation with moderator temperature resulting in changes to the workfunction value. Subsequent studies, such as those performed by Murray and Mills (1980) and Gullikson *et al* (1988), have demonstrated increases in emission corresponding to increases in the magnitude of the workfunction (see Figure 2.8). Although the number of e^+ reaching the surface may remain unchanged, the emission of slow e^+ with respect to other possible processes has been observed to respond to changes in

the surface conditions, thereby revealing another factor, y_0, the slow e^+ branching ratio. The expression from Madansky and Rasetti's estimates can now be modified to include the branching ratio, thus,

$$\varepsilon \propto L_+ \rho y_0 \qquad 1.9$$

Therefore, for good moderation properties, the material must have a large diffusion length. This is achieved by using samples of good crystalline order with relatively low concentrations of vacancies, defects and dislocations which may trap the thermalised positrons in the bulk. A large value of ρ is required as the number of fast β^+ stopped in a particular thickness increases with higher density. On reaching the surface, positrons will be ejected, if the workfunction of the material is negative, with a yield which is seemingly influenced by the magnitude of the workfunction.

In 1980, Dale *et al* performed a study of the emission of slow e^+ from several high density materials, developing a simple annealing treatment and comparing the yields obtained with calculated workfunction values. A 54mCi ^{58}Co source was used to irradiate samples mounted in a flat vane arrangement with 3mm wide ribbons cut into lengths of 10mm. The slow e^+ were electrostatically extracted, guided through a 145° spherical energy selector and detected by a channeltron for analysis of the energy distribution. A variety of methods were employed to prepare and treat the materials investigated which included W, Mo, Ir, Pt and Ni. W samples were found to give the highest yields following an annealing procedure consisting of chemical etching prior to resistive heating for five minutes at 2200° in a vacuum of $5x10^{-8}$ Torr. After correcting for the source-moderator geometry and the transport efficiency, a yield of $7x10^{-4}$ was obtained with a full width at half maximum (FWHM) energy spread of 1.3eV, located at approximately 4V above the accelerating potential. Dale *et al* (1980) found that removal of the surface contaminants by chemical etching was not enough to achieve the high yields and that the annealing procedure was vital in order to recrystallise the structure. The heating process reduces the concentration of defects and so results in an increased value of L_+. After 24 hours they noted that the yield stabilised and, furthermore, exposure to atmosphere was not detrimental to the efficiency.

The importance of this study was not only the determination of W as an efficient moderating material but also the development of a simple method of treatment. Ultra-

high vacuum conditions were not required and the moderator could be annealed in a chamber other than the test apparatus and transported without great loss of efficiency. The inertness of the W samples, noted by Dale *et al* (1980), due to the slow rate of oxidation after two monolayers of coverage renders it a suitable material for use in non-UHV conditions. The efficiency from W was further improved by Vehanen *et al* (1983) when a value of $3x10^{-3}$ was obtained from a single crystal of W in the backscattering mode. This figure is close to that computed by Vehanen and Mäkinen (1985) as the maximum expected yield, $4x10^{-3}$, from such a configuration. Most recently, Lynn *et al* (1989) have developed a new type of W moderator employing a conical configuration. Single crystal W rods were spark-cut and electropolished into truncated cones of various lengths and opening angles. These were annealed in $\approx 10^{-7}$ Torr at 2100°C for a few minutes and subsequently cooled slowly to room temperature. Following transfer in air to the test beam, a maximum efficiency of $1.5x10^{-3}$ was obtained from a 20.8mm long, 85° opening angle sample. A Ni cone was also investigated; this was annealed *in situ* at 800°C for 5 minutes at $5x10^{-6}$ Torr. The efficiency obtained, 10^{-3}, compares well to that from the W. The energy distribution from the emitted e^+ was found to be larger than that from thin W film in transmission mode. The FWHM longitudinal energy spread was measured to be ≈7eV compared to ≈3eV from a thin W(100) film used in the same experiment.

In the studies described above positrons that have backscattered from single crystal or vane arrangements have been extracted. However, the limitations of this mode, discussed in the next section, have given rise to interest in the use of the transmission geometry. In such a configuration, e^+ are extracted from the side opposite to the $ß^+$ entrance surface so thin films of material are required as moderators. Studies have been performed by several workers on their use as $ß^+$ and e^+ moderators including the work detailed in this thesis (Chen *et al*, 1985, Lynn *et al*, 1985, Schultz *et al*, 1986, Gramsch *et al*, 1987, Zafar *et al*, 1988, Poulsen *et al*, 1988, Zafar *et al*, 1989). These investigations will be discussed fully in Chapters 2 and 3.

Since the work of Dale *et al* (1980), the most widely used moderators have been metallic, in particular W. The use of non-metallic substances has recently been revived by the work of Gullikson and Mills (1986) and Mills and Gullikson (1986) where solid noble gases were used as the moderating medium. The configuration employed comprised of a 300μCi ^{22}Na source deposited onto the flat surface of a Cu cylinder which was screwed onto a liquid He refrigerator. With a base pressure of

$\approx 10^{-10}$ Torr, noble gases were condensed onto the arrangement and the emitted e^+ were magnetically guided from this region. The e^+ were monitored with a channeltron in coincidence with a NaI(Tl) detector to determine the absolute efficiency of the moderator. Of the noble gases tested (Ne, Ar, Kr, Xe), Ne was found to give the highest yield and smallest energy spread, however, all the moderators gave results comparable to that from single crystal W in the backscattering mode. Defining the efficiency as the number of slow e^+ per β^+ emitted by the source, a value of $(3.0\pm0.2)\times10^{-3}$ was obtained from a $\approx 1\mu m$ layer of solid Ne deposited onto the source. However, with the attachment of a 16mm long Cu cylinder over the source to form a cup geometry (Figure 1.11d), the efficiency was increased to $(7.0\pm0.2)\times10^{-3}$, more than twice that of the most efficient W moderator (Vehanen *et al*, 1983), with a FWHM e^+ energy distribution of 0.58eV.

Based on incomplete thermalisation before emission, the "hot positron" model was proposed by the authors to account for the slow e^+ yields observed from these materials, the positron workfunctions of which are thought to be positive. The positrons incident on the moderator rapidly lose energy via inelastic collisions until a threshold is reached, due to the wide band gap, where the only means of energy loss is by the less efficient process of phonon excitation. The threshold energy, E_{th}, was identified as the level below which Ps formation cannot occur and, in taking the case of Ar, this value is $\approx$10eV compared to the band gap energy of 14.16eV. Since the maximum phonon energy is small (0.008eV in Ar), the energy loss rate is low and the diffusion length of the pre-thermalised e^+ becomes large; in Ar this was calculated to be $\approx$5000Å. So the probability of e^+ reaching a surface increases substantially below E_{th} and escape from the solid is likely if the e^+ kinetic energies are greater than the e^+ workfunction. This model was substantiated by evidence from the experimental studies: a large energy distribution was observed corresponding to an energy limit of E_{th}; higher implantation energies resulted in lower energy e^+ emission; and extrapolation to zero implantation energies gave y_0 values of 67% - far in excess of that from Ps^* formation, in contradiction with the field-ionisation model.

A yet different type of slow e^+ converter has been discussed by Beling *et al* (1987) - the field-assisted moderator (FAM). This technique relies on the application of an electric field across the moderating material to drift the thermalised positrons to an exit surface, thus enhancing the current in one direction. A thin insulator or semiconductor is required to support the field and silicon was originally suggested.

Moderator & mode	ε	ΔE (eV)	Vacuum (Torr)	Reference
Pt, K, Ga, glass transmission	0	–	–	Madansky and Rasetti (1950)
Cr plated mica transmission	$3x10^{-8}$	–	10^{-7}	Cherry (1958)
Au plated mica transmission	10^{-7}	2	10^{-7}	Costello *et al* (1972a)
MgO coated Au vanes backscattering	$3x10^{-5}$	2.3	10^{-7}	Canter *et al* (1972)
B self-moderator	10^{-7}	0.15	10^{-7}	Stein *et al* (1974)
Al(100) backscattering	$3x10^{-5}$	0.1	10^{-10}	Mills *et al* (1978)
Cu(111)+S backscattering	$9x10^{-4}$	0.3	10^{-10}	Mills (1979a)
Cu(111)+H_2S backscattering	$1.5x10^{-3}$	0.6	10^{-10}	Mills (1980b)
W vanes backscattering	$7x10^{-4}$	1.3	10^{-7}	Dale *et al* (1980)
W(110) backscattering	$3x10^{-3}$	0.7	10^{-10}	Vehanen *et al* (1983)
W(100) transmission	$4x10^{-4}$	3	10^{-10}	Lynn *et al* (1985)
Ne transmission	$7x10^{-3}$	0.58	10^{-10}	Mills and Gullikson (1986)
W(100) Ni(100) transmission	$9x10^{-4}$ $6.6x10^{-4}$	– –	$\approx10^{-8}$ $\approx10^{-8}$	Gramsch *et al* (1987)
W, Ni cone backscattering	$1.5x10^{-3}$ $1.0x10^{-3}$	7	10^{-7}	Lynn *et al* (1989)

ΔE is the quoted energy width

Table 1.2 Chronological summary of developments in $ß^+$–e^+ moderators

The workfunction was later determined to be positive, however it may be possible to change this value by surface coverage with oxygen (or another element) of the order of a few monolayers. Results from the mobility study of Simpson *et al* (1989), using a lifetime technique, indicate that in silicon, a significant fraction (7%) of e^+ can be drifted to an interface at low temperatures (104K) by an electric field.

The discussion above has described some landmarks in the development of a slow e^+ moderator and a chronological summary of these achievements is presented in Table 1.2. The properties required of a metallic moderator have been noted, namely: good crystalline structure, high material density, a favourable positron workfunction and a high positron branching ratio. In addition, several methods of beam production have been outlined employing various means of β^+ production and using different source-moderator configurations. In the following section, the characteristics of these arrangements are discussed more fully.

1.4.3 Source and moderator considerations

As mentioned in the previous section, there are, in the main, two methods of obtaining the β^+ flux: firstly, via pair production from the bremmstrahlung radiation of high energy particle impact and secondly, from the decay of radioactive substances. The former requires the use of a particle accelerators in the creation of the β^+ particles and is, therefore, technically more complex than the latter. Moreover, high background radiation and limitations to the dissipation rate of the heat produced from bombardment are constraining factors. However, with this method, very high primary intensities can be achieved. The use of this technique is exemplified by the facility at the Lawrence Livermore National Laboratory where Howell and co-workers (1986) have generated slow e^+ beams of $1.2 \times 10^9 s^{-1}$ with a thick W converter, employed in producing the β^+ particles, coupled to a W moderator to obtain the slow positrons.

The method of β^+ production using radioactive sources is more widespread and several of the β^+ emitting isotopes are listed in Table 1.3 with their half-life, β^+ branching ratio and the maximum specific activity (from Dupasquier and Zecca, 1985). The use of short-lived isotopes, such as ^{11}C (Stein *et al*, 1974, Section 1.4.2), is restricted by the need to be manufactured close to the site of e^+ beam production. Both the techniques using the short-lived isotopes of ^{11}C and ^{64}Cu, which is reactor-made at the

Brookhaven National Laboratory, thermalise the β^+ particles in the bulk of the source and utilise the materials' negative positron workfunction to produce the slow beam. Thus, the sources are self-moderating. The relatively long-lived isotopes of ^{58}Co and ^{22}Na, with half-lives of 71 days and 2.6 years, respectively, are commercially manufactured and are most often used due to ease of handling and transport.

Isotope	Half-life	β^+ Fraction %	Maximum specific activity (Cig^{-1})
^{58}Co	71 d	15	16.6
^{22}Na	2.6 y	90	1.25
^{68}Ge	288 d	88	6
^{11}C	20 min	99	-
^{64}Cu	12.8 h	19	600

Table 1.3 Properties of some β^+ emitting isotopes (from Dupasquier and Zecca, 1985)

The moderator arrangements of backscattering, vane, grid, cup, cone and transmission, shown in Figure 1.11, are geometries used with these long lived sources. High efficiencies ($3x10^{-3}$) have been achieved using the backscattering mode (Vehanen *et al*, 1983) where fast β^+ particles are impacted onto a flat, (usually) single crystal material and the slow e^+ are extracted from the same surface (illustrated in Figure 1.11a). From clean surfaces, the positrons are emitted normally with a small transverse component due to the thermal energy. However, this configuration is marred by the presence of the source which intercepts a portion of the emitted flux. Hence, the backscattering geometry is only suitable for high specific activity sources, for example ^{58}Co, and is normally deposited onto a fine needle or ribbon. Even so, the strengths of ^{58}Co sources cannot be increased above 100mCi mm^{-2} for technical reasons.

Following the work of Dale *et al* (1980), W is widely used as a moderating material in the vane and grid configurations shown in Figures 1.11b and c. Polycrystalline W ribbon or grids are usually employed after resistive heating at temperatures of $\approx$2200°C to increase the grain size of the crystallites. Although emission is from the

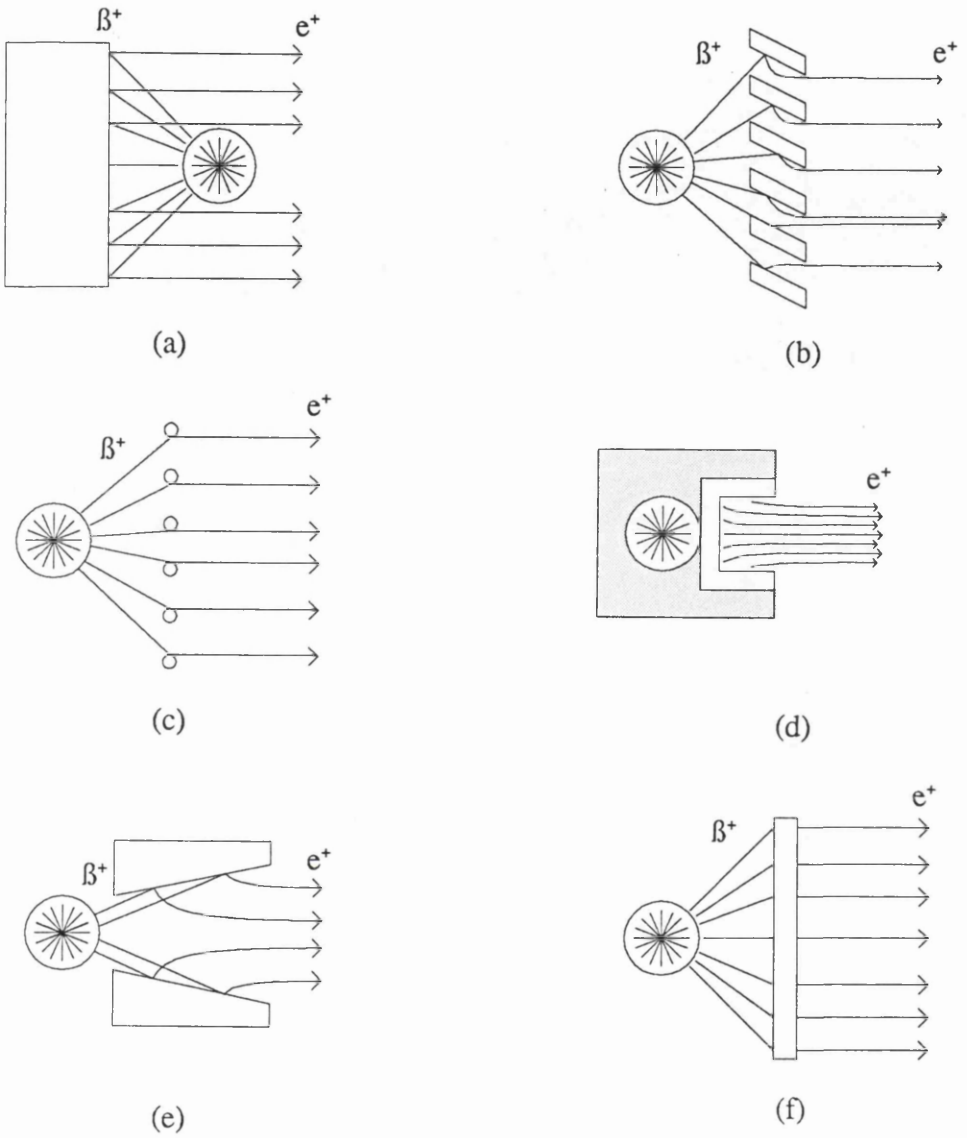

Figure 1.11 Moderator arrangements
(a) backscattering, (b) vane, (c) grid,
(d) cup - solid Ne, (e) cone (f) transmission

same surface as that entered by the β^+ particles, the slow e^+ are extracted on the side opposite the source. Without the shadow problem associated with the backscattering geometry, the relatively large sized, commercially-made ^{22}Na sources can be used in addition to those constructed with ^{58}Co. In both the vane and the grid arrangements, the e^+ may be emitted from surfaces which are not perpendicular to the beam axis, thus resulting in a larger measured (longitudinal) energy width than that from flat single crystal moderators. As in the case of the backscattering mode, the vane configuration can intercept the majority of the β^+ flux, depending on the angle of tilt, but the grid arrangement is disadvantaged by the large open area through which much of the incident flux is lost.

The recent advances in the study of the solid noble gas moderators (Mills and Gullikson, 1986) have resulted in the development of the cup geometry (Figure 1.11d) which was found to increase the yields from solid Ne moderators by over 100%. Figure 1.11e illustrates the forward re-emission cone moderator used by Lynn *et al* (1989) to obtain efficiencies 50% higher than that from thin single crystal films in transmission mode. However, this resulted in a 130% increase in the longitudinal energy spread of the ejected e^+.

Figure 1.11f illustrates the transmission mode where the e^+ are extracted from the side opposite to the implantation surface. Interest in this geometry arose initially for two reasons. Firstly, to produce e^+ with the smaller longitudinal energy distributions associated with e^+ backscattered from single crystals but free from the problems of source shadowing. Secondly, in order to simplify the optics in electrostatic systems using stages of remoderation. The recent availability of thin films, which are self-supporting and low in defect concentrations has enabled investigations into their use as moderators.

The energy spread and spatial distribution of primary moderated beams are too large for some atomic and surface studies such as low energy positron diffraction. To energy select the positrons and aperture down the size, however, would result in a large loss in intensity. Furthermore, electrostatic focusing of the beam also has limitations as discussed by Mills (1980a). From Liouville's theorem, a swarm of particles occupies a constant phase-space volume under conservative forces which can

be expressed thus,

$$B(E) = I/AE\sin^2\theta = \text{constant} \qquad 1.10$$

where B(E) is called the brightness of the beam-per-unit energy and I, A and θ are the intensity, the cross sectional area and the angular divergence of the flux. Thus if one factor is decreased, another will increase in compensation.

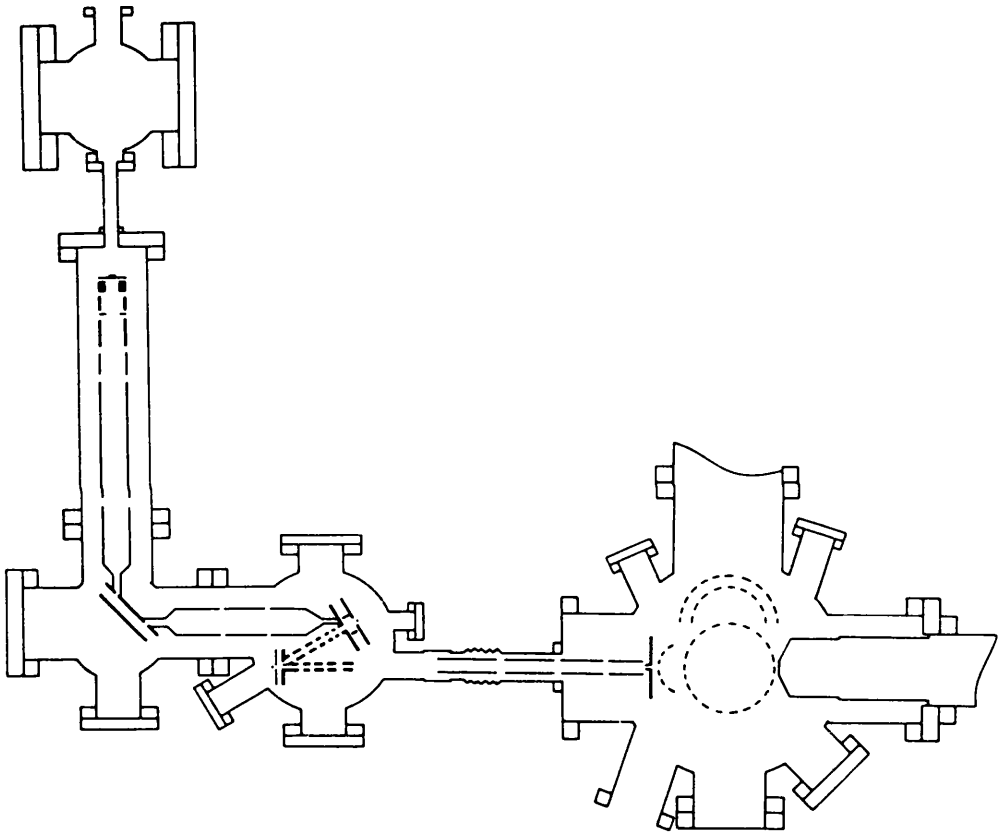

Figure 1.12 Schematic diagram of high brightness e^+ beam at Brandeis (from Canter *et al*, 1987)

Mills (1980a) suggested that, by using the non-conservative process of moderation, it may be possible to produce a brighter flux. By focusing the e^+ of energy 1-10keV onto smaller areas in successive stages of remoderation, B(E) can be increased by several orders of magnitude with some loss in intensity,

determined by the remoderation efficiency. Frieze *et al* (1985) first used this method to achieve a thirtyfold increase in the brightness but with an 80% loss of flux. More recently, Brandes *et al* (1988) have achieved a brightness increase of 500 to produce a e^+ beam of a few microns in diameter. Construction of electrostatic arrangements, such as that shown in Figure 1.12 used by Brandes *et al* (1988), may be aided by the simplification of the extraction optics employed to a linear arrangement. For the uses described above, thin single crystal materials are necessary for maximum yield.

1.5 Slow Positron Beam Experiments in Gases

Slow positron beams have enabled the study of a wide range of atomic processes. Since its initial employment in the study of e^+–He interactions (Costello *et al*, 1972b), many workers have used this technique to perform investigations into partial and total scattering cross section measurements in a variety of gases, for example H_2, N_2, CO_2, O_2, CH_4 (Charlton *et al*, 1983a), noble gases (Canter *et al*, 1974b). The technique of time of flight has been used in most of these investigations as the scattered positrons which are still confined by the magnetic field can be distinguished from the transmitted beam by a delay in arrival time. In the section below, recent studies undertaken with slow e^+ beams and proposals of future investigations are described; achievements in the measurement of e^+–gas scattering cross-sections are summarised in Table 1.4.

As stated in Section 1.1, comparison of the scattering cross-sections of the positron and the electron may aid the understanding of the basic interactions between charged particles and the target atom or molecule. The static interaction, that is the interaction of the particle with the undisturbed Coulomb field of the target, is attractive for the e^- and repulsive for the oppositely charged e^+. However, the polarisation interaction, caused by the distortion of the charge distribution of the target by the projectile, is attractive in both cases. This, therefore, leads to an addition of the effects in the case of electron scattering whilst, for the positron, they are subtractive. Moreover, the exchange interaction, due to the indistinguishability of the projectile and the target electrons, contributes only to e^--atom/molecule scattering. However, for positron scattering, correlation interactions occur between the projectile and the target e^- with the additional probability of Ps formation. In most cases at low energies, these

Cross-section	Gas	Energy range (eV)	Reference
σ_T	He	1-26	Costello *et al* (1972b)
σ_T	He	2-20	Canter *et al* (1972)
σ_T	He, Ne, Ar Kr, Xe	2-400	Canter *et al* (1974b)
σ_T	Ar	1-17	Kauppila *et al* (1976)
σ_T	noble gases	<30	Stein *et al* (1978)
$\sigma(\theta)$	Ar	2.2-8.7 $20°\leq\theta\leq60°$	Coleman and McNutt (1979)
$(\sigma_{Ps}+\sigma_i)$	He	20-500	Griffith *et al* (1979)
σ_{ex}	He	2-≈35	Coleman and Hutton (1980)
$(\sigma_{ex}+\sigma_i)$	He, Ne, Ar	<50	Coleman *et al* (1982)
σ_{ex},σ_i	He	<120	Sueoka (1982)
σ_T	H_2, N_2, CO_2, O_2, CH_4	2-20	Charlton *et al* (1983a)
σ_{Ps}	He, Ne, Ar, Kr, Xe	<150	Charlton *et al* (1983b)
σ_{Ps}	He, Ar, H_2	<80	Fornari *et al* (1983)
σ_{Ps}	H_2, N_2, CO_2, O_2, CH_4	<150	Griffith (1984)
σ_T	Hydrocarbons	5-400	Floeder *et al* (1985)
σ_T	CH_4, CF_4 CCl_4, SiH_4	1-400	Mori *et al* (1985)

Table 1.4 Chronological summary of some major achievements in e^+–gas collision cross-section measurements (continued overleaf)

Cross-section	Gas	Energy range (eV)	Reference
σ_T	K	5-50	Stein *et al* (1985)
σ_i	He	<200	Diana *et al* (1985)
σ_T	H_2O	2-400	Sueoka *et al* (1986)
$\sigma(\theta)$	Ar	100-300 $30°\leq\theta\leq135°$	Hyder *et al* (1986)
σ_{Ps}	He, H_2, Ar	<250	Diana *et al* (1986a,b)
σ_{Ps},σ_i	He	<800	Fromme *et al* (1986)
σ_T	NH_3	1-400	Sueoka *et al* (1987)
$\sigma(\theta)$	Ar	20 $30°\leq\theta\leq135°$ $\sigma(\theta=45°)$	Smith *et al* (1987)
$\sigma(\theta)$	Ar	30	Schwab *et al* (1987)
σ_T	K	50–100	Stein *et al* (1987)
σ_{Ps},σ_i	H_2	<300	Fromme *et al* (1987)
σ_{SR}	O_2	7.8-30.6	Katayama *et al* (1987)
σ_{SR}	H_2O, NH_3	5.7-8.3	Sueoka (1987)
$\sigma_{el},\sigma_{ex},\sigma_i$	He	55	Diana *et al* (1988a)
σ_{Ps}	Xe	7–430	Diana *et al* (1988b)
σ_i^{2+}/σ_i^+	He	≤4000	Charlton *et al* (1988)
σ_i^{2+}/σ_i^+	Ne, Ar	≤4000	Charlton *et al* (1989)
σ_T	C_6H_6	0.7-400	Sueoka (1989)
σ_i	H	30–600	Raith *et al* (1989)

Table 1.4 (cont.) Chronological summary of some major achievements in e^+–gas collision cross-section measurements

effects tend to result in larger e^- cross-sections and the general trends observed in the e^+ and e^- total scattering cross–sections seem to be consistent for all gases investigated at room temperature. Figure 1.13 shows the smoothed $e^{\pm}$–H total scattering cross–sections (Charlton, 1985a) and highlights the features of these interactions such as the difference in the e^+ and e^- values at low energies and the clear indication of the onset of Ps formation. With increasing energy, the relative effects of the polarisation and exchange/correlation interactions become negligible and, as expected, the two distributions merge at high energies as the static interactions begin to dominate all others. However, in the case of He, the convergence (at ≈200eV) appears to occur at substantially lower energies than that of 2keV predicted by theory (Dewangen and Walters, 1977).

A significantly different behaviour has been observed in interactions of e^+ and e^- with K gas. Values of total cross-sections have been determined by Stein *et al* (1985, 1987) for the "one-electron" system of K at greater than room temperature. Using the boron self-moderator system described in the previous section, e^+ and e^- beams were passed through a thermally isolated oven. Flux measurements were taken with two channeltrons situated by the entrance and the exit of the oven for "hot" and "cold" runs and the cross-sections were derived from the ratios of the count rates obtained at both positions. Figure 1.14 shows the results of these studies with the later investigations extending the energy range from 50eV to 100eV. The magnitudes of the cross-sections are much larger than those of gases studied previously and furthermore, the e^+ values exceed those of the e^- until a merger occurs at the remarkably low energy of 30eV.

Initially, Stein *et al* (1985) accounted for these features by suggesting that due to the high polarisability of K, 25 times that of Ar, this effect would be overwhelmingly dominant. The increasing difference of the values at low energies was attributed to Ps formation which can occur at all energies as the ionisation level is below the binding energy of Ps. However, this would not seem to be the case as the differences in the elastic scattering of the two particles have been disregarded. Stein et al (1987) have since noted that in calculations of e^-–alkali collisions polarisation effects lose dominance above the first excitation threshold to flux loss processes (Walters, 1984)

Returning to collisions in He, the elastic cross-sections of e^- scattering have been calculated to be 2.4 times greater than that involving e^+ at 200eV, the point of

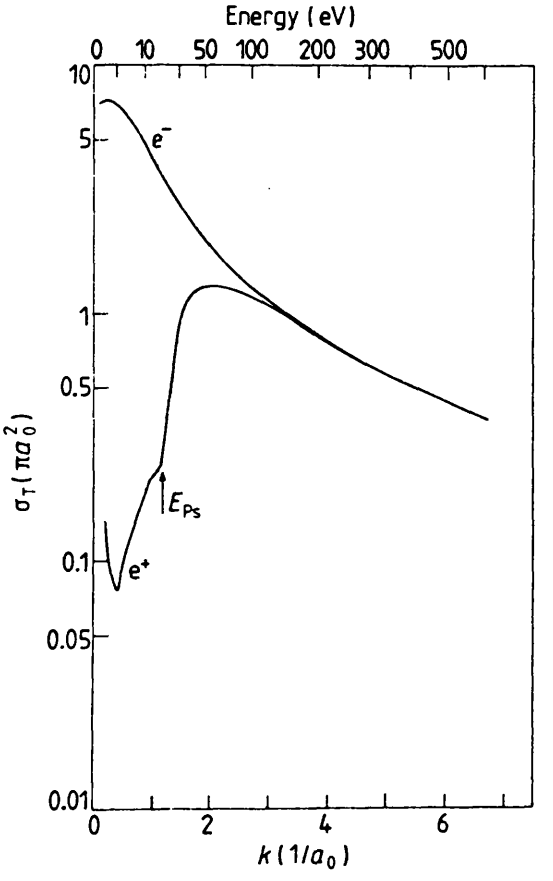

Figure 1.13 Smoothed $e^{\pm}$–He total scattering cross-sections (from Charlton, 1985)

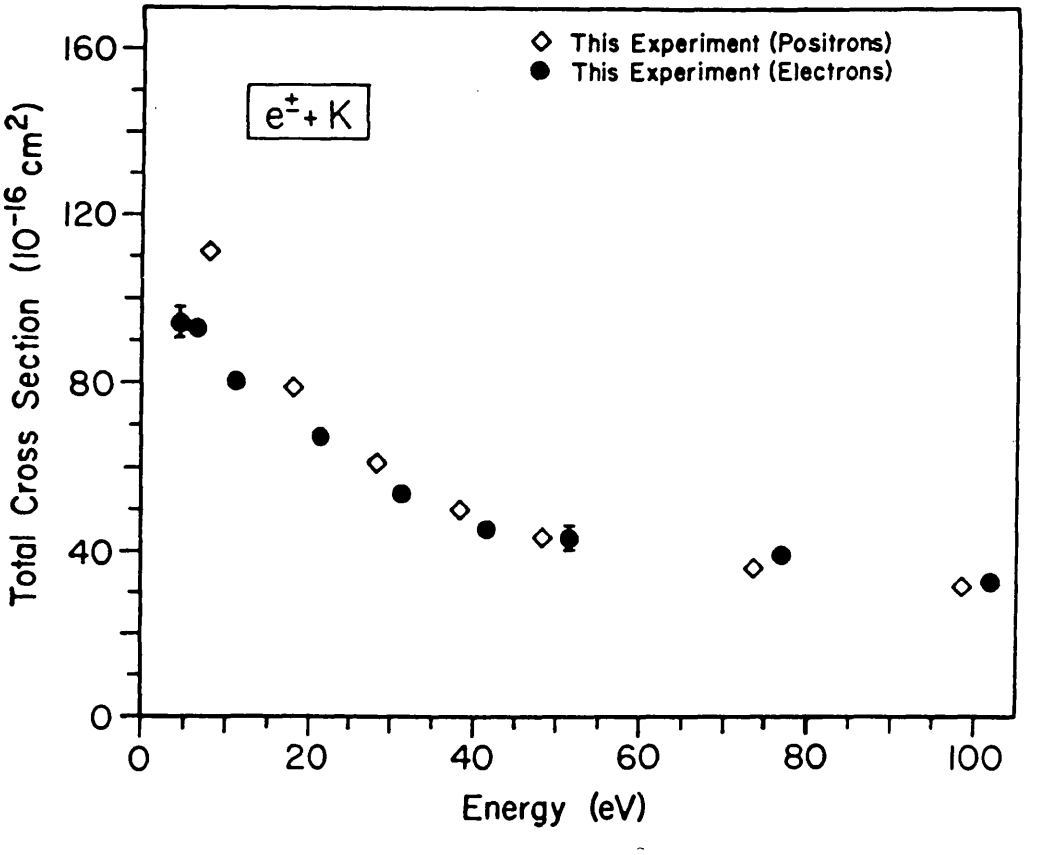

Figure 1.14 Values of σ_T for e^+–K and e^-–K collisions (Stein *et al*, 1987)

convergence. The question remains of why the distributions merge at such low energy where the behaviour of the individual processes seem to differ so markedly. Clearly, further investigations, both theoretical and experimental, are required to resolve these discrepancies.

Few measurements of the angular differential scattering cross-section of e^+ have been made and of these all have studied the interactions with Ar. Two methods have been employed: the time-of-flight and the electrostatic crossed beam technique. The former approach was used by Coleman and McNutt (1979) to obtain values at energies from 2.2 to 8.7eV through angles of 20° to 60°. Positrons were passed through a short (1cm) gas cell and guided by a strong axial magnetic field to a channeltron. Time-of-flight spectra were obtained by detecting the e^+ in coincidence with the light pulses emitted on the passage of $ß^+$ particles through a scintillator placed before the moderator. The forward scattered e^+ appeared as a long tail on the spectra and the angles of scatter were deduced from the time taken to reach the detector.

The second technique is one which is well established in electron scattering physics and routinely used to make such measurements. Hyder *et al* (1986) employed the electrostatic crossed beam technique to obtain values at 100-300eV in the range 30°-135°. Figure 1.15 schematically illustrates their apparatus which was also used, as a check, to measure e^- cross-sections. Both e^+ and e^- studies compared well with theory and the e^- results showed agreement with other experimental values. The e^+ distributions appeared to decrease monotonically with angle at these energies. With respect to the discussion above on the total scattering cross-section, a point of interest was that the elastic values were observed to merge at angles less than 100° at 300eV, in accord with theory (Joachain et al, 1977).

At lower energies, Smith *et al* (1987) have used the same apparatus to obtain results in Ar at 20eV from 30° to 135° and examined the variation with energy at 45°. Schwab *et al* (1987), employing essentially the same technique, determined values at 30eV between 30° and 60°. Both of these studies are in greater accord with the model potential calculations of Nahar and Wadhera (1987) rather than the polarised orbital computations of McEachran and Stauffer (1986).

Deep minima have been noted at certain points in the e^- angular differential elastic scattering cross-sections in all the noble gases bar He at energies of 49-779eV in the

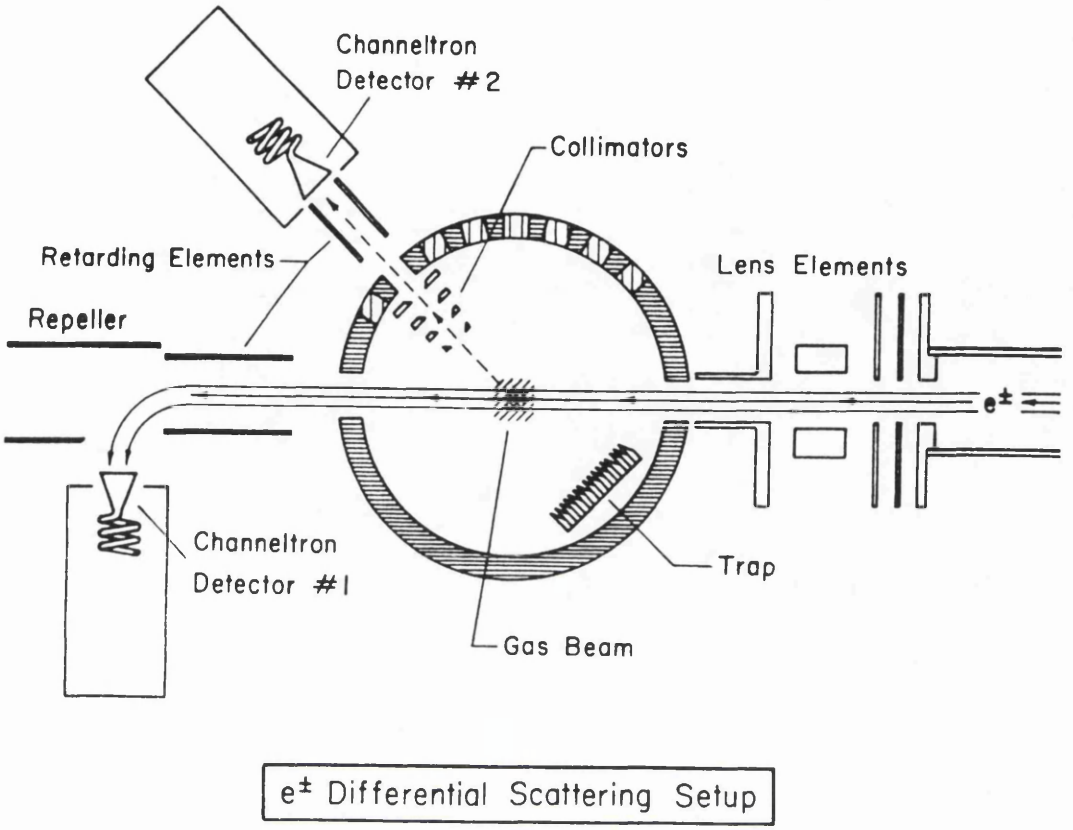

Figure 1.15 Schematic diagram of electrostatic crossed beam apparatus used in differential cross-section measurements (Hyder *et al*, 1986)

angular range 52° to 143° (Lucas, 1979). At so-called critical points, a small change in the scattering angle or e^- energy results in variations of several orders of magnitude in the size of the cross-section; these features can reveal information on the atomic potential (Buhring, 1974). Similar minima have been predicted for e^+ interactions but not observed with the reason being that, for H, He (Nakanishi and Schrader, 1986), Ar, Kr and Xe (Wadhera *et al*, 1984), these have been calculated to occur at much lower energies, 1-3eV, and at an angle of ≈100°. With present beam technology, measurement of such features would not be feasible. However, the alkali metals may be suitable candidates for such an investigation.

The processes of ionisation, excitation and Ps formation have been researched and well documented elsewhere (for example, Charlton, 1985a). Ps formation is discussed in the context of the present study in Chapter 4. Ionisation processes involving e^+ have recently been investigated. Charlton *et al* (1988, 1989) have performed studies into the phenomenon of double ionisation in He, Ne and Ar gases up to 5keV. The ratios of double-to-single ionisation cross-sections were determined for both e^+ and e^- and found to be greater for the latter at most energies. Comparison with similar processes for protons and antiprotons revealed convergence of the ratios at high energies with that of the lighter particle charge counterpart. Thus demonstrating the charge, rather than mass, dependence of the interaction. Divergence at low velocities between the light and heavy particle distributions was attributed to the much lower kinetic energy of the $e^{\pm}$. Charge independence of this effect was proposed by Charlton *et al* (1988) such that the ratio of one of the processes could be determined from direct comparison with the other three. This was verified when the ratios for the e^+ reaction, calculated in this manner, matched those determined experimentally.

Recently, the measurement of e^+ cross-sections in atomic hydrogen has become the subject of much interest. Electron collision studies with H have been performed for many years, however, it is only with current developments in beam and target production that sufficiently intense e^+ and H fluxes can be obtained to make experimentation feasible. Fundamentally, e^+–H interactions are of great importance as theoretical calculations can be performed for this system to high accuracy. Measurement of the collision processes would, therefore, provide a valuable check on the principles upon which they are based.

A programme of e^+–H experiments has been proposed for the high intensity e^+ beam system at Brookhaven National Laboratory (Lubell, 1987). Planned H densities are of the order of 10^{12} atoms cm^{-3} using a radio-frequency (rf) discharge atomic source with a beam flux of $2x10^9$ e^+ s^{-1} employing a cold Ne moderator. An electrostatic crossed beam set-up will be grafted onto the existing apparatus, shown in Figure 1.16, to create a hybrid, split-beam system. Figure 1.16 illustrates the present linear arrangements, characteristically associated with magnetic guidance systems, and the more compact proposed e^+–H experiment located at some distance. Concurrently, an entirely magnetically guided system with electrostatic extraction optics in the interaction region is under development at UCL (Jones *et al*, 1989) An rf H source will also be used with an incident e^+ beam intensity of $\approx 10^4$ e^+s^{-1}.

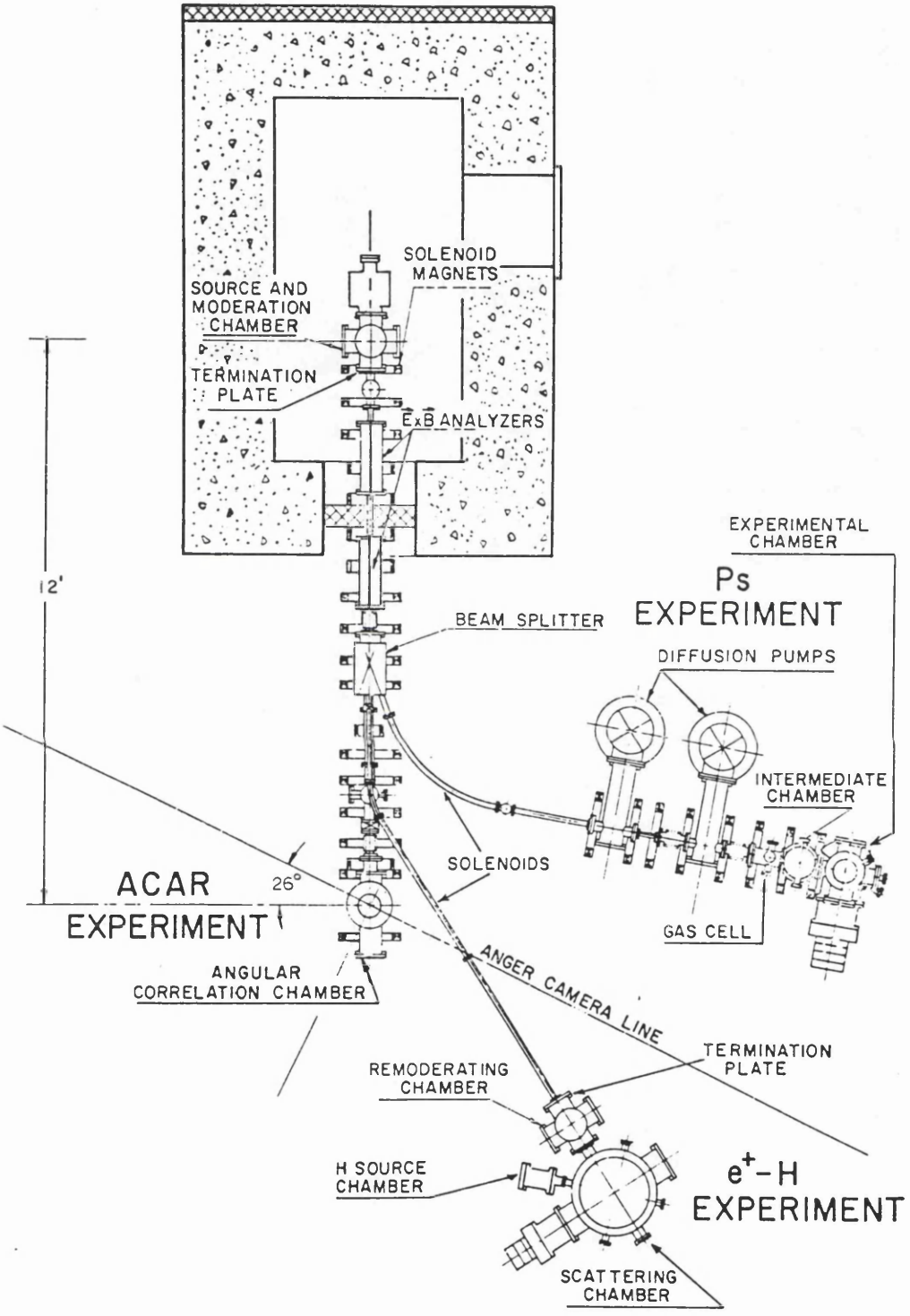

Figure 1.16 Schematic diagram of the proposed arrangement for the BNL high intensity e^+ beam system incorporating the e^+–H experiment (from Lubell, 1987)

The first experimental measurements of e^+–H interaction has been reported by Raith *et al* (1989). In a preliminary study for the Brookhaven proposal, an electrostatic crossed beam system has been used to determine the e^+ impact ionisation cross-sections of H from 17.5eV to 600eV. The arrangement, shown in Figure 1.17, employed a Slevin type rf discharge source to the provide the H and slow e^+ were obtained from a ^{22}Na source with annealed W mesh moderators. The unscattered e^+ and those scattered into a forward cone of 30° half-angle were detected with a channeltron on line with the beam axis and the ions created were diverted to a second channeltron. With shielding of the source and blackening of all internal surfaces, counting rates of 3000 e^+s^{-1} and 10 ions s^{-1} were obtained resulting in a coincidence rate of $0.1s^{-1}$. An inverted time-of-flight system was used (see Section 5.3) to determine the time taken between the correlated events that were detected.

Measurements were made first with e^- and the results obtained compared well with other experimental data, indicating that most of the scattered e^- were registered. By normalising the e^- cross-sections with those of Shah *et al* (1987), absolute values for e^+ impact ionisation cross-sections were determined and these are shown in Figure 1.18. The results for e^+ peak at ≈50eV with a maximum cross-section of $\approx 1.4 \times 10^{-20} m^2$ and are approximately double the e^- values at the same energy. In comparison to theory, the experimental data lie well above all the calculated results, although a similar form of the distribution is noted. In closest agreement are the distorted wave polarised orbital computations of Ghosh *et al* (1985).

And finally, antihydrogen ($\bar{H}$) must be mentioned as the production of the antimatter counterpart of H has recently received much attention. Antihydrogen, the bound state of a positron and an antiproton, is equivalent to hydrogen and as such, should exhibit the same spectroscopic features, thus providing a check on the invariance of the CPT theorem. Gravitation may also be a candidate for investigation with $\bar{H}$ as suggestions have been made from some quantum theories that differences may exist in the behaviour of matter and antimatter in a gravitational field. Three projects have been proposed with the aim of producing sufficient $\bar{H}$ to implement such studies. A review of these methods is referred to Charlton (1988), however the reactions upon which they are based are listed below: e^+ capture of $\bar{p}$ from Ps (Deutch *et al*, 1986); radiative capture in fast merged beams of e^+ and $\bar{p}$ (Poth, 1987); and e^+–$\bar{p}$ combination in dense cold e^+ plasmas (Gabrielse *et al*, 1988).

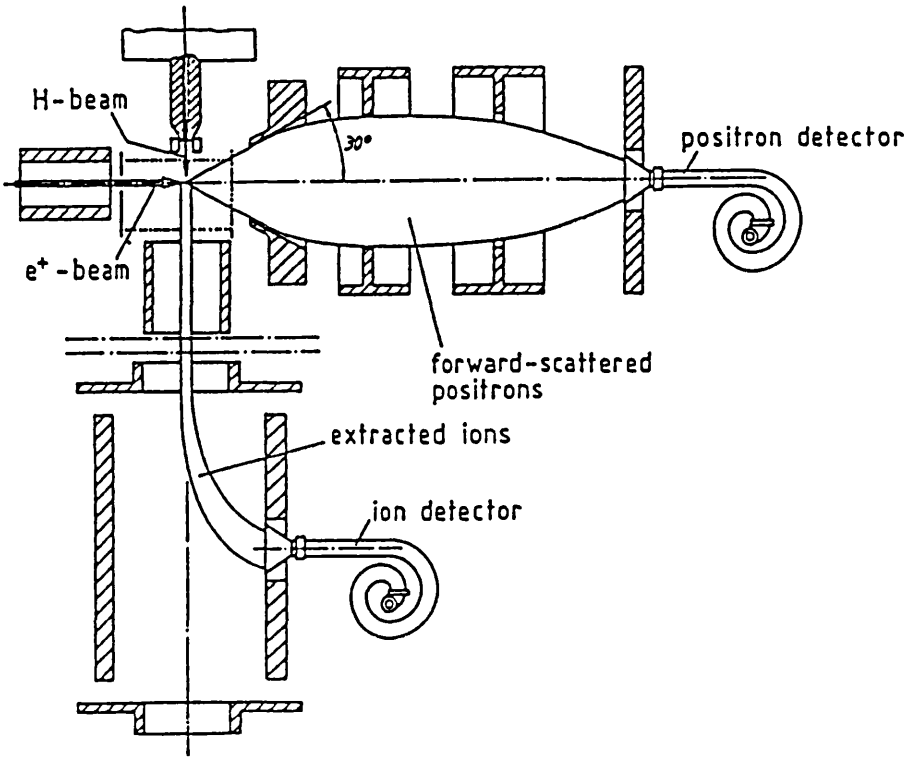

Figure 1.17 Experimental arrangement of e^+–H ionisation cross-section measurement study (Raith *et al*, 1989)

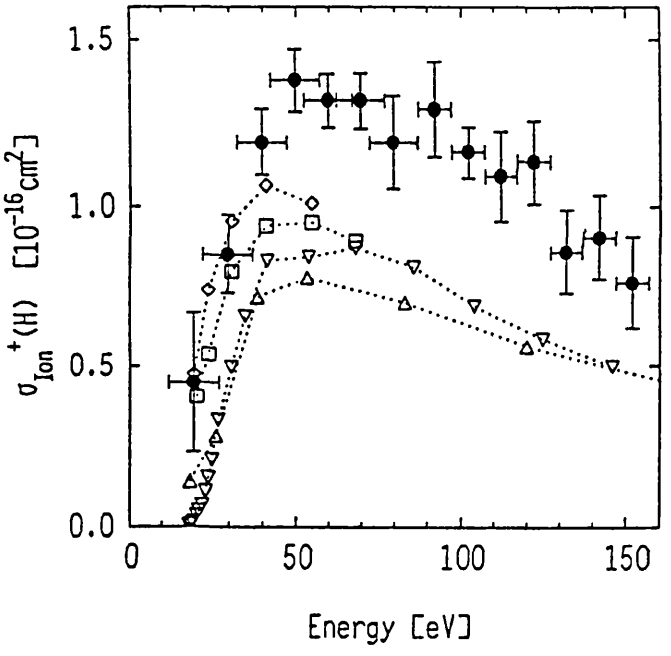

Figure 1.18 Values of e^+–H ionisation cross-sections (Raith *et al*, 1989)

1.6 Motivation of the Present Work

The discussions presented in the previous sections have endeavoured to convey an overall view of the main techniques employed in positron physics and the consequential benefits in the understanding of positron interactions in matter. As the work reported in this thesis is based on the slow e^+ beam technique, particular emphasis has been placed on slow e^+ production and the use of this method in gas scattering studies. In the concluding section of this chapter the general motivation behind these studies is summarised.

The work presented here involved two separate investigations into different aspects of positron physics. As such, the thesis can be divided into two parts with the following two chapters concerned with developments in slow e^+ production and the subsequent two on the formation and interaction of positronium in atomic gases using the slow e^+ beam technique. In each part, the first chapter deals with the background specific to the topic and the second on experimental detail, results and discussions.

In Section 1.4, the efficiency of slow e^+ production has been demonstrated to be critically dependent on the bulk and surface conditions of the moderating material and its treatment before use. Interest has recently arisen in the use of thin single crystal foils as moderators in the transmission mode and some of the advantages of this configuration include: no source shadow problem; larger capture area than grid moderators; narrower energy distribution of ejected positrons than that from vane or grid moderators; use of simpler linear optics in electrostatic arrangements. Therefore, with the purpose of utilising such foils in gas scattering studies, W(100) and Ni(100) foils of various thicknesses (1000-18000Å) were investigated in high vacuum conditions ($\approx 10^{-7}$ Torr).

Some atomic scattering experiments using the slow e^+ beam technique have been described in Section 1.5, however the studies performed to date have mainly involved e^+ interactions. Ps formation is unique to e^+ scattering in matter and the Ps atom is sometimes considered to be a light isotope of H, therefore understanding of basic atomic processes may be enhanced by knowledge gained from light neutral particle scattering. The recent development of the Ps beam technique (Brown, 1985, 1986, Laricchia *et al*, 1987) has made feasible the study Ps-gas interactions at intermediate energies. Thus, the aim of the second study was to investigate the presence of

components in the Ps beam such as n=2 state Ps and once identified, to quantify the proportions of these species. Following characterisation of the flux, measurement of Ps-He and Ps-Ar scattering cross-sections was attempted.

CHAPTER 2
POSITRON MODERATION

2.1 Introduction

The technique of slow positron beam production, as discussed in Chapter 1, relies on the energy moderation of fast β^+ fluxes, emitted from radioactive sources or created in pair production, by interactions with the bulk of the moderating material. The basic principles behind the moderation process are described briefly. The fast β^+ particles rapidly lose energy on impacting with the solid by inelastic collisions. As thermal equilibrium is attained, the positrons diffuse randomly in the solid; some will reach a free surface and if the surface condition of the material permits, a certain fraction will be emitted as free positrons with energies of the order of electron-volts.

However, a number of interactions can occur which influence the production of slow positrons and the brief summary above belies the complexity behind the mechanisms of energy moderation and positron emission. Figure 2.1, from the review by Schultz and Lynn (1988), shows some of the interactions involved with their corresponding time scales. The processes illustrated, albeit for incident positrons of energy $\leq$100keV, are applicable to the β^+ flux from a radioactive source, for example ^{22}Na with a mean positron emission energy of 260keV. Phenomena such as positronium formation and positron trapping in the bulk and at the surface, as well as being of physical interest, can bear upon the β^+–e^+ conversion efficiency of the moderator.

In the following sections, some of the principles underlying the slowing down, diffusion and positron re-emission properties are described with reference to solid media and, in particular, to thin single crystal metals. The importance of such factors as bulk and surface conditions are related to the efficiency of positron production and the application of thin single-crystal W and Ni foils as transmission-mode moderators is discussed in detail.

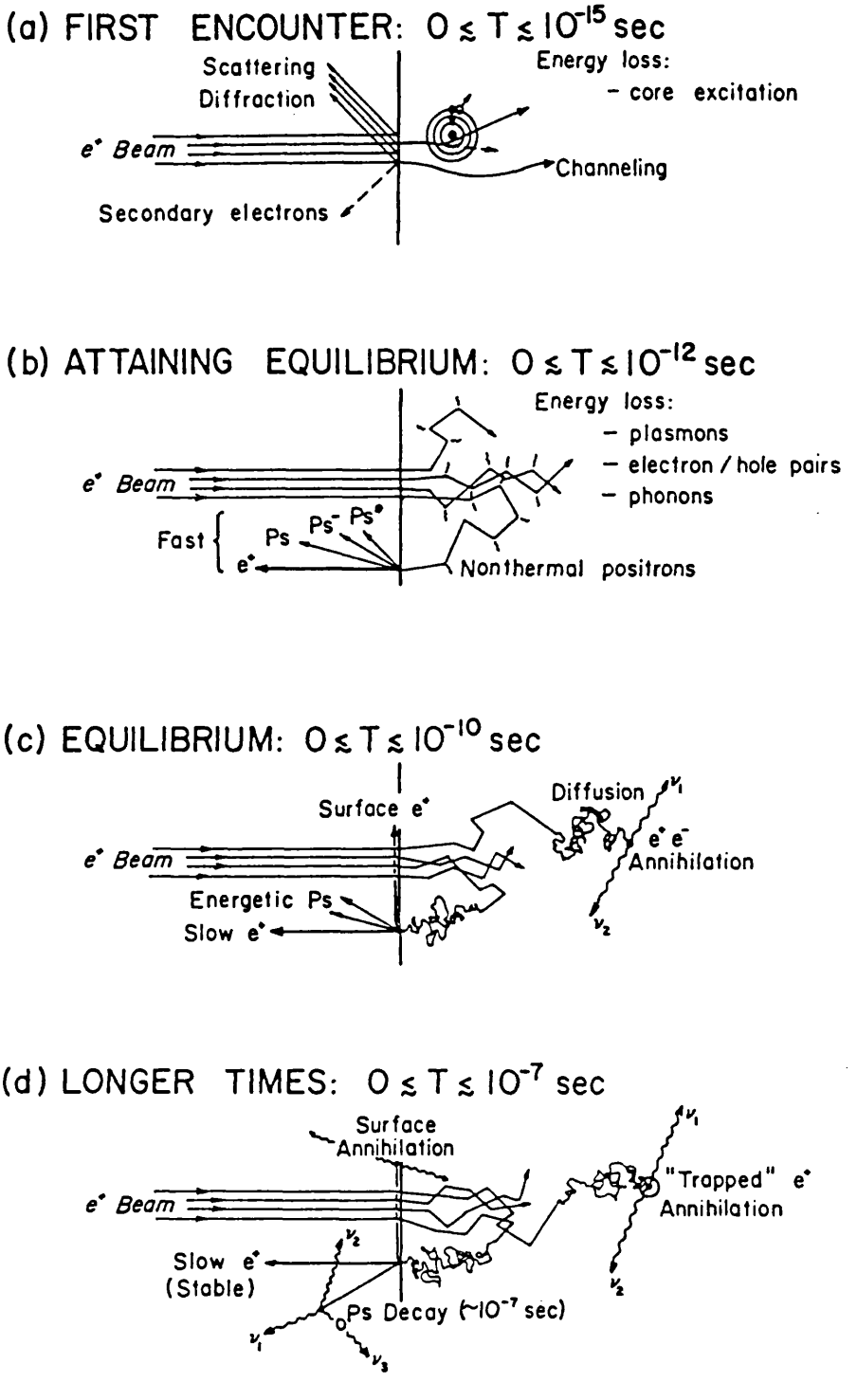

Figure 2.1 The interaction of a positron beam of energy ≤100keV with the near-surface region of a solid (Schultz and Lynn, 1988)

2.2 Bulk processes

2.2.1 Slowing down

Fast β^+ particles, on impacting with the solid, slow down via collisions with the target atoms through mechanisms dependent on the energy of the particle. For positrons with energies greater than a few MeV, energy loss occurs mainly through the processes of bremmstrahlung and Čerenkov radiation (Birkhoff, 1958, Pages et al, 1972). However, for β^+ particles obtained from radioactive sources, such as ^{22}Na with an endpoint energy of 0.54 MeV, the dominant energy loss processes are the inelastic interactions with the electrons of the target, (Figure 2.1a). Excitation and ionisation of the core and conduction electrons swiftly reduce the high initial energies of 100's keV to a few 10's eV. In comparison with the bulk annihilation lifetime of the positron ($\approx 10^{-10}$s), these processes are efficient in slowing down the particles, taking times of the order of 10^{-13}s (Perkins and Carbotte, 1970). The direction of the positrons are randomised by angular deflections from elastic scattering with the ion-cores and the electrons. Due to the large charge difference between the ion-core and the electrons, the size of the differential cross-sections for elastic nuclear scattering is greater by several orders of magnitude. Therefore, energy loss is primarily via interactions with the target electrons, whilst nuclear scattering dominates the directional loss.

From energies of the order of the Fermi level, E_f, the final stage of energy loss is completed in $\approx 10^{-12}$s and is dominated by inelastic phonon scattering (Perkins and Carbotte, 1970), (Figure 2.1b). Figure 2.2 illustrates the results of the calculations by Nieminen and Oliva (1980) of the rate of energy loss from e^+-conduction electron and e^+-phonon interactions in Al in the range 10^{+4} to 10^{-2}eV. The graph shows the domination of the temperature independent processes of positron-electron interactions in the energy loss process. The kink at 33.6eV is associated with the onset of plasmon excitation (e^- gas oscillations) which Oliva (1980) has shown to be more important than particle-hole excitation in the regime $\approx E_f (\approx 12\text{eV})$ to $\approx$1keV.

The two-way energy exchange with the thermally excited lattice vibrations, quantised by phonons, begins to take over from the electron gas processes at about a few eVs. The effects of the temperature dependence on the rate of energy loss become apparent at $\approx$0.2eV as the competing processes of energy loss to and gain from the phonon

field reach equilibrium.

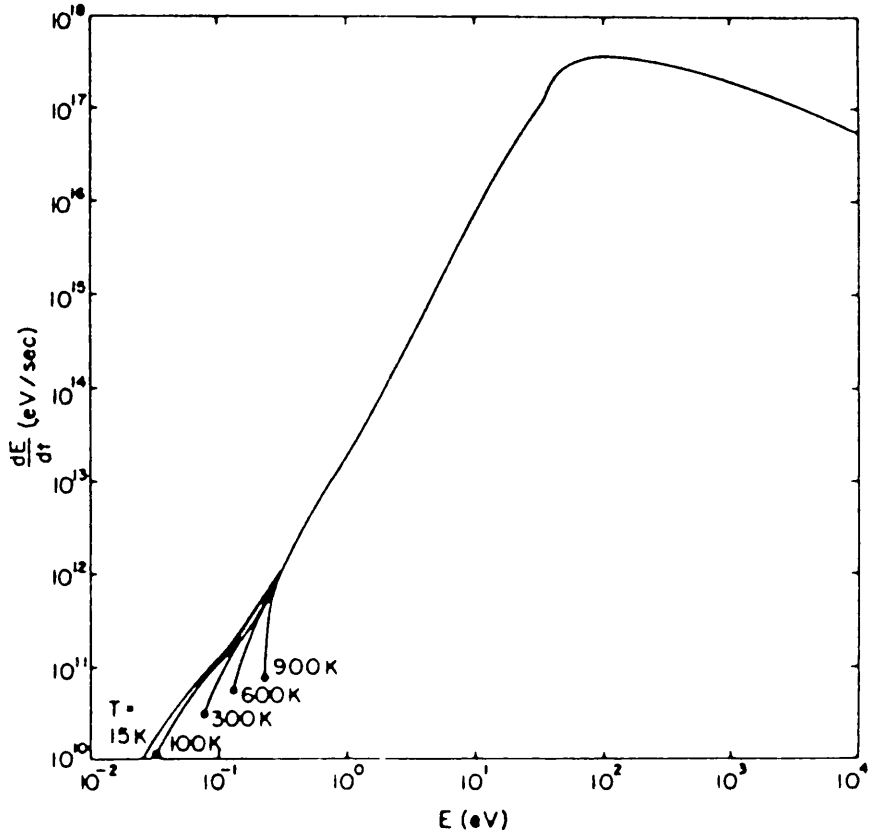

Figure 2.2 Positron energy loss, dE/dt, versus energy, E, in Al (Nieminen and Oliva, 1980)

Conventionally, the e^+ "stops" in the material when its motion ceases to be temperature-independent and the geometrical distance of this point from the entrance surface is known as the implantation depth. For a flux of positrons incident on a target, the probability of stopping in the sample is characterised by the implantation profile, a function dependent on the initial energy of the particles, the target material and, to a lesser extent, on the angle of incidence. The first stage in the calculation of the expected yield from a moderator is based upon the implantation profile. Therefore, an accurate description of the profile is essential in determining the probability of positrons reaching a surface as the implantation depth is used as the

starting point of the subsequent motion. Nieminen and Oliva (1980) have shown that the implantation depth of the e^+ reaches saturation (that is, ceases to increase significantly) well above thermal positron energies. Moreover, Valkealathi and Nieminen (1983), in Monte Carlo studies of the slowing down of e^+ and e^- in solids, calculated that changing the cut off from the point when the e^+ energy has reached 20eV to 100eV results in a 1Å difference in the endpoint of the trajectory. Various theoretical calculations of the implantation profile have been performed for monoenergetic beams of positrons (Rohlich and Carlson, 1954, Nieminen and Oliva, 1980, Hansen and Ingerslev-Jensen, 1983). However, an accurate theoretical description has yet to be made of the implantation of β^+ particles obtained from a radioactive source with the characteristically large distribution of energies.

The implantation profile in such a case has been experimentally deduced by Brandt and Paulin (1977) for a number of materials with densities in the range 0.9-9 gcm^{-3}. In this study, the annihilations from the impact of β^+ particles emitted from a ^{64}Cu source into a thick sample were monitored by a NaI(Tl) detector as it was traversed across a 0.1mm wide slit in the Pb shielding. From a fit to their data, they established that the implantation profile, P(z), was well represented by

$$P(z) = \alpha_+ \exp(-\alpha_+ z) \qquad 2.1$$

where z is the distance from the entrance surface and α_+ is the absorption coefficient.

Mourino *et al* (1979), in a similar study using ^{22}Na, ^{64}Cu and ^{68}Ge sources, found that the mass absorption coefficient, α_+/ρ where ρ is the density, could not be expressed solely by the endpoint energy of the emitted flux as Brandt and Paulin (1977) had suggested. They deduced that it was better described in terms of the mean energy, $\bar{E}$, and the atomic number of the target material, Z. Moreover, they noted the effect of backscattering from the source mount, finding that the mean energy, for example, of 0.26MeV for ^{22}Na, was reduced to 0.15MeV with a Pb support. Fits to their data gave the following expression for α_+:

$$\alpha_+/\rho = 2.8\ Z^{0.15}/\bar{E}^{1.19}\ (cm^2g^{-1}) \qquad 2.2$$

for ^{22}Na and

$$\alpha_+/\rho = 1.1\ Z^{0.25}/\bar{E}^{1.58}\ (cm^2g^{-1}) \qquad 2.3$$

for ^{64}Cu and ^{68}Ge.

Figure 2.3 shows an experimentally obtained implantation profile of β^+ particles from ^{22}Na impacting into a Ni target (Hansen *et al*, 1982). The solid line represents the profile calculated with equation 2.1 and 2.2.

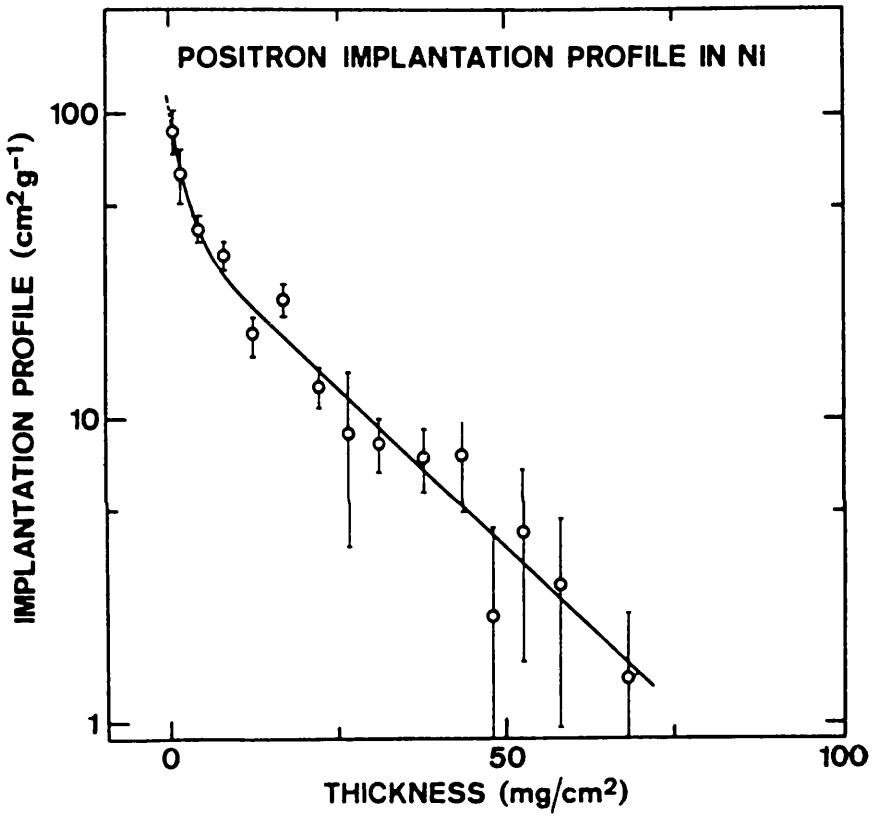

o Experimental profile

—— Calculated profile

Figure 2.3 Positron implantation profile in Ni using a ^{22}Na source (Hansen *et al*, 1982)

Using a different method Vehanen and Mäkinen (1985), derived an expression for the

implantation profile to provide additional confirmation of equations 2.1 and 2.2. They convoluted the shape of the ^{22}Na β^+ spectrum, dN_β/dE (Konopinski, 1966), with the Makhov expression (1960) suggested by Hansen and Ingerslev-Jensen (1983) for a monoenergetic positron beam. The profile, $P_E(z)$, is given by

$$P_E(z) = \frac{mz^{m-1}}{z_o^m} \exp\left(-(z/z_o)^m\right) \qquad 2.4$$

where m is a parameter dependent on the atomic number and the incident particle energy, z is the distance from the surface and z_o is expressed as

$$z_o = \bar{z}/\Gamma(1/m+1) \qquad 2.5$$

where $\bar{z}$ is the mean stopping depth and Γ is the gamma function. z_o is energy dependent through $\bar{z}$ (presumed to be described by the power law derived from electron impact studies) and is given by

$$\bar{z} = AE^n \qquad 2.6$$

E is the energy of the incident particle beam and A is a constant found empirically by Mills and Wilson (1982) and Vehanen at al (1987) to be $\approx 400/\rho$ Å/keV^n. The values of the constants m and n have also been experimentally derived from many electron and positron studies and shown to range from 1.2 to 1.9 for m and 1.4 to 1.7 for n (for references, see Vehanen and Mäkinen, 1985, and Valkealathi and Nieminen, 1983).

Vehanen and Mäkinen (1985) obtained the following expression for the β^+ implantation profile P'(z)

$$P'(z) = \int_o^\infty P_E(z)\,(dN_\beta/dE)\,dE \qquad 2.7$$

which is illustrated in Figure 2.4 for Cu, Al and W. For n, the values used were obtained from the data of Hansen and Ingerslev-Jensen (1983). The constants, A and m, were fitted to achieve agreement between P'(z) and P(z) but were consistent with other experimentally observed values. They found agreement between the values of P'(z) and P(z) except at depths of less than 10μm for Cu and Al. Beling *et al* (1987)

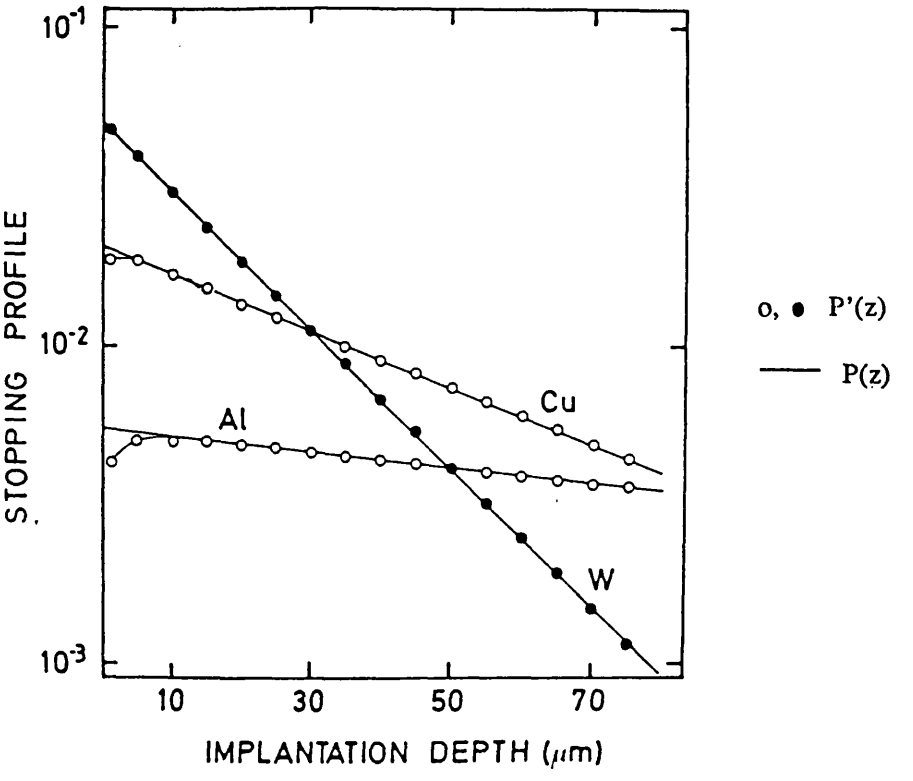

Figure 2.4 Implantation profiles of ^{22}Na β^+ spectrum in Al, Cu and W (Vehanen and Mäkinen, 1985)

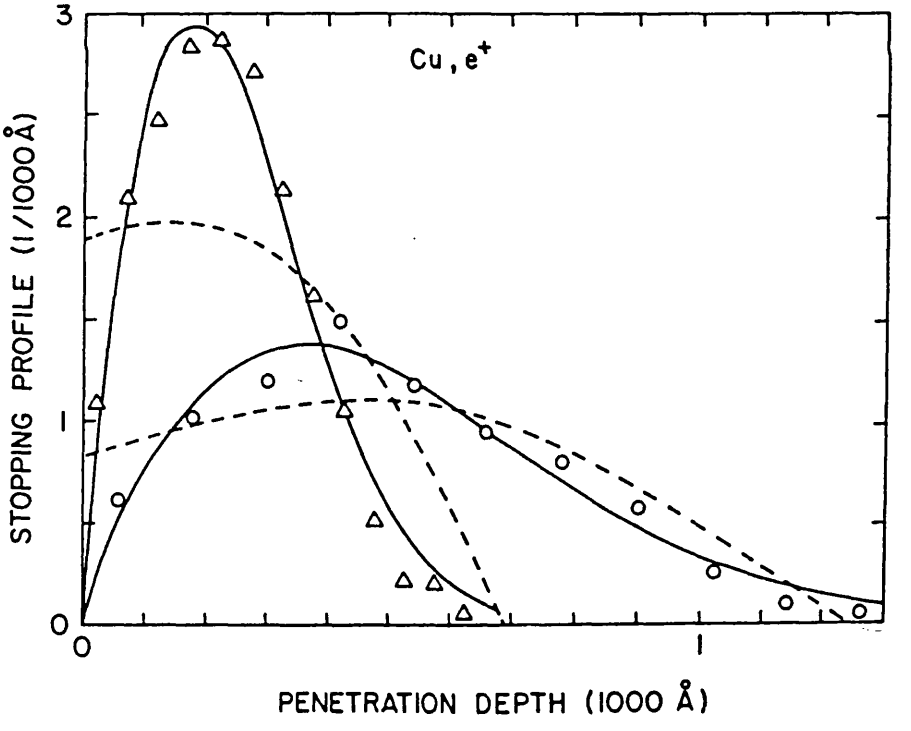

Δ 3keV Monte Carlo simulation data o 5keV Monte Carlo simulation data

---- Thin film data for 3.1 and 5.0keV e^+ from Mills and Wilson (1982)

—— Fit to MC data using Equation 2.4

Figure 2.5 Stopping (implantation) profile for 3 and 5keV incident energy positrons in semi-infinite Cu (Valkealathi and Nieminen, 1984)

have suggested that this may be due to the treatment of the beam distribution as collimated and not isotropic.

Monte Carlo calculations have been performed by Valkealathi and Nieminen (1983, 1984), in a comparative study of the slowing down of positrons and electrons of initial energy 1–10keV. As stated in Chapter 1, this energy range is typical of that employed in the remoderation technique. Using Grysinski's excitation function for the inelastic processes at each level and in the later study, accurate atomic cross-sections for the elastic scattering, they calculated the profile for targets of Al, Cu, Au and W. Figure 2.5 shows the profile for Cu at 3 and 5keV. The fit to the Monte Carlo data using Equation 2.4 (solid line) confirmed the validity of using the Makhov expression for positron implantation. The results are also in agreement with the experimental data of Mills and Wilson (1982) at the higher energy. The discrepancy at the lower energy is suggested by Valkealathi and Nieminen (1984) to be due to the neglect in the experimental work of the effect of backscattering. In the study of Mills and Wilson (1982), the stopping profile was deduced from the number of positrons transmitted through a thin wedge-shaped sample. Therefore, e^+ in the thin film would be detected once traversing the exit surface. However, in the theoretical case where the target was presumed to be semi-infinite, the e^+ crossing the plane at the same depth as the exit surface from the experimental case would still have the probability to scatter back into the region under consideration. The calculations would have included such backscattered e^+, thus resulting in an implantation profile different to that obtained in the transmission study of Mills and Wilson (1982). The effect would be more significant at lower e^+ impact energies due the greater number of positrons stopped at smaller distances from the point of entry.

2.2.2 Diffusion

Following thermalisation, the motion of the positrons become random as they undergo numerous collisions (Figure 2.1c) and their mean lifetime in the solid is relatively long, $\approx 10^{-10}$ s, compared to the time taken to reach equilibrium. During this period, the motion of the delocalised, thermal positrons is dominated by phonon interactions, with contributions two orders of magnitude lower from e^- scattering (Bergensen *et al*, 1974). Depletion of the e^+ population can occur from annihilation and capture into a localised state by defects and vacancies. The distribution of the ensemble of

positrons in the solid is thus described by a Boltzmann equation, subject to boundary conditions.

The Boltzmann transport equation has been applied to specific situations by several workers (Beling *et al*, 1987, Mills and Murray, 1980a, Sferlazzo, 1985, Vehanen and Mäkinen, 1985, Jorch *et al*, 1984). Beling *et al* (1987), in the study of the concept of a field assisted moderator, have applied the diffusion equation to the one dimensional case with the presence of an electric field. The motion is described by

$$\frac{\partial n(z,t)}{\partial t} = D_+ \frac{\partial^2 n(z,t)}{\partial z^2} - v\frac{\partial n(z,t)}{\partial z} - \lambda n(z,t) \qquad 2.8$$

where n(z,t) is the positron probability density at a distance z from the entrance surface and at time t, D_+ is the diffusion coefficient, v is the drift velocity due to the electric field and λ is the (uniform) capture and decay rate.

The diffusion coefficient, D_+, is defined as

$$D_+ = 1/3\ v^2_{th} t_{sc} \qquad 2.9$$

where v^2_{th} is the thermal mean square velocity and t_{sc} is the mean time between collisions. For the diffusion approximation to be valid, t_{sc} must be much less than τ, the mean lifetime of the positron in the solid ($\approx 10^{-10}$s) such that the velocity (V) dependent diffusion coefficient, $D_+(V)$, averages to a temperature dependent value, D_+. Thus, from Equation 2.9, D_+ must be much smaller than $1/3v^2_{th}\tau \approx 3 \times 10^3 cm^2 s^{-1}$; this is consistent with values derived experimentally for many metals, including W and Ni (Jorch *et al*, 1984)

Beling *et al* (1987) have obtained an exact solution for equation 2.8 with the boundary conditions of n(0,t)=n(d,t)=0 and $n(z,0)=\alpha_+ \exp(-\alpha_+ z)$ $(0<z<d)$ where d is the moderator thickness. They determined the probability of positrons diffusing to the surface at z=0 and z=d as

$$q(o) = \int_o^\infty D_+ \frac{\partial n}{\partial z}\Big|_{z=o} dt \ , \qquad q(d) = -\int_o^\infty D_+ \frac{\partial n}{\partial z}\Big|_{z=d} dt \qquad 2.10$$

Using the exponential profile of Equation 2.1, the fraction of positrons reaching the surface was extracted. As no electric field can be applied in the case of the metallic moderator the drift term is set to zero resulting in the same expression derived by Vehanen and Mäkinen (1985), who used a Green's function substitution. Thus, the transmitted current of positrons, assuming no reflection at the surface, is given by

$$J = \frac{1}{(\sinh d/L_+)} \int_0^d \sinh (z'/L_+)P(z')dz' \qquad 2.11$$

where L_+, the diffusion length, is the characteristic distance travelled by a thermal e^+ before annihilation or capture. L_+ is typically of the order of 1000Å and is expressed by

$$L_+ = (D_+/\lambda_{eff})^{1/2} \qquad 2.12$$

where

$$\lambda_{eff} = \lambda_b + kC(z) \qquad 2.13$$

λ_b is the rate of annihilation in the bulk and kC(z) is the depth dependent rate of defect trapping.

Defects in the structure of the material caused, for instance, during growth or by the presence of impurities contribute to the value of kC(z), decreasing L_+, and are thus detrimental to the transport of e^+ to the surface. The efficiency of trapping of thermal positrons has been calculated by Hodges (1970) to be of the order of 10^{15} per second per unit concentration of vacancies and with binding energies as large as a few eVs. Dupasquier and Zecca (1985), in their review, have illustrated the effect of this process by calculating that in Al, a vacancy concentration of only 20 atomic parts per million is required to reduce the L_+ by ≈15%. In addition, non–thermalised e^+ trapping has also been observed by Nielsen B. *et al* (1986). The authors examined e^+ re-emission at various temperatures from Al(111) and noted a sharp drop in the non-thermalised yield above 700K with a maximum decrease for positrons of energies ≈1eV. Corresponding to a regime where the rate of thermally induced vacancies is high, Nielsen B. *et al* (1986) attributed this effect to defect trapping. Moreover, due to the remarkably high cross-section of this process, they suggest the existence of an excited positron resonance state at such defects.

Equation 2.12 shows that a high value of D_+ can also be beneficial to the propagation of the e^+ in the solid. Mills (1979b) demonstrated the effect of increasing D_+ in the investigation of the Cu(111)+S moderator by cooling the sample with liquid nitrogen. Varying reciprocally with temperature, D_+ increased such that the efficiency of the moderator improved from $1x10^{-3}$ (at 300K) to $1.5x10^{-3}$ (at 100K).

2.3 Surface processes

2.3.1 Free positron emission

On reaching the surface, several processes can determine the fate of the positrons and the efficiency of the material as a $ß^+$–e^+ converter. The production of slow positron beams depends on the prompt emission of free positrons, a process only energetically allowed for certain substances and determined by the workfunction of the material. In this section the surface properties of metals and the condition of the surface (for example: adsorbate coverage) are discussed in relation to the emission of slow positrons.

The workfunction of a material is defined as the minimum energy required to remove an/a electron/positron from a point inside to one just outside the surface. Lang and Kohn (1971) expressed this for electrons as the difference between δ, the surface dipole barrier and μ_-, the bulk chemical potential

$$\phi_- = \delta - \mu_- \qquad 2.14$$

The positron workfunction, ϕ_+, was similarly expressed by Tong (1972) as

$$\phi_+ = -\delta - \mu_+ \qquad 2.15$$

where μ_+ is the positron bulk chemical potential and the surface contribution, δ, is the same in magnitude as in the electron case but opposite in sign. Thus, from 2.15, spontaneous emission of positrons is only allowed for negative ϕ_+ values. A diagrammatic representation of the e^- and e^+ workfunctions is shown in Figure 2.6.

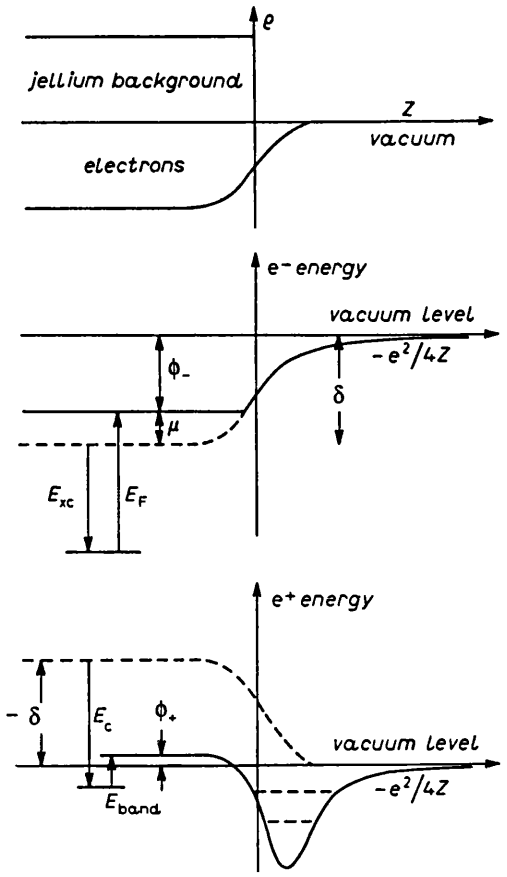

Figure 2.6 Potential energy seen by electrons and positrons at a surface (Mills, 1981a)

Lang and Kohn (1971) and Tong (1972) used the jellium model to illustrate and evaluate the dipole contribution of the surface. In this model, the lattice of positive ions is replaced with a uniform positive background and the electrons form a uniform cloud in the interior of the metal. At the surface, however, the cloud "spills out" creating a double layer of charge separated by a few angstroms (Frenkel, 1928). The double layer, of positive charge inside and negative charge outside the plane of the surface, attracts the electrons whilst repelling the positrons at the surface. Thus the dipole contributions are opposite in sign. The value of δ can change with surface adsorbates and crystal orientation; Lang and Kohn (1971) have shown a general trend of decreasing δ with decreasing density of ions in the lattice plane. The changes with

face orientation are generally of the order of a few tenths of an eV.

The bulk contribution, μ_+, is the positron chemical potential and has been defined by Hodges and Stott (1973b) as the difference between the lowest positron energy state and the electrostatic potential at 0K in the interstitial region (that is the region between the ion cores). Contributions to the chemical potential arise from the strong ion-core repulsion of the e^+ and the e^+–e^- correlation.

In all metals, the e^- workfunction values are positive due to the additive nature of the surface and bulk terms. For positrons, however, the terms cancel out partially, leaving a value usually smaller than the e^- workfunction. More importantly, the value of the e^+ workfunction can be negative, thus allowing the positrons to be ejected from the material with an energy of the order of eV . This property is essential in the production of the slow positron beam using a metallic moderator. First noted by Costello *et al* (1972a), many metals, for example Ni, W, Cu, Pt, have been found to emit e^+ with a characteristic energy.

Many studies have been performed to investigate the emission of positrons from surfaces and these have demonstrated that adsorbates on the surface may influence the yield, workfunction value and the range of angular and energy emission of the e^+. In the remainder of this section, some of these studies are discussed to illustrate the effects of various surface conditions with particular relevance to the present work.

Of the positrons that reach the surface a certain fraction may be emitted into the vacuum; in the adiabatic case the e^+ are ejected perpendicular to the surface with the workfunction energy. However, an additional contribution arises from the thermal spread, which if in the transverse direction, gives a maximum angular distribution of $\approx(k_BT/2\phi_+)^{1/2}$. Thus, emission from the surface should be confined to a narrow cone and with a small thermally caused energy distribution.

The energy distributions of slow positrons emitted from clean and coated surfaces on single-crystal Ni, W and Cu in ultra-high vacuum were studied by Fischer (1984) and Fischer *et al* (1986). Using a high resolution (≈20meV) electrostatic energy analyser, they obtained the spectra of e^+ emitted from clean Ni(100), W(110) and Cu(111) upon bombardment by a 3keV beam of positrons. The emission was found to be primarily

(≈99%) elastic and normal to the surface with energy and angular spreads governed by the Maxwell-Boltzmann distribution. A small continuous distribution of positrons was observed from the elastic peak to 0eV (≈1% of the total yield) which they attributed to electron-hole production and phonon scattering (Nieminen and Oliva, 1980).

The effect of adsorbate coverage on the positron emission properties of the surface is dependent on the adsorbed substance and the thickness of the layer. The presence of an adsorbate can influence the dipole contribution (Murray and Mills, 1980), thus changing the workfunction value. If the layer is of sufficient thickness, the surface properties of the overlayer can dictate the emission energy of the e^+ and in addition, the trapping of positrons at the interface may occur.

The energy distribution of positrons emitted from adsorbate coated surfaces was also studied by Fischer *et al* (1983, 1986). For coverages of the order of a monolayer, they found that positrons were elastically emitted from a number of single-crystals of Ni, W and Cu coated with oxygen, carbon and sulphur, respectively, in the same proportion as that from the clean surfaces. The study of Gullikson *et al* (1985) confirmed the findings of Fischer (1984) (and Fischer *et al*, 1986) on e^+ emission from surfaces of clean Ni(100) and from W(110) with a monolayer coverage of C. The proportion of elastically emitted positrons was found to be ≈97%, but a wide angular distribution was observed, in particular from W(100)+C, the cause of which was uncertain.

Fischer *et al* (1986), however, noted that the size of the energy loss tail on the energy spectrum from a sample of Ni(100), exposed to 300L of oxygen (1L = 10^{-6}Torr s) at a sample temperature of 150°C, decreased from ≈10% of the elastic peak to ≈1% after annealing at 300°C for 1 minute. Auger electron spectroscopy showed the same oxygen coverage before and after annealing but low energy electron diffraction (LEED) patterns indicated greater surface order after heating to 300°C, thus indicating that the surface disorder enhances inelastic emission processes. Furthermore, discrete energy loss peaks were also observed from e^+ emitted Ni(100)+CO and NiO+H_20 surface corresponding to the excitation of the molecular vibrational levels.

It is generally thought that emission from a clean surface is almost entirely elastic and normal to the surface with thermally dependent energy and angular broadening. The

distribution between $-\phi_+$ and 0eV observed in some cases (for example: Wilson 1983) may be caused, in part, by imperfections in the external guiding and extraction fields or emission from rough surfaces. In addition, the phenomena responsible for the broad energy distributions may be due to the presence of adsorbates on the surface. Scattering and excitation of the adsorbed molecules, together with electron-hole creation and, to a secondary extent, phonon and plasmon excitation (Nieminen and Oliva, 1980, Nielson D. *et al* 1986) are some of the factors which lead to a spread in the e^+ energy.

A point of note is that distributions of positrons with energies greater than those determined by the workfunction and the thermal spread have also been observed. Figure 2.7 from Fischer *et al* (1986) illustrates such a spread and the variation with incident positron energy. The tail of the distribution is caused by positrons emitted prior to complete thermalisation in the solid; the yields decrease with increasing incident energy as the positrons are implanted deeper into the bulk, thus undergoing more collisions before reaching the surface.

An important factor in the efficiency of slow e^+ beam production is the branching ratio, y_0. Free positron emission is only one of a number of competing processes which the positrons at the surface can undergo (see next section). The value of y_0 in comparison to the other energetically allowed processes, as yet, has not been experimentally established for each metal. Niemimen and Oliva (1980) have explained the processes of positron and positronium emission from metals with regard to the motion of the e^+ through the surface. In simple terms, slow positron motion would result in Ps formation as this is always more energetically favourable in metals than the competing process of free e^+ emission (see below). However, if the positron was accelerated "downhill" along the surface potential, then the probability of e^- capture would greatly decrease due to the shorter interaction time. Thus a larger surface potential results in a greater e^+ velocity and therefore, a smaller probability of Ps formation. However, a comparison of the y_0 and ϕ_+ values from various experimental studies on single-crystal metal samples (from the review of Schultz and Lynn, 1988) gives little indication of this expected relation. Therefore, further investigations are required to determine the overall effect of the workfunction on the branching ratio.

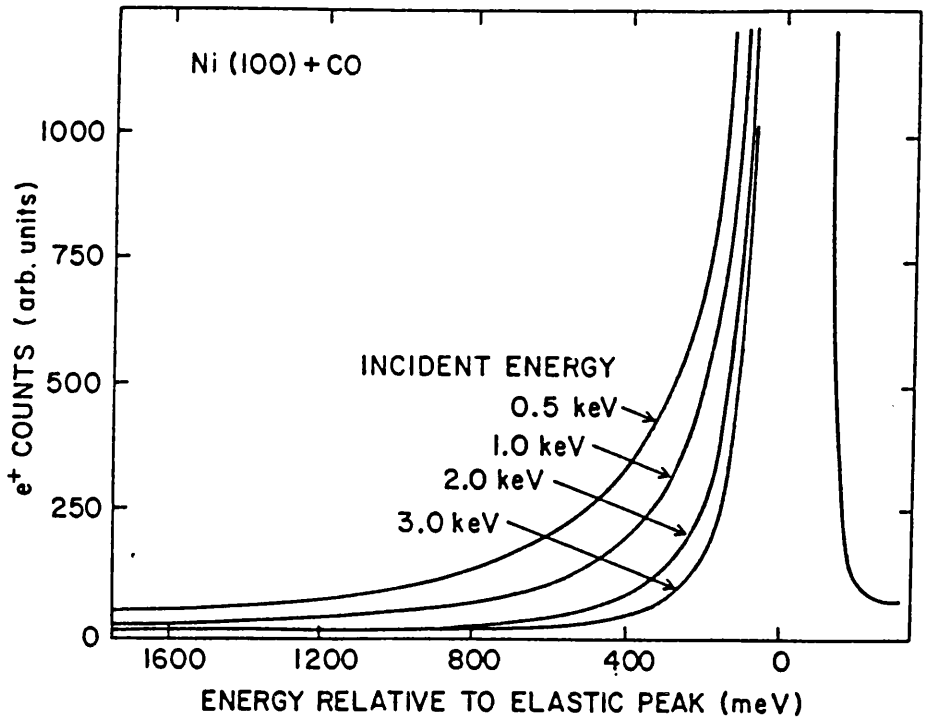

Figure 2.7 Variation of re-emitted positron energy distribution from Ni(100)+CO with incident energy (Fischer *et al*, 1986)

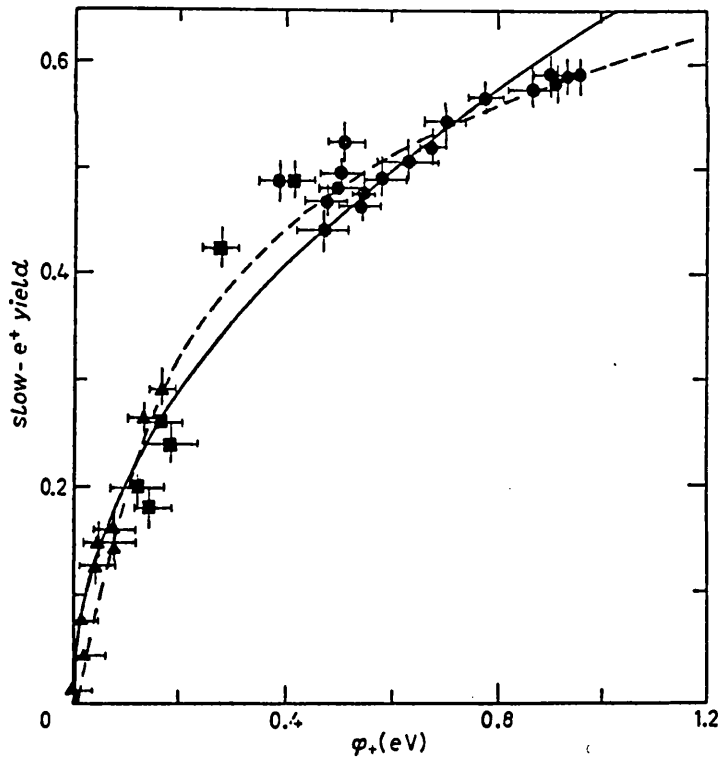

●, ▲, ■ Experimental - - -, —— Theoretical

Figure 2.8 Slow positron yield versus positron workfunction of Cu (Murray and Mills, 1980)

In general, the slow e^+ yield has been observed to increase with the workfunction value of the surface (Murray and Mills, 1980, Gullikson *et al* 1988) for a particular metal. In the study of Murray and Mills (1980), samples of single-crystal Cu and Al of different face orientations were coated with impurities and raised in temperature to achieve a change in the workfunction value. A magnetically guided variable energy (0–3keV) beam of positrons bombarded the samples in UHV conditions and the re-emitted e^+ were detected with a NaI(Tl) detector. They found that the variation of the observed slow e^+ yield with the ϕ_+ value was accountable using the simple picture described above. By considering the time, Δt, spent by the positrons in a region of thickness Δz from where they are accelerated out with a final energy $-\phi_+$ and the capture rate, C, then the probability of e^+ emission, $\exp(-C\Delta t)$ is given by

$$y_0 = \exp(-\phi_0/\phi_+)^{1/2} \qquad 2.16$$

$\phi_0 = 1/2m_eC^2\Delta z^2$ and is constant if C is constant. Figure 2.8 shows this data for Cu fitted with Equation 2.16.

With some relevance to the present study, Wilson and Mills (1983a) observed a change in the ϕ_+ value of single crystal W(111) from $-(2.59\pm0.1)$eV for a clean surface to $-(3.3\pm0.1)$ev and $-(5.0\pm0.1)$eV for C and O coverage respectively. Fischer *et al* (1986) also found similar values of $-(2.95\pm0.1)$ev and $-(4.1\pm0.2)$eV for C and O coated W(110) samples; the differences may be due to the thickness of coverage and the face orientation of the crystals. An oxygen coverage, however, was noted to decrease size of the workfunction of Ni(100) from the clean surface value of −1.4eV to −0.95eV in the study of Fischer *et al* (1986).

An increase in the workfunction by adsorbate coverage has been used to enhance slow e^+ yields by Mills (1979a,b). A coverage of S on Cu(111) of the order of a monolayer was found to increase the efficiency of the moderator by 30% above the pure sample, with a full width at half maximum (FWHM) energy width of 0.2eV. Overlayers greater than a few monolayers can result in the domination of the adsorbate workfunction. Lynn and Lutz (1980) employed this effect in the proposal of a hybrid W+Cu moderator which would incorporate the superior stopping power of W but, due to the small ϕ_+ of Cu ($\approx$0.4eV), produce e^+ with an energy distribution smaller than from W.

Single crystal W moderators with epitaxially grown layers of Cu have been tested by Wilson and Mills (1983a) and Vehanen *et al* (1983) and Schultz *et al* (1983) and found to emit a narrow energy beam of e^+. However trapping at interface defects substantially reduced the efficiency from the single crystal W value. Vehanen *et al* (1983) noted that the β^+–e^+ conversion efficiency of the hybrid moderator was $3x10^{-4}$ compared to $3.2x10^{-3}$ for W(110) and $1.3x10^{-3}$ for Cu(111)+S in the backscattering mode. The FWHM energy spread obtained, 0.4eV, was similar to that from a pure Cu sample. Annealing to below 850°C improved the efficiency to $1.2x10^{-3}$, however, heating to 850°C resulted in islanding of the Cu on the W surface. Thus, the interfacial defects could not be annealed out without evaporation or rearrangement of the overlayer.

2.3.2 Ps emission, trapping and reflection

The main processes which can occur at the surface in competition with the e^+ emission are briefly discussed below. The first is the formation of Ps with energies much greater than the thermal values. Although Hasegawa *et al* (1985), from angular correlation studies, have obtained evidence of the formation of Ps in the voids of neutron-irradiated vanadium, in pure crystalline metals Ps has not been observed to form in the solid bulk. Rather, e^- pick-up by the outgoing e^+ occurs at the surface where the electron density falls to ≈1/10th of the bulk values (Held and Kahana, 1964, Lowy and Jackson, 1975). From conservation of energy, the Ps energy E_{Ps}, can be calculated from

$$E_{Ps} = \phi_- + \phi_+ - E_b \qquad 2.17$$

where E_b is the binding energy of positronium. Ps formation is always a favourable process in metals with negative ϕ_+ since the energy required to remove the electron is compensated by E_b thus making E_{Ps} negative.

A non-adiabatic model of Ps formation at the surface has been proposed by Mills *et al* (1983) in which the removal of the electron leaves the metal in an excited state. The resulting Ps energy has a maximum value of E_{Ps} and a spread corresponding to the density of states of the electrons at the surface. In their investigation, the energy spread of the normal component of the energy of the Ps emitted from an Al(100) surface was measured (Figure 2.9) and found to be in accord with the above model

(represented by the solid line). An adequate explanation for the discrepancy at energies <1eV has yet to be offered.

Ps emitted with energies greater than E_{P_s} have been observed by Howell *et al* (1986) from LiF samples and have been attributed to the formation of Ps by backscattered epithermal positrons. This process is discussed in Section 4.2.1.

The trapping of positrons at the surface in wells created by the attraction from the image induced potential with the correlation potential was first predicted by Hodges and Stott (1973a). Positrons at the surface were estimated to be bound with energies of 1–3eV by Nieminen and Hodges (1978) and possess a lifetime against annihilation of 2–3 times of that in the bulk. Evidence of e^+ trapping was obtained by Mills and Pfeiffer (1979) when the energy distribution of the Ps emitted from a Cu(111) surface was observed to be temperature dependent. In this study, a time-of-flight technique was used to measure the Ps velocity by detecting the Ps annihilation γ–rays in coincidence with the pulsed incident e^+ beam. They observed that at 30°C Ps was formed with energies corresponding to those relating to the workfunction process described above. However, at a sample temperature of 790°C, an additional delayed component was found which correlated to Ps of mean energy 0.14eV and a non-Maxwellian thermal distribution. The authors attribute this to desorption of surface trapped e^+ as Ps. This effect is illustrated in Figure 2.10 from Mills (1981a).

Lastly, the e^+ can undergo reflection at the surface potential. Nieminen and Oliva (1980) have shown this process to be temperature dependent, predicting a decrease in the emission rate of e^+ and Ps to zero at 0K. Trapping of e^+ was calculated to be temperature independent. Subsequent studies did not provide support but indicated a weak temperature dependence (Lynn *et al*, 1981, Schultz and Lynn, 1982). However, the recent study of Britton *et al* (1989) has demonstrated a temperature related variation of the e^+ and Ps yields from Cu(111) and Al(110) surfaces which can be described in terms of quantum mechanical reflection at the surface potential. They demonstrated that the elastically transmitted thermal e^+ flux would vanish at 0K for a negative ϕ_+ surface and attributed the discrepancies with the earlier studies to insufficient separation of the thermal and epithermal contributions.

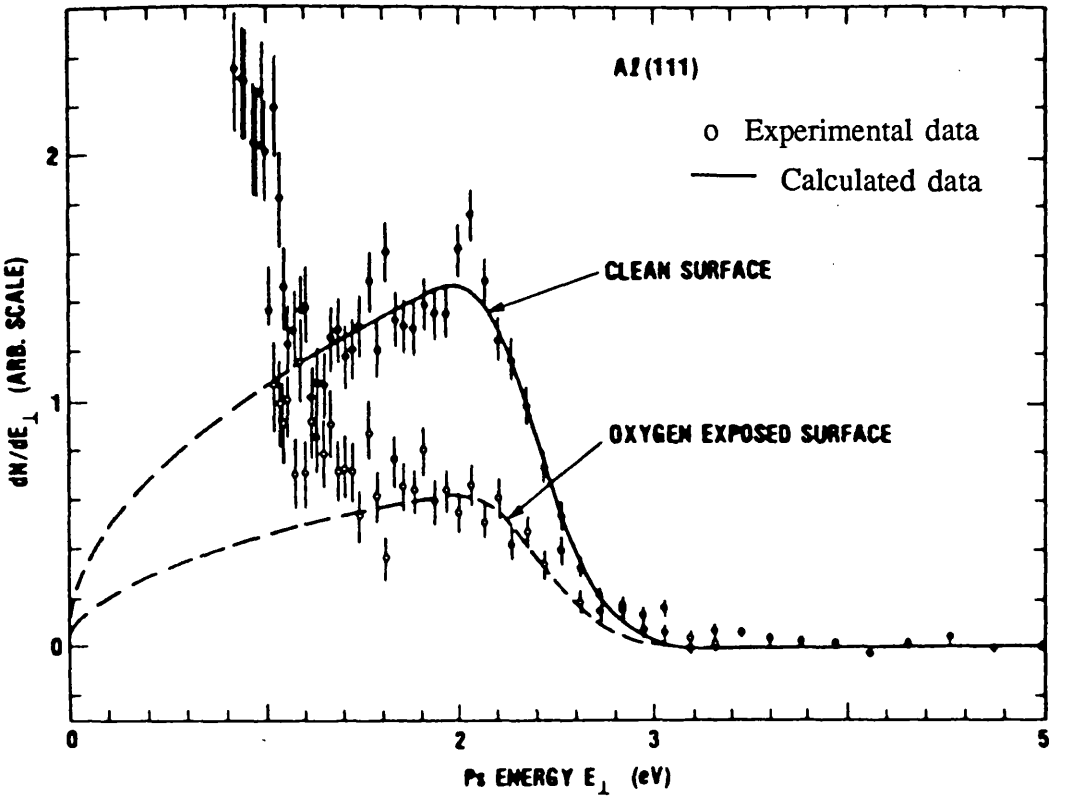

Figure 2.9 Normal component of kinetic energy of Ps emitted from Al(111) (Mills *et al*, 1983)

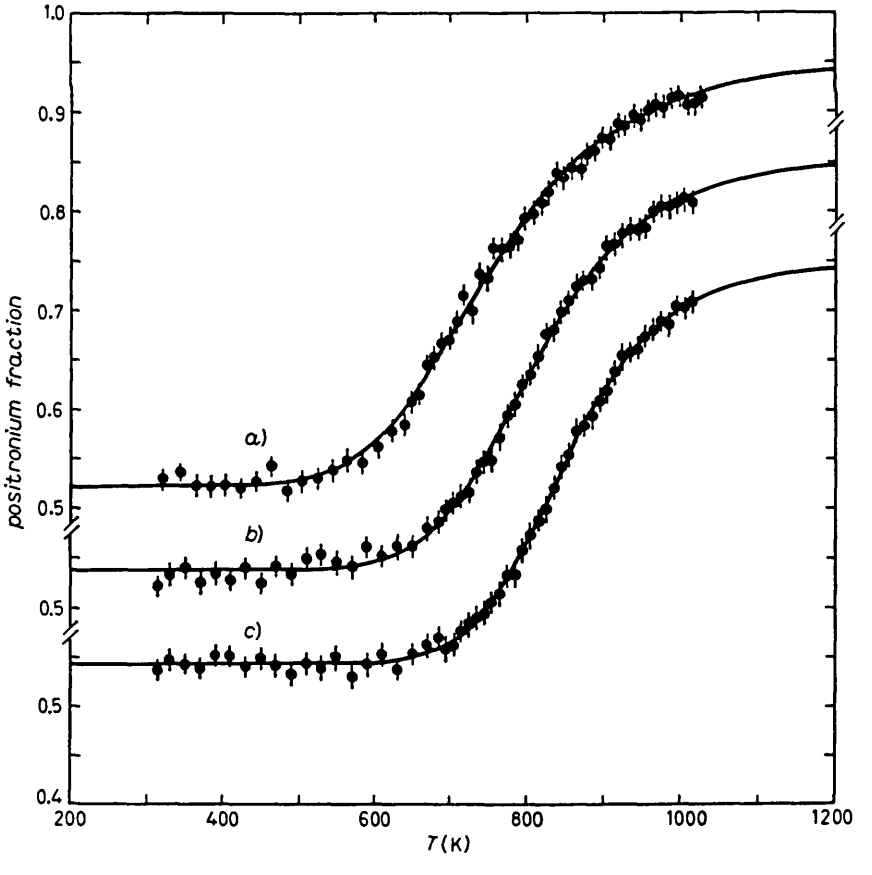

Figure 2.10 Ps fraction versus temperature for Cu(100) with various S coverage (from Mills, 1981a)

2.4 Thin film moderators

2.4.1 Summary of processes

The processes governing the energy moderation of fast β^+ particles in the solid, the subsequent diffusion motion and its eventual fate in the bulk or at the surface have been discussed in sections 2.3 and 2.3 and are briefly summarised below.

1. Bulk processes

The fast β^+ particles quickly lose energy on entering the solid by inelastic collisions with the target electrons and stop at a characteristic distance from the entrance surface. From Figure 2.3, of the implantation profile of β^+ particles from ^{22}Na impacting on a Ni sample, it can be seen that only $\approx$1% of the incident flux is stopped in the first 1500Å. Since the characteristic distance travelled by the positron during its diffusive motion, L_+, is $\approx$1000Å, the majority of the emitted slow positrons will originate from those stopped within the order of 1000Å from the surface. Thus, a large proportion of the incident β^+ flux is unused and a limit is set by the stopping power on the ultimate efficiency of a single-crystal metal converter for β^+ moderation.

Equation 2.1, 2.2 and 2.3 shows the dependence of the implantation depth of β^+ particles from a radioactive source on the target material and the incident energy. For a ^{22}Na source, the values of α_+/ρ for Cu (Z=29) and W (Z=74) are given as 23.0 and 25.8 cm^2g^{-1}, respectively, with $\bar{E}$=O.26MeV (Vehanen and Mäkinen, 1985). Thus the mean implantation depth is smaller for substances with higher densities and so materials such as W are favoured for use as moderator.

For remoderation, however, the requirements are modified by the use of an essentially monoenergetic positron beam. Figure 2.5 shows the implantation profile obtained from Monte Carlo studies by Valkealathi and Nieminen (1984) and illustrates the control of mean implantation depth by variation of the incident e^+ energy. Thus, the energy of the beam can be adjusted to achieve mean implantation depths of the order of the diffusion length from the surface. However, the implantation profile becomes broad with increasing energy and, as the mean depth approaches the transmitting surface a significant proportion of the e^+ are emitted before thermalisation, therefore setting limits on the parameters of energy and thickness.

2. Diffusion

The motion of the positrons become random as thermalisation is attained allowing the transport to be described by the diffusion equation. The proportion of positrons that may eventually reach the surface can be calculated using Equation 2.1 for isotropic $ß^+$ implantation and Equation 2.4 for a monoenergetic, collimated incident beam.

The importance of a pure crystalline structure is reflected by Equation 2.12, in the value of L_+. Large values of D_+, a reciprocal measure of the number of scattering events, and small values of λ_{eff} are desirable to achieve a greater proportion of e^+ at the surface. The single crystal and polycrystalline values of D_+ for the same material differ appreciably. For example, in the case of W, D_+ is $1.5 cm^2 s^{-1}$ for single crystal samples (Vehanen *et al*, 1983) compared to 10^{-2} $cm^2 s^{-1}$ for a polycrystalline form (Paulin *et al* 1974). Thus the use of single crystal material is preferable in obtaining high moderation efficiencies. However, some polycrystalline samples have been observed to give yields comparable to single crystals (Gramsch *et al* 1987), probably due to an increase in the crystallite grain sizes through repeated annealing cycles.

Sample annealing is also relevant to the value of λ_{eff} which is increased by trapping at defects and vacancies in the bulk. Bulk impurities, such as C, can cause vacancies and are present even in high purity single crystal samples. Carbon is incorporated during the fabrication process, but can be removed by heating in the presence of oxygen (discussed below).

3. Surface Processes

At the surface the positrons can undergo a number of competing processes, chiefly: free e^+ emission; energetic Ps formation; trapping at the surface; reflection at the surface potential.

The first phenomenon, free e^+ emission, is only energetically allowed if the positron workfunction, ϕ_+ of the material is negative , although non-thermalised positrons may be emitted from all substances. Moreover, the presence of adsorbate layers has been shown to change the value of ϕ_+. The branching ratio, y_0, of the process has been demonstrated by Murray and Mills (1980) and Gullikson *et al* (1988) to vary with the magnitude of ϕ_+ for a particular metal (Al, Cu) suggesting that larger values of ϕ_+ are beneficial in achieving high yields.

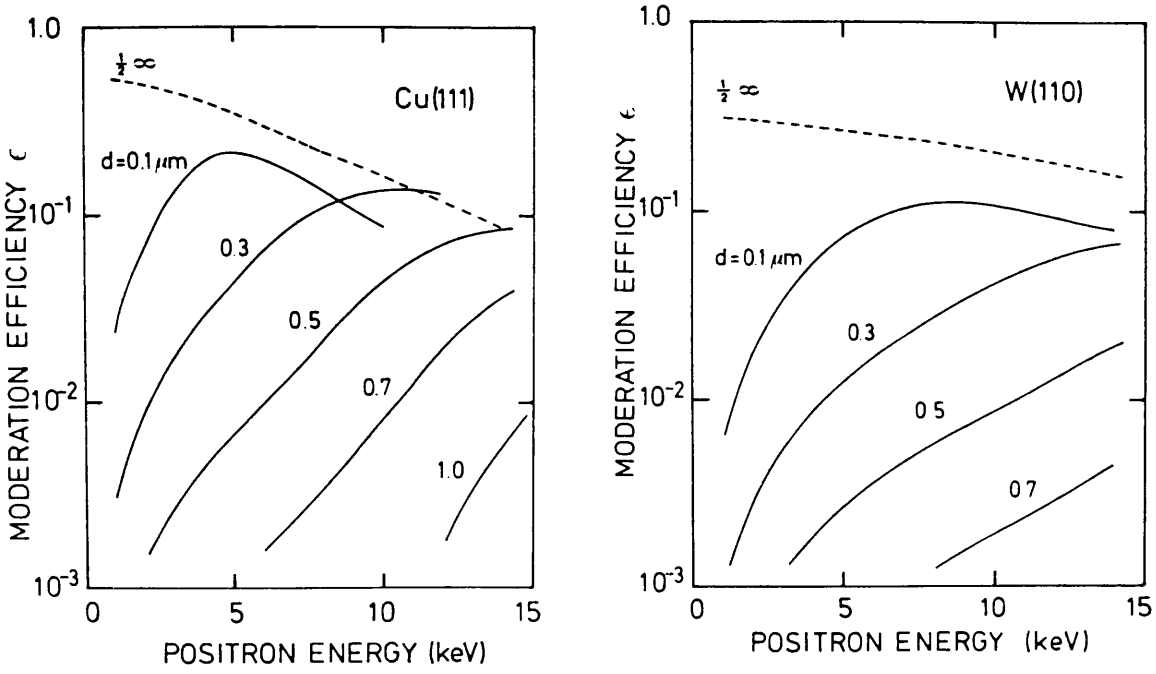

—— Calculated for thin single crystal film in transmission mode

- - - - Calculated for semi-infinite single crystal in backscattering mode

Figure 2.11 Slow positron remoderation efficiencies versus energy in (a) Cu(111) and (b) W(110) (Vehanen and Mäkinen,1985)

The branching ratio of the process of free e^+ emission can be taken together with the implantation profile and the solution of the diffusion equation to calculate the efficiency of moderation of a particular material. Vehanen and Mäkinen (1985) have calculated these values for W(110) and Cu(111) single crystal foils in the back and

forward emission geometries. Using the profile of β^+ implantation from a ^{22}Na source on a high Z backing (Mourino *et al*, 1979) and experimentally derived values of L_+ and y_0 (Vehanen *et al*, 1983), their results showed similar efficiencies for the back and forward emission modes for each metal. W(110) was found to be more efficient than Cu(111) at less than 10μm thickness with a maximum ε of $4x10^{-3}$ compared to $2.5x10^{-3}$; the higher density and larger diffusion length of W (L_+^W=1350Å, L_+^{Cu}=1100Å) offsetting the effect of the larger branching ratio used for Cu (y_0^W=0.55, y_0^{Cu}=0.33). In the case of remoderators, the Cu sample was found to be more efficient than W, at the same thickness and incident beam energy due to the differences in the implantation depth and the branching ratio.

Figure 2.10 illustrates the variation of ε with e^+ energy for different thicknesses for Cu(111) and W(110), the efficiency of the backscattering geometry is represented by the dashed line. The maximum efficiencies in the transmission mode were found to be 22% for Cu(111) at 5keV and 11% for Cu(110) at 8keV for a 1000Å thick foil. Figure 2.11 shows that a thicker Cu(111) foil can be used to achieve the same efficiency as that from W(110) providing the branching ratios used are correct. This is of technical benefit as thicker foils are easier to handle.

2.4.2 Use of thin film moderators

The use of thin films in transmission was first studied by Chen *et al* (1985). Epitaxially grown single-crystal W(100) films of thicknesses 1000, 2500 and 5000Å were investigated using a 0–80keV monoenergetic e^+ beam in ultra-high vacuum conditions. The foils were grown, in high vacuum conditions, on substrates of MgO/Mo using an electron evaporation technique similar to that described by Mertler *et al* (1982). After removal from the substrate by chemical etching, the foils were subjected to *in situ* heat treatment to remove defects and surface contaminants. The optimum procedure was found to be heating in $\approx 10^{-7}$ Torr of oxygen at 700-800°C for 40 minutes to remove C, the main bulk impurity in W, and then increasing to 2000°C for 1 minute in high vacuum ($\approx 10^{-9}$ Torr) to remove the oxide layer.

Figure 2.12a shows the positron emission spectra, after two cleaning cycles, from a 2500Å W(100) foil bombarded with 12keV e^+. The effect of the oxygen overlayer is demonstrated at T=1200°C; the broad energy distribution caused by inelastic

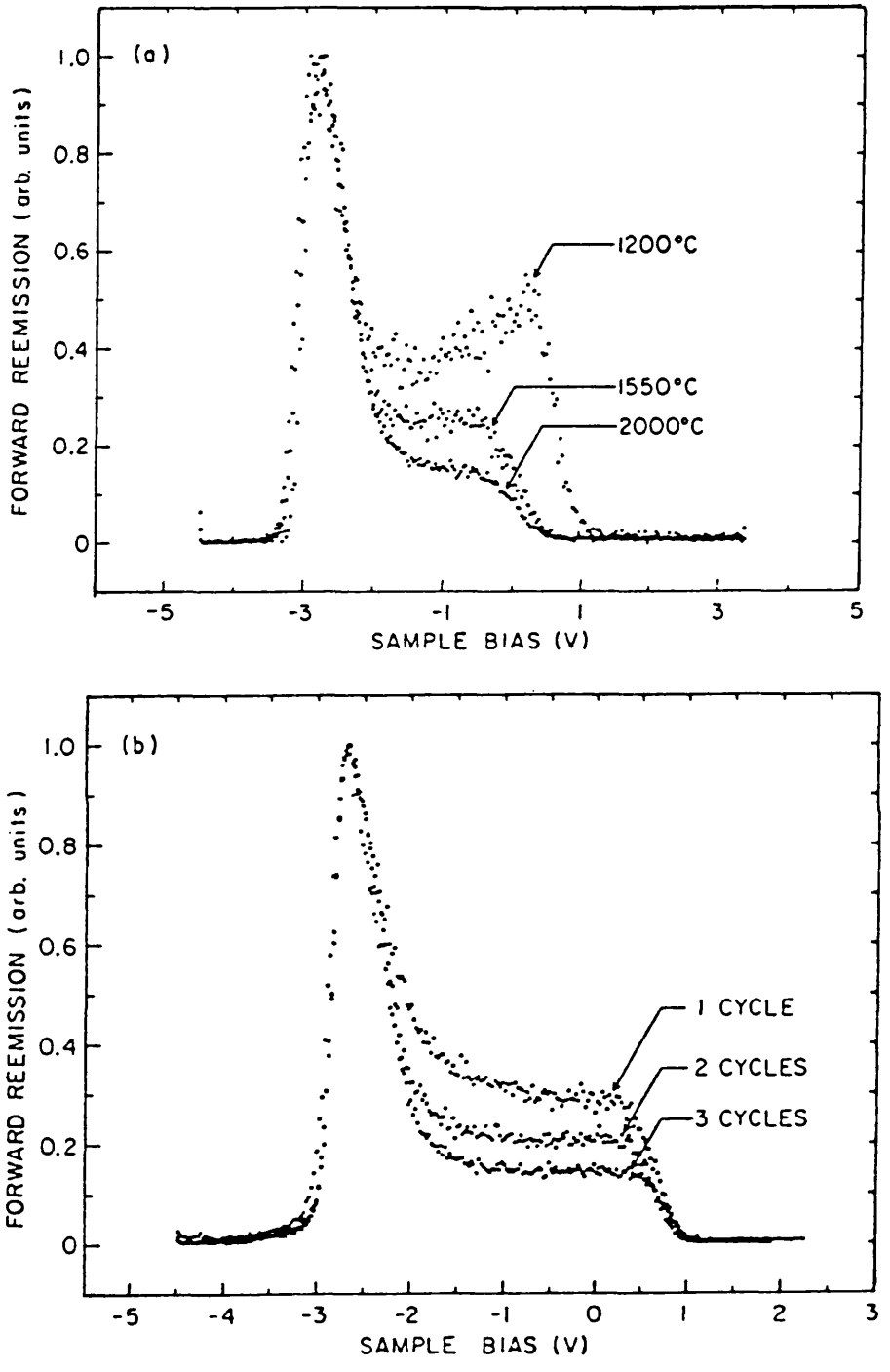

Figure 2.12 (a) Differentiated energy spectrum of forward re-emitted e^+ from 2500Å W(100) foil at incident energy of 12keV after two cleaning cycles

(b) Differentiated energy spectrum of forward re-emitted e^+ from 1000Å W(100) foil at 5.85keV incident energy (Chen *et al*, 1985)

scattering and microscopic roughness of the surface. However, the total yield and theworkfunction value are larger in comparison to that annealed at 2000°C. Figure 2.12b, from 5.85keV e^+ incident on a 1000Å W(100) foil, illustrates the improvement in the peak-to-shoulder ratio after several annealing cycles. Maximum re-emission efficiencies of 18% for 1000Å and 12% for 2500Å thick foils were found at 5 and 10keV respectively and e^+ were emitted within a FWHM cone of 30°,thus demonstrating the feasibility of using transmission mode remoderators after appropriate annealing procedure.

Lynn *et al* (1985), employing a similar method of annealing, investigated the use of a 5000Å W(100)film as a primary transmission moderator and found a maximum efficiency of $4x10^{-4}$ in 10^{-8} Torr. On obtaining an efficiency of $3x10^{-4}$ after exposure to air followed by baking at 135°C, they proposed its use in lower vacuum conditions. Subsequent improvements to this efficiency have been made by Gramsch *et al* (1987) using electron bombardment at $5x10^{-7}$ Torr to heat the samples to 2100°C. They found a maximum value of $9.1x10^{-4}$ from a 10000Å foil, in contact with the ^{22}Na source on a thick W backing.

A number of single crystal and polycrystalline samples were studied by Gramsch *et al* (1987): W; Ni; Ta; Mo; Nb; Cu. Single-crystal W(100), in the configuration described above, gave the highest yield. However, a 10000Å W(100) sample and a 3000Å Ni(100) foil, both placed in direct contact with a Kapton covered ^{22}Na source, yielded comparable efficiencies for the two foils ($\varepsilon_W=5.9x10^{-4}$, $\varepsilon_{Ni}=6.6x10^{-4}$). Moreover efficiencies obtained from polycrystalline W and Ni foils were ≈40% that of the maximum value from the single crystal samples.

The re-emission properties of single crystal Ni were investigated by Schultz *et al* (1986). Their sample, a 1500Å thick Ni(100) foil, was raised to 650°C by electron bombardment and then cooled at a constant rate over a period of 30 minutes. They obtained a yield of 19%, similar to that of W(100) but with a FWHM energy spread of 165meV, a third of that from the sample used by Chen *et al* (1985). Furthermore, they noted that exposure to air did not degrade the foil.

Recently, work has been carried out by Poulsen *et al* (1988) on the effect of laser annealing thin single crystal W foils. Some very promising results have been

obtained. The procedure they employed consisted of a 10s pulse at 1200°C in UHV from a CW–Nd:512 laser of wavelength 1.06μm, followed by an exposure of 20 minutes at 1200°C in 10^{-6} Torr of oxygen, then 2000°C for 1 minute at 10^{-9} Torr. Three foils were tested, of thicknesses 1000Å, 2000Å and 3100Å, and a maximum re-emission yield of 38% was found for the 1000Å sample at 5keV incident beam energy, doubling the efficiency obtained in the study of Chen *et al* (1985). Moreover, they found that 60–70% of the contribution is contained in the FWHM energy band of 150–200meV - a four-fold improvement on the previous work.

2.4.3 Aim of the study

Following the studies discussed in the previous section on transmission mode moderators, the properties thin single crystal W and Ni foil as β^+–e^+ converters have been investigated in conditions of 10^{-7} Torr for use in gas-scattering experiments. Samples of W(100) and Ni(100) foils with thicknesses in the range 1000Å to 18000Å have been studied with reference to (a) the annealing technique, (b) the efficiency of slow positron emission and (c) the energy distribution of the emitted flux.

The calculations of Vehanen and Mäkinen (1985) indicate that high moderator efficiencies are attainable in the transmission mode from the single crystal metal foils and, since the availability of films with good crystalline order and of sufficient rigidity, transmission mode moderators have been demonstrated by several workers to yield high efficiencies (Chen *et al*, 1985, Lynn *et al*, 1985, Schultz *et al*, 1986, Gramsch *et al*, 1987). The aforementioned studies were all undertaken in a high or ultra-high vacuum environment ($\geq 10^{-8}$ Torr). Such conditions are difficult to maintain in gas-collision investigations, where typical base pressures used are of the order of 10^{-7} Torr. However, Dale *et al* (1980) and Lynn *et al* (1985) have noted that the performance of W moderators (both single crystal and polycrystalline) was not greatly degraded by exposure to air for a short time. Thus, W, shown to give high yields, is a candidate for use as a moderator in the lower vacuum environments.

In addition to the yields, the energy distribution of the emitted positrons was also determined as this is an important factor in some experiments such as studies of the collision processes in e^+–molecule scattering where the difference in energy levels can be small. Adsorbate coverage, such as oxide layers, may increase the longitudinal energy distribution of the emitted e^+. W, in poor vacuum conditions, will inevitably

obtain an oxide coating, although Dale *et al* (1980) state that the maximum thickness of such a coverage is ≈2 monolayers. With its large ϕ_+ value, the spread in energies of the positrons can be significantly broadened by such processes as adsorbate scattering. Schultz *et al* (1986) have demonstrated that a Ni(100) foil used in UHV as a transmission mode remoderator yielded an efficiency similar to that from W (Chen *et al*, 1985) but with a much narrower energy spread. Thus, the feature of the small energy spread but comparatively high re-emission yield, motivated the study of Ni foils for use as primary moderators in lower vacuum conditions.

CHAPTER 3
EXPERIMENTAL STUDY ON THE USE OF THIN SINGLE CRYSTAL FOILS AS PRIMARY TRANSMISSION MODERATORS

3.1 Introduction

The fabrication of single crystal films, sufficiently thin for use as positron transmission moderators, has been facilitated by developments in the evaporation growth technique. Unlike other methods of crystal preparation, such as bulk material thinning or melt growth, the evaporation process is advantageous in that it enables the growth of thin films of large areas and almost homogeneous thicknesses with relative ease. In this method, epitaxial layers are formed by the controlled condensation, in high vacuum conditions, of the required substance onto a host crystal of similar structure. The substrate is later removed by chemical processes leaving films of high purity and good structural order.

In the present study, foils of W(100) and Ni(100), fabricated in this manner and with thicknesses of 1000-18000Å and 3000-15000Å respectively, were employed for investigation. An annealing procedure, described in Section 3.3, using resistive heating was developed and the slow e^+ emission properties of the films were characterised in a separate e^+-beam system (Section 3.4).

To derive the yield of slow e^+ emitted upon β^+ implantation, various points were considered and these are discussed in Sections 3.5, 3.6 and 3.7. The corrections required were namely due to the solid angle effect of the source-moderator geometry, backscattering from the source mount, the efficiency of slow e^+ detection, and the transmission of the grids in the beam path. On accounting for these factors, the β^+–e^+ conversion efficiency, ε, of the foils can be derived. The values thus determined are presented in Section 3.8 and discussed in relation to yields obtained from calculations and from other experimental studies. Additionally, the energy distribution of the e^+ emitted from the foils and from the widely used W mesh moderator were measured and these are compared in this section.

3.2 Foil fabrication

3.2.1 W(100) foils

The evaporation technique of crystal growth was employed to fabricate films of high crystallinity with low defect and impurity concentrations. Using a hetero-epitaxial growth method similar to that developed by Mertler et al (1982), W(100) films of various thicknesses were laid onto magnesium oxide-molybdenum hosts in high vacuum conditions (Chevallier, 1987). The use of the hetero-epitaxial technique, where the Mo film is employed as the substrate layer, results in an improved 2-dimensional growth of the foils. Differences in the lattice spacings between the host and the deposited layer can lead to the formation of defects in the structure of the crystal grown. In this case, although both MgO and Mo are epitaxial with W, the lattice misfit between W and Mo is less then that between Mo and MgO (≈5.5%). Thus, better "perfection" is achieved if Mo is used as the substrate layer rather than MgO. This was demonstrated in the study of Mertler *et al* (1982) from the results of x-ray rocking curves which may be considered as a measure of the tilt of the crystallites. The FWHM of the distributions was found, at best, to be 24′ (minutes of angle) for Mo on MgO compared to <10′ for W on Mo. Furthermore, the density of dislocations, also a measure of the perfection of the crystal, was found to be much lower in W films grown on Mo than those grown onto MgO (Chevallier, 1987).

The MgO crystals employed were cleaved in air in the desired orientation, located by x–ray diffraction analysis. However, due to the hardness of the crystal, many high step defects may be created on the surface from the cleaving process leading to an uneven thickness of the deposited layer (Mertler *et al*, 1982). Therefore, the MgO crystals were polished and annealed before use as the substrate. The crystals were mounted on a heater plate in the evaporation chamber and were raised in temperature following evacuation to 10^{-8} Torr. High purity Mo pieces (99.99%), placed in a W boat, were melted by electron bombardment and degassed. Whilst adjustments were made to the Mo evaporation rate, the MgO crystal was protected from deposition by a shutter. On reaching the optimum evaporation rate and substrate temperature, the shutter was removed and the thickness of the subsequent growth was measured with a quartz crystal oscillator accurate to ±10%. During evaporation, the pressure in the chamber rose to $\approx 10^{-7}$ Torr.

The temperature of the host crystal is regarded to be critical for good crystalline growth; for Mo, Mertler *et al* (1982) found that heating the MgO crystal to between 1000°C and 1150°C gave the highest degree of crystallinity. Using transmission electron microscopy, the density of dislocations in Mo crystals, grown in this temperature range, was measured to be $\approx 10^9 cm^{-2}$ and no misorientated areas were observed. Below 850°C Mo was found to be deposited amorphously and above 1200°C the structure became polycrystalline and discontinuous. The Mo layer was grown, typically, to a thickness of 2000Å whereupon the W, (99.99% purity), was similarly deposited onto the Mo at a rate of $5–20 Å s^{-1}$.

Prior to removal from the substrate the films were tested for crystallinity using the Rutherford backscattering technique to find the minimum axial channelling yield, χ_{min}, of 2MeV α–particles impinging onto the samples. The term χ_{min} is defined as the ratio of the backscattered signal when the crystal is in the optimum orientation with respect to the particle beam compared to that when the orientation is random. For W(100) the theoretical value for χ_{min} is 1.1% (for references see Gemmell, 1974); crystals with a measured χ_{min} of less than 1.5% were used as "good" foils although some with χ_{min} greater than 1.5% , referred to as "bad" foils, were also investigated.

The foils were removed from the substrates before transport to UCL. The MgO and Mo crystals were chemically removed from the W films (Chevallier, 1987) which were then washed several times with fresh distilled water and lifted off onto W meshes or rings.

3.2.2 Ni(100) foils

The Ni foils were fabricated in a similar fashion to the W foils. Ni, of 99.99% purity, was evaporated onto NaCl substrates cleaved in the (100) orientation and tested using Rutherford backscattering. For Ni, the theoretical value of χ_{min} is calculated to be 3.3% (for references see Gemmell, 1974) and foils with $\chi_{min} \leq 4.5\%$ were used.

As the process of substrate removal was less complex in the case of the Ni foils, these were transported on the host crystal to UCL to provide greater support. The NaCl was simply dissolved in distilled water and the films were washed 4 or 5 times

with a fresh change of distilled water on each occasion. The foils were then picked up onto high purity (99.95%), 25μm thick Ni rings which had been heat treated. In order to remove contaminants from the bulk which could migrate into or condense onto the foil during the annealing process, the rings had been maintained at 650°C for 30 minutes, followed by flashing at 950°C for a few seconds.

3.3 Annealing

3.3.1 W(100) foils

The foils were annealed in an "oven", shown in Figure 3.1, which was constructed from 2 rectangular pieces of 25μm thick, 99.95% pure W sheet, typically of dimension 1.5cm by 3cm. Two tungsten-alloy clamps held the pieces, outwardly bowed in the centre, such that the samples could be placed in between and heated by passing current through the oven walls. For the purpose of heating, the foils were sandwiched between high purity (99.95%) W meshes which had previously undergone annealing to remove impurities. Most foils required support otherwise crumpling occurred, although some of the thicker foils, such as the 18000Å sample, were of sufficient rigidity to be left free-standing in the oven during treatment. It was found particularly important to avoid contact of the films with the oven walls in order to prevent damage caused to the films from the occurrence of hot spots and partial melting.

The temperature of the foil was monitored externally through a pyrex window with an optical pyrometer accurate to ±100°C. Each sample was heated to a few hundred degrees for a few minutes to remove adsorbed water molecules from the surfaces, then quickly taken up to temperatures of 1800-2400°C. The samples were flashed, that is, held at the temperature for 1–3 seconds, for 2 reasons: (i) it was undesirable to heat materials in the electrode assembly which could contribute to contamination and (ii) temperature control was difficult. Longer heating times often resulted in the evaporation of the sample. This procedure was performed mainly in a low vacuum environment ($6x10^{-2}$ Torr); repeating this cycle at a lower pressure (10^{-6} Torr) using a diffusion pump did not yield any significant improvement.

Carbon is commonly the main bulk impurity in W material and it has long been established that this can be removed by heating in an oxygen atmosphere. Becker

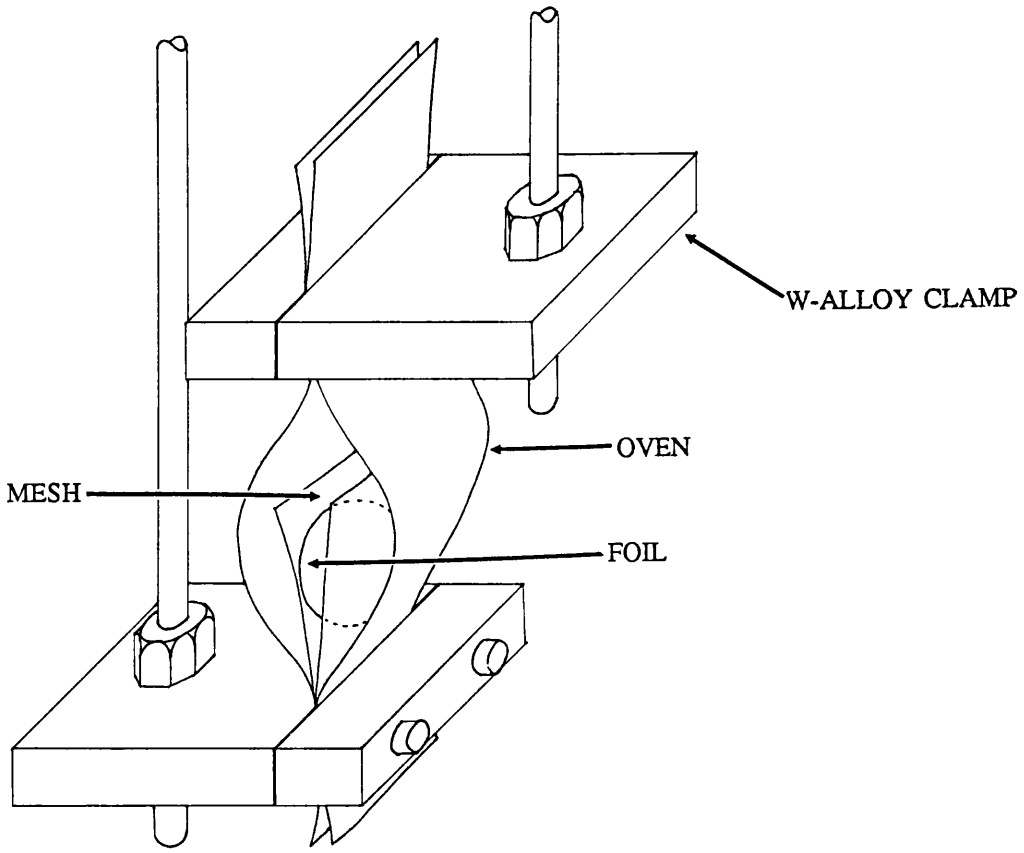

Figure 3.1 Diagram of "oven" arrangement employed in the annealing procedure

et al (1960) found that negligible amounts of C were left in their W ribbon samples when heated at 2200K in 10^{-6} mmHg of oxygen for 10–60 hours. The carbon content of the W material was depleted by the formation of CO_2 with C atoms on the surface which were continuously replenished by migration from the bulk. Other workers, such as Chen *et al* (1985), have demonstrated the effect on the slow e^+ emission properties of W of introducing O_2 into the system during heating (discussed in Section 2.5). The annealing procedure developed in the present study was chiefly carried out at $6x10^{-2}$ Torr giving a partial pressure of the ambient O_2 molecules of $\approx 10^{-2}$ Torr. An 18000Å thick sample, treated at a pressure of 10^{-6} Torr, underwent 10 heating cycles before reaching a maximum which was more than that required by

the other foils. It is uncertain whether this was due to greater thickness or the reduced number of O_2 molecules available.

The foils were allowed to cool to room temperature, then transferred in air to an e^+-beam system where they were mounted in rigid stainless steel or W-alloy push-fit ring holders (opening diameter: 8mm) as the mesh supports were found to be too flexible to contain the foils in the test beam and furthermore, hindered film characterisation. However, this introduced an extra handling process, increasing the possibility of stressing and thus, damaging the crystal structure.

As pure W material is extremely difficult to machine due to its hardness, holders could not be easily constructed from this, therefore W-alloy holders were made with the original intention of supporting the films during annealing. However, these were not employed for such use as it was suspected that substances in the alloy may degas and cause contamination. This had been observed when Ta from the original foil casing evaporated on heating and condensed on the film, resulting in a detrimental effect on the moderator efficiency. Once contaminated, the samples rarely regained their previous performance even after extensive heating. In addition, thermal stress caused by disproportionate heating may have resulted by tightly clamping the fragile films.

3.3.2 Ni(100) foils

The foils, held between pre-annealed Ni rings for support, were placed in a similarly constructed oven made from 25μm thick, 99.95% pure Ni foil. Before annealing any samples, the oven was heated at 650°C for 30 minutes, then flashed a few times at 950°C to reduce contamination. The foils were heated at 100–200°C for 10 minutes to desorb water molecules, then raised to temperatures between 550–950°C for times ranging from a few seconds to 1 hour. The temperature was monitored with a Ni/Cr thermocouple spot-welded to the oven wall. It was found that 2 minutes at 650°C was insufficient to improve the yield much above that from the unannealed state. A minimum of 2 cycles of 2 minutes at 650°C was required to give significant increases; in most cases ≈90% of the final yields were obtained after annealing at 650–700°C for 4 to 8 minutes. A decrease in the e^+ yield was observed after prolonged, continuous heating (≈30 minutes) at these temperatures. This was thought to be due to contamination from outgassing of the surroundings. Therefore, the foils

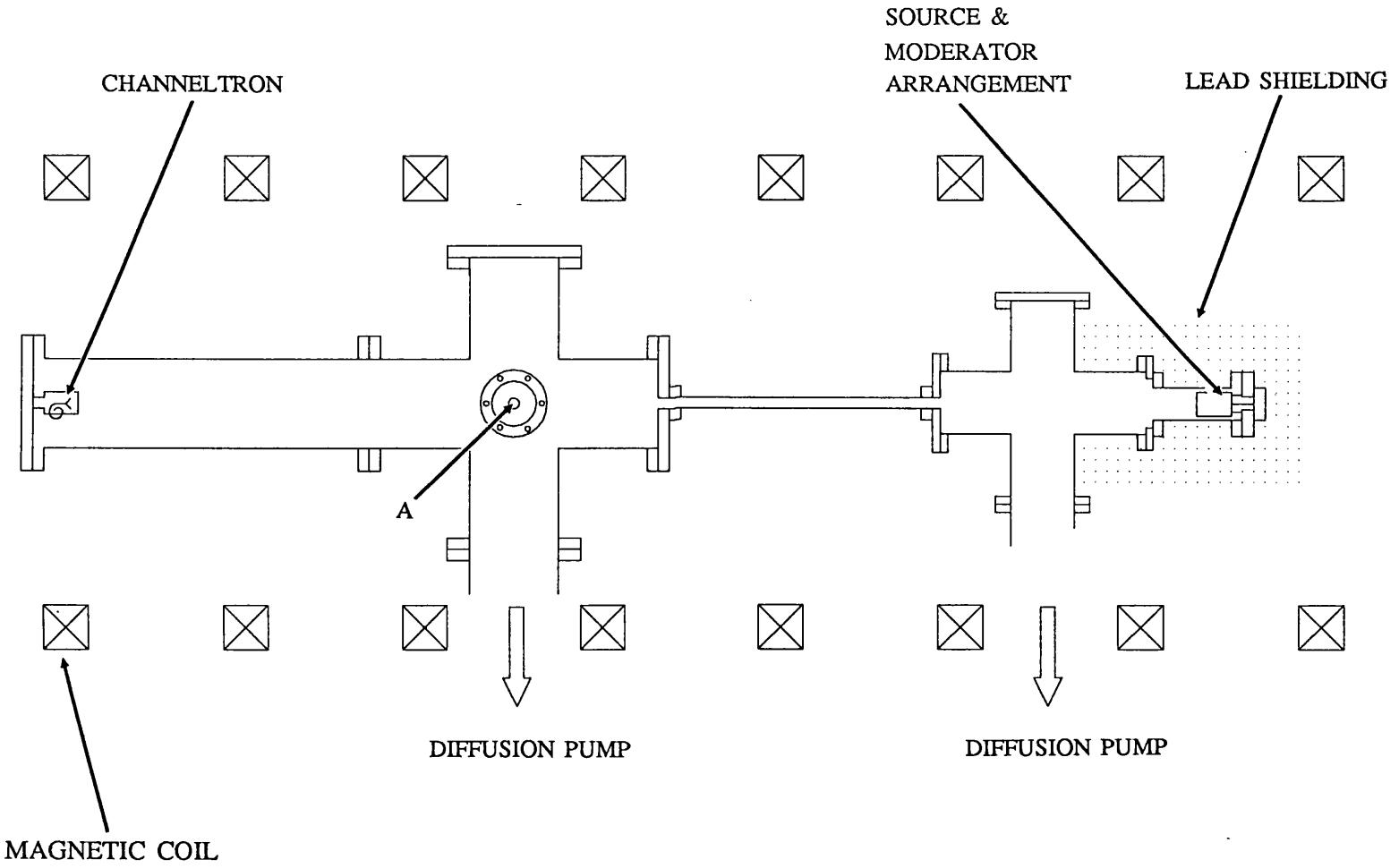

NOT TO SCALE

Figure 3.2 Schematic diagram of test beam apparatus

were heated in cycles of 2 minutes and the pressure was allowed to drop back to its minimum values in the intervals. It was also observed that similar yields could be obtained by taking the foils up to 900–950°C for times of 5 seconds to 5 minutes, again with a maximum period of 2 minutes per cycle.

Upon cooling to room temperature, they were transferred to the test beam in Ni rigid holders of the same design as in 3.3.1 but with a bigger opening diameter (10mm) as the Ni foils were larger in size than the W. Although Ni is machinable and high purity pieces are available, the holders were not used during annealing to avoid the occurrence of damage caused from disproportionate heating. It is also noted that Ni posed additional handling difficulties due to its magnetic property.

3.4 Test beam

The characteristics of the foils were studied in a system, shown in Figure 3.2, typical of those used in e^+-gas interaction experiments. Two unsealed ^{22}Na sources were employed in the W study with activities of (64.4±0.9) μCi and (44.9±0.7) μCi deposited, respectively, onto thick W and Pb discs. These were both 1cm in diameter and 25μm thick for the W backing and 1mm thick in the case of the Pb. For the Ni work, only the Pb-backed source was used and its strength at the time of the study was measured to be (40.0±0.7) μCi.

The source used was held to a brass mount, approximately 20mm in diameter, by a threaded cap and the mount itself was threaded to allow exact positioning. The source and sample were placed in a PTFE capsule, specially designed (figure 3.3) to allow a rapid change-over and minimum handling time so that exposure time to air (of the foil) and to radiation (of the experimenter) was short. As the foils were placed in identical holders each time and the position of the source was unchanged, the source-holder distance remained constant throughout the experiment. The relatively large source-foil distance of 1.5mm was chosen such that the effect of surface distortion would be small compared to the separation and moreover, there would be little danger of contact with the unsealed source. The foils were contained in 3mm thick circular holders (outer diameter:20mm) by a loose push-fit ring and slotted precisely into the assembly in front of a earthed grid, mounted on M3 studding. By a slight turn of the locking nuts, the whole grid and foil arrangement was held firmly in place. An accelerating potential of +100V was applied to the

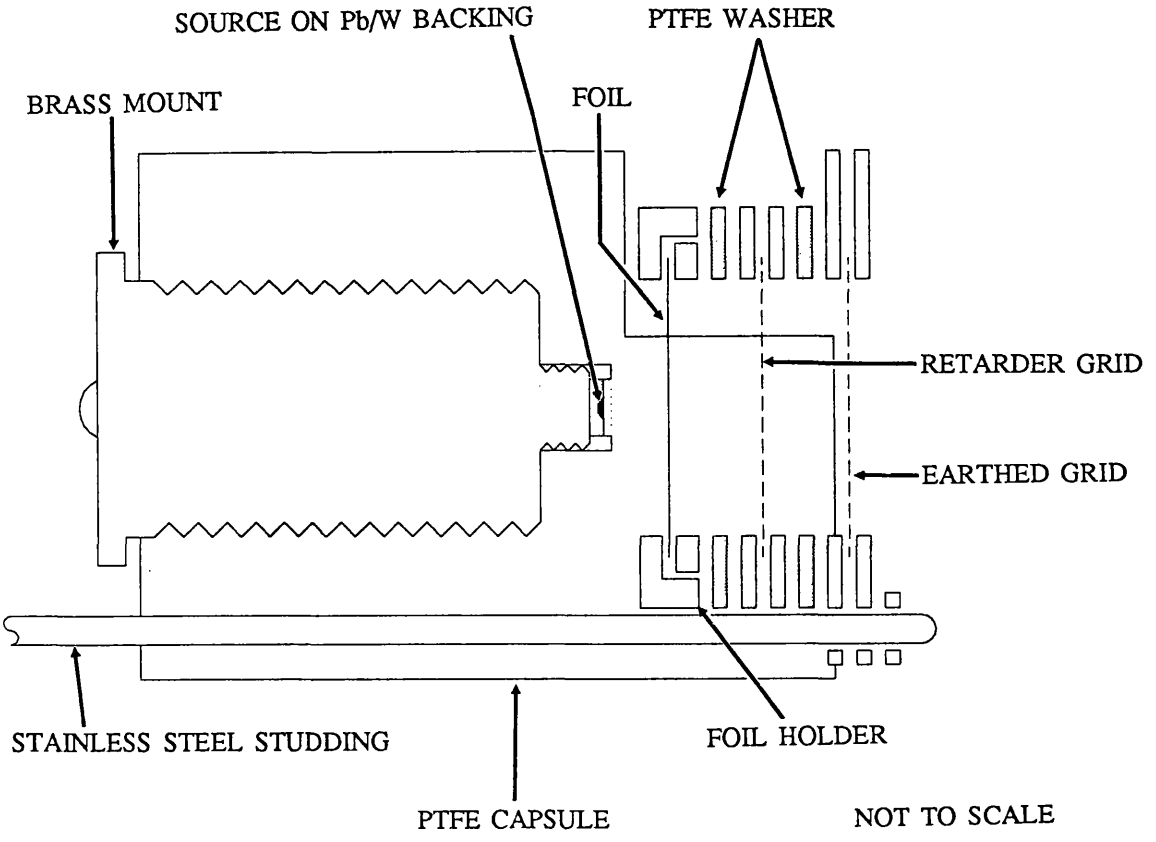

Figure 3.3 Cross-section of source and sample arrangement

foils. Mesh moderators could also be used in the system by simply applying a potential to the source approximately 20V greater than that on the moderator to turn the backwardly emitted positrons towards the detector.

The PTFE capsule housing the source-moderator assembly was mounted from a small (70mm) stainless steel flange by means of M3 studding. This arrangement was bolted to a stainless steel tube connected to a (100mm) stainless steel 4-way cross to allow Pb shielding of the source area. A 20mm diameter, 300mm long brass tube coupled this to a 200mm diameter 5-way cross stainless steel chamber. The final part of the arrangement consisted of a large brass tube, 130mm diameter, at the end of which the detector system was mounted. The 5-way cross chamber was required to support a number of features so that the test beam would be of multi-purpose use. For instance, a gas cell could be accommodated or a ExB filter could be inserted. In this study

an ionisation gauge was originally placed in position A in Figure 3.2 but this was subsequently replaced by a manipulator for the grid transmission measurements (section 3.6). Two vapour diffusion pumps, situated at the source end (E02 2" dia.) and at the 5-way cross (E04 4" dia.), backed by Edwards ED35 and ES330 rotary pumps and protected with Edwards CB4A water-cooled baffles provided efficient evacuation to 10^{-6} Torr.

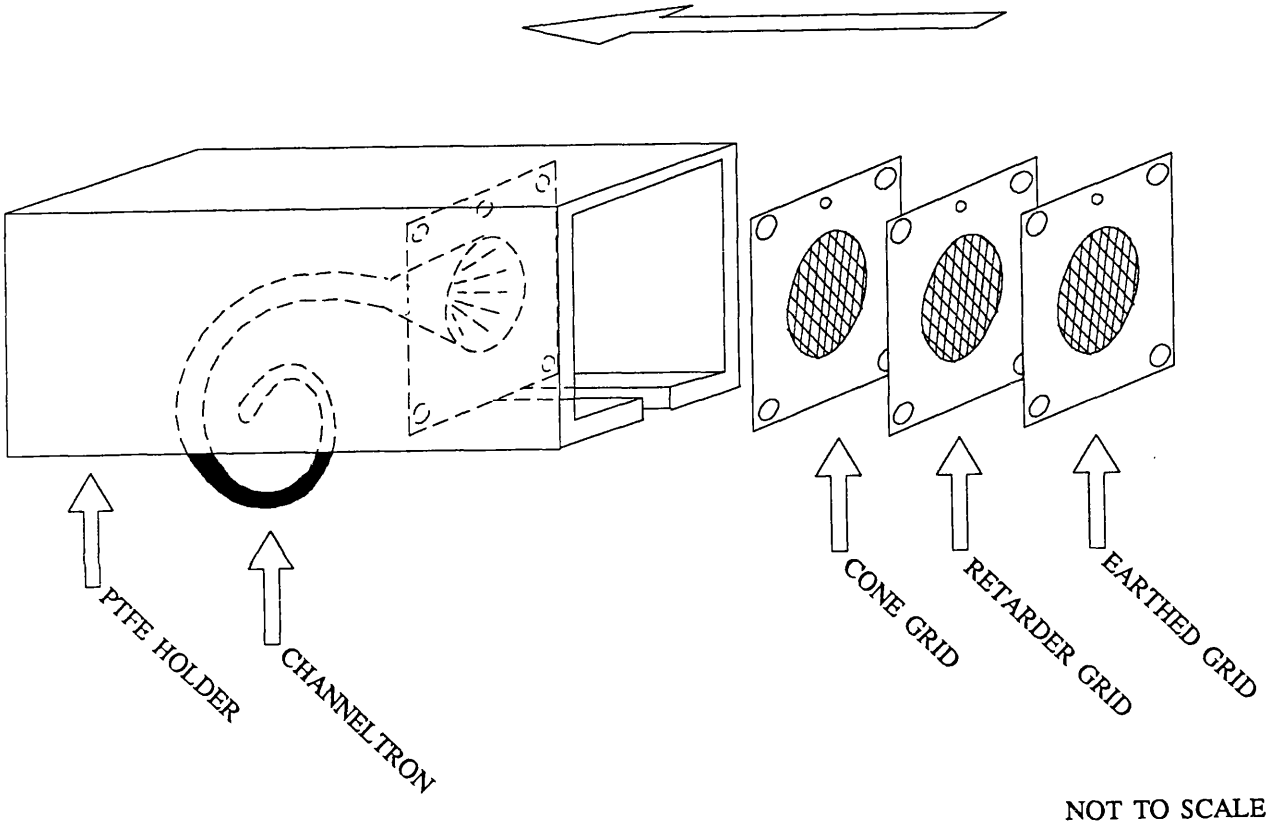

Figure 3.4 Exploded view of channeltron holder and associated grids

The e^+ emitted from the moderator were accelerated by the application of +100V on the foil with respect to the earthed grid. The e^+ were guided by an axial magnetic field along a flight path of approximately 1.5m to a Mullard B419Bl channel electron multiplier (channeltron) where they were further accelerated by −250V for detection. The field, produced by a Helmholtz arrangement of eight coils of mean diameter 24

cm, was 100 Gauss at the e^+ emission site, whilst along most of the path length it was held at 65 Gauss.

Initially, the energy profile of the positrons was examined by the application of a positive potential on a grid near the channeltron. However, imperfections in the magnetic field and **ExB** effects at the channeltron cone led to a broadening of the longitudinal energy distribution following emission. Therefore, in the studies subsequent to the W(100) film work, spectra were generated using an additional grid placed at the source end between the moderator and the earthed grid and separated by 1mm thick PTFE washers.

The channeltron and associated grids, shown in Figure 3.4, were housed in a machined PTFE block. Three grids were placed in front of the channeltron cone; the cone potential (−250V) was applied to the first to present a parallel field to the particle, the second was used for retarding and the third grid was earthed. The grids, nominally 80% transmission Cu micromesh, were held in brass plates by push-fit rings, interleaved with thin layers of PTFE of the same design. The whole arrangement slotted neatly into the holder and was secured by nylon screws. The connecting wires ran along the body of the PTFE block and all surfaces exposed to the particle flux were coated with Ag paint to prevent charge-up.

The cone of the channeltron was held at −250V, to attract positrons whilst repelling electrons, and 3kV was applied to the tube end. Positrons, both fast and slow, were detected by the channeltron from which the signals were extracted via a 300pF HV capacitor terminated by a 1kΩ resistor. These were fed into a fast preamplifier (x10 gain) and the resulting pulses were presented to a scaler counter via an Ortec 473 constant fraction discriminator. By use of a positive potential applied to the central grid in the arrangement prior to the channeltron cone, the flux of fast positrons was measured and subtraction from the total flux gave the number of slow e^+ in the beam. The longitudinal energy spectra of the emitted e^+ from several of the samples were obtained with the use of a voltage ramped retarder at the source end. These were subsequently differentiated with respect to the applied potential to show the measured energy distribution of the e^+ (see Section 3.8). The ramp was incremented in steps of 17mV over a 9V range, however the resolution of the retarder analyser was unknown and in practice, is difficult to obtain. The smallest spread in energies in the spectra obtained was ≈100meV, thus resolution was estimated to be ≤100mV.

3.5 Deduction of β^+ flux

3.5.1 Source calibration

The strengths of the sources were determined by using an intrinsic Ge detector to compare the measured 511keV and 1.27MeV rates with that obtained from a commercially made, encapsulated ^{22}Na source. The activity of the calibrated source was measured to be 1.277μCi on 17/2/1987 by the manufacturers - Amersham International - and the strength at the time of the study was calculated using the known decay rate of ^{22}Na (half-life:2.62 years).

The sources were positioned at distances between 300mm and 600mm from the Ge detector head in order to minimise the effect on the measurements from the differences in the active areas (6mm and 3mm diameter for the test beam sources and 1mm diameter for the calibrated source). The detector head was shrouded with Pb bricks to reduce the background counts. The signal from the detector was fed into an Ortec 572 Spectroscopy Amplifier, then presented to a 5300 Norland Multichannel Analyser where the number of counts in the peaks resulting from the 511keV and 1.27MeV γ-rays were integrated. The background was calculated by integrating regions on either side of the peaks. A number of runs were taken at different source-detector distances and following background subtraction, the strengths were calculated with knowledge of the calibrated source activity. As the count rate is proportional to the activity, a comparison with the results from the calibrated source gave values of (64.4±0.7) and (44.9±0.7)μCi for the W- and Pb-backed sources, respectively, at the time of the W study. The activity of the Pb-backed source, when used again later for the Ni work, was found to have decayed to (40.4±0.7)μCi.

3.5.2 Backscattering coefficient

From studies of β^+ particle impact on various targets (for example: MacKenzie *et al* (1973) and Arifov *et al* (1982)), it is known that materials with higher Z (atomic number) values, such as W (Z=74) and Pb (Z=82), exhibit a greater propensity to backscatter the particles. Thus, the flux incident upon the foil is likely to contain a significant component due to β^+ particles scattered from the source support. In the

present study, measured values of the backscattering coefficient for W and Pb from the Doppler broadening work of MacKenzie *et al* (1973) were used to calculate the total flux in the forward direction (that is, towards the foil). For W, with ^{22}Na, and Pb, using a ^{68}Ge source, the coefficients used were (0.480±0.011) and (0.516±0.012) respectively, thus giving (74.0±0.6)% and (75.8±0.6)% of the total β^+ emission directed towards the moderator. Although the value for Pb was taken with a ^{68}Ge source, which has an endpoint positron emission energy of 1.88MeV, subsequent studies by Kuzminikh and Vorobiev (1979) have produced results for both W and Pb with ^{22}Na which are in accord with those of MacKenzie *et al* (1973).

As stated in Section 2.4, the energy distribution of the β^+ particles emitted in the forward direction is influenced by the process of backscattering from the source mount. In the case of ^{22}Na, this changes the mean energy, $\bar{E}$, of the β^+ emission from 0.26MeV to 0.15MeV for a Pb backing (Mourino *et al*, 1979). However, the effect of backscattering on the geometric distribution is as yet unknown; in this study it has been assumed to be isotropic.

Since the source was deposited directly onto the backing and remained uncovered the effect of self-absorption was presumed to be small. This assumption was confirmed in the study of Massoumi *et al* (1988) who found that the β^+ flux from a ^{22}Na source of strength ≈5mCi and with an active diameter of 4–5mm was as expected from consideration of the activity, the branching ratio and the attenuation by the Ti window. There was, therefore, negligible self-absorption.

3.5.3 Solid angle effect

Of the forward going β^+ particles from the source, only a fraction strike the moderator and this is dependent on the foil size, source area and the source-foil distance. In the two studies, the exposed region of the foil was 8mm and 10mm in diameter for the W and Ni respectively. The sources were approximately 6mm (W-backed) and 3mm (Pb-backed) in diameter and the source-foil distance was ≈1.5mm. From the relative sizes of the sources and the moderator and their separation distance, it is clear that the effective solid angle cannot be calculated by simply assuming a target-point source geometry. By considering the number of β^+ from an elemental area of source activity striking an elemental area on the foil, the mathematical description of this complex

extended-source arrangement can be written as

$$N = \int \frac{s^2 t^2 n ds dt}{t(d^2+s^2)^{3/2}} \int \frac{\cos(\alpha-\beta) d\alpha d\beta}{d^2+s^2+t^2-2st\cos(\alpha-\beta)} \qquad 3.1$$

the solution of which is possible only by iteration (Wonnacott, 1987). In Equation 3.1, N is the number of particles striking the foil per second, n is the number of particles per second per cm^2 per steradian, d is the source-moderator distance and the position of the elemental areas on the source and foil are given in polar co-ordinates by (s,α) and (t,β).

Therefore, an estimate of the flux incident on the moderator was made by dividing the source into six "ring elements" of equal activity and calculating, for each element, the ratio of the solid angle subtended by the foil over 2π. The number of β^+ particles impinging on the foil from each element was deduced by: (a) assuming an isotropic distribution of the emitted particles; (b) including the backscattered flux from the source-mount; (c) using the ^{22}Na β^+ decay branching ratio of 0.906. The values thus determined were summed to give the total number of β^+ particles incident on the foil. Based upon these estimates the number of β^+ particles calculated to strike the W foils were $(8.9\pm0.3)\times10^5 s^{-1}$ and $(7.2\pm0.2)\times10^5 s^{-1}$ with total β^+ emissions of $21.5\times10^5 s^{-1}$ and $15.1\times10^5 s^{-1}$, respectively, for the W– and Pb–backed sources. In the Ni study, this value was deduced to be $(7.2\pm0.2)\times10^5 s^{-1}$ compared to a total β^+ emission of $13.5\times10^5 s^{-1}$ from the Pb-backed source; the greater striking fraction is due to the larger foil size.

3.6 Transport efficiency

The transport efficiency of the axial magnetic field system was assumed to be unity, except for the grid transmission effect. A total of four 10mm diameter grids were employed in the W study for acceleration and retardation, each fabricated from nominally 80% transmission copper micromesh.

In a separate experiment, an identical mesh and holder arrangement was mounted on a manipulator at position A (Figure 3.1) and inserted into the beam. From a measure of the number of slow e^+ detected with and without the presence of the extra grid in

the beam path, the transmission coefficient of the Cu mesh was established to be (0.77±0.01). Thus, giving an overall transmission of (35±1)%. Inserting the holder without the mesh resulted in <0.1% change to the intensity indicating that the beam diameter was less than 10mm. For the Ni study 5 grids were used, therefore the transmission here was calculated to be (27±1)%.

3.7 Detection efficiency

The detection efficiency of the channeltron to slow e^+ was deduced by placing, in its proximity, an auxiliary NaI(Tl) counter. The channeltron and NaI(Tl) pulses were fed into a TAC-MCA coincidence arrangement. The relevant single and double coincidence rates with the slow beam "on" and "off" were counted and the required efficiencies were extracted after allowing for the background events and the annihilations at the grids before the channeltron. A schematic diagram of the timing system is shown in Figure 3.5.

The NaI(Tl) detector monitored γ–rays of ≤511keV energy and the corresponding signal was presented to an Ortec 454 Timing Filter Amplifier (TFA) which integrated and amplified the pulses from the photomultiplier. After shaping, the pulses were fed into an Ortec 473 Constant Fraction Discriminator (CFD) from which the output, with the introduction of a delay, was used as the stop signal of the Ortec 437A Time-to-Amplitude Converter (TAC). The channeltron signal was passed into a fast pre-amplifier (x10 gain) and then fed into an Ortec 473 CFD, with the resultant pulses presented to the TAC as the start signal. For every true and random coincidence event the TAC produced a bipolar pulse with an amplitude proportional to the time interval between the start and stop pulses. The TAC output was recorded with a Norland 5300 Multichannel Analyser (MCA) in the pulse height analysis mode and from this the number of coincidence events was deduced by integration of the spectrum. Runs were taken with the slow beam on (that is, the total flux) and the slow beam off (when the slow e^+ were retarded) and the following procedure was employed to calculate the slow e^+ detection efficiency of the channeltron

The total number of counts monitored by the NaI(Tl) detector, N_{NaI}, can be expressed in terms of counts due to annihilations of slow e^+ at the channeltron (N_s) and at the grids (N_g), annihilations of fast e^+ at the channeltron (N_f) and at the grid (N_{gf}) and the

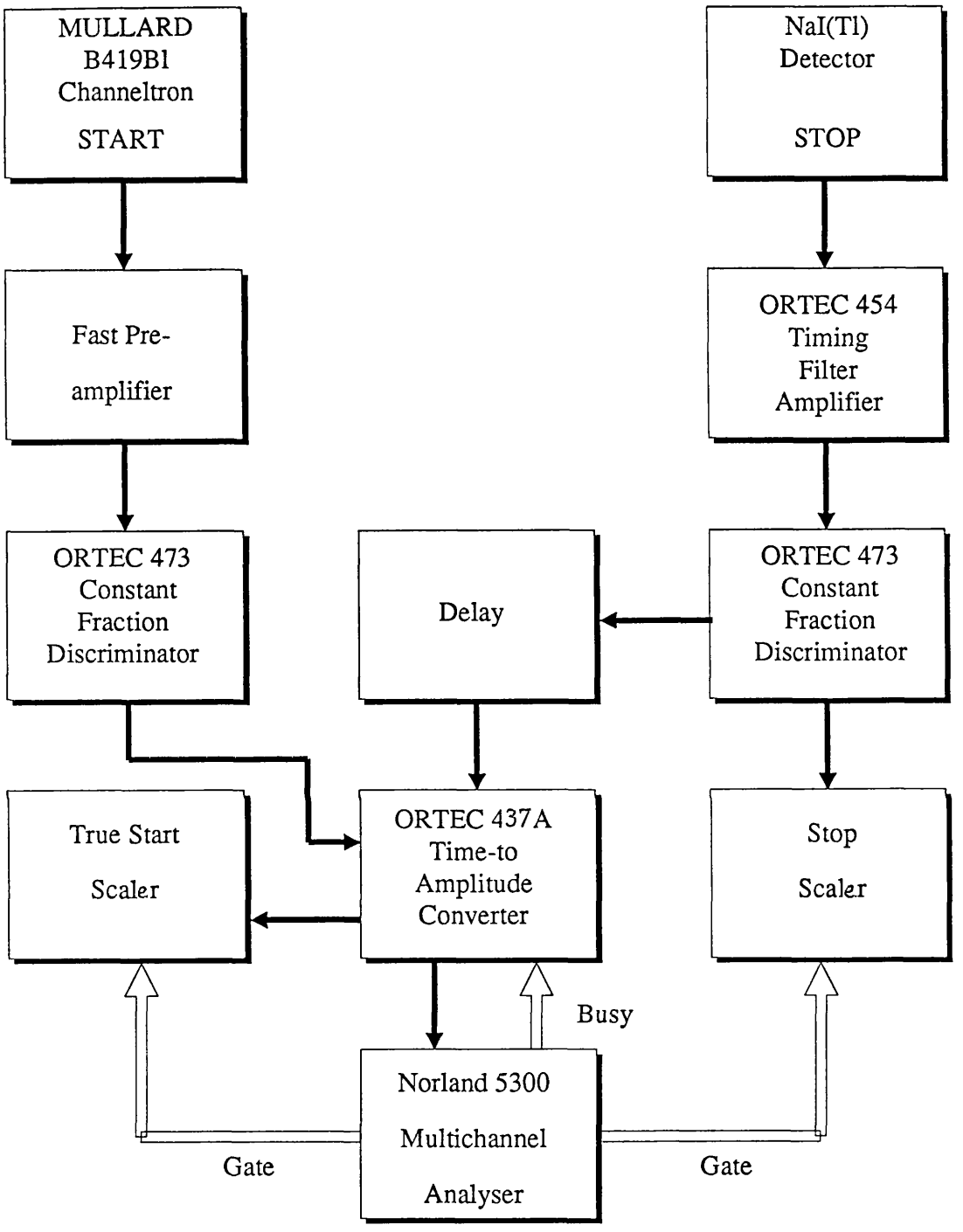

Figure 3.5 Block diagram of the timing electronics employed in the deduction of the channeltron efficiency

background contribution, N_b. Thus

$$N_{NaI} = 2\varepsilon_{NaI}(N_s+N_f+N_g+N_{gf})+N_b \qquad \text{Beam on} \qquad 3.2$$

$$N_{NaI} = 2\varepsilon_{NaI}(N_f+N_{gf})+N_b \qquad \text{Beam off} \qquad 3.3$$

where ε_{NaI} is the efficiency of the NaI(Tl) detector; the factor 2 in the equations allows for the two annihilation γ–rays.

The background count rate was assumed to be the same for beam on and beam off as the slow e^+ were retarded at the moderator which was shielded by 10cm of Pb and also at a distance of 1.5m from the detectors. The NaI(Tl) crystal, too, was wrapped in layers of Pb, thus significantly reducing the contribution from background events.

Subtracting Equation 3.3 from Equation 3.2 gives

$$\Delta N_{NaI} = 2\varepsilon_{NaI}(N_t) \qquad 3.4$$

where

$$N_t = N_s + N_g \qquad 3.5$$

For the channeltron, measuring a total number of counts, N_c,

$$N_c = \varepsilon_s N_s + \varepsilon_f Nf \qquad \text{Beam on} \qquad 3.6$$

$$N_c = \varepsilon_f N_f \qquad \text{Beam off} \qquad 3.7$$

where N_s and N_f are defined as above and ε_s and ε_f are the slow and fast positron detection efficiencies of the channeltron respectively.

Subtracting Equation 3.7 from Equation 3.6 gives

$$\Delta N_c = \varepsilon_s N_s \qquad 3.8$$

From Section 3.6 it was seen that (23±1)% of the slow e^+ beam was stopped by a single grid. Using this value the total transmission after the 3 grids in front of the

channeltron was computed to be (45±1)%. It was assumed that re-emission of the stopped e^+ did not occur in the form of Ps or epithermal e^+. Furthermore, the study showed that <0.1% of the e^+ was intercepted by the grid holder, thus contributing a negligible amount to the measured NaI(Tl) signals.

Equation 3.8, therefore, becomes

$$\Delta N_c = \varepsilon_s(0.45 \times N_t) \qquad 3.9$$

The coincidence events can be expressed thus

$$\Delta N_{coin} = (\Delta N_{NaI} \times \Delta N_c)/N_t \qquad 3.10$$

where ΔN_{coin} is the number of [beam on minus beam off] coincidence counts registered on the MCA. Substituting in equation 3.9 into 3.10 gives

$$\varepsilon_s = \Delta N_{coin}/(0.45 \times \Delta N_{NaI}) \qquad 3.11$$

Using Equation 3.11, the efficiency of the channeltron was found to be (62±8)% at the time of the W work.

This was checked by deducing the absolute efficiency of the NaI(Tl) counter using the ^{22}Na source of known activity employed in the Section 3.5.1. The source was placed close to the channeltron cone and γ–rays of energies ≤1.27MeV were detected by the NaI(Tl) detector. A ^{60}Co source was placed in the same position and the emitted 1.7 and 1.3Mev γ–rays were used to adequately mimic the contribution from Compton scattered 1.27MeV photons. Thus, the relevant correction was applied to the ^{22}Na spectra. This efficiency was calculated using Equations 3.4, 3.5 and 3.9 and found to be in accord with that obtained using the first method. However, the difference in activity sizes and difficulties in the exact positioning of the sources resulted in larger systematic errors. The calibration using the first method was repeated after the Ni work and ε_s was found to (54±9)%.

3.8 Results and discussion

3.8.1 W(100) foils

Six W(100) foils, of thicknesses 1000-18000Å, were employed for investigation into the moderator properties of thin single crystal films. Each sample was subjected to temperatures of 1600-2400°C a number of times until either the increase of the slow e^+ yield was not statistically significant (that is, the yield had plateaued) or the foil was damaged. The maximum number of slow e^+ emitted are listed in Table 3.1 together with the number of heating cycles undergone by each foil. Two efficiencies are noted in Table 3.1: the first is the number of slow e^+ per $ß^+$ particle emitted by the source (after grid correction) and the second is the yield after application of the necessary corrections due to geometry, backscattering, detector efficiency and grid transmission. The large differences in the values clearly illustrates the importance of considering the factors discussed in Sections 3.5, 3.6 and 3.7. when deducing the $ß^+$–e^+ conversion efficiencies of the foils. The correction factors applied are summarised in table 3.3.

In general a number of heating cycles were required (≈5) at temperatures of about 2200°C to gain the highest efficiencies. A maximum yield of $(8.8\pm1.2)\times10^{-4}$ was obtained from a 2000Å "good" foil (that is, with $\chi_{min} \leq 1.5\%$) after the 5th heating cycle, although a 2000Å "bad" foil was found to give a similar value. However, both yields had not reached a plateau before damage occurred to the foil. The χ_{min} value of the "bad" foil was not known, therefore conclusions could not be drawn when comparing its yields with that from the "good" foil. A rough comparison was made with the efficiency obtained from a W mesh moderator, studied under the same conditions. Two overlapping W meshes, nominally 65% transmission, were found to emit slow positrons with an efficiency of approximately 6×10^{-4}. This will increase with the use of a greater number of meshes and as shown in Chapter 5, the yield will reach an optimum value. Beyond this value however, the efficiency begins to decrease with the addition of meshes as the positrons are intercepted before extraction.

The expected yields from the foils were calculated using the exact solution to the diffusion equation (Equation 2.8) obtained by Beling *et al* (1987) with the exponential implantation profile for ^{22}Na (Equations 2.1 and 2.2) (Brandt and Paulin, 1977, Mourino *et al*, 1979). The backward and forward emission efficiencies of single

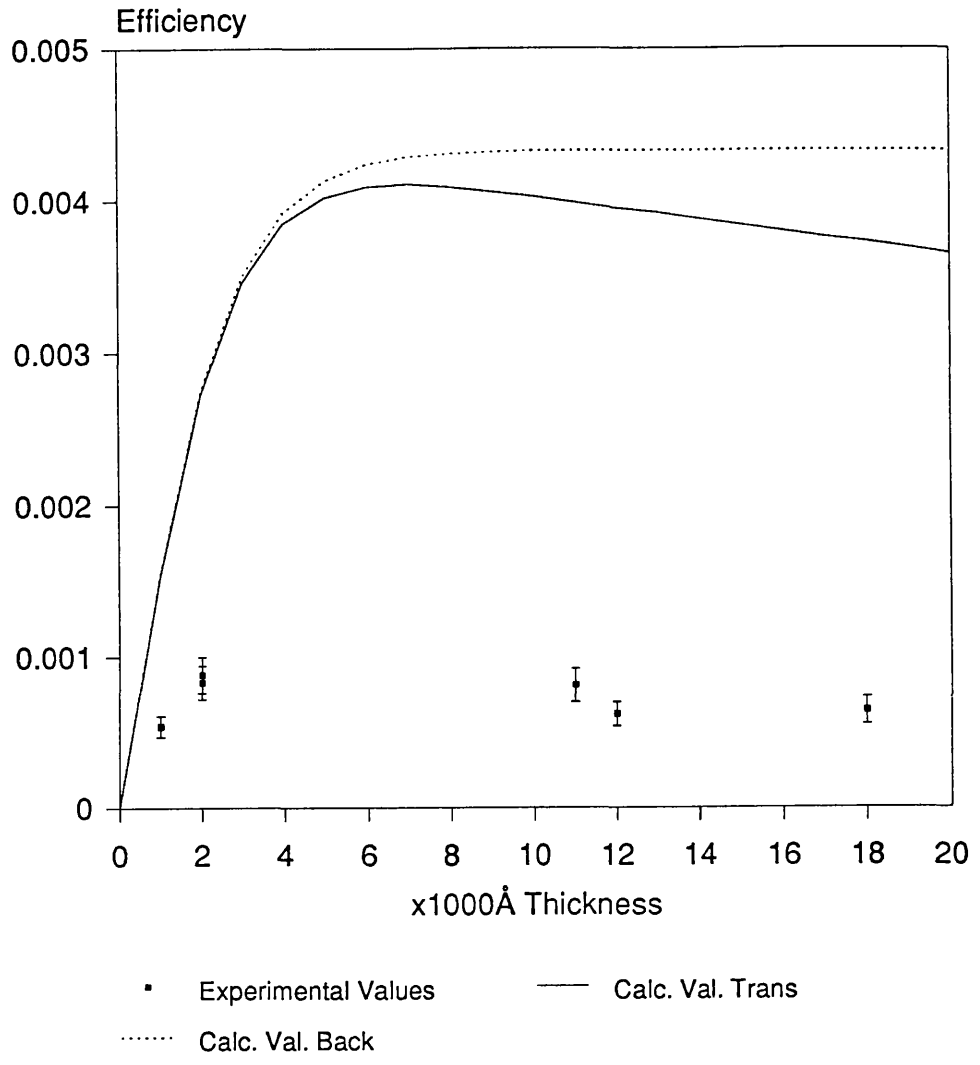

Figure 3.6 Variation of the measured and calculated yield with thickness for W(100) foils

crystal W(100) were computed for various sample thicknesses (Simpson, 1987) and are presented in Figure 3.6, together with the experimental data from the present study. Empirically derived values of 1350Å for the diffusion length of annealed single crystal W (Vehanen *et al*, 1984) and 1/3 for the branching ratio (Schultz *et al*, 1983) were used. The mean energy of the β^+ emission (with a high Z backing) was

estimated to be 0.16MeV (from Mourino *et al*, 1979).

The calculated values shown in Figure 3.6 indicate that the yields expected for primary moderation with thin foils are comparable for the transmission and backscattering modes. These are presented in Figure 3.6 by the full and dotted curves, respectively. The predicted values of the transmission efficiency rise to a maximum of $4x10^{-3}$ at 7000Å and thereafter, decrease very slowly by 10% at 18000Å. The experimental values peak at 2000Å with $8.8x10^{-4}$, a factor of 4.5 less than expected. The shape of the distribution, maximising at 2000Å and falling to 70% of this value at 18000Å, also departs from the expected trend. Both the yield and the distribution indicate that the annealing technique may not have sufficiently lowered the defect concentration, caused by the presence of impurities and by handling, or reduced the surface contamination. Characterisation procedures were not available to determine the effects of such conditions.

Results from other experimental studies are noted below, however, β^+–e^+ conversion efficiencies, ε, defined using different correction factors make comparisons with the present study difficult.

The use of W(100) as a primary transmission mode moderator was first investigated by Lynn *et al* (1985) in a short study using a 5000Å film. In this work the film was heated in 10^{-7} Torr of O_2 for 20 minutes then flashed three times at temperatures of 1800-2000°C in 10^{-8} Torr vacuum before insertion into an e^+ beam apparatus. An efficiency of $\approx 3x10^{-4}$ was observed, which rose to $4x10^{-4}$ after repeated *in situ* annealing (1500-1800°C) and O_2 treatments. However, Lynn *et al* (1985) do not define their conversion efficiency or state the corrections used.

More recently, using a somewhat different annealing procedure, Gramsch *et al* (1987) have studied a 10000Å W(100) foil and obtained a value of $\varepsilon \approx 5.9x10^{-4}$. The foil was initially heated to 800°C, then annealed at 2100°C for 2 minutes at a pressure of $5x10^{-7}$ Torr. Thereafter, it was transferred to a test system and placed in direct contact with a 0.9mCi, Kapton covered, ^{22}Na source. This process was repeated until the maximum efficiency was obtained.

Gramsch *et al* (1987) have defined ε as the number of slow e^+ leaving the foil on the side opposite the source divided by the β^+ activity. This convention produces a

figure-of-merit by ignoring geometry considerations and losses of β^+ in the source but allows for the correction of the measured flux due to transport and detection efficiencies (points discussed in sections 3.6 and 3.7). This results in a combined source-moderator efficiency which as Gramsch *et al* (1987) note, may be much less than the true efficiency of the moderator when large ^{22}Na sources are used for which self-absorption of the β^+ flux is not negligible. However, as noted above, a study by Massoumi *et al* (1988) has shown that self-absorption is negligible for sources below an activity of 5mCi, so in the case of Gramsch *et al* (1987) the true efficiency could be calculated by considering the points discussed in section 3.5. It is thus pertinent in the determination of moderator performance to use small, specially constructed sources in which self-absorption is minimised and the contribution of β^+ backscattered from the source mount can be estimated.

The highest value obtained by Gramsch *et al* (1987) for ε was $(9.1\pm0.4)\times10^{-4}$ when a ^{22}Na source was deposited onto a 1.5mm thick W substrate and placed in direct contact with the W(100) foil. The geometry of this arrangement is such that the solid angle effect does not need to be considered. The authors have allowed for the transport and detection efficiencies, however, they have not accounted for backscattering from the substrate. If a rough correction is made for this effect, it can be seen that the value obtained in the present study is about 73% of that from the investigations of Gramsch *et al* (1987).

Turning to the energy profile of the emitted beam, the full width at half maximum, FWHM, of the longitudinal spread was found to be ≈5eV when examined close to the channeltron. The distribution was deduced by differentiating the flux obtained in the spectrum with respect to the applied voltage on the retarder. The point of retardation was subsequently moved to the source end, 4mm from the moderator. However, the electronic voltage ramping system, used in the Ni investigation, was not available for the W(100) study, therefore a 5000Å W(110) sample was tested after the Ni work. The e^+ energy spectrum from W(110) was assumed to be similar to that of W(100) as the different face orientation changes the dipole contribution of the work function by only a few tenths of eV.

For the same 5eV FWHM spread obtained at the channeltron, a value of 1.7eV FWHM was found for retardation at the source end, located at 2.57V above the applied potential. This is shown in Figure 3.7, where the relative voltage, V, is the

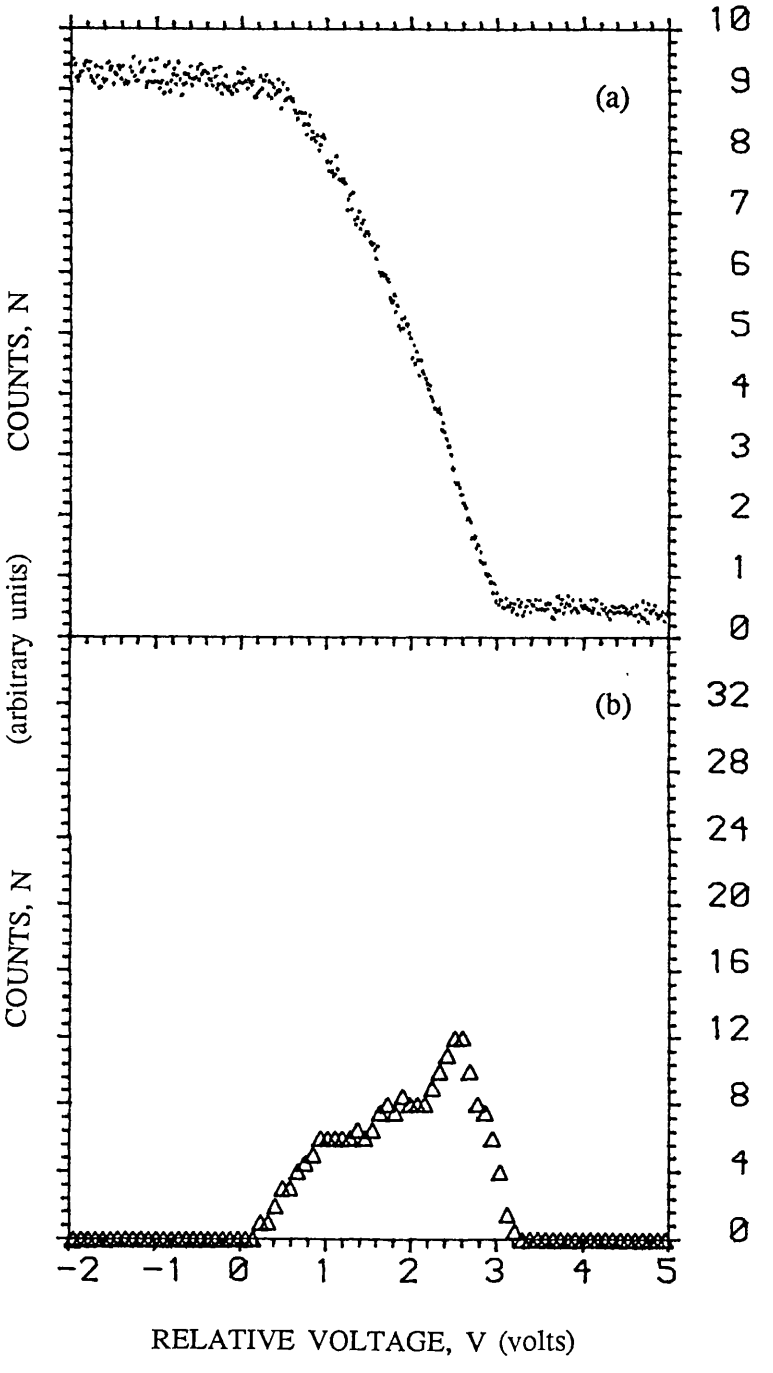

Figure 3.7 (a) Retarding spectrum of 5000Å W(110) foil

(b) Differentiated spectrum of 5000Å W(110) foil where relative voltage, V, is the difference between the potentials applied to the foil and the retarder

difference between the potentials applied to the moderator and the retarder (all measured energy spreads refer to the longitudinal component). By varying the cone potential, the cause of the broadening in the energy distribution was discovered to be due to **ExB** effects at the channeltron entrance. For a perfect single crystal with a clean surface, the energy of emission of the e^+ is governed by the workfunction value of the material and the thermal kinetic energy. However, the energy distribution obtained from the W(110) sample is two orders of magnitude larger than that accounted for by thermal spread. Possible causes of this may be from: coupling between the transverse and longitudinal velocity components in the magnetic field; elastic scattering (Gullikson *et al*, 1985); surface roughness; inelastic scattering with surface adsorbates. Observation of the surface clearly showed distortions which would enhance the angle of emission of the positrons. Dale *et al* (1980) have stated that a clean W surface rapidly oxidises on exposure to air. However, growth of the oxide layers greatly decreases after two monolayers of coverage, thereby the surface is passivated. The annealing procedure developed in this study involves the exposure of the films to air, therefore, the sample surfaces, if clean, will inevitably gain some oxygen coverage. However, the location of the spectrum peak, at 2.57V above the applied voltage, questions the identity of the adsorbate species. The peak position, after consideration of contact potentials (≈few tenths of V) and angular effects, is indicative of the workfunction of the material. In the case of W, the value of $-\phi_+$ has been shown by Wilson (1983) and Gidley *et al* (1987) to change with adsorbate coverage (Section 2.4). For layers of the order of a monolayer, $-\phi_+$ was found to be 2.95eV for (W(110)+C) and 4.1eV for (W(110)+O) (Gidley *et al*, 1987). Although the value obtained in the study infers a C overlayer, conclusions cannot be drawn without further investigation.

A W grid moderator, annealed in a similar way, was tested and found to have an energy spread of 2.8eV FWHM. The emission of e^+ from surfaces which are not parallel to the longitudinal axis is reflected in the larger energy spread observed from the mesh thus demonstrating one of the benefits of using foil moderators.

3.8.2 Ni(100) foils

In this study, five Ni foils in the thickness range 3000-15000Å were investigated. An annealing procedure was developed which consisted of heating the samples for 5–10 minutes at ≈200°C followed by cycles of up to 2 minutes at 650–950°C. The resultant slow e^+ yields which were measured are presented in Table 3.2 with the correction factors applied listed in Table 3.3. All the films were repeatedly heat-treated until the yields plateaued; unlike the W foils none of the Ni samples were damaged by evaporation due to greater temperature control. The highest yield obtained was $(6.5\pm1.0)\times10^{-4}$ from a 5000Å foil annealed for a total of 25 minutes at 650°C, however, all samples were found to convert β^+ to e^+ with an average efficiency of 1×10^{-4} prior to annealing at temperatures greater than 200°C. The maximum yield obtained in this study is similar to that measured by Gramsch *et al* (1987), $(6.6\pm0.3)\times10^{-4}$, from a 3000Å foil annealed *in situ* and under vacuum conditions of 10^{-8} Torr at ≈1400°C. However, these authors have not considered the points discussed in Section 3.5 on the proportion of the β^+ particles striking the foil, therefore, comparison between the values from the two studies is not strictly valid.

The experimental results as a function of thickness, together with the expected efficiency of the foils as calculated in Section 3.8.1, are shown in Figure 3.8. The transmission efficiency is denoted by the full curve and the dotted line represents that of the backscattering mode. The discrepancy, of about factor 2.5, between the maximum predicted and obtained values is not as large as that found for W. The calculated values used a diffusion length of 1100Å (Vehanen *et al*, 1984) and a branching ratio of 0.45 deduced by Gullikson *et al* (1985); substituting the latter value with that of 0.39 found by Mills (1981b) leads to a difference with the measured yields of factor 2. Again the variation of ε is not expected for the 5000-15000 range since the ^{22}Na β^+ mean implantation depth is much larger than the foil thickness for single crystal Ni.

The diffusion length employed in the computation of the efficiency was reduced from the annealed single crystal Ni value of 1100Å until a value of 777Å (dashed curve in Figure 3.8) when the resultant efficiencies maximised at 5000Å, coinciding with the experimental data. Two points are indicated by the distribution. First, the highest measured yield is still less than that expected by ≈38%, implying that the discrepancy cannot be attributed to bulk defects alone if the concentration is uniform throughout

the foil. Therefore, surface contamination must also be a factor. Secondly, the sharp decrease in ε between 5000Å and 15000Å in the experimental data cannot be accounted for by a constant value of the diffusion length in this thickness range. Such behaviour might be associated with problems in fully annealing the thicker foils such that e^+ may become trapped in the bulk before reaching the surface.

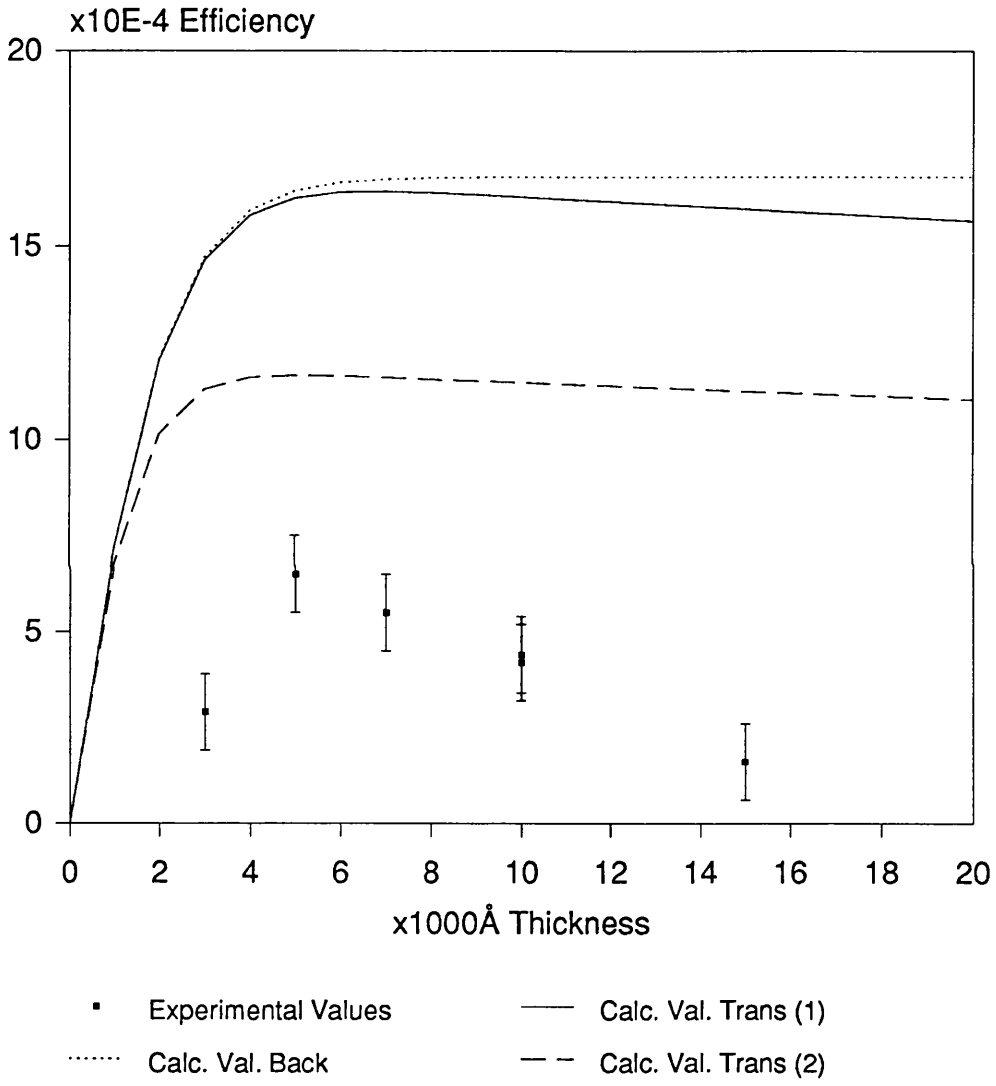

Figure 3.8 Variation of measured and calculated yield with thickness for Ni(100) foils

The FWHM of the e^+ energy spread parallel to the magnetic guiding field, uncorrected for analyser response, ranged from 250 to 450meV though most typically obtained values were (330±70)meV. Approximately 60% of the total number of e^+ were contained in this energy region. The spectrum taken from a 3000Å sample, shown in the integral and differential forms in Figure 3.9, has a FWHM of 330meV located at a measured energy of 1.3±0.1eV above that gained from the moderator by the applied potential. The latter result is consistent with the e^+ workfunction, ϕ_+, measurements of Gullikson *et al* (1985) who find a value of ϕ_+=−1.4eV for a clean Ni(100) surface. Surface contamination and distortion, contact potentials and angular effects must be considered if deducing the work function. In addition, the effect of the magnetic property of Ni is unclear, however this may give rise to angular effects and so contribute to the tail observed between 0 and −1V in Figure 3.9.

Although the maximum efficiency of the Ni foils is about (74±22)% that of the W samples, the FWHM of the Ni (330meV) is 5 times narrower than that for W (1.7eV) shown in Figure 3.7. Furthermore, this is only about a factor of 2 larger than the value of 165meV obtained at ϕ_+=1.1eV by Schultz *et al* (1986) using electron heating in UHV. Again, as in the case of W, contribution to the measured spread in energy can arise from surface distortion (which was observed), angular effects and inelastic interactions on emission. The species of surface adsorbate was uncertain; similarly with W, C is the major bulk impurity in the Ni foils and migration to the surface can occur on heating. Also, oxide build up is rapid up to a few monolayers, whereafter the rate of formation is significantly reduced.

3.9 Summary

The developments in the technique of film growth using the evaporation method have resulted in the ability to fabricate epitaxial films of uniform thickness and large area (Mertler *et al*, 1982). The availability of such thin self-supporting films of almost perfect crystalline structure and high purity has enabled the study of their use as $ß^+$ moderators in the transmission mode. In this work six W(100) foils, with thicknesses in the range 1000-18000Å, and five Ni(100) foils from 3000Å to 15000Å were subjected to heat treatment and investigation of the slow e^+ emission characteristics.

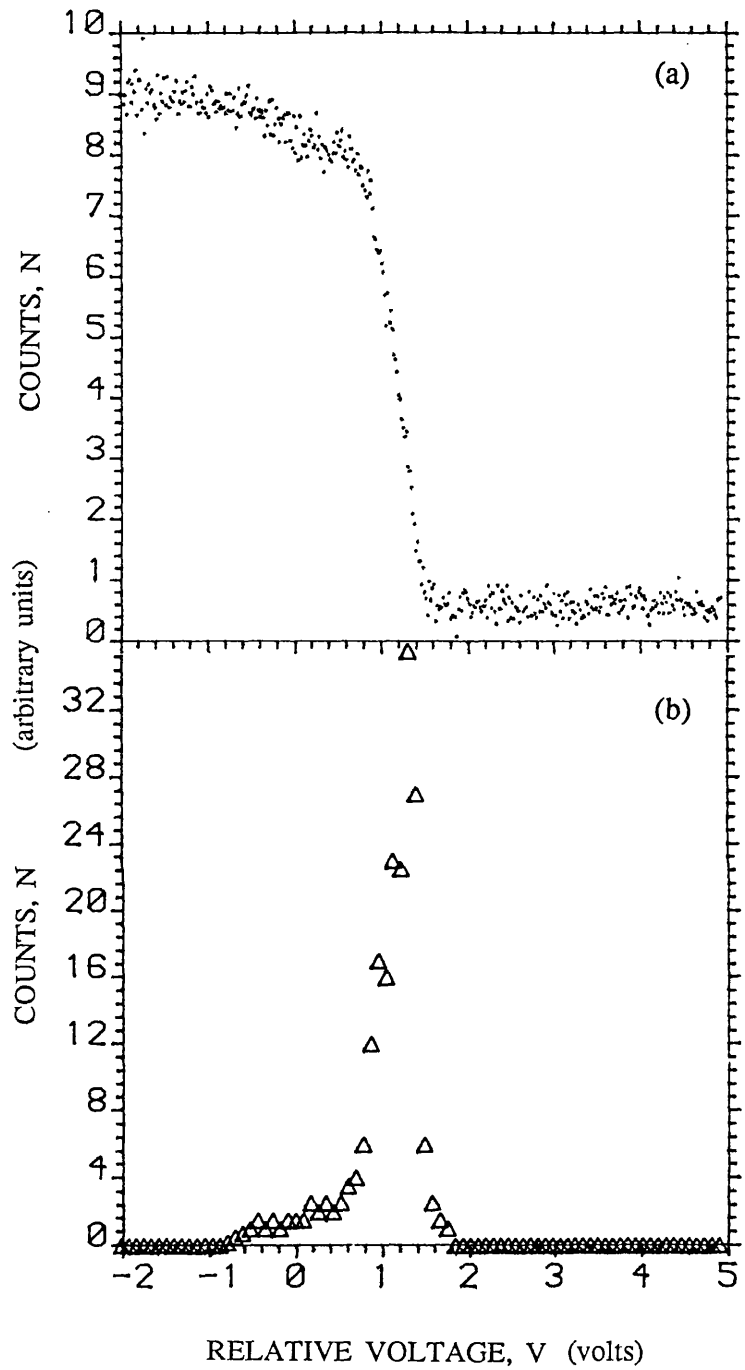

Figure 3.9 (a) Retarding spectrum of 3000Å Ni(100) foil
(b) Differentiated spectrum of 3000Å Ni(100) foil where relative voltage, V, is the difference between the potentials applied to the foil and the retarder

A simple annealing technique was developed whereby foils, supported between meshes or rings of the same material, were resistively heated in low vacuum conditions ($6x10^{-2}$ Torr). The heating cycle consisted of 5–10 minutes at ≈200°C followed by flashing at ≈2200°C for the W foils and longer periods of up to 2 minutes at 650–950°C for the Ni samples. The foils were found to emit slow e^+ upon transfer, in air, to a test system.

In order to make a meaningful comparison of the slow e^+ flux not only with theory but also with experimental values obtained by using different techniques it was found essential to allow for certain factors. In this investigation these were:

(i) the number of β^+ which strike the moderator including source strength, backscattering and solid angle considerations;
(ii) the absorption of the slow e^+ in the beam by the grids;
(iii) the detection efficiency of the channeltron to slow e^+.

These factors were considered in Sections 3.5, 3.6 and 3.7 and summarised in Table 3.3.

The total number of slow e^+ produced at the moderator was obtained by dividing the measured fluxes by the transport efficiency due to grid losses and the channeltron detection efficiency. The final efficiency was then computed by dividing this number by the total number of β^+ particles impinging upon the foil. Thus, the efficiency has been defined as the total number of slow e^+ per fast β^+ particle *incident on the foil.* These values were listed in Tables 3.1, 3.2 and 3.3.

The maximum efficiencies obtained were $(8.8\pm1.2)x10^{-4}$ for the W(100) from a 2000Å foil and $(6.5\pm1.0)x10^{-4}$ from a 5000Å Ni(100) sample. These values are a factor of 4.5 (W) and 2.5 (Ni) less than the maximum yields predicted from calculations using the experimentally derived implantation profile (Brandt and Paulin, 1977, Mourino *et al*, 1979) and the solution to the diffusion equation (Beling *et al*, 1987). However, they are comparable to the results obtained by Gramsch *et al* (1987) employing a more complex annealing technique of electron bombardment heating in high vacuum conditions.

The FWHM of the longitudinal energy spread from W foil was found to be 1.7eV

compared to 2.8eV from a W grid, measured close to the moderator. Furthermore, the FWHM of the energy distribution of the e^+ emitted from the Ni samples was found to be ≈0.3eV, six times narrower than that from W samples annealed in a similar fashion.

Thus, the study has shown that thin W and Ni film moderators can be annealed in a simple manner and employed, in vacuum conditions typical of those in gas-collision experiments, to efficiently produce slow e^+ with a longitudinal energy spread much narrower than that from the widely used W mesh moderators.

Foil thickness Å	No. of times heated	Temperature range °C	Maximum number* of slow e^+ s^{-1}	Slow $e^+/ß^+$ emitted $x10^{-4}$	Corrected yield** $x10^{-4}$	Comments
1000	5	1800	298±9	1.25±0.04	5.4±0.7	"Bad" foil, yield plateaued Source: 64.4µCi
2000	5	1800-2200	486±14	2.04±0.07	8.8±1.2	Yield did not plateau Source: 64.4µCi
2000	5	1600-2200	368±11	2.22±0.07	8.3±1.1	"Bad" foil, yield did not plateau Source: 44.9µCi
11000	6	1800-2200	362±11	2.18±0.07	8.1±1.1	Yield plateaued Source: 44.9µCi
12000	2	2200-2400	277±8	1.67±0.05	6.2±0.8	Yield did not plateau Source: 44.9µCi
18000	10	1600-2200	284±8	1.71±0.06	6.4±0.9	Yield plateaued, annealed at 10^{-6} Torr Source: 44.9µCi

* Number of slow e^+ s^{-1} after grid correction
** Yield after grid, solid angle and detection efficiency corrections

Table 3.1 Slow e^+ transmission efficiencies of thin W(100) foils

Foil thickness Å	Total annealing time to reach maximum yield minutes	Temperature range °C	Maximum number* of slow e^+ s^{-1}	Slow e^+/β^+ emitted $x10^{-4}$	Corrected yield** $x10^{-4}$
3000	27	650-950	148±9	0.99±0.06	2.9±1.0
5000	25	650-700	325±13	2.17±0.09	6.5±1.0
7000	54	600-750	273±11	1.83±0.07	5.5±1.0
10000	37	650-750	211±8	1.41±0.05	4.2±1.0
10000	12.5	650-900	218±9	1.46±0.06	4.4±1.0
15000	30	650	81±3	0.54±0.02	1.6±1.0

* Number of slow e^+ s^{-1} after grid transmission correction
** Yield after grid, solid angle and detection efficiency corrections

Table 3.2 Slow e^+ transmission efficiencies of thin Ni(100) foils

Study	Calibrated source strength μCi	Size of activity (backing)	Number of e^+ emitted $x10^5$ s^{-1}	Fraction of forward going e^+	Fraction of e^+ striking foil	Number of e^+ striking foil $x10^5$ s^{-1}	Total grid transmis-sion (number of grids)	Detection efficiency
W	64.4±0.9	6mm dia. (W)	21.5±0.3	0.740 ±0.006	0.559 ±0.017	8.93±0.26	0.35±0.01 (4)	0.62±0.08
W	44.9±0.7	3mm dia. (Pb)	15.1±0.2	0.758 ±0.006	0.630 ±0.018	7.19±0.19	0.35±0.01 (4)	0.62±0.08
Ni	40.4±0.7	3mm dia. (Pb)	13.5±0.2	0.758 ±0.006	0.699 ±0.021	7.18±0.22	0.27±0.01 (5)	0.54±0.09

Table 3.3 Summary of correction factors applied to obtain slow e^+ transmission efficiencies

CHAPTER 4
POSITRONIUM BEAM DEVELOPMENT

4.1 Introduction

Since its discovery, the positronium atom has been of continuing interest as a testing ground for fundamental theories of physics. Measurements of fine structure transitions and self-annihilation rates are a valuable check on the accuracy of QED calculations. A number of spectroscopic studies have been performed. Fine structure measurements were first obtained by Mills *et al* (1975) by enhancing the $2^3S_1 \rightarrow 2^3P_2$ transition with an rf field in a weak magnetic field. Their result, (8626.4±2.8)MHz, was within two standard deviations of the theoretical value calculated by Fulton and Martin (1954). The role of Ps as the marker for QED calculations has been supported by the work of Chu *et al* (1984) in the study of the $1^3S_1 \rightarrow 2^3S_1$ transition. Using Doppler-free two-photon spectroscopy, the frequency interval was measured to an accuracy comparable to those in studies with H (Hildum *et al*, 1986, Barr *et al*, 1986).

Also of fundamental interest is the scattering of electrons and positrons from positronium as such experiments provide a test for the invariance of charge conjugation in the leptonic systems of $(e^+e^-e^-)$ and $(e^-e^+e^+)$. If charge conjugation holds, then the ratio of cross-sections for e^+ and e^- should be unity. Calculations of the elastic scattering cross-sections of these interactions have been made by Ward *et al* (1987), together with photodetachment cross-sections for Ps^-, revealing structures close to the first excitation threshold which are similar to those seen in hydrogen (Branscomb 1969) and alkalis (Moores 1976).

Charlton (1987) has proposed a "Ps gas cell" using an intense ($10^9 s^{-1}$) e^+ beam impinging into a box constructed from a suitable converter which may be crossed by the projectile stream of electrons, protons or anti-protons. The last is of particular interest as the reaction,

$$\bar{p} + Ps \rightarrow \bar{H} + e^- \qquad 4.1$$

has been proposed as a viable means of producing anti-hydrogen, $\bar{H}$, by Deutch *et al*

(1986, 1988). Calculations by Humberston *et al* (1987) indicate that the cross-section for this reaction is of the order of 10^5 times greater than the corresponding e^+–$\bar{p}$ radiative capture (Berger *et al*, 1985) and 10^3 times higher if the latter process is laser enhanced (Neuman *et al*, 1983). Recent experiments have achieved optical saturation in thermal Ps of the $1^3S \rightarrow 2^3P$ transition using a frequency doubled, pulsed dye laser (Ziock *et al*, 1990). Excitation to high Rydberg states of Ps have been suggested as a means of cooling Ps for accumulation and subsequently experimentation with anti-protons.

Other projects also await investigation and the recent interest in Ps as a "probe" has, in part, spurred the development of Ps beams. For instance, low energy positronium diffraction technique has been proposed as an investigative tool in analogy to the counterparts with e^- and e^+. This method also possesses certain advantages over other neutral species in surface characterisation. Due to its small mass, higher energies can be used to probe the surface structures not accessible to particles such as He. The first stage of development of this technique has been pioneered by Weber *et al* (1988) in the study of Ps reflection from surfaces; this is discussed below.

In the field of atomic physics, basic collision interactions concerning Ps have yet to be fully investigated. It is, therefore, with the motivation of elucidating some of these processes that the present work has been performed. In the following section Ps emission from solids and gases is discussed in the context of energetic Ps beam production with particular emphasis on gaseous reactions. Advances in the development of the beam technique are described in Section 4.3 and a selection of predicted Ps interactions are presented in Section 4.4.

4.2 Positronium Formation In:

4.2.1 Solids

Since the discovery of Ps formation in a powdered insulator by Paulin and Ambrosino (1968) and the detection of Ps emerging from MgO powder by Curry and Schawlow (1971) following the implantation of e^+, Ps emission has been observed from a large variety of solid surfaces. Three basic processes have been found to govern Ps production from solid media. Two of these, as described in Chapter 2 with reference to metals, are Ps formation by (i) thermal desorption of surface trapped e^+ and (ii)

electron pick-up on ejection of workfunction energy e^+. Ps of such energies (of 0(meV) and 0(eV)) have also been observed from non-metals, for instance quartz (Canter *et al*, 1974a) and the examples given above. Conversion efficiencies are known to be high for these processes, however, with regard to the generation of a variable energy beam, the Ps produced in this way are limited in their use.

In the context of a thermal Ps source, Mills *et al* (1989) have recently investigated the formation of low energy Ps from SiO_2 powder at 4.2K. Cold Ps produced in this manner are advantageous over those that are thermally desorbed from surfaces at higher ambient temperatures in such studies as precision spectroscopy. A time of flight system was employed to deduce the velocity of Ps produced on impacting a high energy pulsed e^+ beam onto a powder target. The 0.3mm thick layer, formed on a liquid He cold finger, was composed of fumed silica grains, estimated to be $\approx$35Å in radius. Positrons incident on the target form Ps within the powder grains which diffuse to the surfaces and escape into voids between the grains (Brandt and Paulin, 1968). The energetic Ps atoms are subsequently slowed down by collisions with surface atoms. As thermal equilibrium is approached, localisation should occur which Mills *et al* (1989) suggest might be seen as a low-energy cut-off in the Ps velocity. However, no cut-off was observed, but a 2% thermalisation of the Ps flux was detected at 4.2K with 19keV implantation energy.

The third mechanism noted is that of epithermal Ps formation where the energy of the ejected Ps implies a lack of thermalisation. This phenomenon has been attributed to surface electron pick-up by non-thermal e^+ scattering out of the solid and as such the energy distribution of Ps formed in this manner will be determined by the epithermal e^+ energies and the formation cross-section at the surface. The formation of epithermal Ps was noted by Howell *et al* (1986) in a study of Ps emission from various clean surfaces. Single crystal samples of Al(111), Au(100), Cu(100) and Ni(100) were bombarded, in UHV, by a pulsed e^+ beam of energy 50–3000eV. The time of flight spectra of the resultant Ps were obtained at a number of energies and Figure 4.1 shows examples of spectra taken at 50eV incident energy. The two peaks at 0 and 200 ns were identified as arising from the annihilation of p–Ps and o–Ps, respectively, with the long decay of the second peak corresponding in energies to the distribution expected from workfunction and thermal Ps. However, a prominent third peak can also be seen in all the spectra at short times (therefore high energies) and has been attributed to fast, epithermal Ps. Howell *et al* (1986) observed epithermal

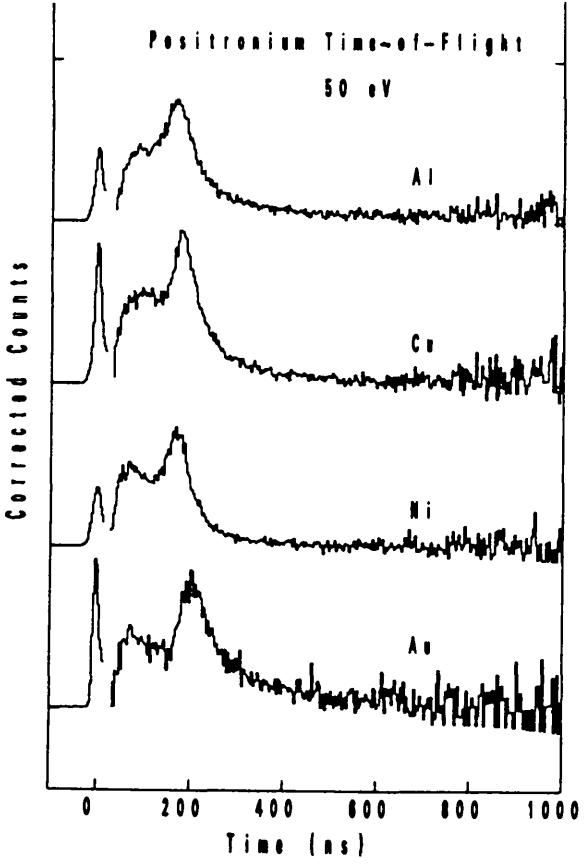

Figure 4.1 Time-of-flight spectra of Ps emission from Al(111), Cu(100), Ni(100) and Au(100) at 50eV incident e^+ energy (Howell *et al*, 1986)

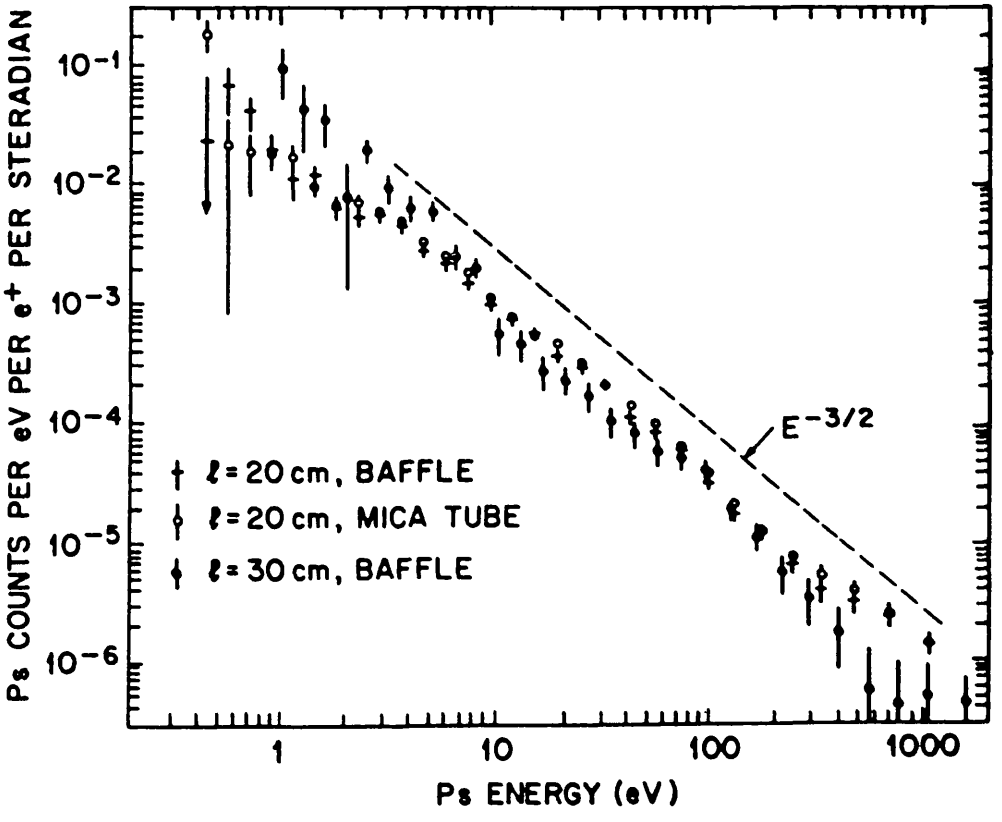

Figure 4.2 Energy spectra of the Ps detected using the beam-foil technique (Mills and Crane, 1985)

Ps formation to be greatest at low energies. These authors estimate that 20–40% of the detected Ps flux was composed of these fast Ps at 50eV incident e^+ energy, with a peak value at ≈10eV Ps energy and a range extending to beyond 40eV.

Fast Ps^- have been observed using the beam-foil technique developed by Mills (1981b). This stable ion composed of e^+ and two e^- has been calculated to be bound with a ground state energy of 0.327eV (Haftel and Mandelzweig, 1989). In the study of Mills (1981b), e^+ were impacted into a thin (40Å) C film in high vacuum conditions and the annihilation quanta were monitored with a high resolution Ge(Li) detector. Ps^- emitted from the surface of the C were accelerated by the application, on a grid following the convertor, of a positive voltage with respect to the foil. The blue-shifted signal from Ps^- annihilation were thus discerned from the 511keV contributions. Ps^- yields were seen to increase with accelerating voltage and at maximum, gave a e^+–Ps^- conversion efficiency of $(2.8\pm0.3)\times10^{-4}$. It has been suggested that, by photodetachment of the extra electron, a variable energy Ps beam may be produced, however a constraint of this method, amongst others, is the short lifetime (500ps) of the Ps^- ion (Mills, 1983).

Using a similar technique, Mills and Crane (1985) observed the production of fast Ps from a 50Å thick C foil. Time of flight spectra were obtained from the detection of o–Ps with a channel electron multiplier array (CEMA) in coincidence with the pulsed e^+ beam. Baffles were positioned prior to the CEMA to reduce the effect of any "bouncing" Ps, thus making the Ps path length purely geometrical. Negative ions and e^- were biassed away by potentials on the baffles and detectors and the remaining e^+ were retarded by a 1500V potential on a grid preceding the baffles. The time of flight data were converted to an energy scale, shown in Figure 4.2, for three different arrangements. The baffles were replaced with a freshly cleaned roll of mica with the expectation of high Ps reflection. However, this was not indicated in the results and, moreover, no change was observed when the baffles were completely removed.

The fast Ps formation was observed to have an energy dependence of $E^{-3/2}$ and extended in range to ≈1keV. From an initial flux of 10^6 e^+s^{-1}, approximately 10 Ps atoms $eV^{-1}s^{-1}$ of energy 10eV were estimated to be emitted into a 3° cone. The efficiency of Ps production with energies between 10–500ev is approximately 2% times the detector solid angle. Though efficient in Ps production and giving a large range of energies, the generation of a Ps beam using this technique would require a

timing system with high resolution.

4.2.2 Gases

Ps formation in dilute gases occurs mainly by the process of charge transfer,

$$e^+ + A \rightarrow Ps + A^+ \qquad 4.2$$

where electron pick-up by the incoming e^+ from the target atom or molecule, A, leaves behind a positive ion. In principle, the energy of the Ps, E_{Ps}, is variable with that of the e^+ and, for the interaction described in equation 4.2, given by

$$E_{Ps} = E_{e+}-E_I+E_b \qquad 4.3$$

where E_{e+} is the energy of the incident e^+, E_I is the ionization energy of the target gas and E_b is the binding energy of the Ps atom formed. For ground state Ps produced in this manner, E_b is 6.8eV. However, processes such as excited state Ps (Ps^*) formation and excitation of the target species have bearing on the production with the resultant effect of Ps with kinetic energy lower than that expected.

Observation of Ps formation in gases is well documented and several workers have made measurements of the total formation cross-sections employing a variety of techniques. From threshold to intermediate energies, in low density gases, three main methods have been employed:

(i) measurement of the triple coincident γ–rays from the decay of o–Ps in all noble and some molecular gases (Charlton, 1980, Charlton *et al*, 1983b and Griffith, 1984);

(ii) measurement of all remaining e^+ following interaction in He, Ar, H_2 and Xe (Fornari *et al*, 1983, Diana *et al*, 1986a,b and Diana *et al*, 1988);

(iii) measurement of total ion yield in conjunction with e^+–ion coincidences in He and H_2 (Sinapius *et al*, 1986, Fromme *et al*, 1986 and Fromme *et al*, 1987).

The first attempt to predict the total Ps formation cross-section was made by Massey and Mohr (1954), using the first Born approximation with H as the target atom. In

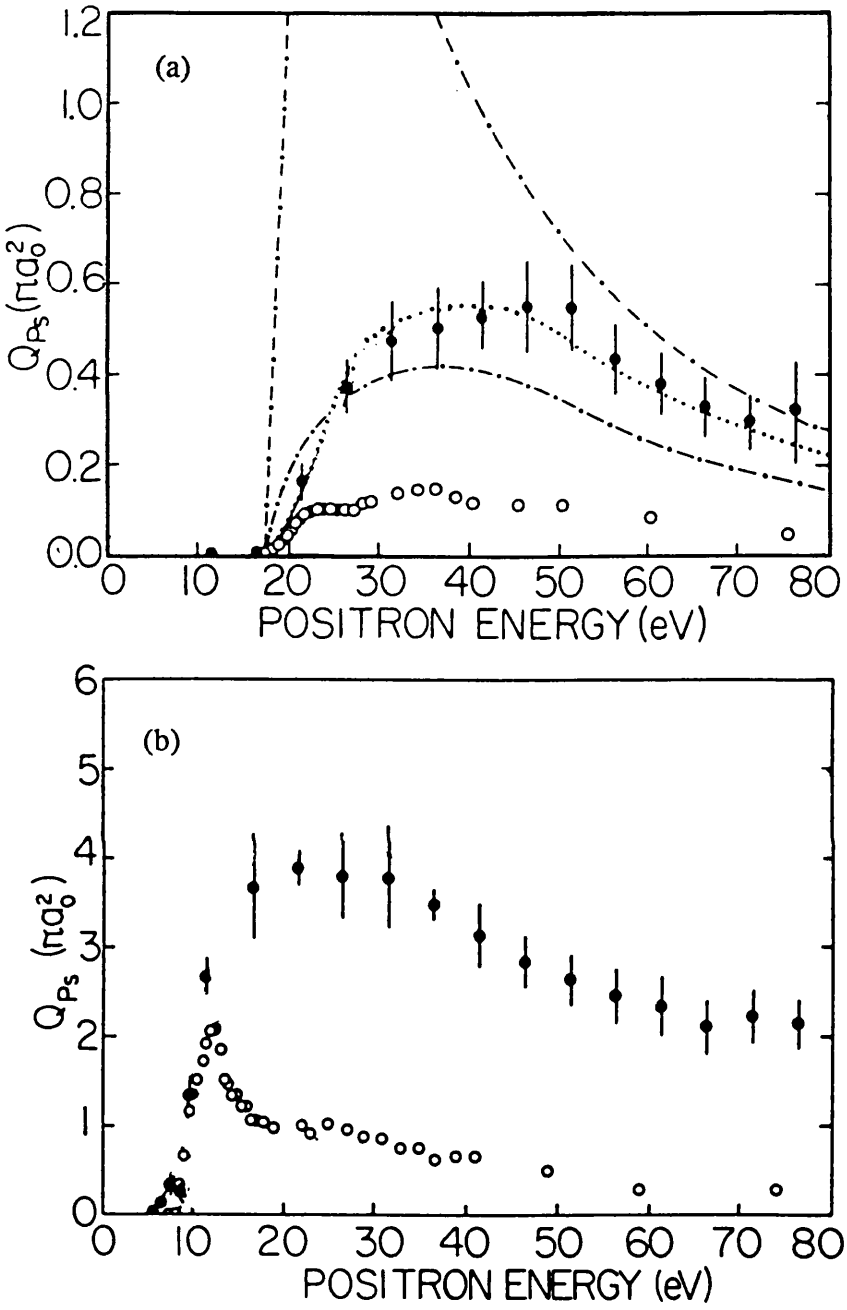

o Charlton *et al* (1983b) • Fornari *et al* (1983)

—•— Mandal *et al* (1975) ••••• Mandal *et al* (1979)

—•—•— Khan and Ghosh (1983)

Figure 4.3 Ps formation cross-sections in (a) He and (b) Ar

addition they computed values with a form of distorted wave approximation which yielded results 50% lower than those obtained by the former method. Since then, many workers have also calculated the Ps total formation cross-section for a range of atoms and molecules. Some examples are cited below. Drachman *et al* (1976), Mandal *et al* (1979), Khan and Ghosh (1983), Humberston (1984) and Brown and Humberston (1985) have employed different methods to deduce σ_{Ps} for atomic hydrogen. Calculations on the "one-electron" systems of Li and Na have been performed by Nahar and Wadhera (1986) and Mazumdar and Ghosh (1986) and also for formation of excited states in e^+–Li collisions by Guha and Saha (1980).

Detailed comparison on the merits of the various techniques and the reliability of the obtained cross-sections, both theoretical and experimental, are noted elsewhere (see for example Charlton 1985a). In the context of the present investigation, it suffices to draw attention to the points of interest from the studies of He and Ar. Figure 4.3 shows the measured value of σ_{Ps} obtained by Charlton *et al* (1983b) using (i) and Fornari *et al* (1983) using (ii) together with some theoretical calculations for He. On inspection of the graphs, a large discrepancy is apparent between the values obtained from the two experimental studies for both gases. The distorted wave model calculations by Mandal *et al* (1979) and those by Khan and Ghosh (1983), accounting for polarization effects, appear to be in closer accord with the latter study. First Born approximation calculations by Mandal *et al* (1975) are also displayed; however it is clear from the distribution that this method is not adequate for the re-arrangement process of Ps formation where accurate descriptions of the system are necessary.

Results from the third experimental technique noted above also lend support to the cross-sections derived by Fornari *et al* (1983) rather than those of Charlton *et al* (1983b). Therefore, taking the experimental values of σ_{Ps} at its peak value from the former study and of σ_T from Kauppila *et al* (1981), about 40% and 90% of the scattered e^+ form Ps in He and Ar, respectively. In terms of a "Ps source" for beam development, the requirement is of efficient Ps production per incident e^+. On inspection of Figure 4.3, it can be seen that the Ps flux from Ar is much greater than that from He. Computations on the efficiency of Ps formation (Section 5.4.3) show that total production from Ar is approximately an order to magnitude larger than from He at a particular density. For example, at 4μmHg gas pressure, the conversion of incident e^+ to Ps is 2.5% in He and 23% in Ar at 50eV (e^+ energy). However, for the specific purpose of beam development, the variation of Ps formation with angle

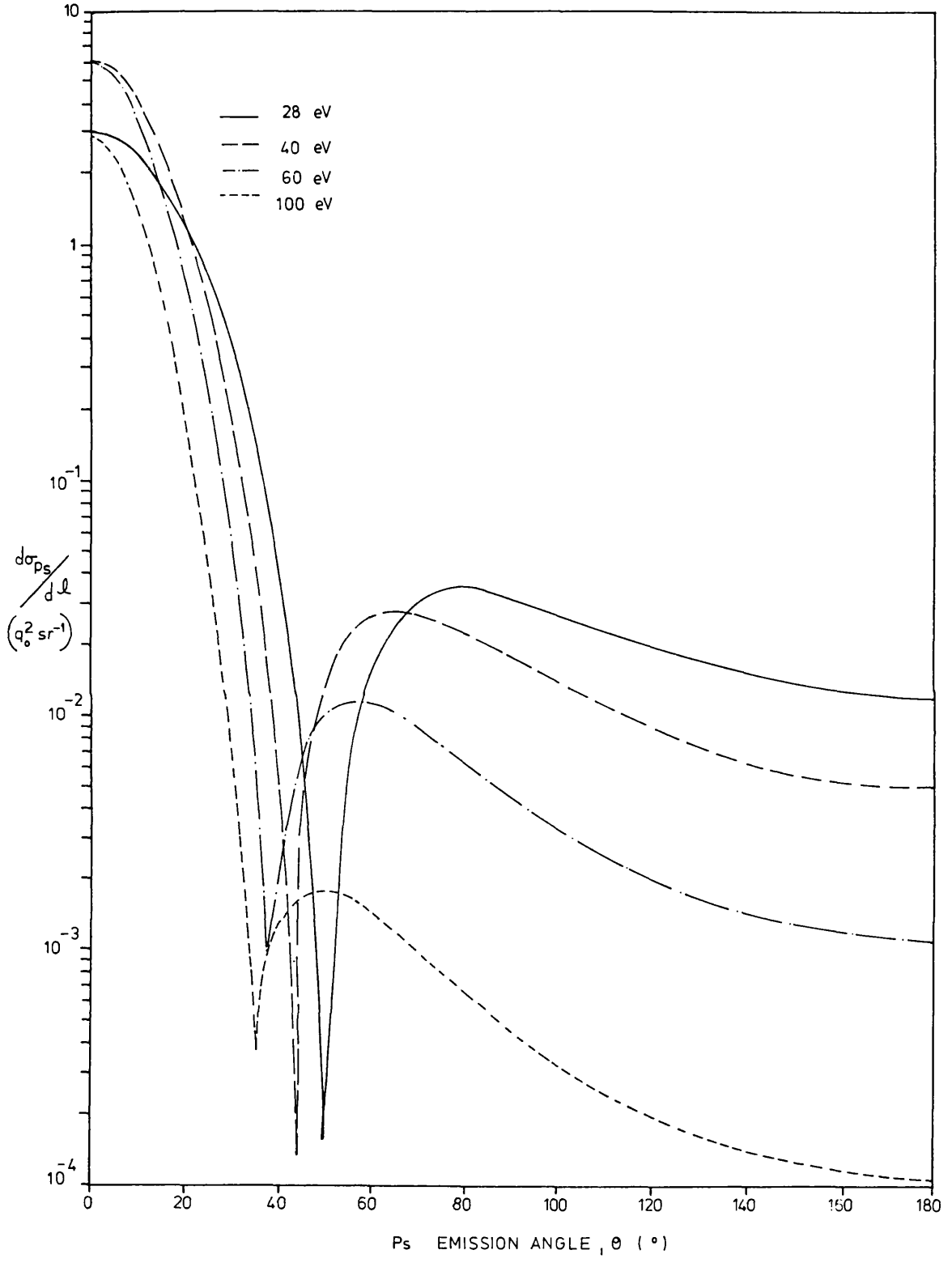

Figure 4.4 Differential Ps (n=1) formation cross-sections for e^+–He scattering (Mandal *et al*, 1979)

must also be investigated.

The theoretical calculations on the angular differential formation cross-sections in He by Mandal *et al* (1979), shown in Figure 4.4, and in H and He by Khan and Ghosh (1983) and Brown and Humberston (1985) reveal that $d\sigma_{Ps}/d\Omega$ becomes progressively more forward peaked with increasing energy. The yields derived by Mandal *et al* (1979), using the distorted wave approximation, indicate that over 50% of the total Ps flux will be contained in a 20° cone at ≈20eV Ps energy. Computation of these values together with experimental evidence of this feature is discussed in Section 4.3.

Although the study of Charlton *et al* (1983b) would appear to have suffered from systematic effects, it is nevertheless instructive to compare the cross-sections with reference to a Ps source. Of the range of gases investigated, Xe gave the largest peak value with $\sigma_{Ps}=13\pi a_o^2$ compared to $\sigma_{Ps}=0.15\pi a_o^2$ from He. However, the expense of Xe and Kr ($\sigma_{Ps}=4.5\pi a_o^2$) rule out the feasibility of these options. Ar ($\sigma_{Ps}=2.3\pi a_o^2$) together with methane, CH_4, ($\sigma_{Ps}=5\pi a_o^2$) rank as the best alternatives known in terms of total Ps production but, as asserted above, the relative differential formation cross-sections must be known in order to make full comparison with regard to Ps beams.

4.2.3 Gases - excited states

In addition to the formation of the ground state positronium, a number of processes can occur to increase the energy distribution of the Ps produced, for example Ps scattering and Ps^* formation. Both processes are of great interest in themselves, however, in order to use the Ps flux as a probe, the presence of such species must be fully characterised. In the case of Ps formation in gas collision, the excited state was first observed unambiguously by Laricchia *et al* (1985), following the preliminary work of Clark (1984). The arrangement used was similar to that employed by Canter *et al* (1975) in the study of Ps^* emission from solid surfaces and comprised of a u-v sensitive phototube detecting the 243nm signal in coincidence with the annihilation quanta of the de-excited o-Ps. Insertion of a borosilicate filter, opaque to photons ≤285nm, provided explicit proof of the presence of Lyman–α radiation in a number of gases. The highest yields extracted were 5.7% from H_2 and 4.0% from Ar per stopped e^+.

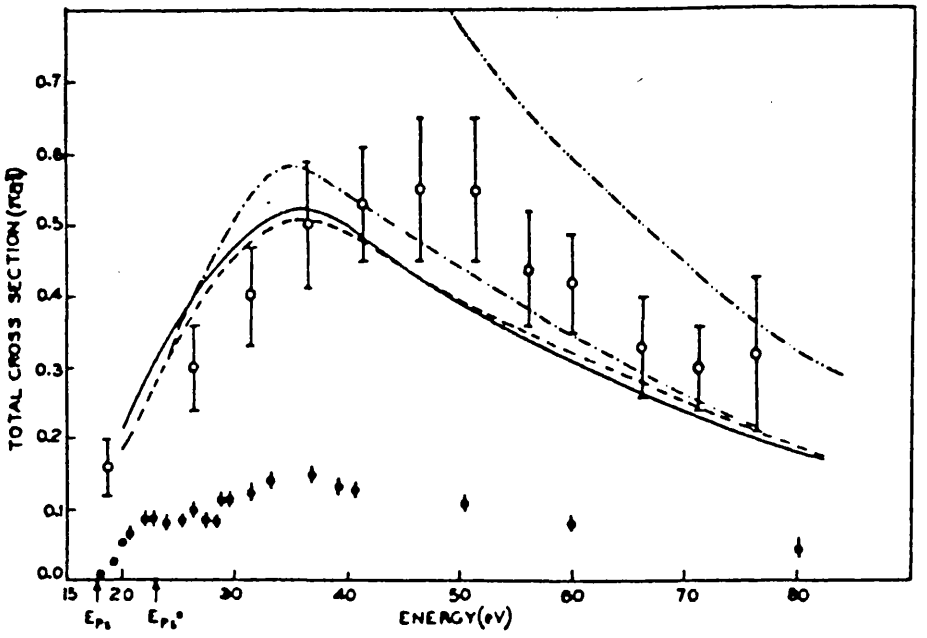

—— Polarised orbital, Khan *et al* (1985) [n=1+2]
---- Adiabatic, Khan *et al* (1985) [n=1+2]
—•• First Born approx., Khan *et al* (1985) [n=1+2]
• Charlton *et al* (1983b)
o Fornari *et al* (1983)
—•—• Mandal *et al* (1979) [n=1]

Figure 4.5 Total Ps formation cross-sections for e^+–He scattering

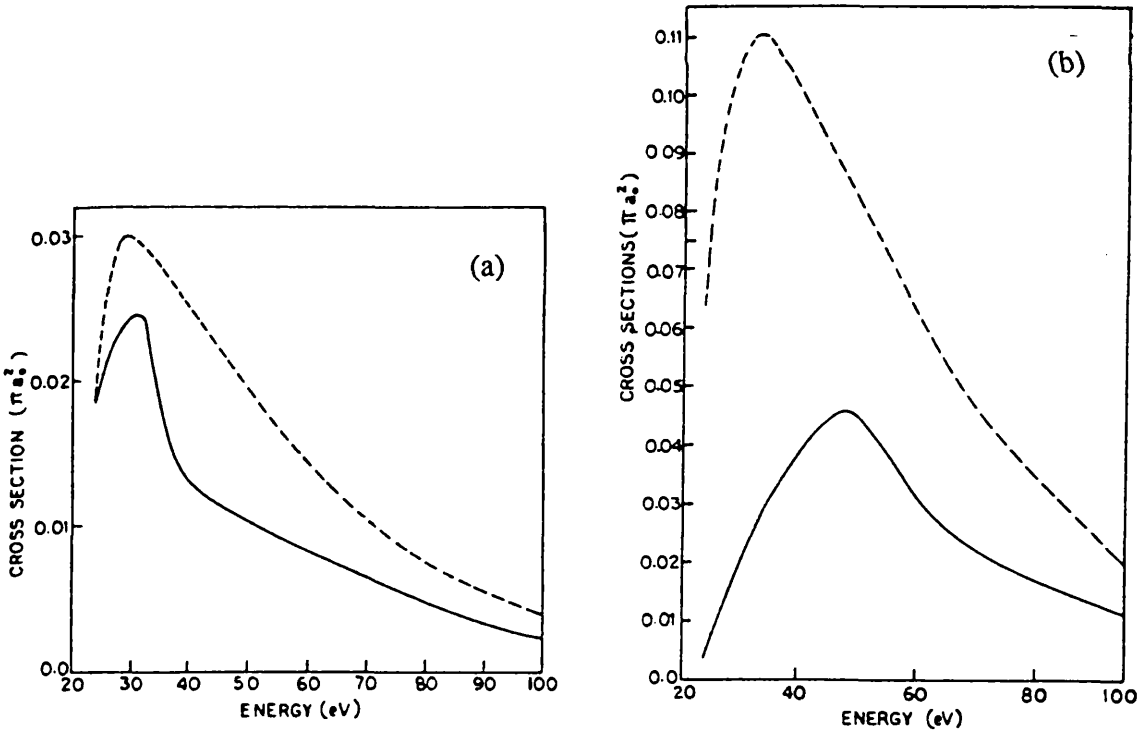

—— Polarised orbital, Khan *et al* (1985)
---- First Born approx., Khan *et al* (1985)

Figure 4.6 Total Ps (n=2) formation cross-sections for e^+–He scattering, (a) 2P states and (b) 2S states

An interesting outcome of this investigation was the first observation of simultaneous positronium formation and excitation of the ionic species in e^+–CO_2 and e^+–N_2O scattering (Laricchia *et al* 1988a). In terms of beam production, this may contribute to degradation of the energy resolution.

Theoretical studies on the formation of excited states have been performed with H and He by Mandal *et al* (1980), Khan and Ghosh (1984) and Khan *et al* (1985). Figure 4.5 shows the distorted wave polarised orbital calculations of total cross-section for Ps formation into the n=1+2 states and the n=2 state calculated by Khan *et al* (1985) for He. The Ps^* formation cross-section is approximately an order of magnitude lower than the ground state. The variation of the cross-section with energy for the individual states reveal greater structure (Figure 4.6), with a sharp maximum at 35eV for the P state followed by a broader peak at 50eV for the S state.

The proportion of n=2 state Ps detected in an experimental arrangement is dependent on the differential formation cross-section integrated over the solid angle subtended by the detector. The calculations performed by Mandal *et al* (1980) on Ps formation into excited S states reveal a forward peaked nature of the angular distribution similar to that predicted for the ground state. Although the magnitude of the excited state (n=2) cross-section may be approximately a factor of ten less than the ground state, a significant proportion of the signal detected in an experimental set-up may be contributed by Ps^* due to two factors: firstly, the angular variation mentioned above and secondly, the relatively long (≈1100ns) lifetime of the metastable 2S state. Substantial contamination of the beam may thus occur. However, this also indicates the possibility of Ps^* beam generation.

4.3 Developments in the Ps Beam Technique

In the last section, some of the processes of Ps emission from solids and gases have been described and the efficiency of Ps formation noted for both. In terms of a solid Ps source, the mechanism of fast Ps emission allows a wide range of energies while the other two processes result in Ps with energies of the order of a few meV to eV . The production of Ps (and Ps^-) from thin C foils (Mills and Crane, 1985 and Mills, 1981b) and the glancing angle technique of Gidley *et al* (1987) have been suggested in conjunction with the generation of energetic Ps beams. However, due to technical difficulties associated with these methods, such as energy selection, the

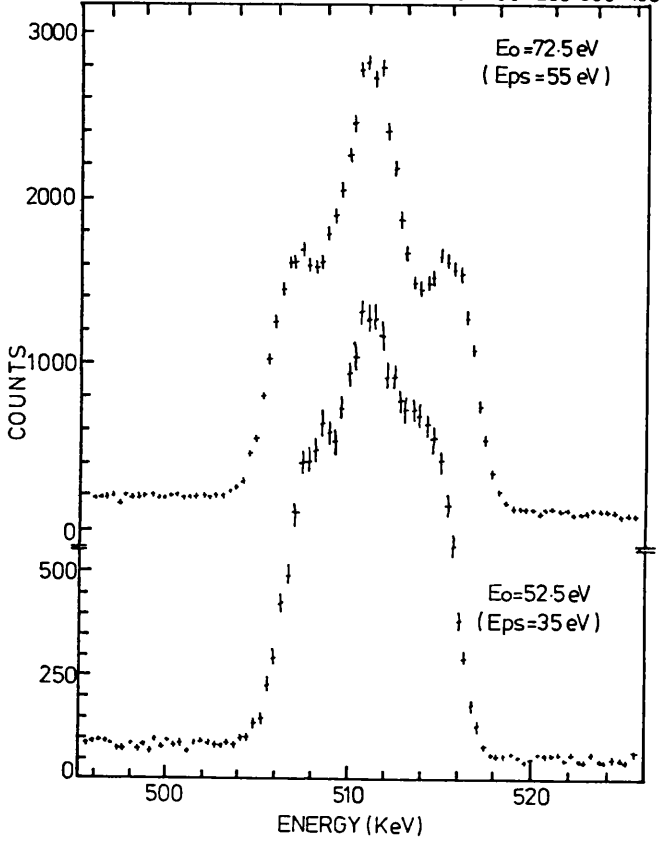

Figure 4.7 Annihilation spectra of e^+ in He showing the Doppler-shifted p–Ps contributions in the wings (Brown, 1986)

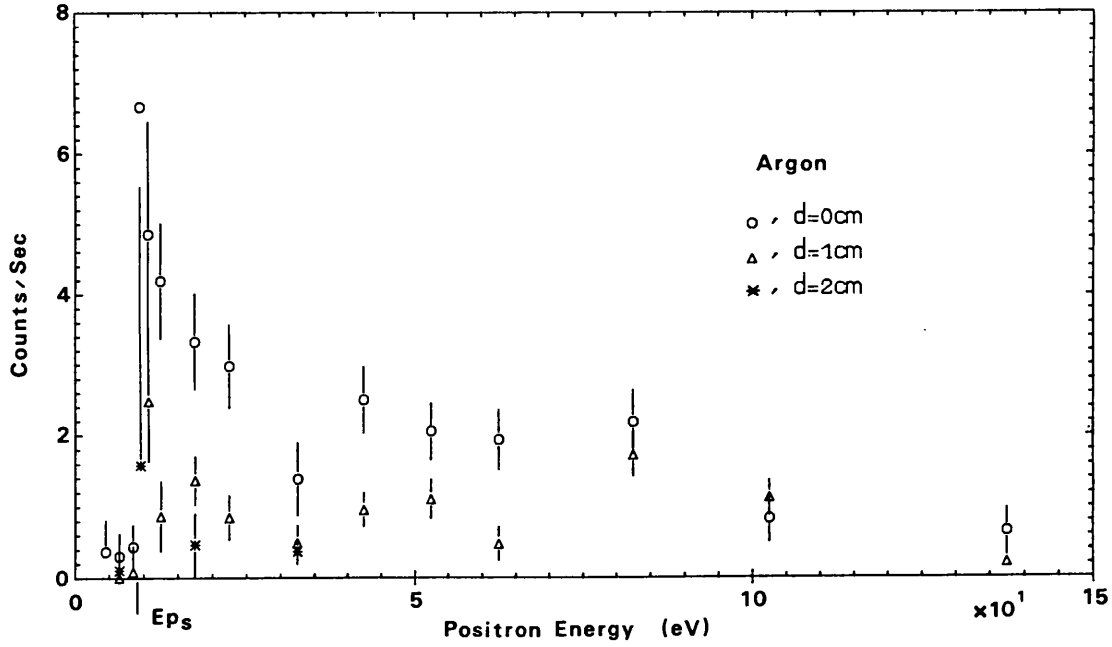

Figure 4.8 Ps detected from e^+–He scattering versus e^+ energy at various distances normal to the beam axis (Laricchia *et al*, 1986a)

main developments in the Ps beam method have concerned the use of a gaseous Ps source. Furthermore, the theoretical studies mentioned above have suggested that such Ps formation is preferentially forward directed. However, the effect of break-up and conversion to the p–Ps state in the production cell is unknown as reliable values for the cross-section of these processes have yet to be reported. Thus, in an effort to verify these predictions and to assess the feasibility of this method a number of studies were performed by Brown (1985, 1986) and Laricchia *et al* (1986a,b, 1987).

In the preliminary study of Brown (1985, 1986), a beam of e^+ was magnetically guided along a 1m long gas cell containing 10^{-4} Torr of He. The e^+ remaining after interaction with the gas were reflected at grid on the exit to allow a second traversal of the cell. A high resolution Ge(Li) γ-ray was used to monitor the annihilation events at two incident e^+ energies, 72.5 and 52.5eV. Figure 4.7 shows the results as a function of energy; the peak centred at 511keV is due to the 2-γ annihilation of free positrons and o-Ps quenching on the cell walls and the wings on either side are attributed to the Doppler shifted annihilation events of p-Ps travelling along the axis of the incoming e^+.

Further evidence of this nature was forthcoming from the work of Laricchia *et al* (1986a,b) in which Ps formation in Ar was investigated from threshold to 130eV. A magnetically guided e^+ beam was passed into a differentially pumped gas cell, 20mm in length with 8mm wide U-shaped apertures containing 4μmHg of Ar. Of the Ps produced, the longer lived o-Ps atoms were detected by a channeltron mounted on a manipulator at a distance of 120mm from the gas cell, whilst all charged particles were prevented from reaching the detector by means of retarder grids. The lifetime of the singlet p-Ps, 125ps, was too short in comparison to the flight times for survival to the channeltron. Gas and background runs were taken for various energies at 3 positions: on axis, 10mm and 20mm above axis. The obtained data is shown in Figure 4.8 and demonstrates the preferentially directed formation of Ps from Ar gas.

The investigations were improved and extended by Laricchia *et al* (1987) to include He. The channeltron was replaced by an arrangement of channel electron multiplier arrays (CEMA) mounted on an axial linear shaft to allow angular variation. In order to improve the signal to background ratio, the pulses were registered in coincidence with either of the two Na(Tl) detectors placed in close proximity to the CEMA. The e^+ remaining after interaction were biassed away by electrostatic plates, one of which

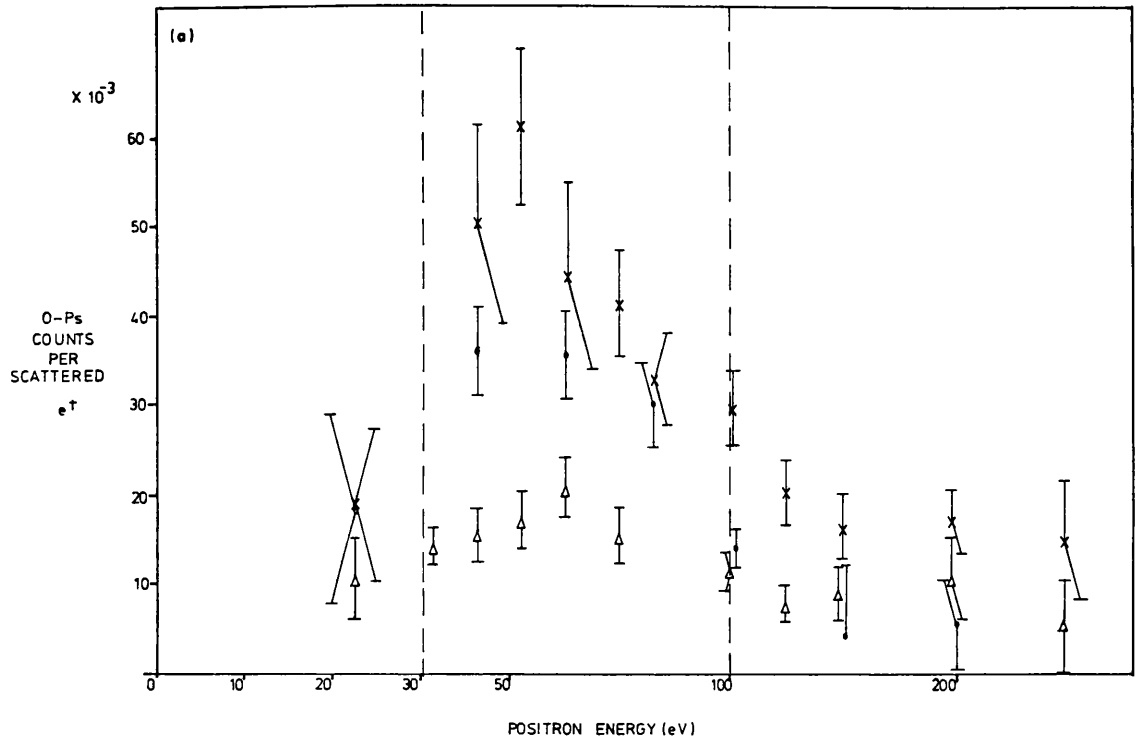

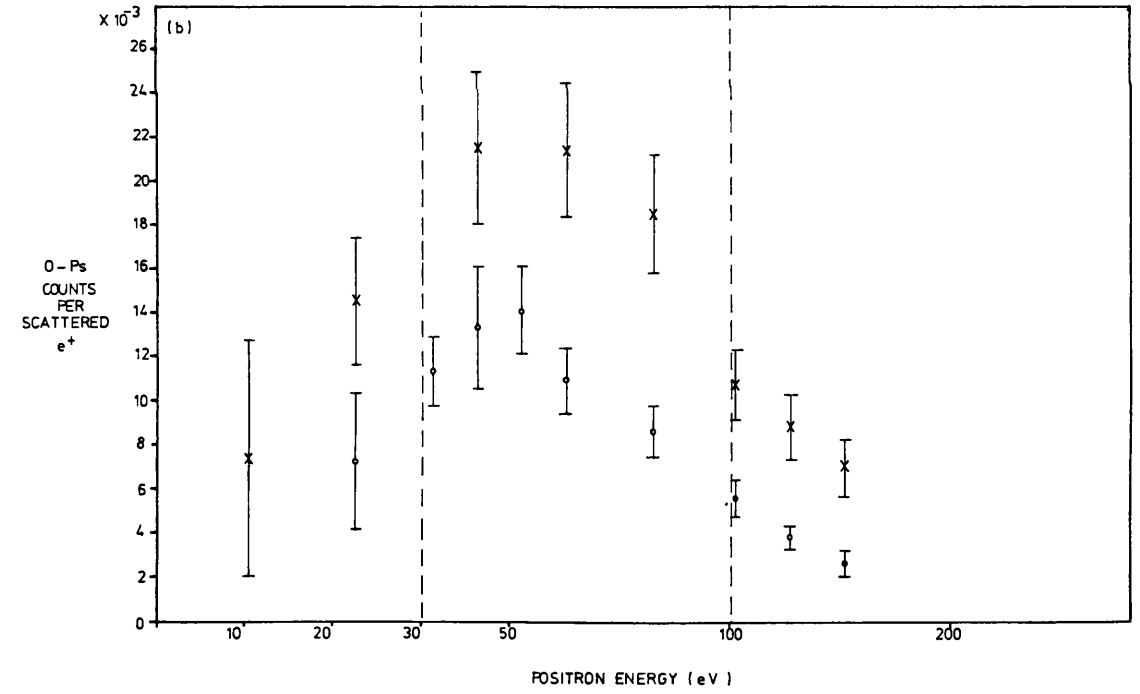

o 6° (½ cone angle) x 8° (½ cone angle)

Δ 6° (½ cone angle, low magnetic field at source end)

Figure 4.9 o–Ps formed per scattered e^+ in (a) He and (b) Ar (Laricchia *et al*, 1987)

was held at earth whilst 1-2keV was applied to the other. Multiple scattering events in the cell were minimised by confining the gas pressures to values within the approximation given by Equation 5.13 in Section 5.4.3. The results obtained in 6° and 8° cones are shown in Figure 4.9 for He and Ar normalised the number of scattered e^+ per second.

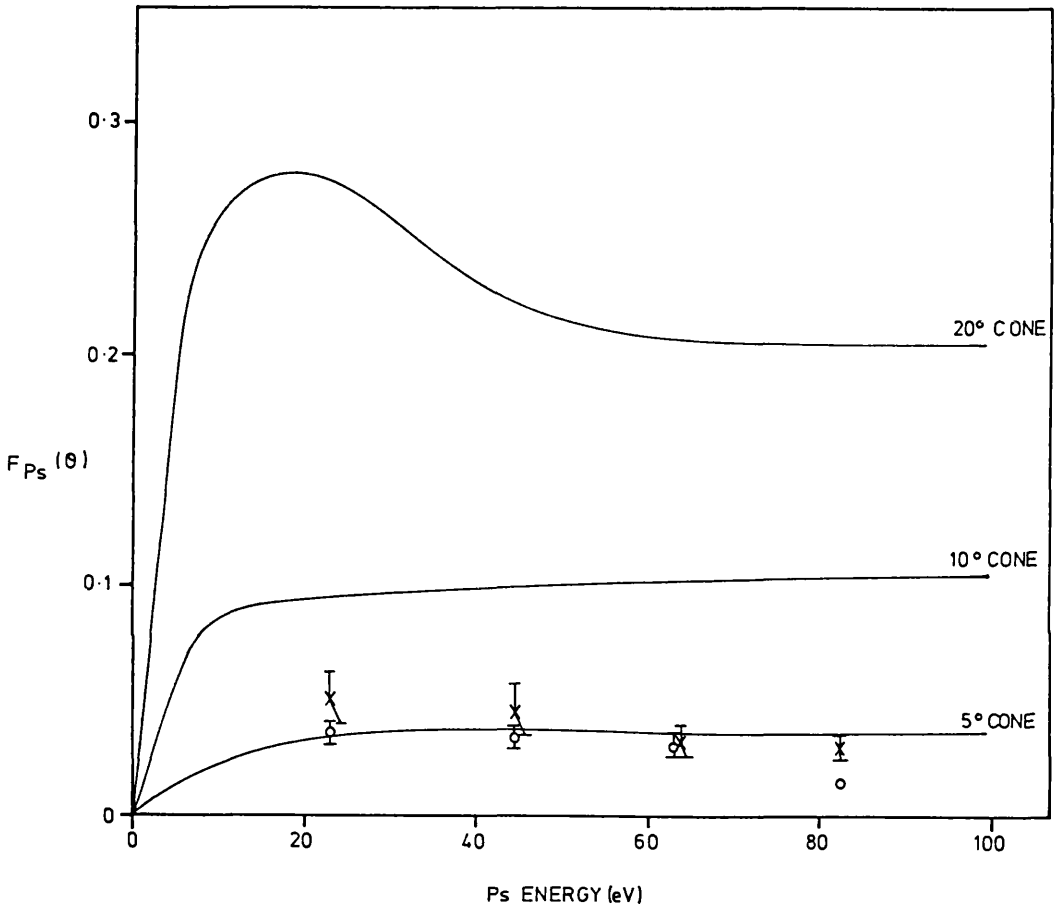

—— Computed from Mandal *et al* (1979)

o, x Experimental values from Laricchia *et al* (1987)
(Notation as in Figure 4.9)

Figure 4.10 Variation of e^+ fraction forming Ps in He in 5°, 10° and 20° angular ranges about the incident e^+ direction

Using the calculations of $d\sigma_{Ps}/d\Omega$ by Mandal *et al* (1979) and the value of σ_{Ps} from Fromme *et al* (1986) for He, they computed the fraction of Ps formed in both spin

states between angles 0 and θ' to the incident e^+ direction from

$$F_{Ps}(\theta') = (2\pi/\sigma_{Ps}) \int_0^{\theta'} (d\theta_{Ps}/d\Omega)\sin\theta d\theta \qquad 4.4$$

Figure 4.10 illustrates the variation of the fraction of Ps emitted in 5°, 10° and 20° cones derived using equation 4.4, together with the experimental data for He. Evidently, there is good agreement between the calculated and measured values in the 5° angular region with ≈5% collimation of the Ps flux above 10eV energy. The results indicate that, with He and Ar gases, Ps "beams" can be formed with an efficiency of 10^{-3}–10^{-4} per incident e^+.

The investigations outlined above have shown that the production in gases is far from isotropic and demonstrated the feasibility of using the gas charge exchange method in the generation of energy-tunable, collimated Ps beams. However, from the discussions in the previous section it is apparent that the n=1 state Ps is only one of a number of species possibly formed in this process. In order to identify these components, a timed Ps beam system was developed by Laricchia *et al* (1988b). A remoderation stage was incorporated into the flight path and the e^+ emitted were "tagged" by the detection of the secondary e^- released on impact. Subsequent formation of Ps and the measurement of the time of flight to the detector allowed the determination of the energy distribution of the beam. This technique and its application are discussed in the next chapter.

The use of a gaseous Ps source has been demonstrated in the study of Weber *et al* (1988) to observe positronium specular reflection from LiF (100). Figure 4.11 shows a schematic diagram of the experiment. The Ps was formed via gas charge exchange with 10^{-3} Torr Ar in a 200mm long gas cell. The energy of the incoming 150eV e^+ was varied by electrically floating the gas cell to the desired potential. Those e^+ remaining after interaction with the gas were retarded by t. With an incident e^+ beam of 8×10^6 s^{-1}, an o–Ps production efficiency of $\approx10^{-3}$ was obtained. The sample was held at a few hundred °C to prevent adsorption of contaminants on the surface. Annihilation quanta of the reflected o-Ps were detected by means of a pair of bismuth germanate (BGO) scintillators coupled to photomultipliers placed outside the chamber, above and below the annihilation plate. The angular distribution of the Ps was measured whilst changing θ_i (by rotating the sample) but keeping the total scattering angle constant as:- $\Psi=\theta_i+\theta_r$ where θ_i and θ_r are the incident and reflected angles

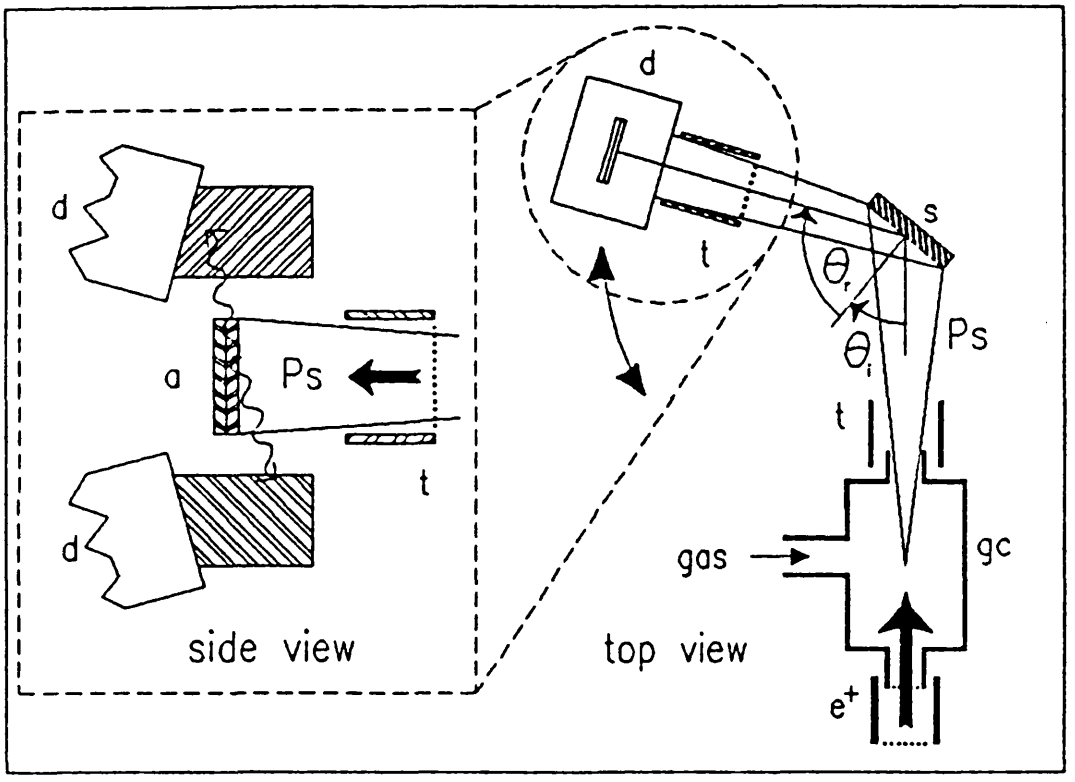

Figure 4.11 Experimental arrangement of Ps reflection study (Weber *et al*, 1988)

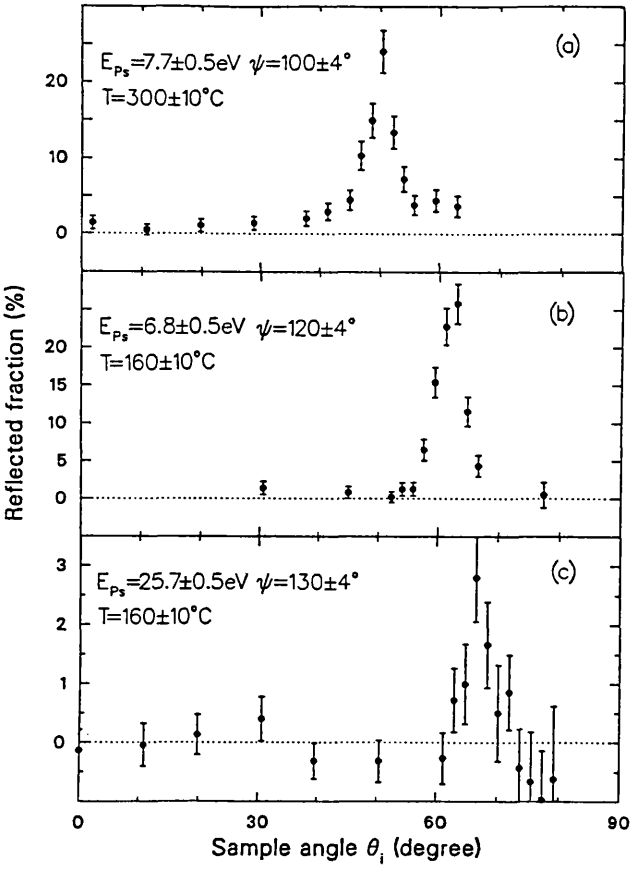

Figure 4.12
Ps reflection from LiF(100)
(Weber *et al*, 1988)

respectively. Their results are shown in Figure 4.12; between incident angles of 50° to 60°, they observed reflection of the beam with a maximum fraction of (30±5)% at of 7eV Ps energy. The authors hope to extend this study to the observation of Ps diffraction from surfaces.

4.4 Positronium Scattering

The possibility of energy-controllable Ps beam production affords the opportunity of investigating a variety of interesting processes. Comparison of the collision channels and their counterparts in e^+ and H scattering may be instructive in understanding these phenomena. Furthermore, exotic reactions such as Ps complex formation have been postulated. However, calculations in all aspects of Ps interaction with dilute gases are limited.

Published theoretical work on total scattering cross-sections is confined to the classic study of Massey and Mohr (1954) on Ps–H scattering using the first Born approximation. These calculations, although approximate, give an indication of the magnitude of the interaction between Ps and H. The scattering of the neutral Ps atoms differs from that of the e^+ and e^-. In the case of the charged particles at low energies, the static and polarization effects are dominant factors in determining the size of the interaction with atoms, with exchange/correlation effects between the incident species and atomic e^- contributing accordingly. However, for the Ps atom, long range static interactions are negligible due to the coincidence of the centre of mass and charge. The influence of polarization from the induced dipole is also limited, being most effective at the lower energies. Hence, in elastic collisions, the exchange interaction is an important factor.

Massey and Mohr (1954), on application of the Born-Oppenheimer approximation (which they state is a rough estimate), found that the elastic cross-sections in Ps–H scattering was highly energy dependent due to the strong coupling of the exchange interaction. Values obtained ranged from $230\pi a_0^2$ at 0eV (Ps energy) to $25\pi a_0^2$ at 6.7eV, revised to $4\pi a_0^2$ on consideration of the s-wave contribution only, and $0.4\pi a_0^2$ at 27eV. Fraser (1961), in an extension of this work using relatively more accurate integro-differential equations, obtained similar results which are displayed in Figure 4.13.

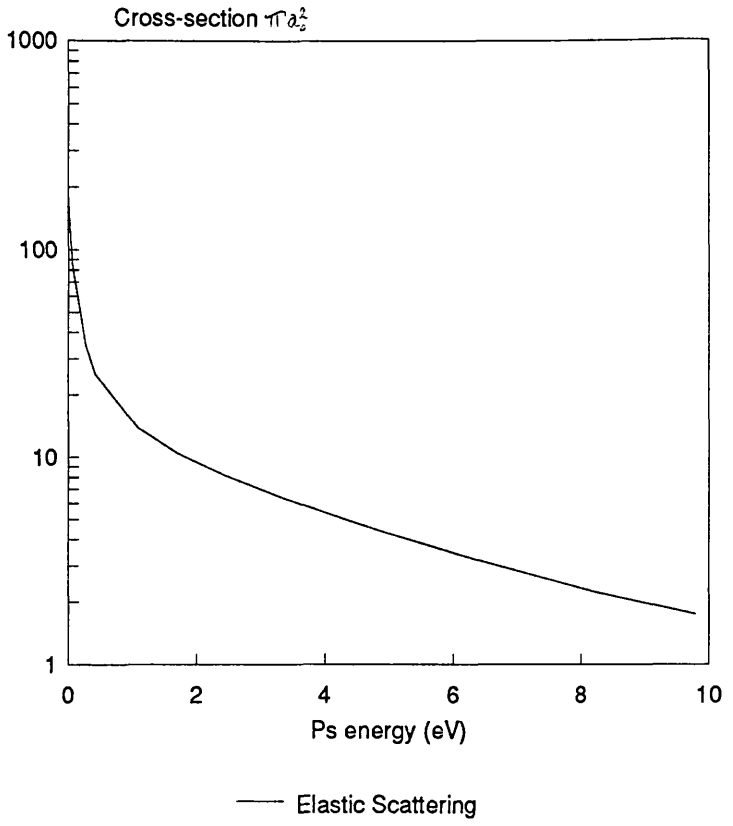

Figure 4.13 Theoretical values of Ps–H elastic scattering cross-section (Fraser, 1961)

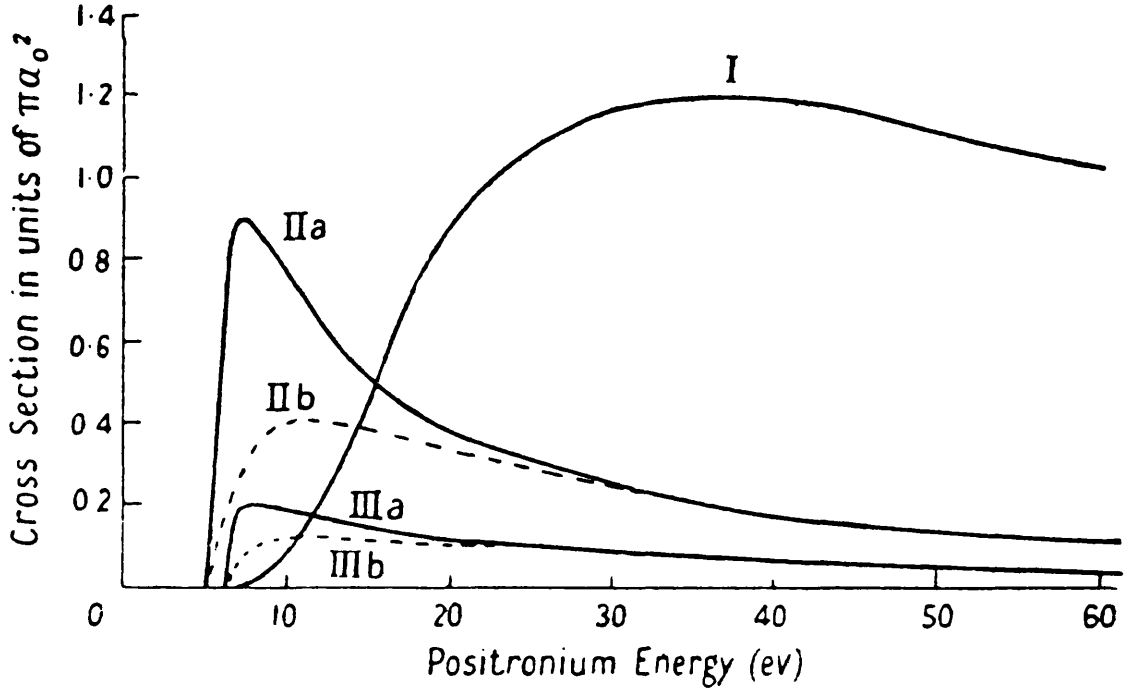

I—— Ps ionisation cross-section

II—— Ps excitation into 2P states II- - - - Ps excitation into 2P states (corrected)

III—— Ps excitation into 3P states III- - - - Ps excitation into 3P states (corrected)

Figure 4.14 Theoretical values of Ps–H inelastic scattering cross-section (Massey and Mohr, 1954)

The quenching process of conversion from o-Ps to p-Ps by spin exchange was considered by the above authors and estimated by Massey and Mohr (1954) to be about a quarter of the elastic cross-section, showing a strong energy dependence of this interaction. Quenching by direct spin-reversal was estimated to be of the order of $10^{-6}\pi a_0^2$, that is, negligible. Fraser's work (1961) did not find the same relationship with the conversion/total elastic scattering cross-section ratio ranging from 0.176 at 0eV to 0.07 at 6.8eV.

The study of Massey and Mohr (1954) dealt in part with the inelastic collisions in Ps-H scattering. From the first Born approximation, they state that there is a vanishingly small probability of excitation of either the Ps or the H. Excitation of the Ps atom was presumed to be more likely as its threshold is lower than that of the H atom. The results obtained are shown in Figure 4.14 by lines II and III; the dashed curves are the adjusted excitation cross-sections with corrections derived from those applied to first Born calculation of e^-–atom excitation. An estimation of the ionisation, that is break-up, cross-sections of Ps was also made and is represented in Figure 4.14 by line I. These calculations indicate that the scattering of Ps by H is dominated by the short range exchange process at low energies, resulting in a strong energy dependence where the cross-section rapidly decreases with increasing kinetic energy. At intermediate energies, however, the break-up process may be the greatest contributor to the scattering interaction. Below 5.1eV, the cross-sections, in comparison to those of the corresponding e^+–H interaction (Humberston, 1979), were noted to be greater by an order of magnitude or more, giving rise to the expectation of relatively large cross-sections for Ps–atom/molecule collisions. This generalisation has yet to be verified.

Apart from these studies, calculations concentrate on resonances (Drachman and Houston 1975, 1976, Drachman 1979, Ho 1978) and the bound state PsH (Drachman 1979, Ho 1978). The presence of a number of resonance levels in Ps–H interaction has been predicted with all bar one state lying above the n=2 threshold (Drachman, 1979). The lowest resonance state has been computed by Ho (1978) to correspond to a Ps scattering energy of 4.01eV with a width of 74±27meV. The stability of positronium hydride, PsH, an "isotope" of H_2, has been theoretically established since the early work by Ore (1951) and Ho (1978) has theoretically determined the binding energy of such a "molecule" to be 1.0211eV.

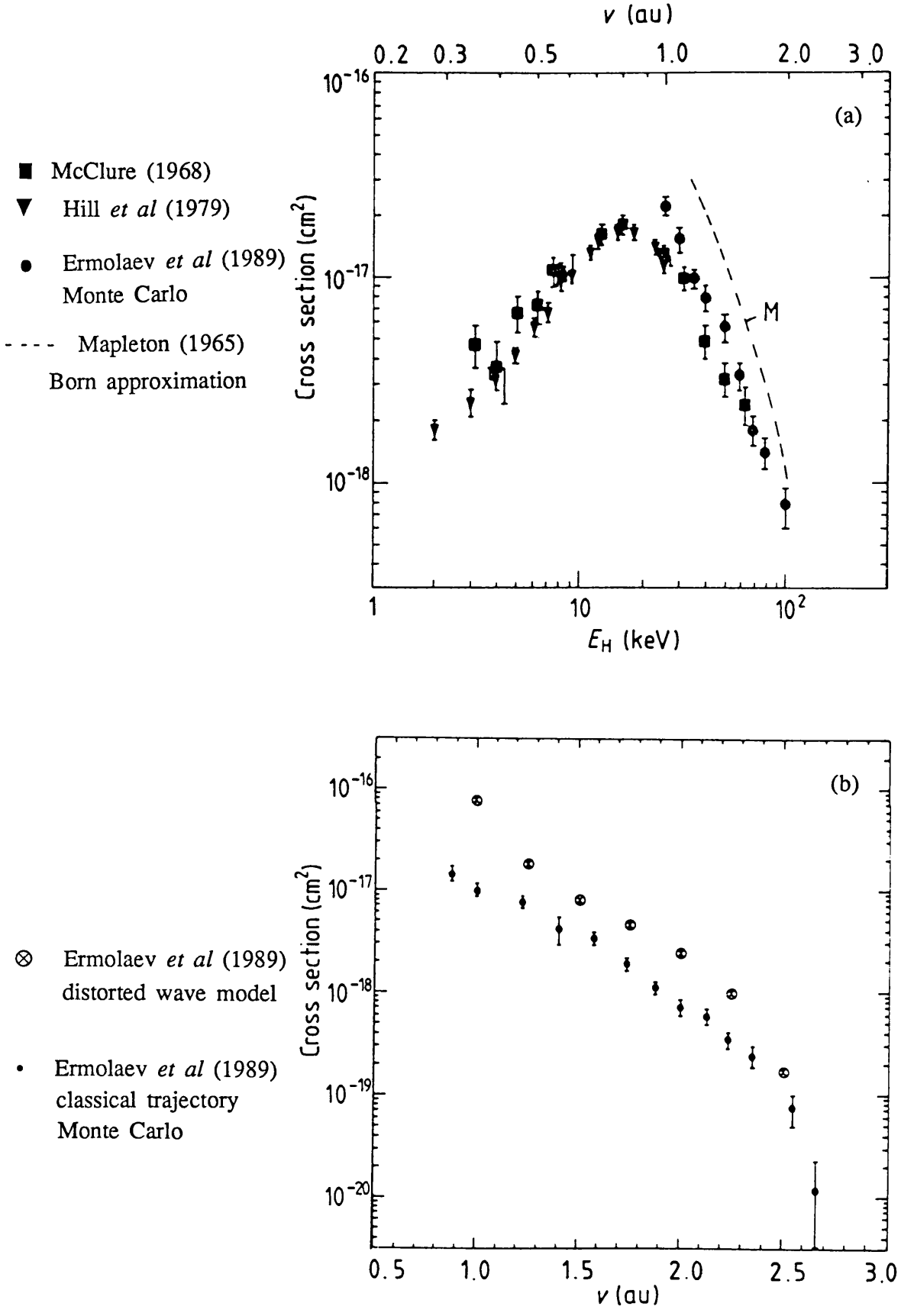

Figure 4.15 (a) Formation cross-sections of H^- in H–H scattering
(b) Calculated formation cross-sections of Ps^- in Ps–H scattering
(Ermolaev *et al*,1989)

Recently, Ermolaev *et al* (1989) have calculated the cross-section of formation of Ps^- in Ps–H collisions. Using the distorted wave model, they obtained results for Ps impact energies in the range 27-170eV. For confirmation, classical trajectory Monte Carlo calculations were also performed for this process in Ps–H scattering and also the analogous reaction of H^- formation in H–H collisions. Their results for the latter interaction are illustrated in Figure 4.15a and show good agreement with the experimental data above ≈30keV H impact energy. Such close accord is not predicted for values of the Ps–H interaction computed with this method because of the lighter incident particle. The distorted wave and Monte Carlo results for Ps–H collision are presented in Figure 4.15b and exhibit the expected trend of decrease with increasing energy associated with e^- capture processes upon reaching the maximum cross-section, however divergence of the two distributions is apparent at the lowest energy in the range of the calculations. Both methods of computation are expected to be more reliable at the higher energies where the velocity of the impacting particle is greater than the Bohr velocity of the target e^-. Ermolaev *et al* (1989) state that high accuracy is not predicted for these calculations, although the order of magnitude of the cross-sections is expected to be correct. In comparison to the Ps break-up process discussed above, the magnitude of this process is small, $0(10^{-21}m^2)$.

The theoretical work for He, too, is limited, with little agreement between the various calculations. Fraser (1962, 1968), Fraser and Kraidy (1966) and Barker and Bransden (1968, 1969) deal with the low energy regime 0-7eV, using the static exchange approximation to calculate the elastic scattering cross-section of o-Ps with pick-off quenching. Barker and Bransden (1968, 1969) also computed values using an approximation to allow for the long range van der Waal's forces. In contrast to Ps–H scattering where quenching by e^- pick-off is masked by that of e^- exchange, the latter process cannot occur in this interaction below the He triplet excitation threshold of 19.8eV. Peach (1984) has obtained the elastic scattering cross-sections by treating the He atom as a polarisable core and describing the e^-–He and e^+–He interactions by local model potentials.

The values from Fraser (1968) are 14.2 to $7.5\pi a_0^2$ in this energy regime, whilst those presented by Barker and Bransden (1968) range from 13 to $7.7\pi a_0^2$ and 16.9 to 7.6 πa_0^2 for the two approaches employed. Corrections were later made to this work (Barker and Bransden, 1969) which modified the values to 10.4-$6.7\pi a_0^2$, however it is not clear to which of the two methods they relate. The reliability of both these

studies is uncertain as values of $_1Z_{eff}$ determined from these calculations are inconsistent with experimentally extracted results. Nevertheless, as expected for He, the rapid change in cross-section at low energies is not as marked as for H. The elastic collision and in particular, the quenching process will be reduced as He possesses a full complement of outer electrons compared to the incomplete shell system of H, which is known to be an effective quencher. The values of elastic scattering cross-sections derived by Peach (1984), plotted in Figure 4.16, are smaller than those of the above study, ranging from 4.1 to $2.6\pi a_0^2$ (3.6-2.3 $x10^{-20}m^2$) in the same energy regime. Although the energy dependence of the cross-section is presumed to be less than in H, a greater variation was expected than that obtained in these results by the author herself.

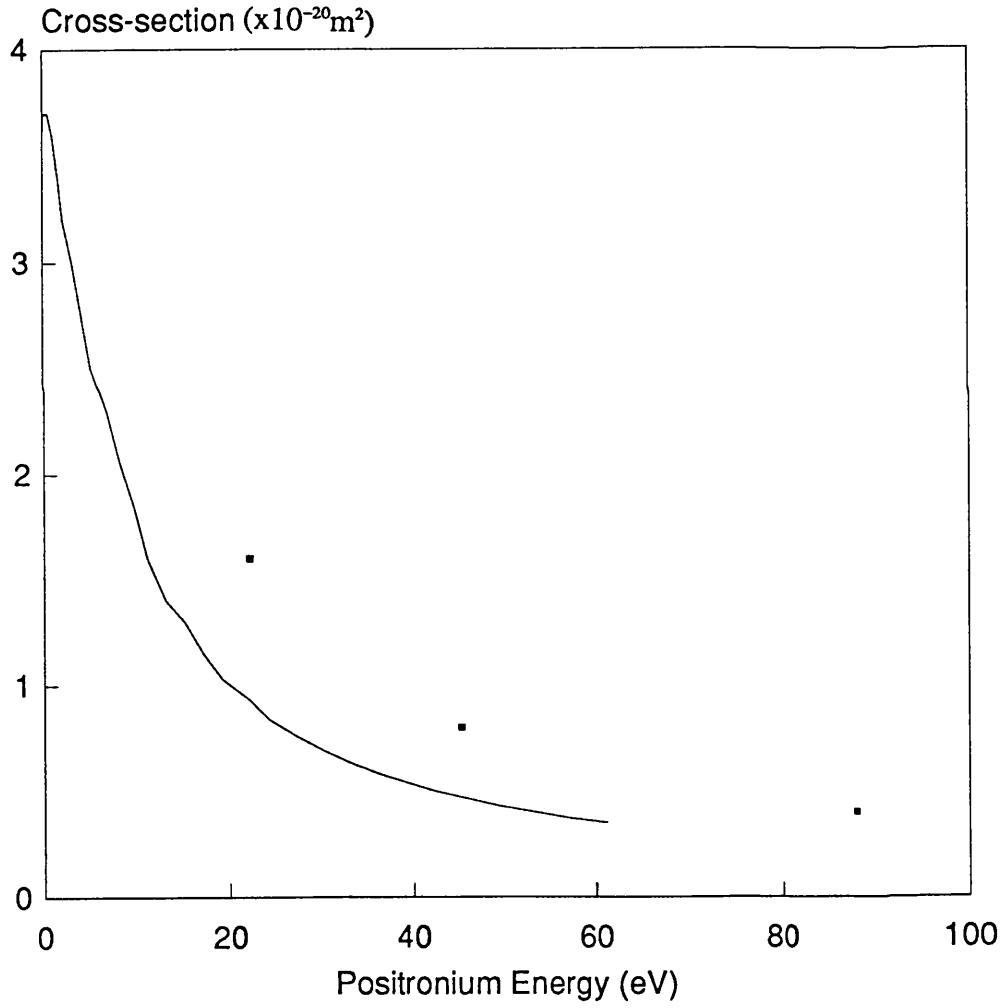

Figure 4.16 Theoretical and experimental Ps–He cross-sections

—— Ps–He elastic scattering (Peach, 1984)

▪ Ps–He total scattering (Brown, 1987)

(i)	$Ps + He \rightarrow Ps^* + He$
(ii)	$Ps + He \rightarrow Ps + He^*$
(iii)	$Ps + He \rightarrow Ps^* + He^*$
(iv)	$Ps + He \rightarrow Ps + He^+ + e^-$
(v)	$Ps + He \rightarrow e^- + e^+ + He$
(vi)	$Ps + He \rightarrow e^+ + He^-$
(vii)	$Ps + He \rightarrow Ps^- + He^+$

Table 4.1 Some inelastic processes in Ps-He scattering

A number of inelastic processes can occur in Ps–He collisions and some of these are noted in Table 4.1. In the study of Ermolaev *et al* (1989), discussed above, the cross-section of the last reaction listed in Table 4.1 was also computed for the range 51.4–137.7eV. Although the authors state in the report that the values at the lowest energies must be treated with reserve, an idea of the magnitude of the cross-section may be gained. More recently, the results from the application of the classical trajectory Monte Carlo method on reactions (iv), (v) and (vi) have also been obtained and made known in a private communication (Ermolaev, 1989). These values are presented in Figure 4.17 and show that the inelastic contributions peak at ≈20eV with a value of $0.11\pi a_o^2$ ($0.097 \times 10^{-20} m^2$) of which the largest contribution is made by the Ps break-up process.

It has been predicted that the bound state PsHe does not exist (Gertler *et al*, 1968). However, Drachman *et al* (1976) suggest the possibility of $(PsHe)^+$ formation via interaction with the metastable 3S He atom:

$$Ps + He^* \rightarrow (PsHe)^+ + e^- \qquad 4.5$$

Even more exotic bound states of Ps with atoms and molecules have been proposed (Gol'danskii, 1968) and theoretical proof of the stability of such complexes has been provided by Karl *et al* (1984). In the latter study it was shown that Ps can bind to a number of atoms, listed below: Al, Au, Cu, Pt, alkali metals, C, F, O, S. In addition, negative species of the form PsA^- have been predicted to be exist where A can be Be, Mg, C, O or Si.

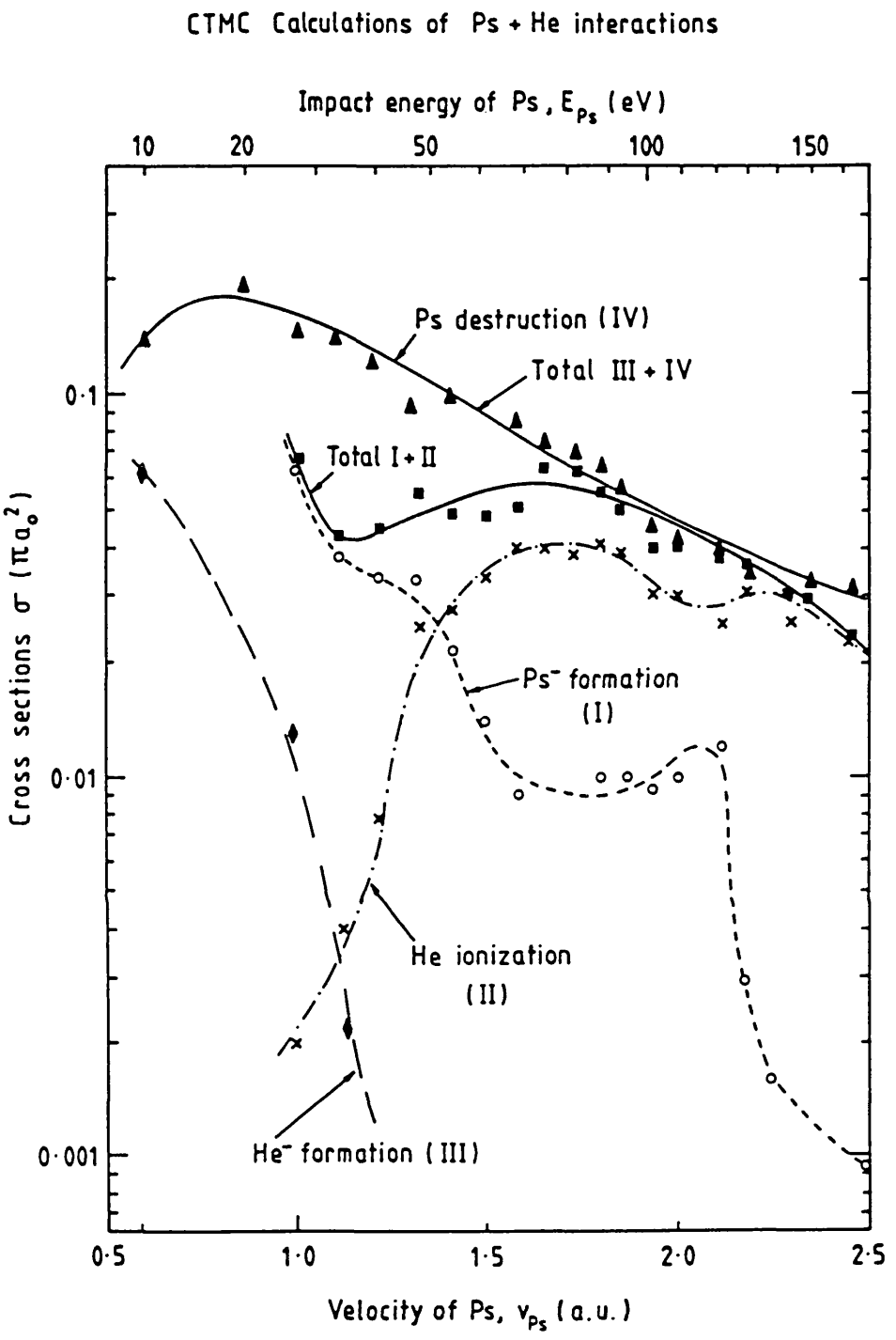

Figure 4.17 Calculated cross-sections of some inelastic processes in Ps–He scattering (Ermolaev, 1989)

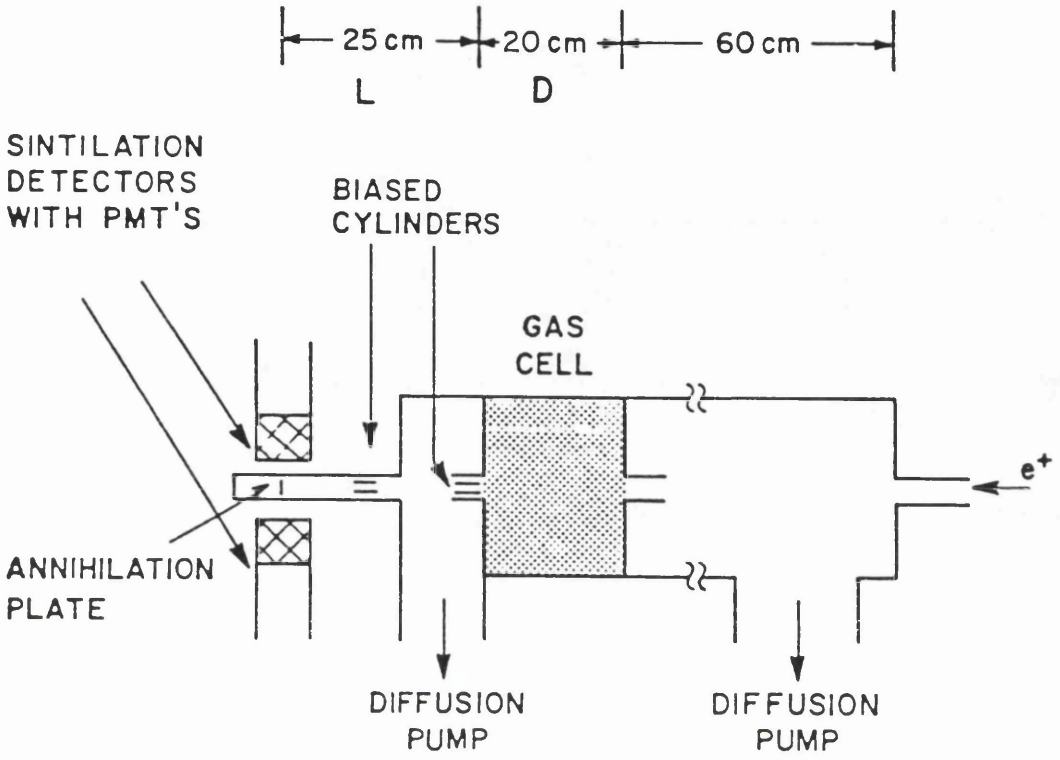

Figure 4.18 Experimental arrangement of Ps–He collision study (Brown, 1987)

The examples cited above demonstrate that there is much scope for experimentation employing Ps beams with many interesting processes that warrant investigation. On the experimental front, however, results are few and values for the basic scattering interactions have yet to be established. In 1987, Brown reported measurements of total Ps–He scattering cross-section in an investigation of Ps production efficiency. The apparatus used is shown in Figure 4.18. A gas cell of length 20cm was placed

at a distance of 25 cm from an annihilation plate about which NaI(Tl) detectors were positioned to monitor the 511keV photons. Positrons were repelled using biassing cylinders and efficiencies were measured at 2 pressures - high ($1.6x10^{-3}$ Torr), and low ($0.3x10^{-3}$ Torr). The effect of scattering in the production cell was apparent at the higher pressure. Thus, values for the total scattering cross-sections were determined using the observed deviation of the measured data from theoretically predicted yields; these are shown in Figure 4.16, alongside the calculations of Peach (1984). Although the errors attributed to the measurements are not reported, the results are in broad agreement with the extrapolation of the theoretically derived elastic values. However recently, Laricchia (1989) has noted that the values deduced by Brown (1987) are in error, possibly by as much as an order of magnitude.

4.5 Aim of the study

The time of flight technique, developed by Laricchia *et al* (1988b), has been demonstrated to be a viable means of determining the energy distribution of the Ps emission. Therefore, with the ultimate aim of the study of Ps–gas scattering interactions, the timed beam method has been employed to investigate the components of the neutral flux ensuing from slow e^+ interaction with He and Ar gases.

The discussions presented in Section 4.2.2 indicate that various species may be formed in e^+–gas collisions other than ground state positronium. The predictions from theory indicate that formation into the excited states of Ps via gas charge exchange is generally $\approx n^{-3}$ that of the ground state where n is the principle quantum number (Mandal *et al*, 1980). Therefore, approximately 11% of the total Ps yield is expected to be formed in the n=2 state. However, in experimentation with Ps beams, the actual composition of the flux may be considerably different at the point of interaction due to the presence of the long lived metastable state. Thus, characterisation of the flux is necessary prior to investigation of Ps interactions.

As reported in Section 4.4, interactions involving Ps collisions with gases have yet to be fully investigated. Therefore, following resolution of the beam components, the timed Ps beam technique has been employed to investigate Ps scattering in He and Ar gases. Measurements of the Ps total scattering cross-section have been attempted from interpretation of the data obtained on increasing the gas density in the cell. Comparison of the departure from the expected value has been made, however, in

contrast to Brown (1987), experimentally predicted yields have been used. The timed Ps beam technique and the results obtained from its employment are presented and discussed in the following chapter.

CHAPTER 5
EXPERIMENTAL STUDY ON THE PRODUCTION OF A POSITRONIUM BEAM AND ITS INTERACTION WITH ATOMIC GASES

5.1 Introduction

The investigation into Ps production and interaction in He and Ar gases was undertaken on the apparatus used by Laricchia *et al* (1988b) in the development of the timed Ps beam technique. Modifications were made to this system to allow further study of components in the flux, in particular the formation of excited state Ps. The changes that were required for this purpose and to measure Ps total scattering cross-sections are detailed below in the description of the system and summarised in Section 5.4.

Also presented in Section 5.4 are the results obtained in this work which can be divided into three parts. Firstly, the decay rate of the signal with distance was extracted to confirm the identification of the peaks observed in the time of flight spectra. Secondly, the yields of the various components were computed and their relative abundances compared. Finally, Ps total scattering cross-sections were derived using a single cell for production and attenuation. The results are collectively summarised in Table 5.1.

5.2 Slow positron production

A slow positron beam was produced from the moderation of fast β^+ particles obtained from a commercially manufactured ^{22}Na source; from consideration of the initial calibrated strength and the half-life of the isotope (2.62 years), the activity was calculated to be approximately 9mCi at the time of the investigation. The source, made by Amersham International, was composed of radioactive NaCl compound deposited onto a thick platinum backing in a 4mm diameter well in a stainless steel disc. Two, 5μm thick, titanium windows sealed the activity, but reduced the transmission of the β^+ particle by 20%. The source capsule, 15mm in diameter and

6mm in length, was mounted on a mobile shaft along the beam axis by means of a stainless steel jig screwed into the source capsule and onto the shaft.

The linear shaft was mounted on axis from a 70mm flange on a stainless steel chamber composed of two concentric cylinders, of which the inner one was partially filled with Pb (Figure 5.1). On retraction of the source along a 23mm diameter tube in the shielding, the inner cylinder could be rotated about the axis perpendicular to the beam line in order to block this channel with Pb. Rotation by 90° provided adequate shielding from the source for the safe withdrawal of a small Pb plug supporting the moderator assembly.

The moderator was comprised of layers of annealed, 90% transmission W meshes (100 lines per inch); experimentation showed that, for the type of mesh used, four were required for the optimum slow e^+ yield. The annealing was performed in a separate chamber under vacuum conditions of $\approx 6 \times 10^{-2}$ Torr and the procedure used was similar to that described in Chapter 3 for the foils. Meshes were placed in a W oven and after pumping for a minimum of 30 minutes, heated to a few hundred °C for approximately 20 minutes to remove surface adsorbates. This was followed by cycles of annealing for short bursts of 2-5 seconds at 2400°C and cooling to allow the pressure to drop back to the base value. The meshes were "flashed" until the increase in pressure was less than 1×10^{-2} in 2 seconds, usually attained after ten to fifteen cycles. A long period of post-annealing pumping (overnight) was found to be beneficial for good moderation properties. If sparking or oven breakage occurred during the annealing procedure, the meshes were re-heated as such effects were observed to result in low efficiencies. After taking up to air, the meshes were inserted into the system within 15 minutes since long exposure to air was found to decrease the reduce the slow e^+ yield.

The meshes, cut into 13mm diameter discs, were placed in a 1mm thick, recessed PTFE ring and held by a 0.5mm thick, brass push-fit ring, to which a potential was applied. An unannealed, 90% transmission W grid, positioned 1mm away, was earthed for extraction of the positrons. An annealed W mesh, held in a similar fashion to the others, was placed between the moderator and the source. The application of a potential to this mesh, some 20-30V greater than the moderator voltage, resulted in a doubling of the slow e^+ yield as those emitted towards the source were turned around. Here, this voltage will be referred to as the source potential.

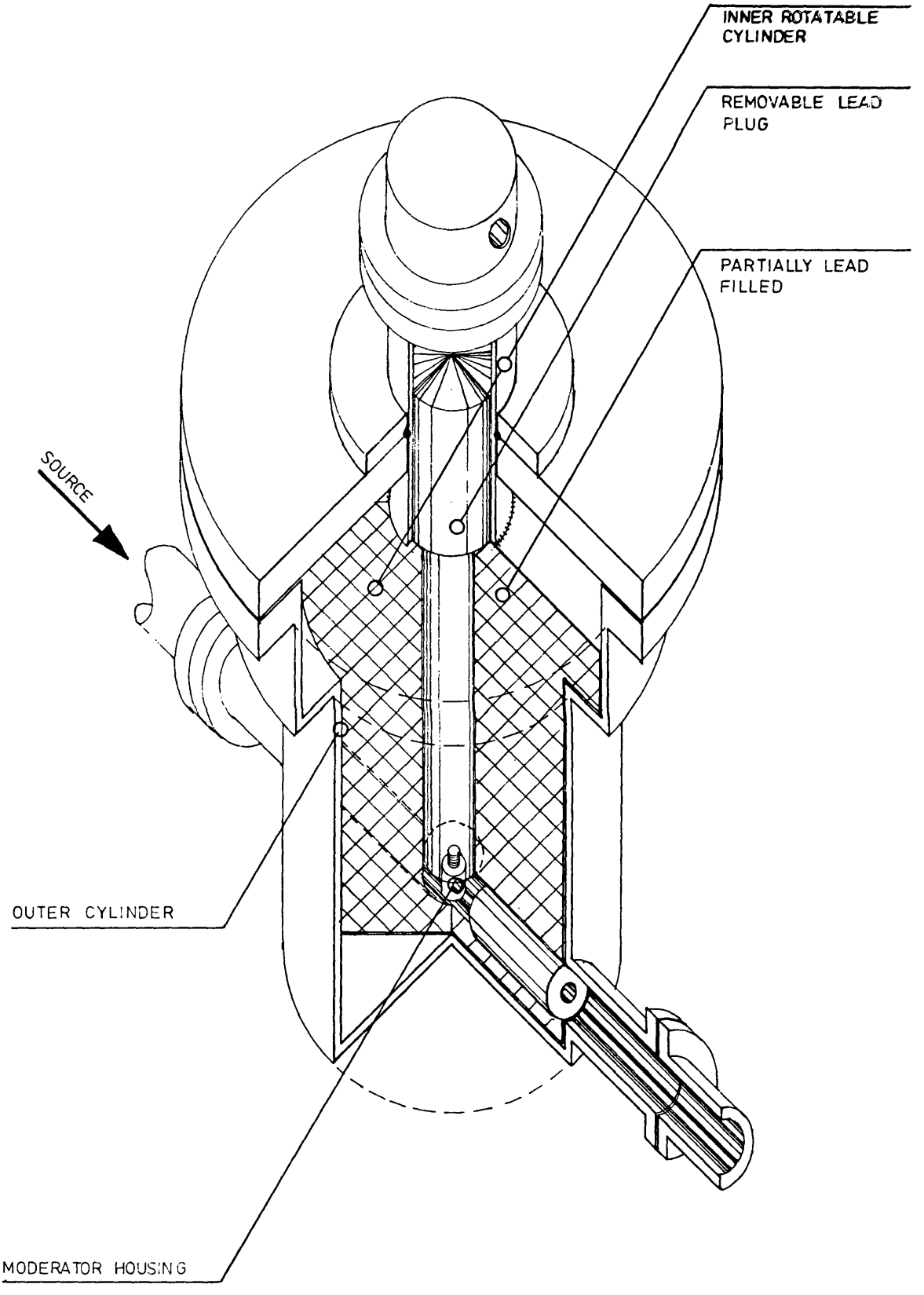

Figure 5.1 Cut away diagram of the source area

The arrangement of meshes was held in a small brass cylinder, of 20mm outer diameter and 9mm long, whilst insulation between the components was made by the PTFE rings and 0.2mm thick PTFE washers. The opening diameter of the moderator was 12mm. The brass cylinder was fixed to the base of the Pb plug by a length of 3mm diameter, stainless steel studding and its position adjusted to achieve maximum interception of the fast β^+ flux when the source was pushed flush against it. Moderator and source potentials of +400V and +420V, respectively, were applied via wires glued into the body of the Pb plug; curved grooves were cut in order to minimise the γ–ray shine-paths. The entire source chamber was clad in a 10cm thick layer of Pb and was evacuated by an E02 (2" dia.) vapour diffusion pump, backed by an Edwards ED35 rotary pump and protected with an Edwards CB4A water-cooled baffle.

The positrons were transported along the beam line, shown schematically in Figure 5.2, under the influence of an axial magnetic field. Guidance from the source region was provided with an arrangement of Helmholtz coils (2 pairs) and a curved solenoid. The 15° bend in the solenoid allowed the removal of many of the fast components from the beam, such as high energy e^+ and e^-, as the field strength was insufficient to confine these species. Slow e^+ transport was aided by an additional coil at this position. Much of the radiation produced in the creation and annihilation of positrons was prevented from reaching the detectors by the insertion of two Pb collimators. The first, 300mm long and 13mm in diameter, was placed directly after the moderator arrangement and the second, 245mm in length and 13mm in diameter, was situated at the entrance of the solenoid. Pb shielding was also placed at the bend of the solenoid.

A set of five coils, 16cm (mean) diameter coils, was employed to maintain a magnetic field along the interaction region. Attempt was made to reduce the effects due to the spiralling of the positrons by keeping the field low in this region in comparison to the source area in order to "parallelise" the beam. That is, to increase the ratio of the longitudinal velocity to the transverse component. Under conservative forces, $\mathbf{B}/\sin^2\alpha$ is constant, where $\mathbf{B}$ is the magnetic field and α is the pitch angle of the helical motion. From the expression, a decrease in the value of $\mathbf{B}$ would, therefore, lead to a corresponding decrease in the pitch angle and thus increase the longitudinal velocity component of the particles in the beam. The magnetic field strength was maintained at approximately 60 Gauss around the source end and 30 Gauss about the

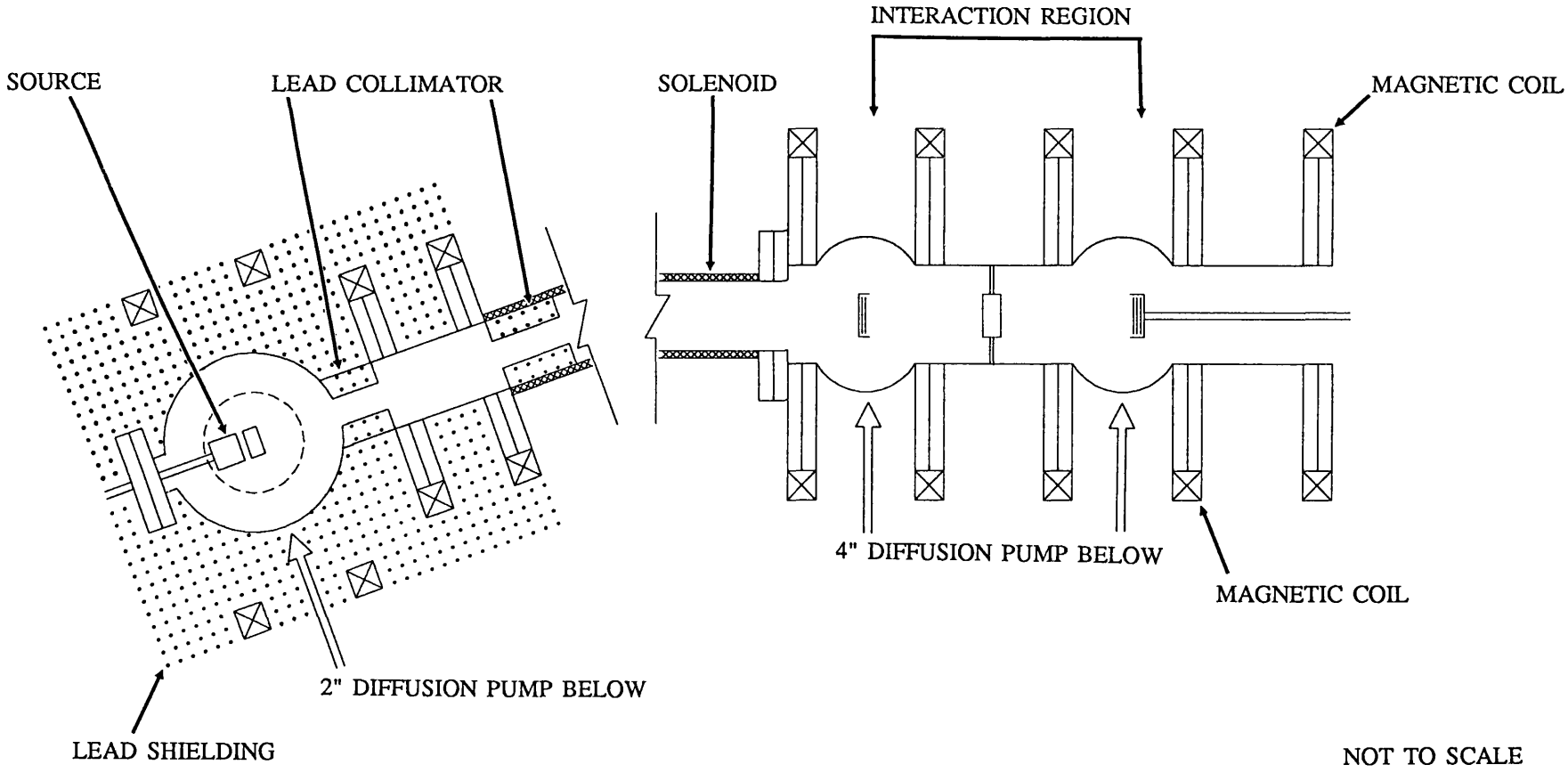

Figure 5.2 Schematic diagram of the timed Ps beam apparatus

interaction region. These were varied occasionally when the beam intensity was maximised by slight adjustment of the field strengths. However, the values of **B** provided by the system of coils resulted in only about a factor 1.4 change in the ratio of the longitudinal and transverse velocities. A more significant point concerning the magnetic field in this region was the value of **B** over the length of the gas cell. Variations in the strength of the field along the cell would lead to changes in α, resulting in corresponding changes in the angle integrated differential Ps formation cross-section. It was therefore imperative to hold the magnetic field constant in this area.

The interaction region, shown in Figure 5.3, consisted of two brass, 4-way pumping ports, 10.6cm in diameter, joined by a 10.6cm diameter brass tube in which the cylindrical gas cell was mounted. The brass gas cell, of inner diameter 30mm and 20mm long, was held centrally by two 1/4 inch diameter copper pipes screwed into the body of the cell and soldered into the supporting brass tube. Gas was admitted through one of the pipes via an Edwards LV5 precision leak valve and the pressure was monitored through the other using an MKS 220-1 Baratron head. A mercury thermometer in direct contact with the brass tube measured the temperature. Long brass extensions pieces were attached to the 7mm apertures on both sides of the cell to aid the confinement of the gas. A cylindrical tube, 7mm in diameter and 11.8mm long, and a conical tube, 22mm in length and 7–10mm in diameter, were placed at the entrance and exit, respectively, of the cell. The conductance of the apertures, at pressures required in the experiment, was reduced by 60% with the use of this configuration. For the latter extension, a conical shape was employed in order to minimise the interception of the Ps flux whilst decreasing the rate of gas outflow.

A further set of three apertured, brass discs were placed directly after the gas cell and these were used to retard the remoderated positrons. The retarder system consisted of a disc (aperture:12mm dia.) to which a potential, V_A, was applied, sandwiched by two larger earthed discs (aperture:10.5mm dia.). The larger discs were connected with Al mesh to form a cylindrical shape and this was also earthed to prevent electric field penetration into the cell. A sizeable potential (+500V) was required to repel e^+ of up to 100eV energy. Therefore, to test the effect of the field on the trajectory of the e^+, a negative potential was applied to accelerate the positrons of initial energy 50eV and their times of flight were monitored. The voltage was increased until a discrepancy between the calculated and measured flight times was observed and it was found

that potentials of up to 1kV could be applied without affecting the e^+ trajectory. The remoderated e^+ were retarded at this point initially to prevent entrance to a second gas cell where Ps scattering interactions were to be studied. The second cell was removed when it was found that the e^+ beam intensity and the pumping speeds were not adequate for this experiment. However, the retarder continued to be employed in repelling the emerging e^+ in order to inhibit Ps production outside the gas cell.

Baffles and E04 (4" dia.) vapour diffusion pumps backed by Edwards ED250 rotary pumps were placed at each brass port and differentially pumped the cell. Pressures of up to 10^{-2} Torr were used in the gas cell in these investigations. Due to their proximity to the cell, the detectors used were positioned above or close to the pump stacks as operating conditions of 10^{-5}–10^{-6} Torr were recommended by the manufacturers. However, the gas loads used required a high evacuation rate which could not be provided by the pumps protected with the standard Edwards CB4A water-cooled baffles. Therefore, specially designed, slim baffles were constructed and placed between the chambers and the pumps. A narrow, louvre arrangement of copper vanes, soldered into a 45mm thick brass tube, ensured a conductance rate higher than that previously obtained with the Edwards CB4A baffle whilst effectively trapping backstreaming vapour. The optically opaque baffles were externally cooled with water which was passed through Cu pipes soldered round the body of the tube. The base pressure was measured to be $4\text{x}10^{-7}$ Torr by an ionisation gauge placed above the second pumping port.

5.3 Time of Flight Method

In order to obtain the energy distribution of particles traversing along the flight path, a time of flight method was developed by Laricchia *et al* (1987). Following van House *et al* (1984), the e^+ beam was "tagged" and this was achieved in the present arrangement by the incorporation of a remoderation stage. The secondary electrons emitted upon impact of the incident beam on the remoderator were registered, initiating a timing sequence. The termination of the sequence was provided by the coincidental detection of the particle (e^+, e^-) or atom (Ps) at the end of the flight path. From a knowledge of the path length and the time taken, the energies of the particle/atom were deduced.

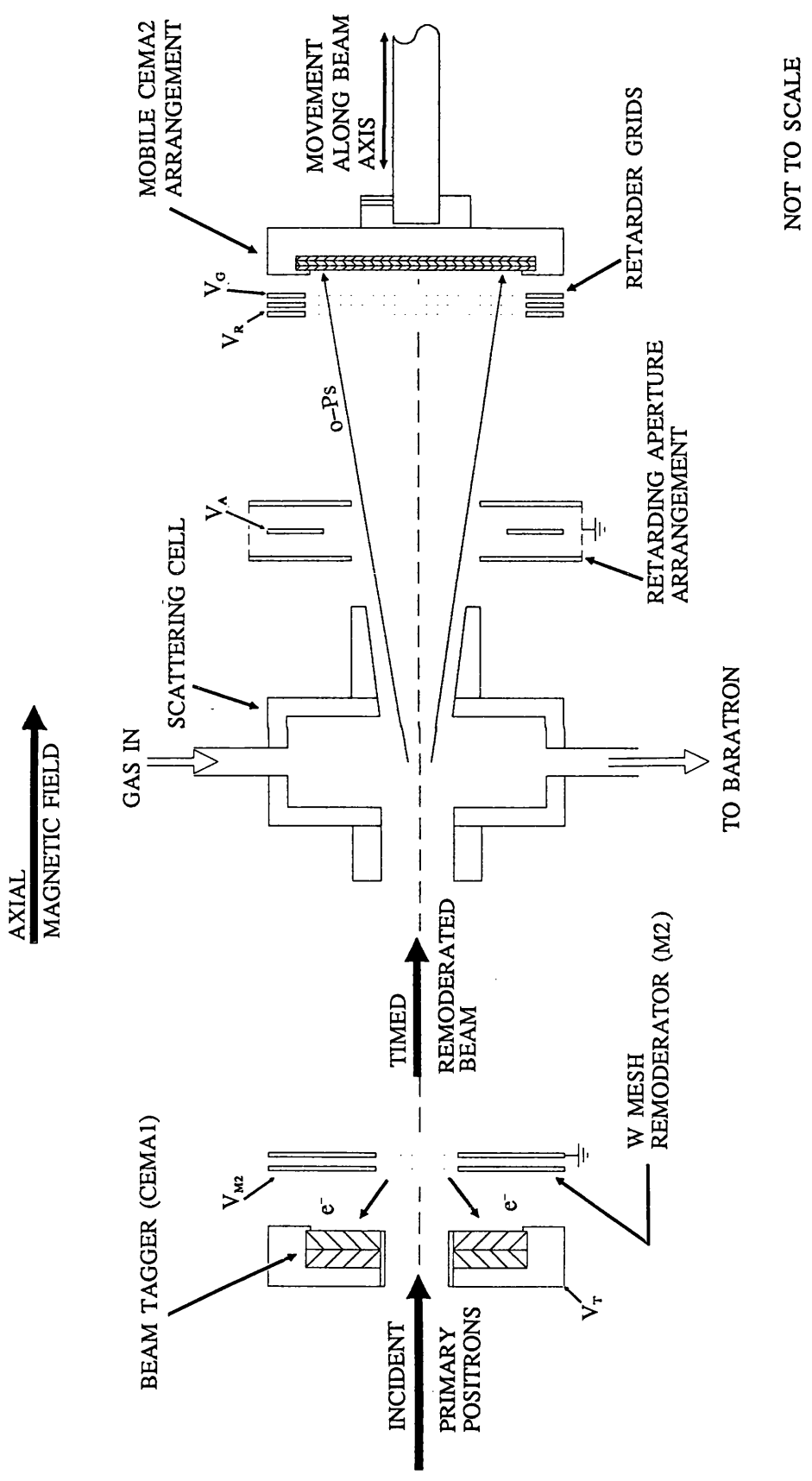

Figure 5.3 Schematic diagram of the interaction region

5.3.1 Remoderation and detection

The particles were timed over various distances between the pumping ports and the components in this region are schematically illustrated in Figure 5.3. The incoming beam of e^+, of energy ≈400eV, was passed through an 8mm diameter tube in the centre of an arrangement of channel electron multiplier array plates and impacted onto a set of W meshes (M2). A fraction of the incident e^+ were remoderated by the meshes which were annealed in the same manner as that described above; four, non-aligned layers were found to give the highest yield. The energy of the remoderated e^+ was determined by the voltage, V_{M2}, applied to the meshes and the workfunction-contact potential value. The latter contribution was found, experimentally, to be 2.7±0.5eV by the method described in Section 5.4.1. An unannealed, 90% transmission W grid, which was earthed and positioned 3mm from the meshes, was employed to extract the positrons.

The secondary electrons released from the impact of the incident beam on the meshes were detected using a set of channel electron multiplier arrays (referred to as CEMA1) placed 14mm from the moderator. CEMA1, illustrated in Figure 5.4a, consisted of two 32.5 mm active diameter, 1mm thick, Galileo MCP10 48–208 MCPs (microchannel plates) each with a central hole, 10mm in diameter. The MCPs were composed of arrays of parallel Pb glass channels, 10μm in diameter and with a centre-to-centre spacing of 12μm. These were set in the glass plate at an angle of 10° from the normal to the face so that all particles incident upon a channel would strike a surface. The interiors of the tubes were coated with semiconducting material of high secondary emission properties. This allowed a potential difference to be applied to the ends of the channels so that, when bombarded by particles/atoms/photons, the ensuing cascades of electrons are accelerated along the tube to the output.

The plates were mounted in a machined ceramic holder with an Ag-coated recess which was used as the charge collection plate (referred to as the screen). They were placed in a chevron arrangement to reduce ionic feedback from the ionisation of gas molecules in the channel. This effect causes spurious output pulses which are not representative of the input and may reduce the gain. A ceramic tube, of 8mm inner diameter, placed in the central hole of the MCPs, allowed the passage of the incident beam. The inner surface of this tube was coated with Ag paint and electrically

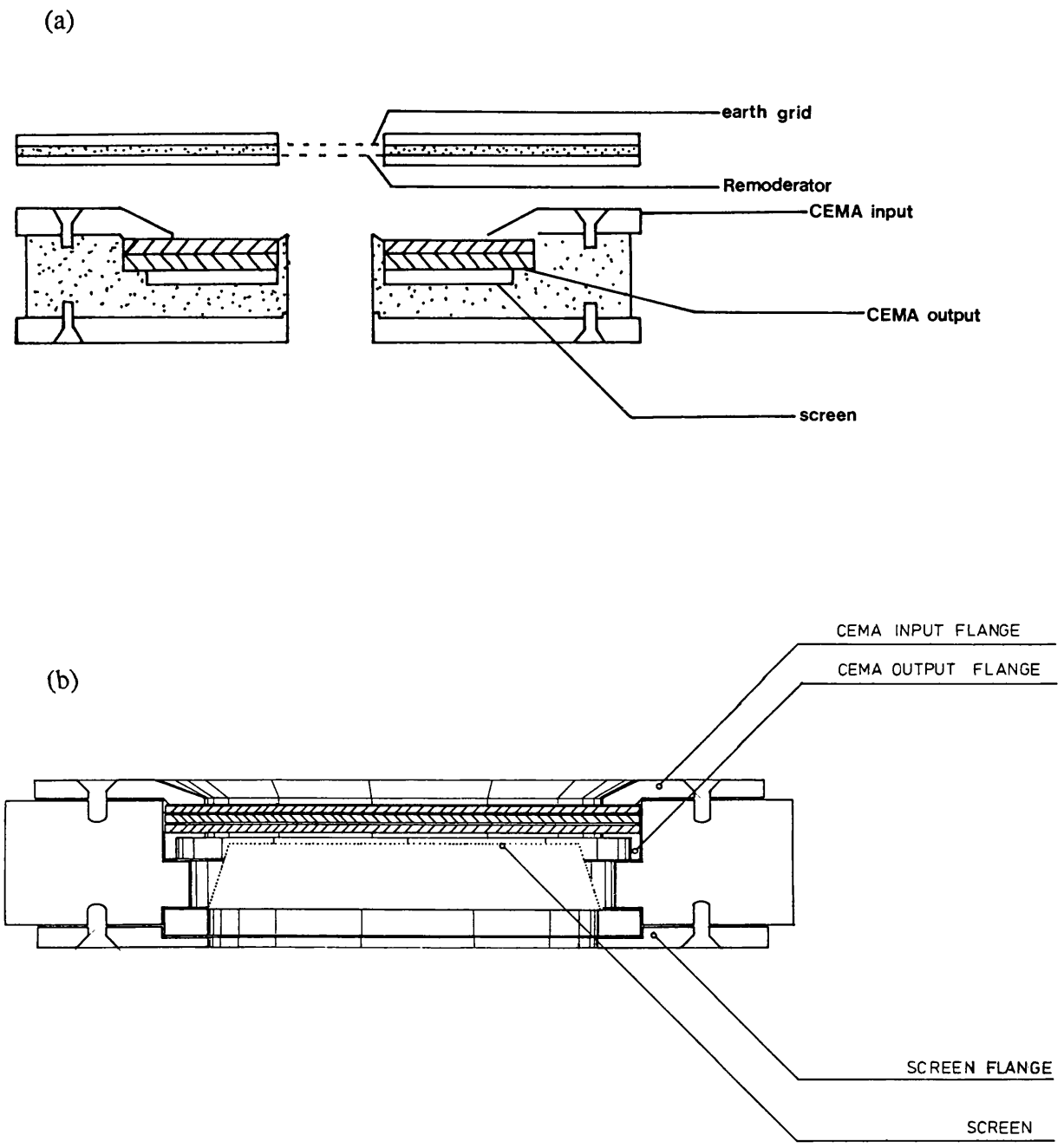

Figure 5.4 Diagram of (a) CEMA1 and (b) CEMA2

connected to a stainless steel disc to which the ceramic holder was fixed. A potential, V_T, of −325V was applied to the tube and the disc, which was positioned to face the incoming beam. To obtain gains in excess of 10^8, the MCPs were operated with the front face of the first plate maintained at +275V, to attract the secondary e^- whilst returning the e^+ which were emitted in the backward direction, and the back of the second plate held at +3.5keV. A voltage of +3.7keV was applied to the screen from which the signal was extracted.

The CEMA1 moderator arrangement was mounted on a linear shaft with motion perpendicular to the beam axis, which also allowed rotation about this axis. Thus, positioning for maximum interception of the incident beam was made by slight adjustment of the shaft. This also enabled the measurement of the incident beam by withdrawal of the arrangement from the beam axis.

The remoderated beam was guided to the gas cell and following interaction, the emergent particles were detected by a second set of channel electron multiplier arrays (CEMA2). CEMA2 consisted of three 25mm active diameter microchannel plates (Varian 8946), similar to those described above and arranged in the chevron formation (Figure 5.4b). A voltage of −450V was applied to the front face to retard electrons whilst accelerating the e^+ and the output of the back plate was held at +2.8keV. An Al-coated glass screen at +3.0keV, placed 2mm from the back plate, served to collect the charge.

An unannealed W grid, directly preceding the plates, was biassed at −520V (V_G) to return to the plate secondary e^- liberated by particles incident upon the surface. Two further unannealed W grids were placed in front of CEMA2 and maintained at earth for the e^+ measurements. For the Ps measurements these were held at +500V (V_R) to retard the e^+ from the primary beam. The entire grid-CEMA2 arrangement was also mounted on a linear shaft but on beam axis in order to vary the distance travelled by the particles before detection.

5.3.2 Timing Electronics

An inverted time of flight method was employed where the second detector in the sequence, CEMA2, gave the start signals and the first detector, CEMA1, provided the stop pulses. This system was used because of the low count rate from CEMA2

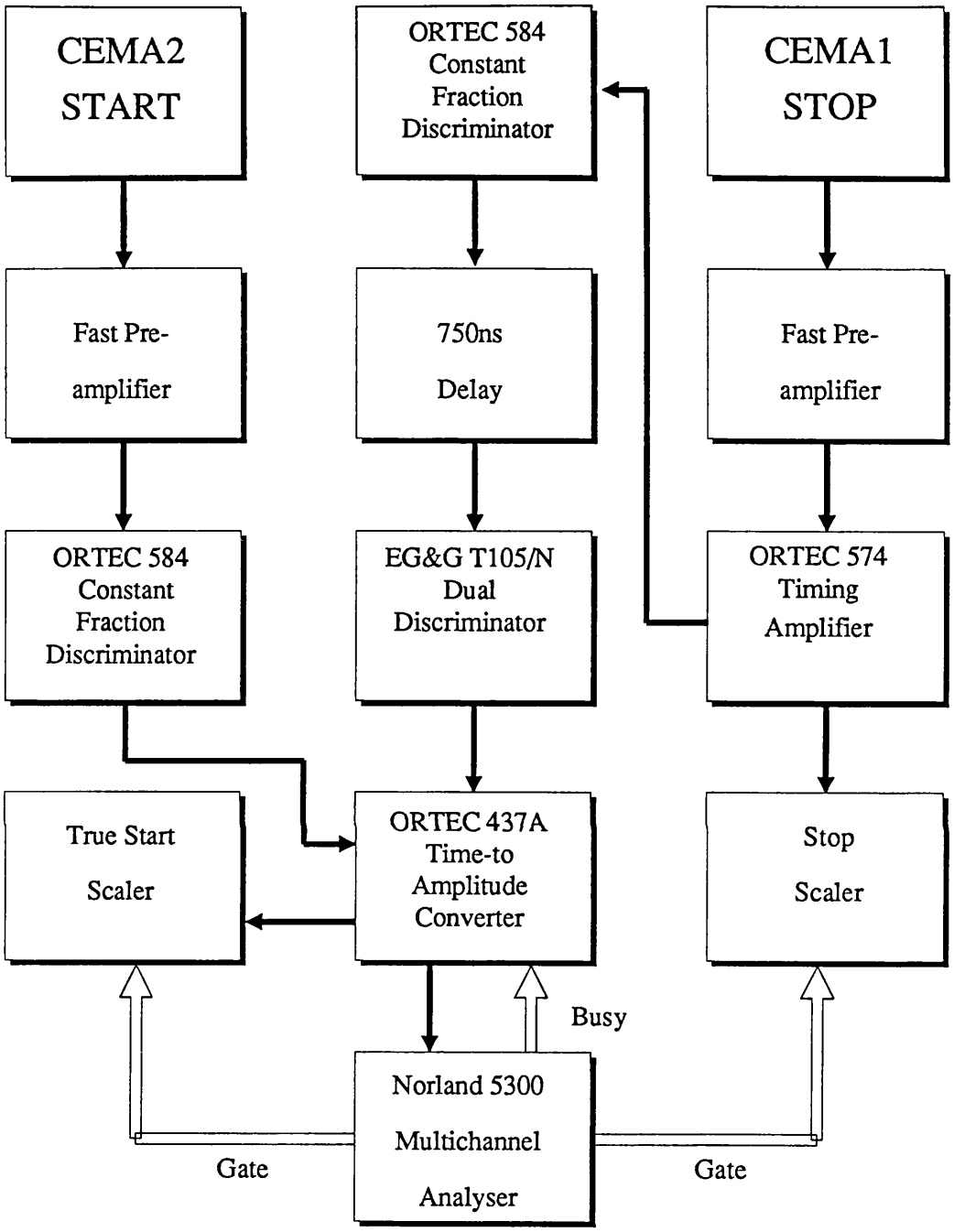

Figure 5.5 Block diagram of the timing electronics

during Ps runs ($\approx 10^1 s^{-1}$) compared to the signal from CEMA1 ($\approx 10^4 s^{-1}$). If pulses from CEMA1 were used as the start signal, some coincidences with CEMA2 would not be registered due to the dead time (7μs) of the Time to Amplitude Converter (TAC). A block diagram of the timing electronics involved is shown in Figure 5.5.

The signal resulting from the detection of secondary e^- at CEMA1 was extracted from the screen potential via two 470pF capacitors in parallel, terminated by a 1kΩ resistor and passed into a fast pre-amplifier through a Si IN4148 diode. Following x10 amplification, the signal was further enhanced by a factor of nine by means of a fast Ortec 574 Timing Amplifier and presented to an Ortec 473 Constant Fraction Discriminator (CFD) on scint mode. The discriminator levels were set accordingly to reject the noise contributions. The resulting pulses were fed through a 650ns delay line and the attenuated signal was boosted by an Ortec T105/N zero crossing discriminator before input to an Ortec 437A TAC as the stop signal.

The signal from CEMA2 was similarly extracted and amplified. An Ortec 473 discriminator was employed with the setting on NaI as the long dead time on this mode (1μs) ensured rejection of any tail on the pulses which may have led to double counting of the signal. The pulses were then fed to the start input of the TAC set on a nominal 1μs range and the resulting signals of various time-dependent amplitudes were registered by a Norland 5300 Multi-Channel Analyser (MCA) on pulse height analysis mode. The data was subsequently saved onto disc for analysis. Scalers recorded the total number of start and stop pulses. Calibration of the TAC time range was performed by feeding the signal from a pulse generator through the timing system via the fast pre-amplifiers. On varying the delay used on the stop line, the peak position registered by the MCA changed correspondingly. A least squares straight line fit to the peak channels and the respective delay times gave the time-per-channel over the region situated by the Ps peaks in the spectra. For the argon and helium studies, these were 1.1544±0.0015 ns/channel and 1.1433±0.0075 ns/channel, respectively.

5.4 Results and Discussion

5.4.1 Preliminaries

The study reported by Davies (1987) detailed the development of the timed Ps beam technique described above. In this work it was demonstrated that the energy of Ps

formed via charge exchange in Ar gas was tunable with the remoderated e^+ energy in the range 16–150eV. Various components of the spectra obtained were identified, however, due to insufficient resolution of the Ps peak, excited state (n>1) Ps was not observed. It was also noted that negligible signals were obtained from Ps with energy less than 7eV, thereby indicating that break up of the atom may be required for detection with CEMAs.

The motivation behind the generation of a timed Ps beam was the measurement of Ps-atom/molecule scattering cross-sections. However, progression to this stage required improvements to the technique in order to resolve the species in the beam which may affect these measurements. The investigation, reported below, undertook to separate the ground and excited states of Ps, quantifying the components produced in He and Ar gas. A method was also developed for deducing values of the total scattering cross-sections of Ps with both of these gases.

In an effort to increase the intensity and reduce the spread in time of the Ps signal, several modifications were made to the apparatus described by Davies (1987) in the initial development of the timed Ps beam. To preserve vacuum conditions suitable for the operation of CEMAs with the density range required in the cell, the pumping speed was increased by the incorporation of high conductance baffles. Furthermore, confinement of gas was aided by a 60% decrease in the conductance of the cell apertures by the addition of extension tubes. This proved to be beneficial in narrowing the time spread of the Ps peak as the region through which the e^+ beam passed was reduced, thereby shortening the distance over which Ps formation could occur. Thus, the time separation between the Ps formed at either extremes of the range would be smaller. A retarding system positioned immediately after the cell, in place of the **ExB** deflectors used in the previous study (Davies, 1987), was also of aid in preventing Ps formation beyond this point. The configuration of the magnetic field was changed to accommodate a greater difference between the source and the interaction region and in particular, to maintain a constant value along the cell to ensure uniformity of the angle integrated differential formation cross-section of Ps. The FWHM of the Ps peak was thus reduced to typically ≈4eV from the previously obtained spread of ≈10eV.

In the study of Laricchia *et al* (1988b), the short Ps flight path together with the spread of the peak did not allow adequate time separation of the signal for

identification of excited states of Ps, the energy of which are ≤5.1eV below that of the ground state. Therefore, the range of the distance travelled by the Ps before detection was increased by extending the linear shaft on which CEMA2 was mounted. Furthermore, this reduced the acceptance angle of the detector from 12° to a minimum of 3.3°.

Significant improvements to the intensity of the beam were achieved by three further modifications. Firstly, a potential of -325V was applied to the mounting and the tube of CEMA1 to divert the flow of secondary e^- from the remoderator away from the central hole and onto the plate. This resulted in a threefold increase in the number of timed e^+. The negative voltage on the mounting also repelled e^- from the source end, preventing impact onto the moderator and the consequent liberation of secondary e^-. The signal from CEMA1 was reduced by 30% without any loss of the timed beam and thus decreased the background caused by random coincidences. Secondly, the distance between the moderator and CEMA1 was increased from 7mm to 14mm with a 50% increase to the timed flux. This was due to an improvement in the electric field configuration in this region allowing more linear e^- trajectories to CEMA1. Finally, an additional grid was placed between CEMA2 and the existing grid arrangement employed to retard e^+. The introduction of this grid with the application of −520V, was found to substantially improve the timing efficiency and increased the timed beam rate by 30%. As the open area of the plate (that is the channel coverage) is about 55% of the total plate area, a number of the incident particles may not strike a channel but nevertheless release secondary e^- on impact. The purpose of the negative potential was, therefore, to return such e^- to the plate and hence increase the probability of detection.

By withdrawal of the CEMA1 arrangement from the beam line, the number of slow e^+ originating from the primary moderator and transported through the various grids and apertures to CEMA2 was measured to be $\approx 11000 s^{-1}$. Approximately $6000 s^{-1}$ of these were intercepted by the secondary moderator, producing ≈900 remoderated $e^+ s^{-1}$ and thus giving a conversion efficiency of ≈15%. On integration of the peak on the time of flight spectrum, the number of timed e^+ was found to be $\approx 400 s^{-1}$ and the timing efficiency of the system was deduced to be 45%. With these conditions of operation, o–Ps produced from interaction of the e^+ with He and Ar gas were detected by CEMA2 and the time of flight measured by the coincidental detection of the secondary e^- at CEMA1. Runs were taken at various gas densities (0.5–12μmHg),

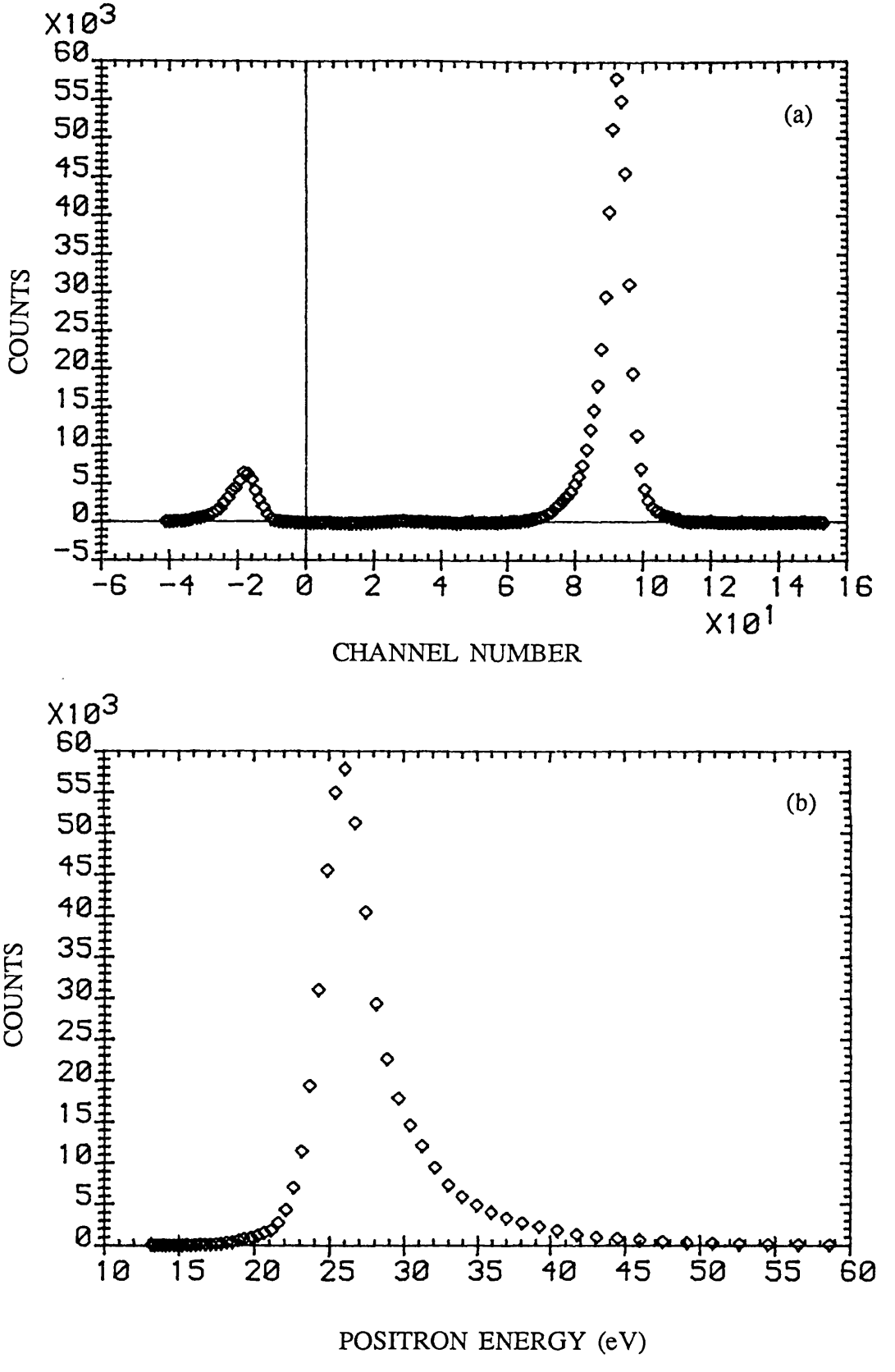

Figure 5.6 Positron TOF spectrum at V_{M2}=23.5V as a function of (a) channel and (b) energy (eV)

incident e^+ energies (16–52.5eV) and o–Ps flight lengths (0.137–0.431m) over times of 10,000 to 250,000s.

Figure 5.6a shows an example of a e^+ time of flight spectrum obtained over a period of 1000s with a potential of 23.5eV applied to the moderator. As the random coincidence count rate in the spectrum was uniform, the background was calculated by averaging a 100 channel portion in a flat region of the spectrum and the value obtained was subtracted from each data point. This was checked by applying the data restoration procedure developed by Coleman *et al* (1974) and Coleman (1979) to a number of spectra. Two peaks are observed in Figure 5.6a; the larger of the two is due to remoderated e^+ and the smaller one, at negative channel numbers (or negative times if multiplied by the time per channel), is a result of the coincidental detection of a particle at CEMA2 with e^- liberated at CEMA2 but escaping the retarding field and travelling back upstream to be registered by CEMA1. The zero time channel was identified by replacing the meshes at CEMA1 with an Al plate and monitoring the e^- coincidences with γ-rays detected at CEMA2 from the annihilation of the incident beam. Figure 5.6b shows the conversion of this spectrum onto an energy scale and illustrates the energy spread of the remoderated e^+ beam. The peak of the signal located at 26eV, demonstrates that, as previously stated, the workfunction of the W mesh is $\approx$2.7eV. The long tail on the high energy side of the peak is caused by the presence of epithermal positrons, that is, positrons emitted from the moderator with non-thermal energies. Even so, over 80% of the e^+ are contained in a 5eV region about the peak energy.

Spectra from both e^+ and Ps runs were transformed from times/channel numbers to the corresponding energies by the application of the following equations. For e^+, the energy, E_{e+} (in eV), is given by

$$E_{e+} = (m_o/2e)(d_{e+}/t_{e+})^2 \qquad 5.1$$

where m_o and e are the mass of the positron and the electronic charge, respectively and the distance d_{e+} is that travelled by the e^+, in this case, from the remoderator to CEMA2. However, it was possible that this length could be considerably greater than the physical value as a result of the spiralling motion. The actual path length of the e^+ was, therefore, deduced by varying the e^+ energy, at constant d_{e+}, and noting the change in the peak position and therefore the time taken (t_{e+}). The energy of the

e^+, as mentioned in Section 5.3.1, was composed of contributions from V_{M2} and the workfunction-contact potential component. Therefore, as the latter value was constant, a plot of V_{M2} versus $(1/t_{e+})^2$ (Equation 5.1) yielded a straight line from which d_{e+} was extracted. The derived result was consistent to within 2% of the geometric value, thus demonstrating that the physical distance could be used without significant error. Furthermore, the workfunction-contact potential value was determined to be 2.7±0.5eV from the intercept of this graph.

The time taken by the e^+ to travel this distance was deduced from the inverted time of flight spectrum using

$$t_{e+} = t_m + t_{e-} \qquad 5.2$$

where t_m is the measured time taken, calculated by multiplying the difference in channels from zero time by the time per channel, and t_{e-} is the secondary e^- flight time to CEMA1. Assuming constant acceleration from the remoderator to CEMA1 with zero initial velocity and a linear, geometric trajectory, the value of t_{e-} was computed according to

$$t_{e-} = (2m_e/Fe)^{1/2}d_{e-} \qquad 5.3$$

where F is the electric field across the distance, d_{e-}, traversed by the electron. With 23.5V applied to M2 and taking d_{e-} and F from above, t_{e-} is 3ns. Compared to typical values of t_m (of the order of 100's ns), t_{e-} is much smaller than t_m, therefore the assumptions of linear path and zero initial velocity are justified. Moreover, the increase in the M2–CEMA distance from 7mm to 14mm reduces the percentage error arising from the use of the geometric value, d_{e-}.

On application of potentials on the arrangement following the gas cell and the grids preceding CEMA2, and with He or Ar in the cell, o–Ps spectra were obtained and similarly converted to an energy scale. The time taken, t_{Ps}, by the o–Ps to travel from the point of production to the CEMA2 is given by

$$t_{Ps} = t'_m + t_{e-} - t'_{e+} \qquad 5.4$$

where t'_{e+} is the time taken by the e^+ to travel from M2 to the gas cell prior to Ps

formation and t'_m is the measured time taken of the total (e^+–Ps) flight. From e^+ runs, illustrated above, the mean value of the remoderated beam was accurately ascertained. Thus, by using Equation 5.1, t'_{e+} was computed assuming that the e^+ had travelled from M2 to the mid-point of the cell. The mid-point was defined to be the position by which half the total number of Ps produced are formed from the point l=0 where l is the effective length over which e^+ scattering can occur in the cell. This was determined by the procedure described in Section 5.4.3. The use of this distance was justified as Ps peaks on the spectra taken were located at the expected energies. Conversion to the energy scale with the distance from the geometric centre of the cell to CEMA2 gave discrepancies of up to ≈1eV on the peak energy. From Equation 5.5, it can be seen that the width of the Ps peak caused by formation at different points in the cell would be greater at lower energies. At 7eV Ps energy (the lowest value of this investigation) the spread in energy from Ps produced at either extreme of the extended cell arrangement was ≈7eV. This distribution was further enhanced by the energy width of the e^+ beam, e^+ spiralling, the thermal motion of the gas atoms and the resolution of the system. The last factor was determined to be ≈4ns (FWHM) by progressively increasing V_{M2} until no change was observed in the width of the peak obtained on the spectrum. The energy of the o–Ps, E_{P_s}, was, therefore, evaluated according to

$$E_{P_s} = (m_{P_s}/2e)(d_{P_s}/t_{P_s})^2 \qquad 5.5$$

where m_{P_s} is the mass of Ps (=2xm_o) and d_{P_s} is the distance travelled by the Ps, taken to be the length from the mid–point to CEMA2.

An example of a Ps spectrum, collected over 63,000s at a Ps flight length (d_{P_s}) of 0.431m and with 7.49μmHg of He gas, is shown in Figure 5.7. Background subtraction was performed in the same manner as that described above for the e^+ spectra. For most runs, this procedure was adequate in eliminating the random coincidences, however, in some of the spectra taken at small d_{P_s} (≈0.14m), and therefore, at large acceptance angles, a significant number of coincidences were found to be emanating from the annihilation of e^+ about the cell-retarder arrangement. These appeared on the high energy side of the Ps peak due to the detection of γ–rays, therefore, at these distances vacuum runs (that is, with no He or Ar in the cell) were taken and subtracted from the corresponding gas spectra.

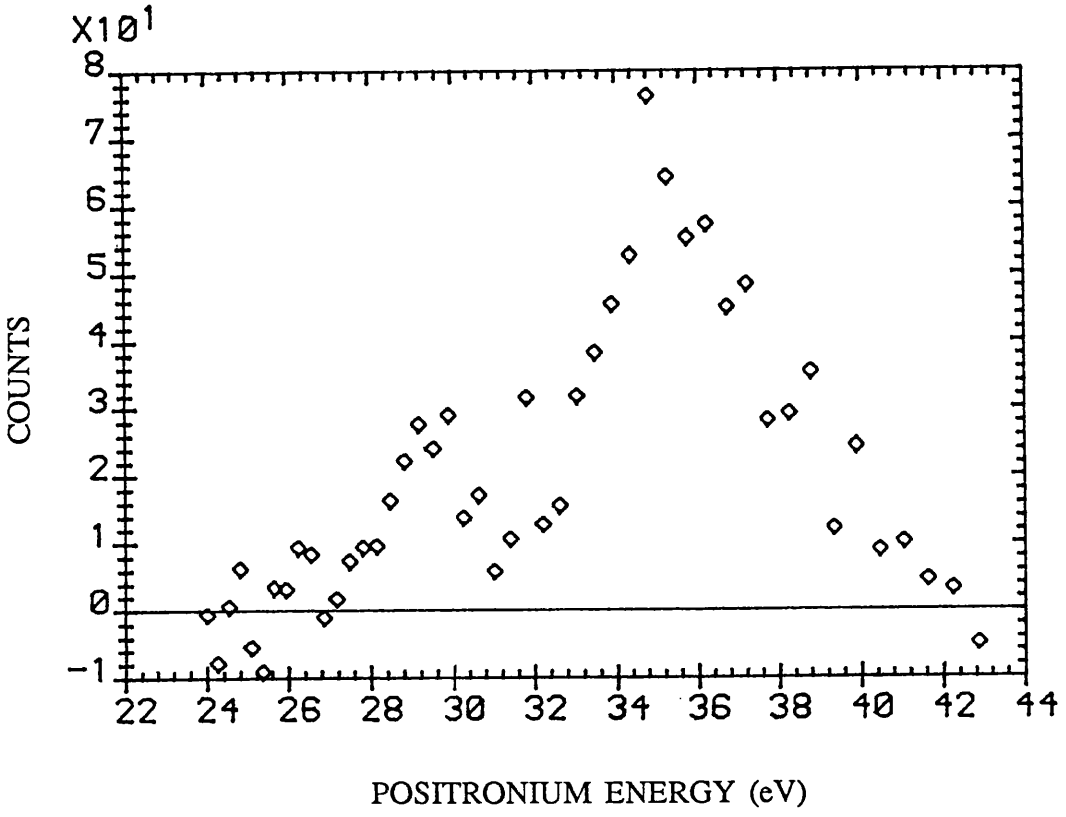

Figure 5.7 Positronium TOF spectrum taken at V_{M2}=50.0 V with 7.49μmHg as a function of energy

The energy of the Ps can be calculated according to

$$E_{Ps} = E_{e+} - E_I + E_b \qquad 5.6$$

where E_I is the ionization energy of the target species and E_b is the binding energy of the Ps atom. For He and Ar, E_I is 24.6eV and 15.7eV respectively. E_b is 6.8eV for ground state Ps and reduces by 5.1 eV to 1.7eV for n=2 excited state Ps (Ps^*). For the spectrum shown above, E_{e+} was 52.5eV, therefore o–Ps and Ps^* of 34.7eV and 29.6eV would be expected. Two peaks, located about these energies, are clearly discernable, demonstrating the ability of this technique to separate the Ps components. The total number of Ps counts (ground and excited states) is 0.015 o–Ps atoms s^{-1}; p–Ps atoms are not detected as a negligible amount survive beyond ≈1cm in flight due to their short lifetime. The number of o–Ps atoms counted per scattered e^+ in a cone of acceptance angle 3.3° was 4.7×10^{-3}. If isotropic production is assumed, then the total number of o–Ps atoms formed in 4π solid angle would be 22 per

scattered e^+; this is indicative that, as Ps formation is known to be forward directed, substantial spiralling has not occurred.

With a typical FWHM of the Ps peak of ≈4eV, an appropriate distance was chosen for each energy investigated to allow enough time separation of the ground and excited state Ps signals for analysis. From Equation 5.5, it can be seen that the time difference, Δt_{Ps}, between the n=1 and n=2 states is given by

$$\Delta t_{Ps} = (m_o/e)^{1/2} (E_{Ps^*}^{-1/2} - E_{Ps}^{-1/2}) d_{Ps} \qquad 5.7$$

Increasing d_{Ps} results in a greater loss of counts due to decay in flight, therefore the distance set was balanced with above requirement. The property of self annihilation, however, was employed to verify the identity of Ps signal obtained.

5.4.2 Lifetime measurements

Measurements of the positronium decay rate (the reciprocal of the lifetime) were made in both He and Ar with approximately 4μmHg gas pressure at e^+ impact energies of 35eV in He and 26, 35 and 50eV in Ar. At each energy, the geometric distance was varied between 0.148m and 0.431m with corresponding acceptance angles of 9.7°–3.3° subtended to the centre of the cell. The Ps counts per scattered e^+ per steradian per second, I, were plotted against flight time according to

$$\ln I = \ln I' - \lambda t_{Ps} \qquad 5.8$$

where I' is the initial number of Ps formed in a particular state and λ is the measured decay rate of Ps. The differential formation cross-sections in this angular range were assumed to be constant so adjustments were made only for the solid angle; the theoretical calculations by Mandal *et al* (1979) and Khan and Ghosh (1983) and Khan *et al* (1985) show the variation to be small for (n=1 and n=2) Ps at these energies.

With the intensity and time spread of the available Ps flux, it was not possible to completely resolve the states without losing most of the signal. Therefore, the Ps counts in a 4eV portion, 2eV on either side of the peak energy, were summed for the component states in Ar. Due to low count rates, the full Ps peak was used in He as less than 11% of the total number of counts appeared in the n=2 region. Employing

Equation 5.8, the lifetime in He was deduced to be 128±28ns, whilst in Ar the weighted mean of the values obtained at 25, 35 and 45eV was 152±16ns (Figure 5.8). Both of these results compare favourably with the expected value of 142ns, which is contained within the limits of the errors, and provide further confirmation of the detection of o–Ps.

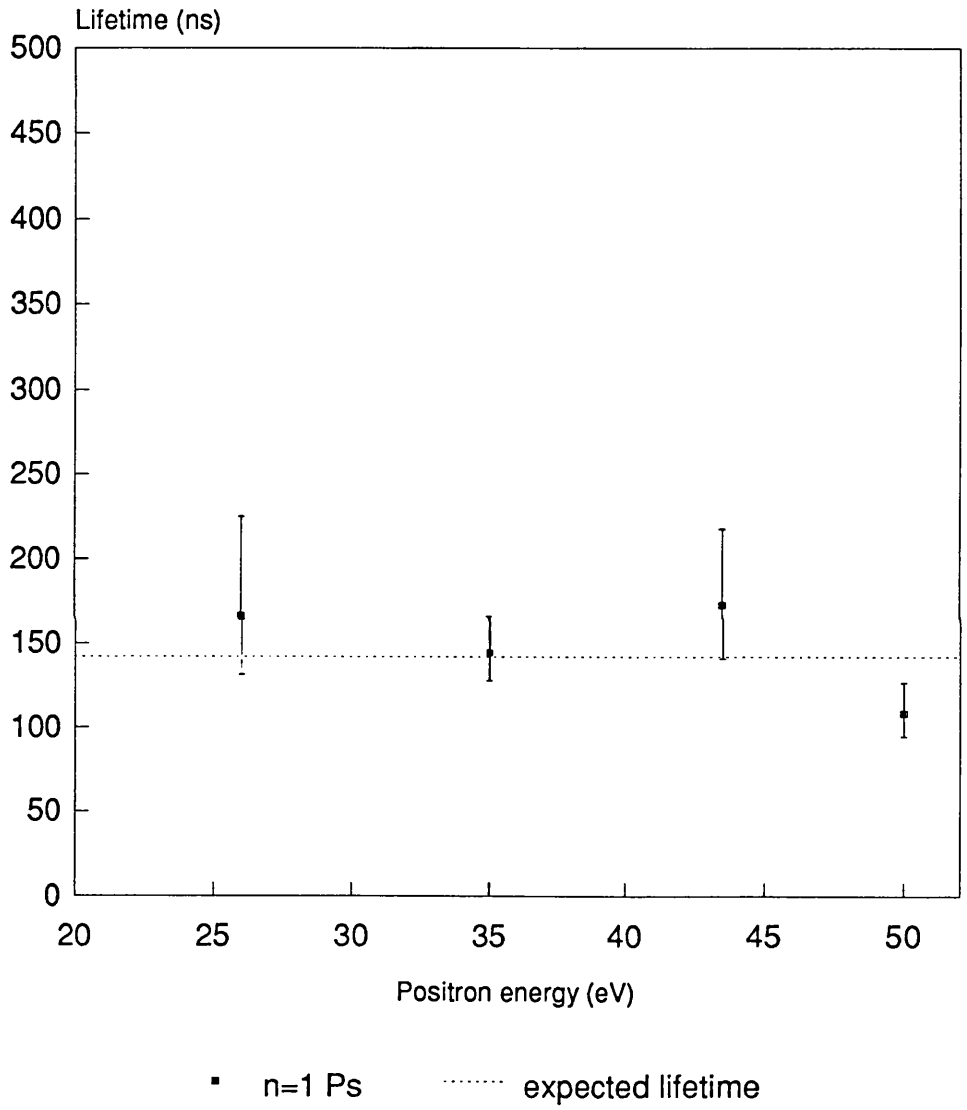

Figure 5.8 Measured lifetimes of Ps (n=1) obtained from Ar gas

At 50eV in Ar, however, the lifetime obtained from a straight line fit, 108±16ns, is much lower than expected which indicates that, at the higher energy, constrained by

the travel of the shaft, the flight path was not sufficient in length to allow adequate separation of the peaks. The logarithmic plot of the sum of the two exponentials results in a curved line from which the decay rate of one of the species cannot be extracted without knowledge of the other's decay rate or the relative number of Ps initially formed in the two states. This is further complicated by the possibility of detecting a number of n=2 substates.

Of the sixteen n=2 Ps sublevels, only those formed in the metastable S state ($2\,^3S_1$) and the triplet P states ($2\,^3P_{0,1,2}$) can survive in sufficient numbers to the detector. The former has a lifetime of 1100ns and the latter preferentially de-excites to the o–Ps ground state within 3.2ns, giving a lifetime of ≈145ns. It was hoped that the decay rate extracted for the n=2 Ps would indicate whether mainly S, P or a mixture of S and P states were being detected. However, with insufficient data and the probability of a sizeable contribution from the ground state, especially at small d_{Ps}, it was not possible to draw any conclusions. Moreover, contamination of the n=2 peak with a higher state Ps cannot be dismissed as the energy separation rapidly decreases between increasing n values (as a function of n^{-2}), making the resolution of these components impossible to achieve in this arrangement. Although the relative formation of Ps in any state can be estimated from proportionality to the n value (αn^{-3}), the number detected is a function of the differential formation cross-section, the lifetime of the substates and the detection efficiency. The n=3 state Ps is estimated to form only ≈4% of the total number of Ps produced which, in this system, would be barely distinguishable from the background. Some suggestion was found on a few spectra of a peak at an energy 6eV below the main signal, coinciding with the expected location of the n=3 state. However, as this state lies 0.94eV below the n=2 level, the flight path required for separation to establish the proportions would not be feasible.

5.4.3 Yield measurements

As in the lifetime measurements, the counts were summed in a 4eV portion about the energies corresponding to the n=1 and n=2 states of Ps. In addition, for Ar, 2eV regions (1eV on either side of the peak energy) were integrated in order to reduce contributions from other states. The counts were normalised to the number of scattered positrons, the solid angle subtended to the mid-point of the cell and for n=1, also corrected for in-flight decay. The number of scattered e^+ was calculated

according to the Beer-Lambert law,

$$N = N_o e^{-nl\sigma} \qquad 5.9$$

where N and N_o are the numbers of unscattered and initial particles, respectively and l is the length over which the interaction can occur. The target number density, n, is given by

$$n = 9.67 \times 10^{21} \rho/T \qquad 5.10$$

where ρ is the pressure in μmHg at temperature T(K). The interaction cross-section, σ, which in this case was the total e^+ scattering cross-section (σ_T), was derived from the experimental work of Griffith *et al* (1979) and Kauppila *et al* (1981). End effects from the use of a short gas cell, as in this experiment, can cause a marked departure of the length over which the particle can scatter (known as the cell length) from its geometric value. Therefore, the effective cell length and its dependence on the pressure measured at the centre of the cell were determined by performing attenuation experiments. Using Equations 5.9 and 5.10 with known σ_T values (Griffith *et al*, 1979, Charlton *et al*, 1984) l was extracted for various densities. Over the range of the Ps study, the effective cell length did not seem to exhibit a trend with density and was hence presumed to be constant for each gas (Figure 5.9). Weighted mean values were thus employed, which were 44.3±1.3mm and 43.8±1.9mm for He and Ar, respectively, compared to the physical value of the extended cell arrangement of 53.8mm. Following consideration of e^+ multiple scattering and Ps scattering, the density below which runs were taken was constrained to 4μmHg in He and 1μmHg in Ar. These conditions are discussed below in the context of Ps scattering cross-sections.

The yields of Ps and Ps^* atoms detected, normalised to scattered e^+ and solid angle, are illustrated graphically in Figure 5.10, together with the n=1 component following correction for decay in flight. These corrections were made by the application of Equation 5.8 using the reciprocal of the known lifetime ($1/142ns^{-1}$) for the decay rate of the n=1 component and the time taken to travel the distance d_{Ps}. The general trend with *Ps energy* appears to be similar in both gases for the corrected n=1 contributions, rising sharply by (68±7)% from 7.2eV to a maximum at 34.7eV in Ar and by (73±7)% in He over the same energies. The distributions of the Ps^* yields,

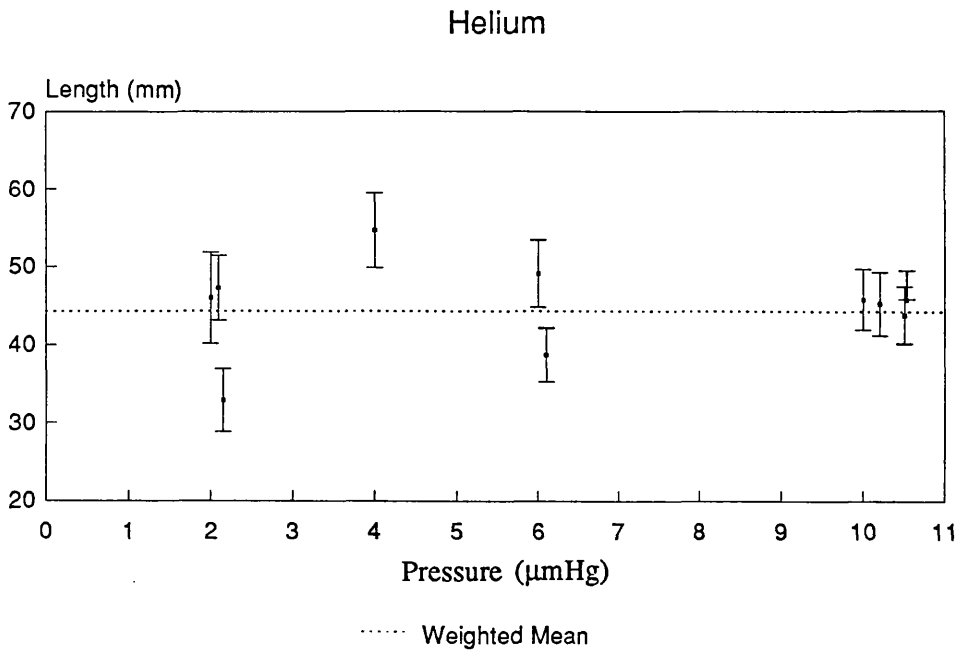

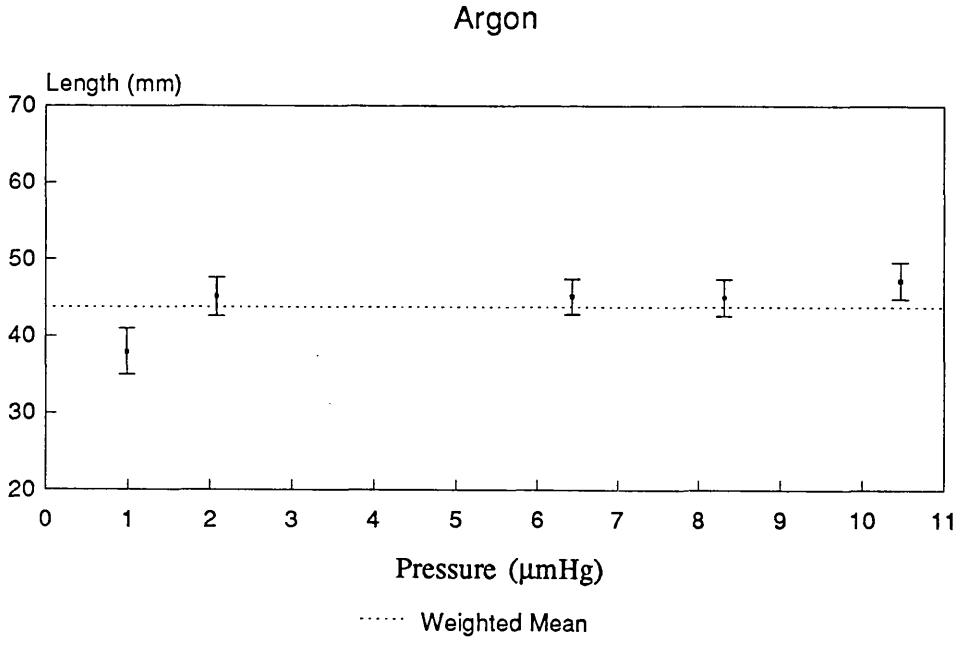

Figure 5.9 Measured cell lengths in (a) He and (b) Ar versus pressure

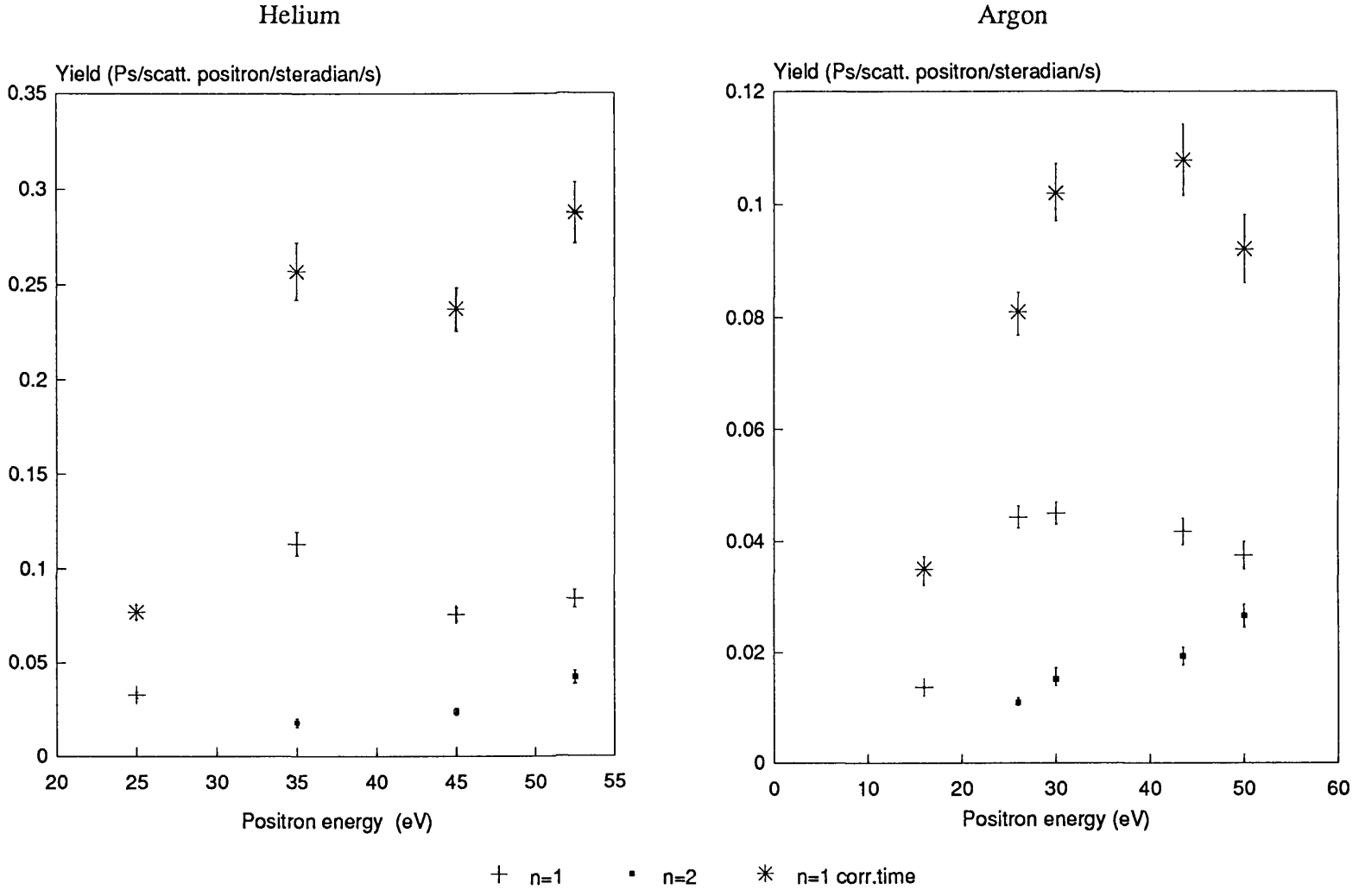

Figure 5.10 Measured yields of n=1, n=1 (corrected for decay in flight) and n=2 Ps in 4eV regions from (a) He and (b) Ar

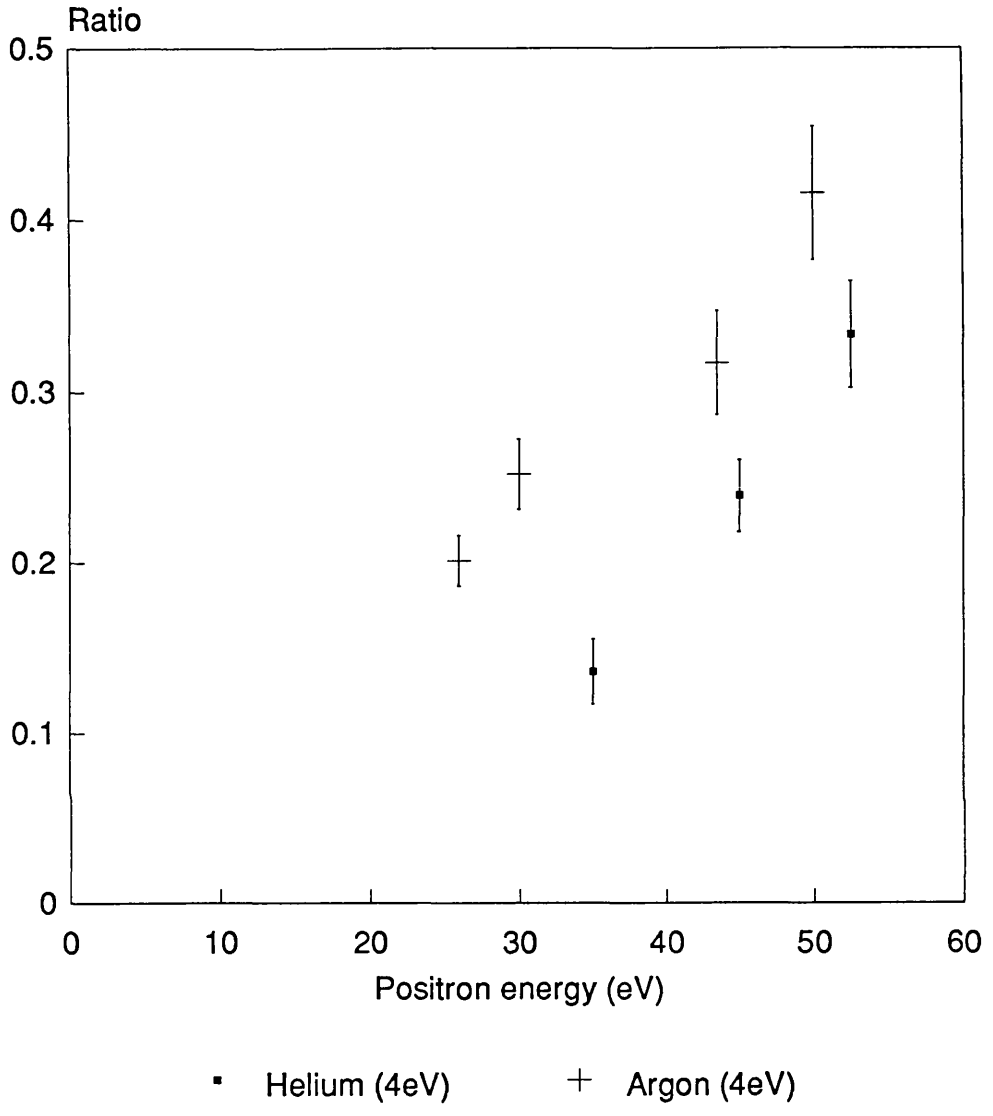

Figure 5.11 Ratio of measured n=1+2 and n=2 Ps yields in 4eV regions from He and Ar

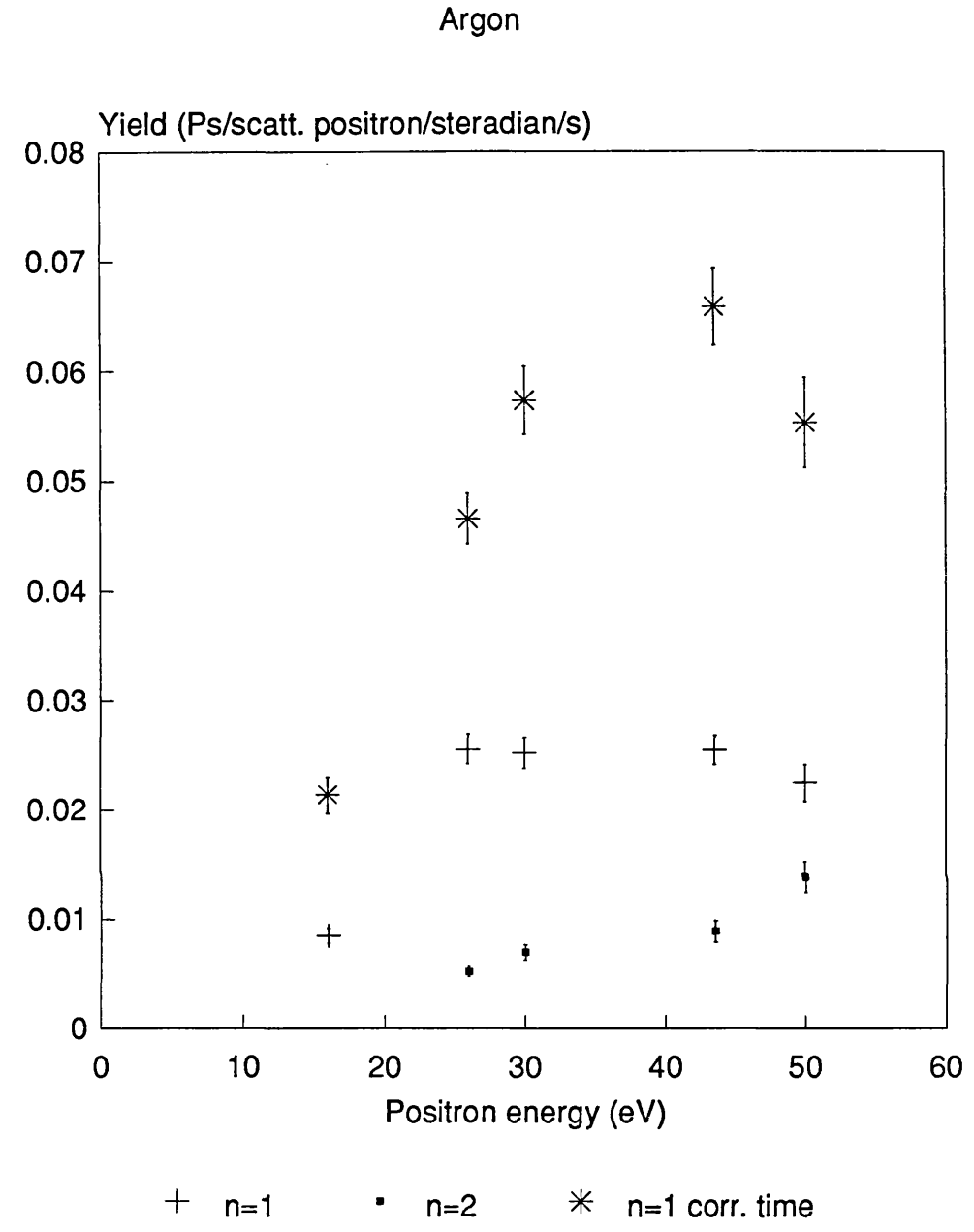

Figure 5.12 Measured yields of n=1, n=1 (corrected for decay in flight) and n=2 Ps in 2eV regions from Ar

uncorrected for decay, increase continuously by (57±11)% (He) and (42±10)% (Ar) over the range of the two common energies investigated. At the lowest e^+ energy in both cases, Ps^* was not detected in statistically significant quantities. The excited state yields were not corrected for in-flight annihilation as the proportions of the metastable S and triplet P, with their vastly differing lifetimes, were not known.

The ratio of the uncorrected yields are presented in Figure 5.11 and show that, over the energy range studied, Ps^* atoms compose (14±2)-(33±3)% and (20±1)-(42±4)% of the detected beam produced from He and Ar, respectively. For Ar, yields from the integration of the 2eV regions are also shown (Figure 5.12). The ratios of n=1 and n=2 Ps are slightly less than those from the 4eV portions at the same energies. Due to the Ps flight paths set and hence the peak separations obtained, a certain proportion of the signals from the n=1 and n=2 states were likely to overlap on the time-of-flight spectra. Therefore, the probability of containing signal from the other state was greater in the 4eV regions. Differences in the formation cross-section of n=1 and n=2 Ps (of about an order of magnitude - see below), would cause proportionately greater contamination of the n=2 portion by n=1 Ps signals and would thereby result in larger ratios. This effect is less apparent for He as the distances set were longer and hence the peak separations on the spectra at the corresponding Ps energies were greater.

Direct comparison cannot be made with the results obtained by Laricchia *et al* (1987) prior to the introduction of the timing system. Differences arise from the allowance of grid absorption, summation of the total Ps count rate and the assumed presence of solely ground state Ps in the beam. However, on correcting the n=1+2 yields from the present study for ground state Ps decay only as in the previous work, illustrated in Figure 4.9, excellent agreement is obtained between the He/Ar ratios at the peak values. The He yield is approximately 2.7 times greater than that of Ar in both studies at e^+ energies of 40-50eV.

In the study of Laricchia *et al* (1987), the Ps counts in the 26-50eV region rise by a factor of (3.0±1.6) in He and (1.6±0.8) in Ar. The same regions in the present work show an increase of x(5.6±0.4) in He and x(4.6±0.4) in Ar. A much sharper rise is observed in both gases which may be indicative of a more favourable magnetic field configuration. It is noted from the data of the previous work that the magnetic field influences not only the magnitude of the yield, but also the rate of increase with energy.

The "absolute" yield can be roughly estimated, solely for the purpose of comparison, by implementing the following:
(i) normalisation to an 8° half angle of acceptance;
(ii) allowance for grid absorption (nominally 90% transmission), although the effect of grids is unknown as the mechanisms of Ps detection have yet to be established;
(iii) correction for the total Ps yield - at the highest energies the n=1 region contained approximately 40% of the beam.

Application of these factors at 40-50eV gave values for He and Ar of ≈60(±3) and 23(±1) respectively, comparing very favourably with the previous values of (60±10) and (22±4) (Ps atoms per scattered $e^{+}x10^{-3}$).

The theoretical computations on the differential formation cross-section are, in the main, limited to H and He target gases using first Born approximation and distorted wave models. Complete calculations on the total and differential formation cross-section of both 2P and 2S state Ps with the same method have yet to be reported over the energy range investigated in this study. Hence, the absolute yields expected could not be derived. Moreover, comparison with theory requires knowledge of the relative formation of the 2S and 2P states of Ps in the experiment. The lifetime measurements, discussed above, did not convey any conclusive information on this matter. Nevertheless, comparison was made in the manner described below.

Plotted in Figure 5.13 are the ratios of the experimental values corrected for in-flight decay with the assumption that the n=2 yield consists entirely of either metastable S or triplet P atoms (denoted by (2S/1S)exp and (2P/1S)exp on the graph). Alongside the experimentally derived values in Figure 5.13, are theoretically calculated ratios of total Ps formation into (2P+2S) states to the ground state, derived from the distorted wave polarised orbital calculations of Khan and Ghosh (1983) and Khan *et al* (1985). Also performed was the application of the reverse process - corrections of the theoretical values for in-flight annihilation using the known lifetimes of the individual states over the time taken in flight by the Ps at each energy in the experiment. These numbers were derived for each state from the work of Khan *et al* (1985) and are plotted in Figure 5.14 with the detected (uncorrected) ratios.

The comparison of the experimental values with the total predicted yields is not strictly justified, however, this was prompted by the results obtained by Mandal *et al*

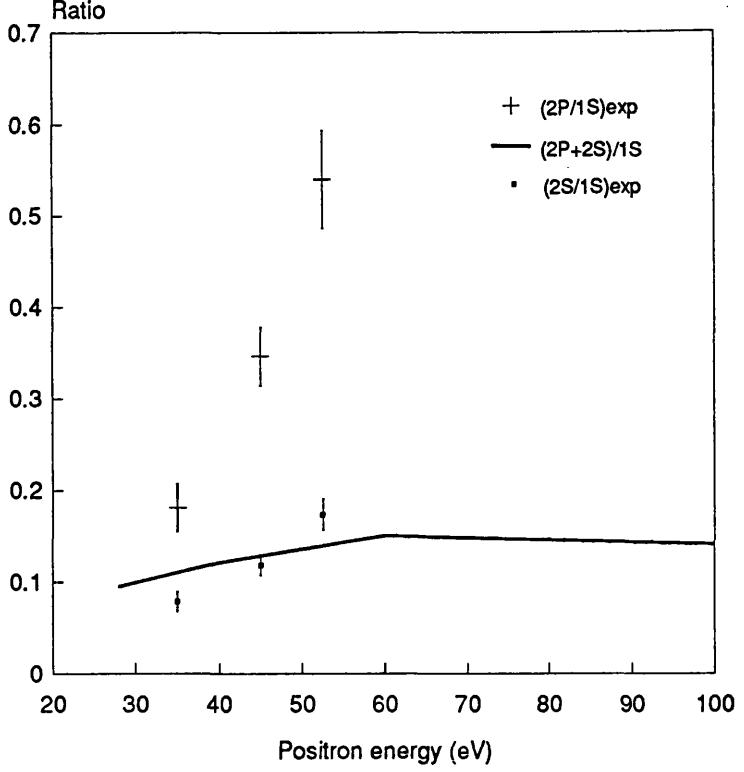

Figure 5.13 Theoretical ratios Ps and Ps* formation yields in He (Khan *et al*, 1984, 1985) and the measured ratios corrected for decay in flight with the assumption of either entirely 2^3S or 2^3P state formation for the n=2 yields

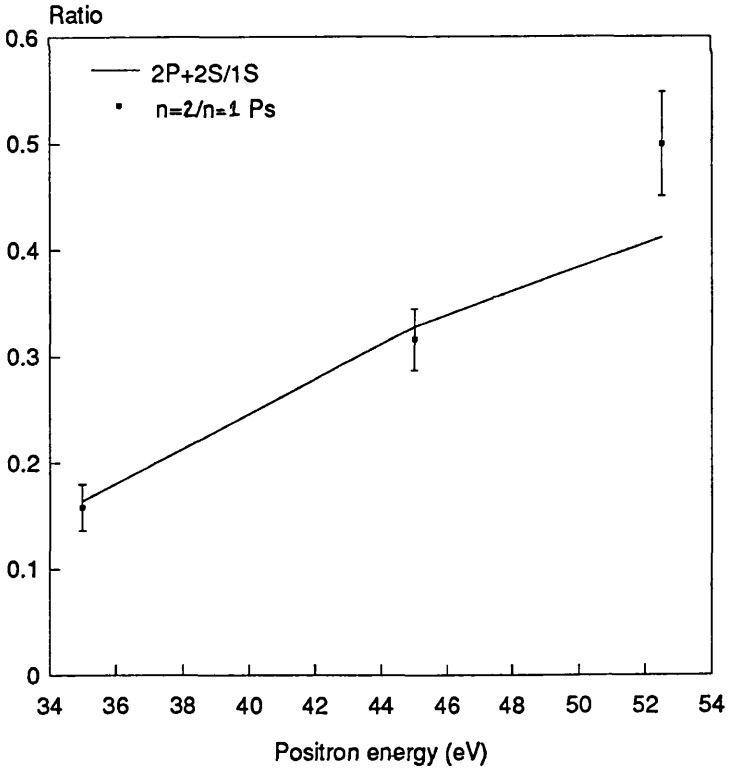

Figure 5.14 Theoretical ratios of Ps and Ps* formation yields in He, corrected for decay in flight (from Khan *et al*, 1984, 1985) with uncorrected measured ratios

(1979, 1980), using the distorted wave model, of the differential formation cross-sections at 100eV e^+ energy. For ground and 2S state Ps, $(\int d\sigma_{Ps}/d\Omega)_{average}$ from 0–5°, was computed, and the ratio derived, 0.1176, was found to be in close accord with that of 0.1183 from the total formation cross-sections at the same energy.

As three-quarters of each of the 2P, 2S and 1S states that are initially formed can survive to the detector, comparison with the theoretical ratios is straightforward assuming that the detection efficiency of the CEMA is constant for the various states. From Figure 5.13, the experimentally derived (2P/1S) values shows a very much larger discrepancy with the calculated (2P+2S)/(1S) distribution than the (2S/1S) ratios. Moreover, the similarity of the two latter distributions implies that the composition of the n=2 yield is dominated by the metastable state atoms. Clearer indication of the proportions may be gained by inspection of Figure 5.14; the experimental and calculated ratios of (2P+2S)/(1S) are in good agreement at the lower energies. If this comparison is valid, then in He, 10-12% of the Ps initially formed in the system are in the n=2 state and that, of these, approximately 70% can be attributed to the metastable S state at Ps energies in the range 17.2-34.7eV. The deviation at the highest energy may be caused by contributions to the yield from Ps of another state. Due to the physical restrictions of the apparatus, a sufficiently long flight path could not be chosen to achieve the same peak separation as at the lower energies, thereby increasing possibility of overlap between the two states and as explained above, resulting in larger values of ratio than expected.

Perhaps the most useful comparison, bearing in mind the ultimate aim, is that of the actual intensity of the Ps flux from the two gases. The initial method proposed utilised two gas cells in order to separate the production and the scattering processes. Although discarded in this study, future investigations will re-incorporate the second cell. Essentially, the requirement of a production cell is to form the maximum quantity of Ps possible in a preferentially forward direction. From Figure 5.10, the yield per scattered e^+ is greater in He by a factor of (2.7±0.2) for the maximum n=1 values, suggesting a more pronounced forward peaked nature for the differential formation cross-section of He. However, on inspection of the total scattering and formation cross-sections of the two gases, the numbers of e^+ scattered and Ps formed are greater for Ar by approximately an order of magnitude. Therefore, it may be instructive to examine the yields with respect to the incident e^+ count rate. These are represented graphically in Figure 5.15 for He and Ar at 1μmHg gas pressure and also

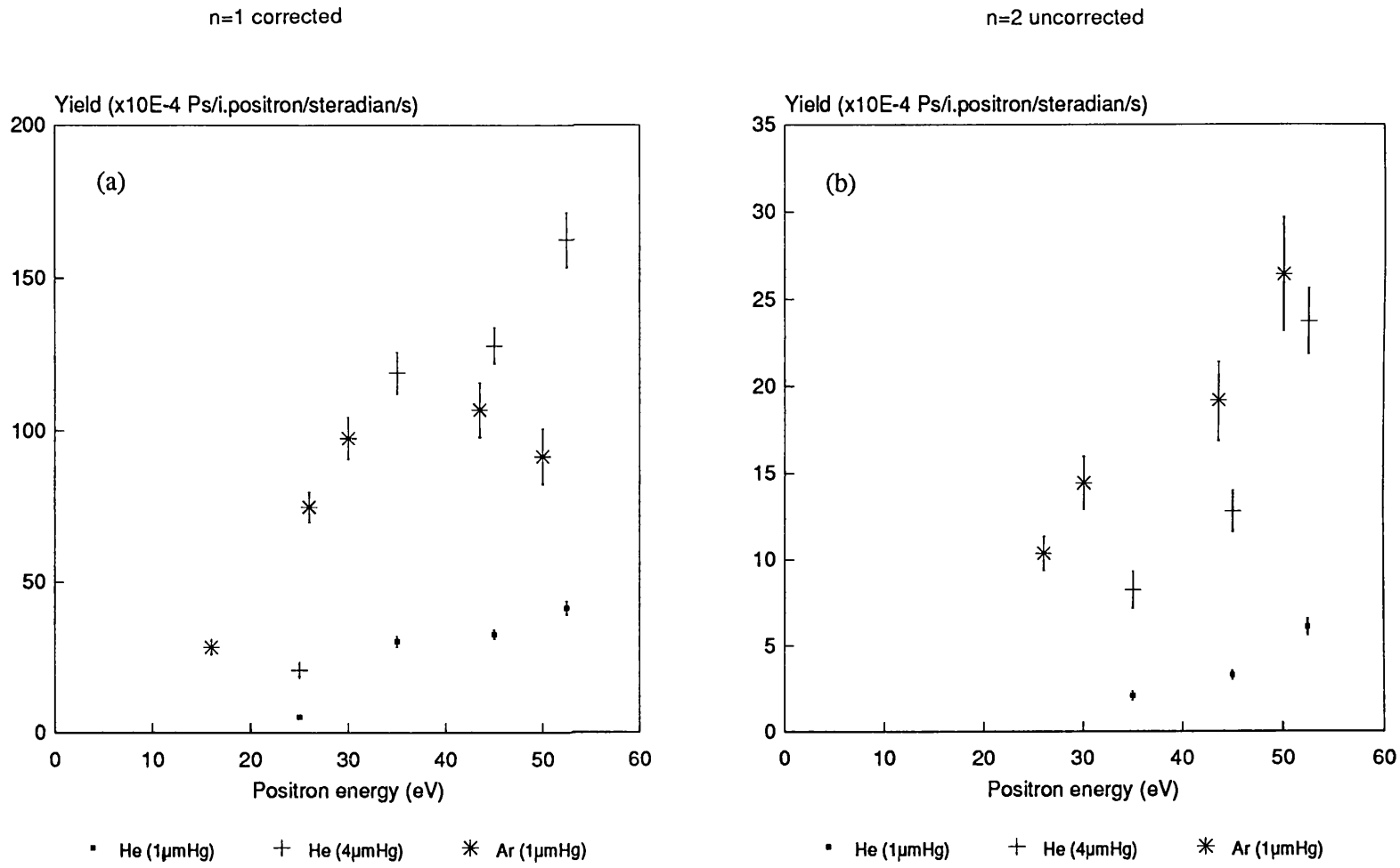

Figure 5.15 Derived yield (per incident e^+) at 1μmHg and 4μmHg in He and 1μmHg in Ar for (a) n=1 and (b) n=2 state Ps

at 4μmHg for He. Allowance has been made for in-flight decay only in the n=1 case while the n=2 yields are presented without correction. The graphs show that, at the same pressure, over twice the n=1 yield and 3 to 5 times the n=2 yield are obtained from Ar as from He. At 4μmHg in He, the values become comparable and at the higher energies, 80% greater for n=1 Ps formed in He. From these results, it can be seen that the Ar produced beam contains more Ps atoms per μmHg of gas, however, factors such as Ps scattering in the production cell, gas evacuation rates and the presence of excited states of Ps must be considered in terms of the constraints particular to the experiment.

5.4.4 Cross-section measurements

The initially proposed scheme of the double cell arrangement for the measurement of the Ps–atom total cross-section (TCS) was revised when it was found that the intensity of Ps detected, following traversal of the second cell, was statistically inadequate for this purpose. However, significant deviations from the expected yields were observed on increasing the gas density in the first cell. From this, values of TCS were extracted.

The estimation of the expected, unscattered Ps yield and the subsequent derivation of the TCS involved three main factors which are listed and detailed below:
(i) calculation of expected Ps yield from the formation cross-sections;
(ii) correction of the incident e^+ beam for attenuation across the cell;
(iii) estimation of the effective Ps cell length.

Point (i): from Equation 5.9, the number of Ps formed, I_{Ps}, can be related to the incident e^+ beam, I_o, and the formation cross-section σ_{Ps}, according to

$$I_{Ps}/I_o = 1-\exp(-nl\sigma_{Ps}) \qquad 5.12$$

where n and l are as defined above.

However, the experimental arrangement does not permit the use of the total formation cross-section but rather requires the integral $\int d\sigma_{Ps}/d\Omega$ which is individual to the gas and the detector-cell configuration.

For simplification, Equation 5.12 was approximated to a linear dependence of the Ps yield per incident e^+ per second with pressure; the integral was thus deduced from a weighted straight line fit to the plot. The approximation made,

$$1\text{-}nl\sigma \approx e^{-nl\sigma} \qquad 5.13$$

is only valid if the size of the exponential power is such that contributions from second order and higher terms in the expansion are small. For a particular σ, the limit of the approximation is governed by the density and covers a range where only single scattering events occur. The limits chosen, ≈4μmHg in He and ≈1μmHg in Ar, were constrained by two conditions: e^+ multiple scattering and Ps scattering. The latter includes break-up of the atom and pick-off quenching. The effects of these processes would cause deviation from the linear distribution expected from Equation 5.13, which at the lower pressures may not be detectable within the error on the yield. If the fit is not made at pressures where these factors are small, then an underestimation of $\int d\sigma_{Ps}/d\Omega$ may result. At the densities stated above, the discrepancy of the approximation (Equation 5.13), an indication of multiple scattering, is less than 1% for both gases using values of σ_T from Griffith *et al* (1979) and Kauppila *et al* (1981). If the Ps total scattering cross-section, σ_T^{Ps}, is larger than σ_T, then greater restrictions will arise from this effect. However, σ_T^{Ps} was unknown. Therefore, σ_T^{Ps} was derived at an arbitrary pressure using the procedure described in this section. Then, by an "iterative" process, the density regime of the straight line fit was reduced until values obtained for σ_T^{Ps} were consistent across the high pressure range. The limits obtained by this method were also used for the Ps yield study in Section 5.4.3. The integral, $\int d\sigma_{Ps}/d\Omega$, was determined for each energy investigated in both gases.

Point (ii): the amount of Ps formed is dependent on the number of e^+ available along the length of the gas cell and is close to the incident e^+ flux at the lower pressures in this investigation. However, at higher pressures a significant proportion of this beam is attenuated, in particular for Ar where only 30% of the e^+ survive to the exit at 12μmHg. The incident flux available for Ps formation, I_i, can be calculated by integration of Equation 5.9 with respect to cell length and is consequently given by

$$I_i = I_o(1\text{-}\exp[-nl\sigma_T])/nl\sigma_T \qquad 5.14$$

which at low pressures reduces to $I_i = I_o$. Therefore, the expected Ps yield per

incident e^+ can be determined from

$$I_{P_s}/I_o = (1-\exp[-nl\sigma_T])(1-\exp[-g\rho])/n\sigma_T l \qquad 5.15$$

where g is = $\int d\sigma_{P_s}/d\Omega$ per unit of pressure, ρ, and is obtained from the gradient of the straight line fit at low densities.

In the case of He, the above identity can be reduced, according to the approximation of Equation 5.13, to

$$(I_{P_s}/I_o)_{He} = g\rho \qquad 5.16$$

For Ar, Equation 5.15 was applied using σ_T from Kauppila *et al* (1981).

Point (iii): the Ps total scattering cross-sections were deduced using the expected Ps yield, as calculated above, at pressures above the chosen limits by

$$(I_{P_s})_m = I_{P_s} \exp[-n\sigma_T^{\&} l_{P_s}] \qquad 5.17$$

where $(I_{P_s})_m$ is the measured Ps yield per incident e^+ per second and l_{P_s} is the effective Ps cell length.

It was not possible to measure l_{P_s} directly as in the case of the positron cell length, l. Since the effective length over which an individual Ps can interact with the gas is that remaining of l from the point of its formation, the following supposition was made. The value of l_{P_s} was estimated to be equivalent to the difference between l and the mid-point of the cell as defined in Section 5.4.1. For He, this point coincided closely with half the value of l, however in Ar, a strong dependence on pressure was apparent with l_{P_s} ranging from l÷2 - 0.0219m - to 0.0284m (with 6% error). Corrections were consequently necessary for (a) decay of the Ps signal due to the increase in the flight length and (b) increase in the acceptance angle subtended by the detector from that at the low pressure regime where the fits were made. It was assumed that there was no divergence of the e^+ beam along the cell so that the differential formation cross-section integrated over the acceptance solid angle of the detector remained constant. Changes in the angular resolution from the different distances set for each energy investigated would result in a systematic error in the

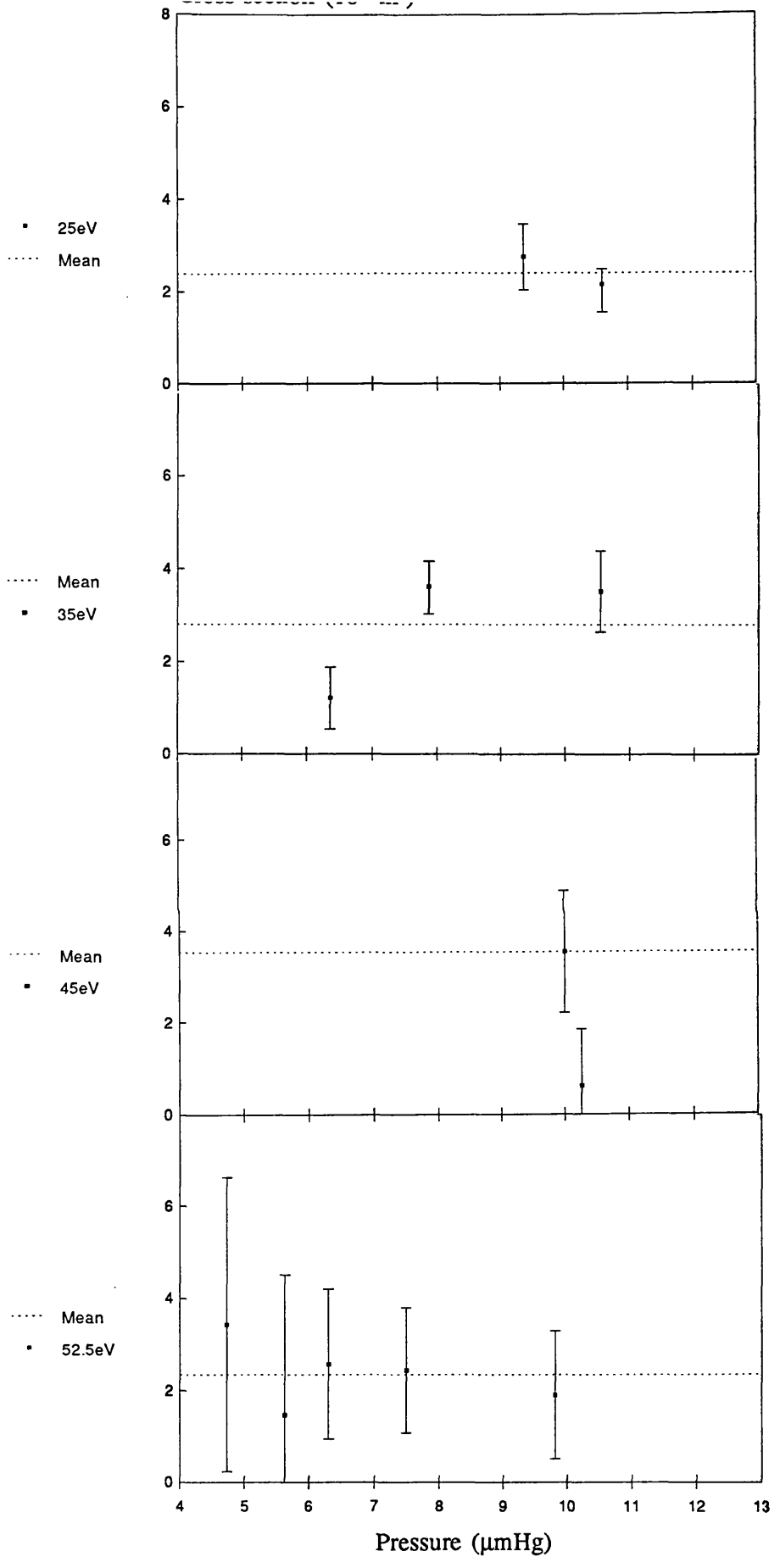

Figure 5.16 Measured Ps (n=1) total scattering cross-sections in He versus pressure at various energies

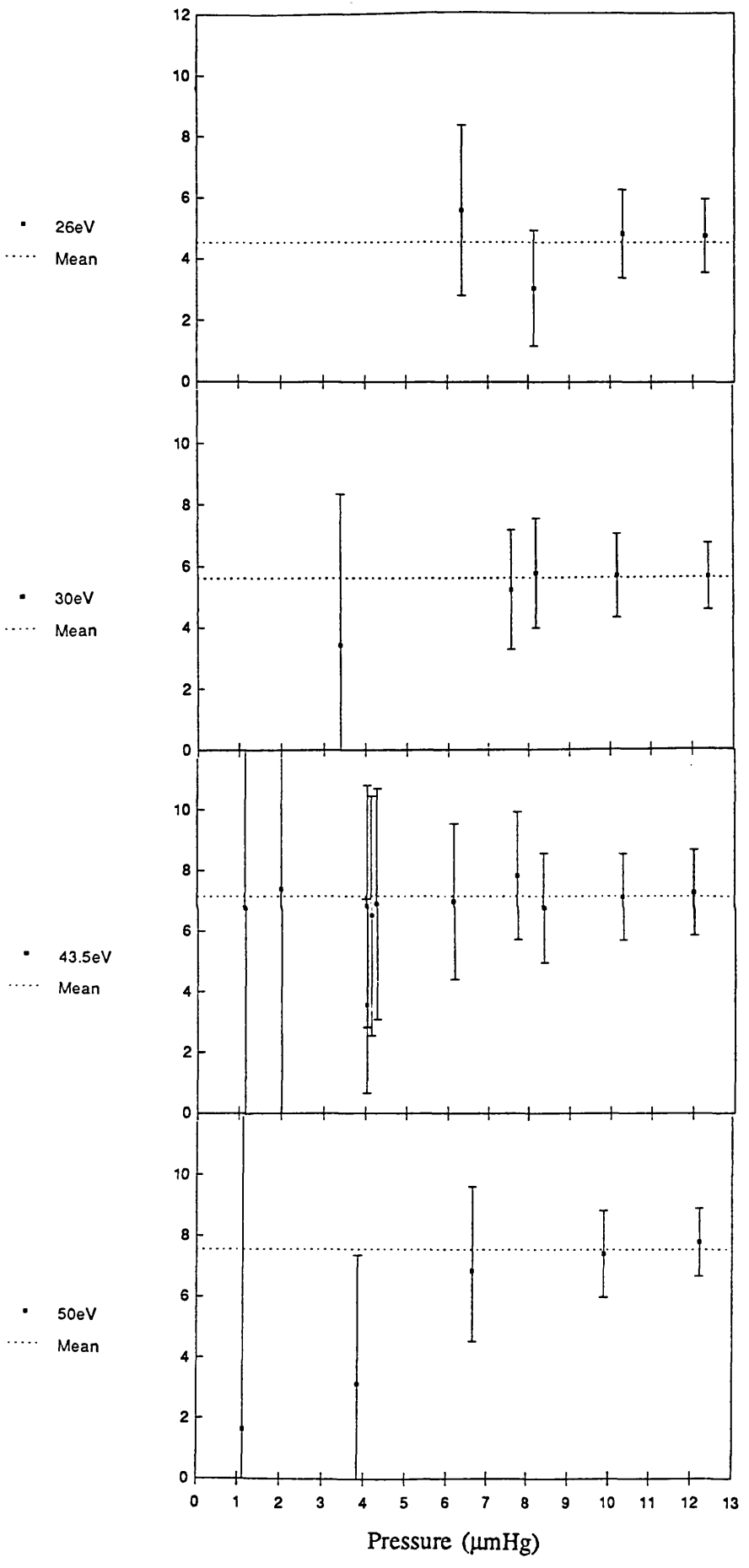

Figure 5.17 Measured Ps (n=1) total scattering cross-sections in Ar versus pressure at various energies

measurement of the cross-sections by this method. This factor could not be calculated but was assumed to be small.

The values of Ps TCS obtained for the n=1 state are presented in Figures 5.16, 5.17 and 5.18. Application of the above method to the n=2 yields was deemed unsuitable for a number of reasons, namely: poorer statistics, possible contamination by n=1 states and the limitation of the fitting procedure to ≈1μmHg. From purely geometrical considerations, the cross-sections of the n=2 state are presumed to be much larger (x16) than the n=1 state, and would thus require measurements at comparatively lower pressures.

Figures 5.16 and 5.17 illustrate the distribution of the n=1 TCS at individual energies with pressure, showing that, in general, they do not exhibit a trend and fluctuate about a mean value. The accuracy of the results increase with pressure; the errors in the case of Ar are 15-20% at best, becoming more unreliable for He (35-40%) as smaller amounts of Ps are formed. A number of runs were taken at high densities at each energy and so the weighted mean values, plotted in Figure 5.18, attained relatively high accuracies of ≈10% in Ar and ≈25% in He. The mean cross-sections derived for n=1 Ps (disregarding those results with >100% error) ranged from (4.5±0.8) to (7.6±0.8) $x10^{-20}m^2$ in Ar and fluctuated between (2.4±0.5) and (3.5±1.3) $x10^{-20}m^2$ in He over 7eV to 41eV Ps energy.

As covered in Section 4.4, available theoretical studies on Ps–He interactions centre mainly on elastic scattering (Fraser, 1968, Barker and Bransden, 1968 and Peach, 1984) with only the work of Peach (1984) extending to the energy range investigated in this study. The inelastic processes of Ps break-up, Ps^- formation, He ionisation and He^- formation have been considered by Ermolaev *et al* (1989) and Ermolaev (1989). No theoretical calculations have been reported for processes in Ps–Ar collisions.

In order to gain some idea of the cross-section expected from theory, the calculations of Peach (1984) and Ermolaev (1989) for He were summed and these are plotted in Figure 5.18 alongside the weighted mean results from the present experiment. There appears to be little agreement, both in size and form, of the two distributions. The only notable similarities are that the values are of the same order of magnitude in the energy range investigated and the close accord of the results at 7eV. However, from this point in energy, the distributions quickly diverge. Doubts have been expressed

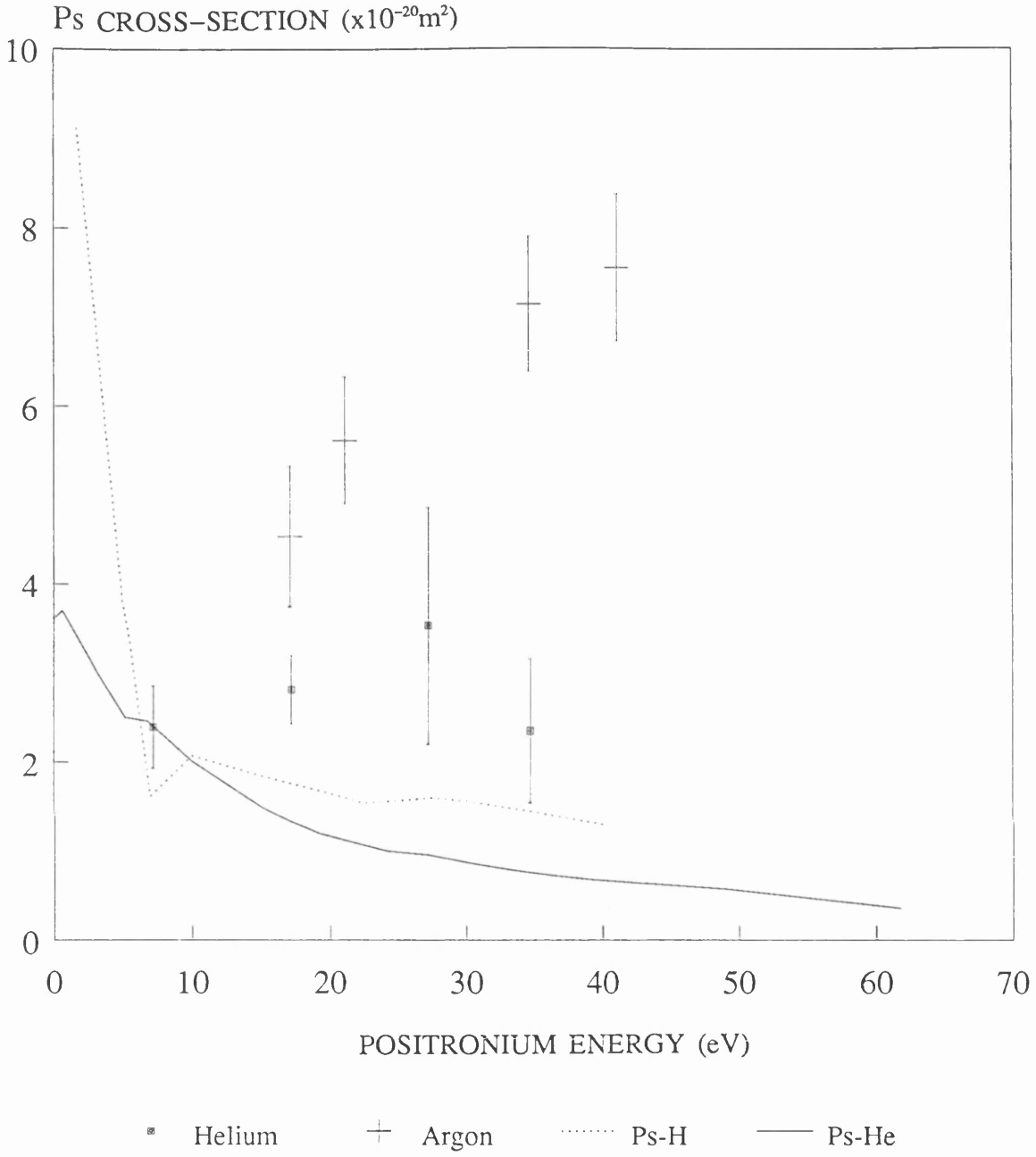

Figure 5.18 Averaged values of Ps (n=1) total scattering cross-section measurements in He and Ar with calculated "total" scattering cross-section for Ps–He (Peach, 1984 and Ermolaev, 1989) and Ps–H (Massey and Mohr, 1954) collisions

by both authors on the reliability of these calculations, especially at lower energies (Ermolaev *et al*, 1989), therefore the discrepancy between the experimental and calculated values may not be surprising. Furthermore, other processes such as target and incident particle excitation and Ps quenching have not been considered.

The shape of the theoretical distributions follows closely that of the elastic scattering cross-section as the contributions from the inelastic processes are of an order of magnitude smaller. This is substantially different from the Ps–H case where the large elastic scattering values quickly decay at intermediate energies as the inelastic processes emerge. The elastic cross-sections of Massey and Mohr (1954) were judiciously extrapolated between 6.7eV and 27eV, following the shape of the curve obtained by Fraser (1961) in the 0–6.8eV limit, and added to the excitation and ionisation cross-sections of Ps estimated by the former authors. The "total" cross-sections, plotted in Figure 5.18 as the dotted line, exhibit the typical dependence at the elastic regime, however start to regain in value slightly at 20-30eV as Ps break-up begins to dominate. Unaccounted interactions such as excitation of S states of H, which the authors state may be quite significant, would further accentuate this feature.

In the case of Ar, the experimental TCS distribution seems to rise more sharply than the He values over the same energy range. The elastic interaction and in particular pick-off quenching is expected to be greater for Ar than He due to the increase in the number of outer electrons. The Ps break-up interaction would also, presumably, be greater because of the larger size of the target atom. The form of the TCS is dependent on the relative magnitudes and increase with energy of the values of the individual processes. On inspection of Figure 5.8, it is clear that the Ar distribution does not exhibit the decay associated with dominant short range elastic processes. However, the shape is more characteristic of increasing inelastic (ionisation or break-up) interactions. Thus, the results obtained both for Ar and He suggest that the magnitude of the inelastic processes are comparable with those of the elastic, if not larger, at the intermediate energies.

The Ps atom is occasionally referred to as isotope of H and, as such, it may be of interest to compare the information on the interactions of these two species with He and Ar. The scattering of H from atoms and molecules differs from that of Ps for a number of reasons. Unlike Ps, the H atom undergoes static interaction with the target, however the polarisation interaction is much stronger in the case of Ps as this

effect is eight times greater than in H. Reiterating the physical aspects stated in Section 1.2, the size of Ps is larger than H with a Bohr radius of $2a_o$ and consequently its binding energy is half that of H. Furthermore, Ps can be removed from the beam by quenching via annihilation. It is, however, difficult to assess the relative importance of these factors in the energy ranges of interest. In the remainder of this section, H collisions with He and Ar are briefly examined to obtain a rough guide on the size of the cross-sections in relation to those of the corresponding Ps–atom scattering. In discussing the cross-sections of projectiles of different masses, the values obtained at equal velocities must be related and not kinetic energy as the magnitudes are dependent on the duration of the interaction. Therefore, results for H impact energy of ≈17keV have been compared to those of Ps with an incident energy of ≈17eV.

For H–He collisions, experiments performed to measure the elastic scattering cross-section are limited to a maximum energy of 2keV, corresponding in velocity to Ps of ≈2eV. Amdur and Mason (1956) have investigated this process in the range 700-2100eV and observed a continuous decrease in cross-section value from 2.2 to $1.1\times10^{-20}m^2$. Extrapolation of these results to 17keV impact energy gives $\approx0.4\times10^{-20}m^2$.

Data on inelastic collisions involving H with He and Ar are available in the energy range corresponding to interactions with Ps of energy 7–50eV. Excitation of the H atom with a He target has been investigated by several workers, both theoretically and experimentally (Orbeli *et al*, 1969, Birely and McNeal, 1972, Sauers and Thomas, 1974, Kimura and Lane, 1988) and the results obtained are in broad agreement. The cross-sections for production of 2S and 2P state H from impact of the ground state atoms are $\approx4\times10^{-22}m^2$ and $\approx10^{-21}m^2$, respectively. Excitation of the target atom has been predicted to be small in comparison (Massey and Gilbody, 1974) and the process of simultaneous target and projectile excitation has been calculated to be of the order of $10^{-22}m^2$ or less (Hartley and Walters, 1987).

The most significant contributions to the interaction in this energy range are made by the ion formation processes involving both the target and projectile atoms. These reactions include ionisation of the target and projectile atoms and negative ion production. The sum of the cross-sections for these individual processes has been determined over a wide energy range for H–He collisions by several workers (Solov'ev *et al*, 1962, McNeal *et al*, 1970, Anderson *et al*, 1980, Van Zyl *et al*, 1981,

DuBois and Kövèr, 1989). At 17keV H impact energy, the cross-section is generally $\approx 2 \times 10^{-20} m^2$ with the largest contribution, $10^{-20} m^2$, from the H ionisation process which is analogous to Ps break-up (Solov'ev *et al* 1962, Stier and Barnett, 1956, Williams, 1967). A rough estimate of the TCS for H impact on He may be obtained by the addition of the total ion formation and excitation cross-sections to the elastic contribution. Thus, the inferred TCS at this energy is $\approx 2.5 \times 10^{-20} m^2$ (with an estimated combined error of 20%) compared to $(2.8 \pm 0.4) \times 10^{-20} m^2$ for 17eV Ps.

For Ar, the elastic scattering cross-sections with deuterium atoms have been measured to 2keV by Ruzic and Cohen (1985). In this work, a number of noble gases were investigated and the results for He, estimated at 17keV, were in accord with the aforementioned study of Amdur and Mason (1956). A rough extrapolation of the D–Ar collision results indicates that the elastic contribution at 17keV impact energy is no greater than $1 \times 10^{-20} m^2$.

Similarly with He, the process of projectile excitation for H–Ar scattering has been investigated by a number of workers (Orbeli *et al*, 1969, Birely and McNeal, 1972, Hughes and Choe, 1972a,b, Van Zyl *et al*, 1980). For excitation to the 2S and 2P states of H, the cross-sections have been measured to be $\approx 2 \times 10^{-21} m^2$ and $\approx 4 \times 10^{-21} m^2$, respectively. The largest value for n=3 H formation is $6 \times 10^{-22} m^2$ for the 3P state (Orbeli *et al*, 1969). Again, as with He, the major component of the H–Ar scattering interaction is comprised of the ion formation process discussed above. However, in this case, the dominant process in the energy range of interest is that of target ionisation. This reaction is be expected to be more significant than for He due to the comparability of the ionisation energies of the H and Ar atoms. The cross-section for H ionisation is $\approx 3 \times 10^{-20} m^2$ with negative ion formation results being more than an order of magnitude smaller (Stier and Barnett, 1956, Solov'ev *et al*, 1962 and Williams, 1967). The value of single ionisation of Ar has been determined to be $\approx 4.5 \times 10^{-20} m^2$ with $\approx 0.8 \times 10^{-20} m^2$ for the formation of doubly charged ions at this energy. The addition of the cross-sections for the individual processes mentioned above gives a "total" cross-section value of $\approx 10 \times 10^{-20} m^2$ (with an estimated combined error of 30%) and is larger than the corresponding Ps–Ar result of $(4.5 \pm 0.8) \times 10^{-20} m^2$ obtained in the present study by a factor of 2.

Figures 5.19 and 5.20 illustrate the H ionisation cross-sections measured in He and Ar gases; a point of note is that the shapes of the distributions in both gases bear

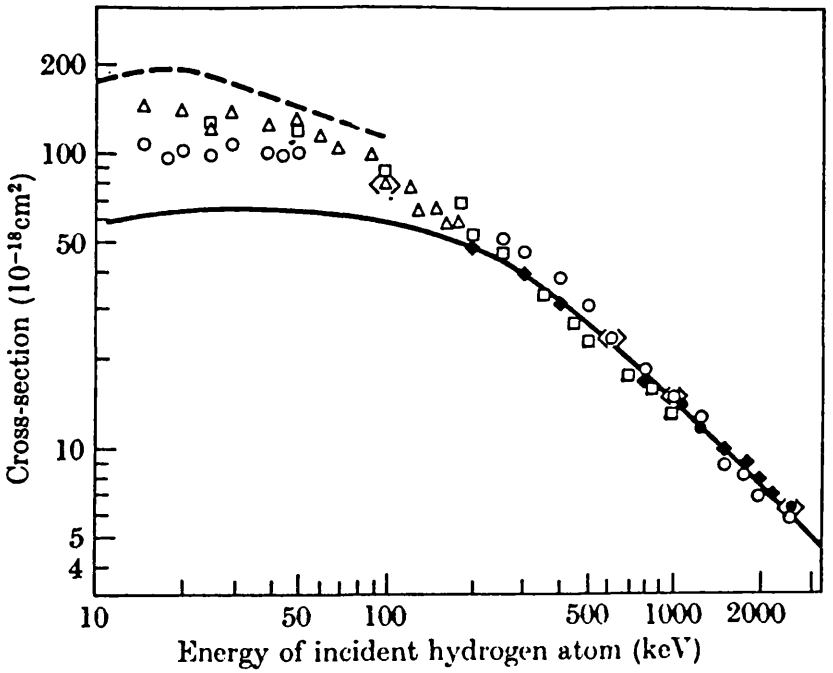

Figure 5.19 Cross-section of H ionisation in H–He collision (from Massey and Gilbody, 1974)

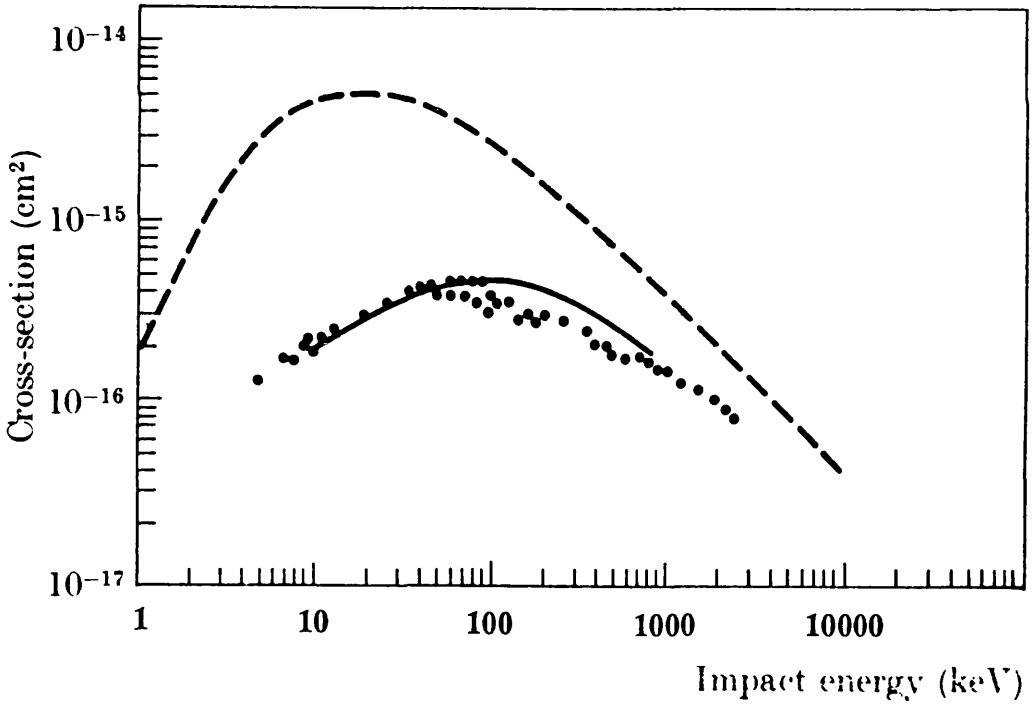

Figure 5.20 Cross-section of H ionisation in H–Ar collision (from Massey and Gilbody, 1974)

some resemblance to those obtained in this study for Ps TCS over the corresponding energy range. The Ar plot, showing the greater variation, may be more pronounced if target ionisation was included. Figure 5.21 shows the cross-sections of the ion formation processes involving incident H ionisation in H–H collisions. In contrast to the Ps case, the results at 17keV, $\approx 2 \times 10^{-20} m^2$, are approximately an order of magnitude lower than for H–He scattering. However,cross-section results similar to the maximum values in H–He scattering are reached at higher impact energies.

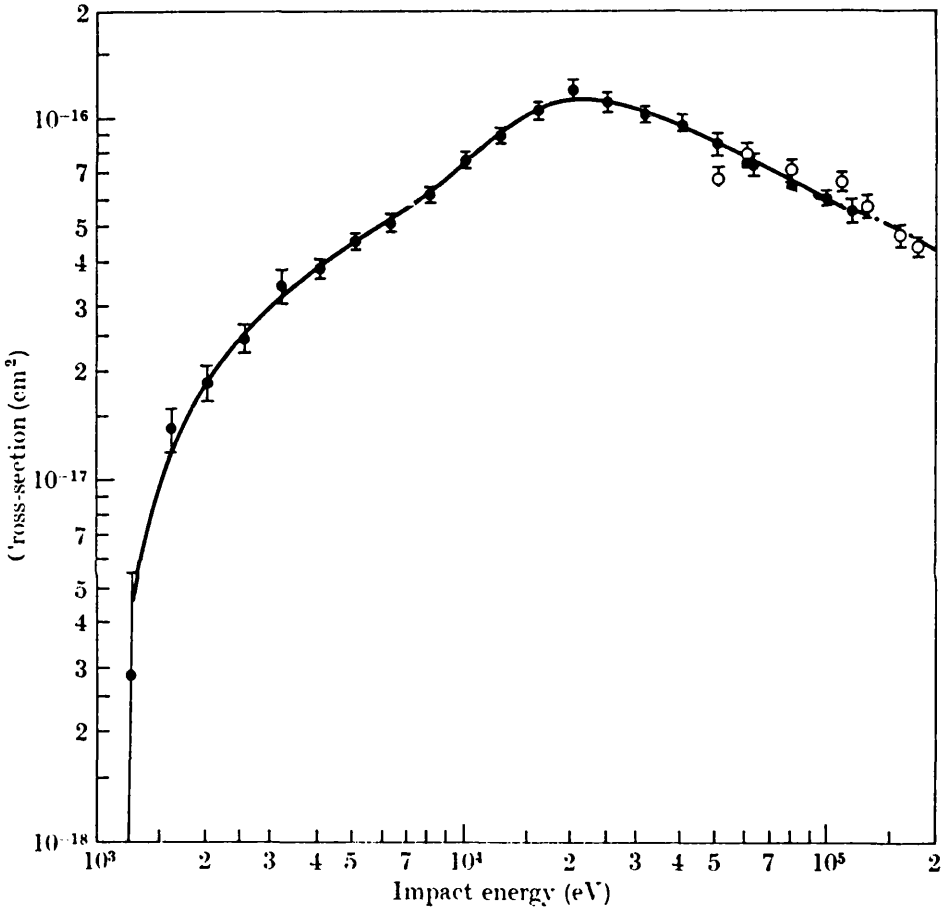

Figure 5.21 Cross-section of H ionisation in H–H collision
(from Massey and Gilbody, 1974)

Comparison of the cross-sections available for H–atom scattering shows that the order of magnitude of these values are the same as those obtained in the present experiment for Ps collision with He and Ar at similar impact velocities. In relation to the total

scattering cross-section of e^+, the Ps results are 2-3 times that of the maximum e^+ values for He. In Ar, the results bear some similarity with those of the e^+, which vary from 6.05 to $7.4 \times 10^{-20} m^2$ with ≈5% error (Kauppila *et al*, 1981) over the e^+ energy range, 25-50eV, corresponding to Ps formation in Ar with Ps energies, 17-41eV. However, this may only be coincidental as the interactions involved in the collision of the two species are significantly different.

5.4.5 Summary

The timed Ps beam technique has been employed to investigate the formation of Ps in He and Ar and subsequently measure the total scattering cross-section of Ps in both of these gases. Modifications made to the system resulted in sufficient separation of signals on the time of flight spectrum to allow the observation of excited state Ps from He and Ar. On conversion to an energy scale, the peaks were situated at the positions expected from Equation 5.5, with the second at an energy ≈5eV below the first. The positions on the spectrum varied with the incident e^+ beam energy and further verification of the presence of ground state Ps was forthcoming from decay rate measurements of the main peak.

Yields of Ps and Ps^* were quantified, in 4eV portions, at various energies and below certain densities, which were 4μmHg in He and 1μmHg in Ar. The results were comparable with those previously obtained by Laricchia *et al* (1987). Maximum yields measured were at ≈35eV Ps energy for both He and Ar with the slow n=2 component, in the case of Ar, continuing to increase with energy. The ratios of the $Ps^*/(Ps+Ps^*)$ yields were also found to increase with energy and at maximum, composed 33% and 42% of the detected Ps flux in He and Ar, respectively. Comparison with theory indicates that a large proportion of the n=2 signal is comprised of the long-lived metastable S state of Ps^*.

Cross-section measurements of Ps scattering in He and Ar were performed on increasing the pressure of the gas in the Ps production cell. Several factors required consideration before TCS values could be extracted. These were:

(i) calculation of the expected "unscattered" Ps yield at high densities from extrapolation of low density values
(ii) correction for the attenuation of the incident e^+ beam across the cell at high

densities

(iii) estimation of the effective length over which Ps scattering may occur.

Values were thus extracted for n=1 Ps. These ranged from (4.5±0.8) to (7.6±0.8) $x10^{-20}m^2$ in Ar for Ps energies of 17-41eV and fluctuated about $3x10^{-20}m^2$ in He in the regime 7-35eV from a minimum of $(2.4\pm0.8)x10^{-20}m^2$ to a maximum of $(3.5\pm1.3)x10^{-20}m^2$.

Thus, the study has demonstrated that the timed Ps beam technique can be employed to discern components of the Ps flux sufficiently to allow characterisation of the beam and consequently to permit the measurement of ground state Ps total scattering cross-section.

	e^+ energy (eV)	Ps energy (eV)	Dist. d_{Ps} (m)	Ps yield† (scatt.$e^{+\,-1}$ $\Omega^{-1}s^{-1}$) x10^{-2}	Ps^* yield† (scatt.$e^{+\,-1}$ $\Omega^{-1}s^{-1}$) x10^{-2}	$\frac{Ps^*}{(Ps+Ps^*)}$ ratio†	Ps TCS (x10^{-20} m^2)
Helium	25.0	7.2	0.1366	3.3±0.2	-	-	2.4±0.5
	35.0	17.2	0.2026	11.3±0.6	1.8±0.2	0.14±0.02	2.8±0.5
	45.0	27.2	0.3546	7.6±0.4	2.4±0.2	0.24±0.02	3.5±1.3
	52.5	34.7	0.4306	8.4±0.5	4.2±0.3	0.33±0.03	2.4±0.8
Argon	16.0	7.1	0.1476	13.7±0.1	-	-	-
	26.0	17.1	0.1476	4.4±0.2	1.1±0.1	0.20±0.01	4.5±0.8
	30.0	21.1	0.2246	4.5±0.2	1.5±0.1	0.25±0.02	5.6±0.7
	43.5	34.6	0.3326	4.2±0.2	1.9±0.2	0.32±0.03	7.1±0.8
	50.0	41.1	0.3436	3.7±0.3	2.7±0.2	0.42±0.04	7.6±0.8

† in 4eV portion uncorrected for decay in flight

Table 5.1 Summary of results obtained for positronium formation and interaction in He and Ar gases

CHAPTER 6
CONCLUSIONS

The work presented in this thesis has involved investigations in two different, though not unrelated, aspects of low energy positron physics, namely: slow e^+ moderator development and Ps beam production and interaction with atomic gases. In this chapter the results and conclusions from each of these studies are assessed and future possibilities are discussed.

Interest in single crystal moderators of thicknesses in the order of 100s to 10000s of Å has arisen for a number of reasons. The employment of a slow e^+ moderator in the transmission mode eliminates the source shadow problem associated with the backscattering geometry and intercepts a larger proportion of the flux than a grid arrangement. It allows the use of simpler linear optics in the remoderation stages of electrostatic transport systems. Furthermore, the longitudinal energy distribution of the ejected e^+ is likely to be narrower than those from the vane, grid or cone configurations as the surface of emission is normal to the beam axis. However, the use of thin film moderators is not without difficulties. Defects in the crystal structure can arise from handling of the fragile films and, moreover, the annealing procedure must be implemented with care as damage can occur from hot spots and evaporation. As discussed in Chapters 2 and 3, work on the performance of thin single crystal films has been carried out in vacuums of $\geq 10^{-8}$ Torr with *in situ* heating facilities. Following Lynn *et al* (1985) and Schultz *et al* (1986), the present study undertook to develop an annealing technique and subsequently, to investigate the moderator properties of thin single crystal W(100) and Ni(100) foils of thicknesses 1000-18000Å in vacuum conditions of $\approx 10^{-7}$ Torr, similar to those of most gas scattering experiments.

A simple annealing procedure was employed, using resistive heating in a low vacuum environment of 6×10^{-2} Torr. After transfer in air to the test system, the maximum efficiencies obtained were $(8.8 \pm 1.2) \times 10^{-4}$ for a 2000Å W(100) foil and $(6.5 \pm 1.0) \times 10^{-4}$ for a 5000Å Ni(100) sample. The longitudinal energy distribution from both W and Ni single crystals were found to be smaller than that from a W mesh annealed in a similar manner under the same conditions. The FWHM of the positrons emitted from

the crystals were measured to be 1.7eV and 0.3eV for W and Ni, respectively, compared to 2.8eV from the W mesh.

The maximum efficiencies determined are in good agreement with those from the study of Gramsch *et al* (1987), using a somewhat more complex annealing technique in higher vacuum conditions (10^{-8} Torr), but are a factor of 2.5-4.5 lower than those predicted from calculations. Moreover, the variation of the efficiency with thickness is also inconsistent with that computed. This is suggestive of the presence of defects and/or contaminants in the bulk and on the surface of the samples. However, efficiencies matching those from calculations based on perfect crystalline structure with no contamination cannot be expected since the procedure employed in the present study involved handling of the foils and exposure to air. On the subject of contamination, annealing in low vacuum may have been of benefit as it is known that carbon, the main contaminant in both the Ni and W foils, can be removed by the formation of gaseous oxides at the surface (Becker *et al*, 1961). The workfunction determined in the present study did not indicate the identity of the surface adsorbate(s), although carbon and oxygen are the most likely candidates. Bulk and surface analysis tools are required to further elucidate and quantify the effects of contamination. Nevertheless, the aim of this project was fulfilled and thin single crystal W and Ni foil moderators were demonstrated to produce slow e^+ in vacuum conditions similar to those of most gas scattering studies.

Extensions of this study can be made to include other single crystal transition elements. It is noted that the majority of the metals that have been observed to emit slow positrons are either of body centred or face centred cubic structures. Tungsten, the most efficient metallic moderator discovered to date, has a body centred cubic (BCC) structure. It may be of interest to examine other BCC crystals such as tantalum, molybdenum, chromium and vanadium which all possess melting points lower than W and so may facilitate greater temperature control in the annealing procedure. In contrast to Cu, W and Ni moderators perform efficiently following exposure to air as these metals are resistant to substantial oxide build up on the surface. Cr and, particularly, V are also known to exhibit such a resistance to oxidation (Nordlander and Ronay, 1987). Metallic moderators emitting e^+ with the narrowest energy distribution in non-UHV conditions are those with the smaller positron workfunctions, such as Ni, Cu and Pt which all have a face centred cubic (FCC) structure. Therefore, it may be of interest to study iridium which possesses

a FCC structure and is more dense than W. Nieminen and Hodges (1978) have calculated the positron workfunction of Ir to be −1.4eV which is comparable to that determined experimentally for Ni by Gullikson *et al* (1985). Furthermore, Dale *et al* (1980) found that polycrystalline Mo and Ir emitted e^+ with yields approximately 80% and 65%, respectively, of that from W in the same study. On the subject of Ni, the magnetic property of this element in relation to the e^+ yield and energy distribution obtained was not conclusively determined. The magnitude of the magnetism differs with face orientation, for example, Ni(111) possesses the largest proportion of magnetically aligned domains. Therefore, further investigations, such as the comparison of yields from various crystal orientations of Ni in magnetic and electrostatic systems, may reveal the effect of this property.

The original motivation of this work was to develop a transmission mode moderator for use in gas scattering investigations, therefore the next step might be to utilise the foils in experiments which may benefit from the generation of slow e^+ beams with narrow energy spreads. These include the measurements of excitation, ionisation and differential scattering cross-section from molecular gases. Beams of widths in the order of 10s to 100s of meV are required for molecular targets due to the presence of vibrational and rotational levels and these may be achieved by remoderation and filtering. Additionally, investigation of the higher excitation states in atomic gases and studies into the behaviour of the individual cross-sections at thresholds, such as the onset of Ps formation, also require systems with high resolution.

The second part of the work discussed in this thesis concerned the production and employment of energy-controllable Ps beams. The technique developed by Laricchia *et al* (1988b) was used to generate a timed Ps beam which, following modifications, allowed the identification of excited state Ps produced in e^+ collisions with He and Ar gases. Ps and Ps^*, formed in the beam in the energy range 7-41eV (Ps energy), were quantified in 4eV portions and the maximum yields of n=1 Ps were obtained at ≈35eV in both gases with the n=2 component exhibiting a gradual increase with energy. The highest ground state Ps yields, following correction for decay in flight, were (0.28±0.02) in He and (0.108±0.006) in Ar per scattered e^+ per steradian per second. The ratios of Ps^* to the total ($Ps+Ps^*$) yields were also found to increase with energy to maximum values of (33±3)% in He and (42±4)% in Ar. A comparison with theory (Mandal *et al*, 1980, Khan *et al*, 1984, 1985) was made which indicated the dominant presence of the long lived metastable S state in the excited Ps

component of the beam.

With regard to the measurement of Ps cross-sections, the original proposal of the double cell arrangement (Laricchia *et al*, 1988b) could not be employed as the pumping speed of the system was not sufficiently high to provide adequate evacuation of the gas from the interaction region at the densities required in this experiment. Furthermore, attenuation of the beam by the apertures in the arrangement caused significant loss of the e^+ and the Ps intensity. Therefore, the second gas cell was removed. However, on increasing the pressure in the Ps production cell, a deviation from the expected yields was observed and from interpretation of these results, Ps total scattering cross-sections were measured at intermediate energies in He and Ar gases.

The values of cross-sections were extracted following a number of assumptions listed in Chapter 5, nevertheless, results with accuracies of 25% in He and 10% in Ar were obtained. These values increased from $(4.5\pm0.8)\times10^{-20}m^2$ at 17eV to $(7.6\pm0.8)\times10^{-20}m^2$ at 41eV in Ar and fluctuated between $(2.4\pm0.8)\times10^{-20}m^2$ and $(3.5\pm1.3)\times10^{-20}m^2$ at energies of 7–35eV in He. Comparison of the He results with available theoretical data (Peach, 1984 and Ermolaev, 1989) showed little agreement in both size and shape with the calculated values, which followed the characteristic decay of elastic scattering with increasing energy. The distributions of the experimental results, in particular Ar, were more indicative of a sizeable contribution to the total cross-section from inelastic processes. Further work is required on both theoretical and experimental fronts.

It is preferable to make cross-section measurements based on as few corrections as possible, therefore, the next development of this investigation must be the re-introduction of the second gas cell in order to check the results obtained in the present study. The problems of gas evacuation and Ps flux intensity, stated above, may be resolved to some extent by (a) the redesign of the interaction region to accommodate a third pumping port and (b) the use of W or Ni single crystal foils in place of the W mesh remoderators. On the latter point, the studies of Chen *et al* (1985) and Schultz *et al* (1986) have shown that such foils, 1000-1500Å thick, can remoderate e^+ with efficiencies of 18-19% at 5keV incident energy in $\approx10^{-9}$ Torr. These efficiencies are similar to that obtained in the present study using W grid moderators, however, the foil will intercept all the incident flux. Therefore, if a thin

film was substituted in place of the W meshes and performed with the same efficiency, approximately 2000 slow e^+ s^{-1} would be emitted resulting in ≈900 timed e^+ s^{-1}, thereby doubling the count rate. The e^+ beam energy cannot be raised to 5keV in this arrangement as the source is earthed so the incorporation of a ceramic break would be required. The aforementioned studies found FWHM e^+ energy distributions of about 0.6eV (W) and 0.2eV (Ni). If thin single crystal foil remoderators were implemented in this system, an energy spread comparable to these values might be obtained which would significantly decrease the FWHM of the Ps peaks on the time of flight spectra and moreover, reduce the proportion of epithermal e^+ in the beam.

Loss of slow e^+ flux may have been incurred in the present study due to the difficulty in guiding the beam along the bent solenoid, therefore, its replacement with a set of cylindrically curved **ExB** plates, developed by Hutchins *et al* (1986), may increase the intensity. The curved **ExB** system has been demonstrated to transport e^+ with little distortion to the cross-section of the beam and this may be of aid when tuning the incident flux through the CEMA1 arrangement.

With an increased flux, the mechanism of Ps detection can be investigated by variation of Ps energy at ≤7eV. If Ps break-up is involved in this process then a cut-off will be apparent in the peak distribution as the energy is reduced to less than the binding energy of Ps. The elucidation of this mechanism could be of benefit in the development of a more efficient Ps detector.

Further to the determination of the total cross-sections of Ps in various atomic and molecular gases, studies on the scattering of n=2 state Ps may be feasible. Although quantitative measurements of the cross-sections of Ps^* were not made in the present study, attenuation of the signal was observed on increasing the density of gas in the cell. As stated in Chapter 5, Ps^* cross-sections are expected to be much larger than those of ground state Ps due to the greater physical size. The improvements discussed above may increase the Ps^* component of the timed beam, thereby allowing the investigation of Ps^* interactions in gases.

REFERENCES

Amdur I. and Mason E.A. (1956) J. Chem. Phys. **25**, 630

Anderson C.D., (1932) Phys. Rev. **41**, 405

Anderson C.J., Girnius R.J., Howald A.M. and Anderson L.W.
(1980) Phys. Rev. **A22**, 822

Arifov P.U., Grupper A.R. and Alimkulov H., (1982) "Positron
Annihilation" (Coleman P.G., Sharma S.C. and Diana L.M., eds;
North-Holland, Amsterdam) 699

Barker M.I. and Bransden B.H. (1968) J. Phys. **B1**, 1109
(1969) J. Phys. **B2**, 730

Barr J.R.M, Girkin J.M., Tolchard J.M. and Ferguson A.I.,
(1986) Phys. Rev. Lett. **56**, 576

Becker J.A., Becker E.J. and Brandes R.G.,
(1961) J. Appl. Phys. **32**, 411

Beling C.D., Simpson R.I., Charlton M., Jacobson F.M., Griffith T.C.,
Moriarty P. and Fung S., (1987) Appl. Phys. **A42**, 111

Bell K.L., Dose V. and Kingston A.E. (1969) J. Phys. **B2**, 831

Bell R.E. and Graham R.L. (1953) Phys. Rev. **90**, 644

Berger J. *et al*, (1985) CERN proposal PSCC/P86

Bergersen B., Pajanne E., Kubica P., Stott M.J. and Hodges C.H.,
(1974) Solid State Commun. **15**, 1377

Birely J.H. and McNeal R.J. (1972) Phys. Rev. **A5**, 257

Birkhoff R.D., (1958) Handbuch der Physik **34**, (Berlin: Springer), 53

Blackett P.M.S. and Occhialini G.P.S., (1933) Proc. Roy. Soc. **A139**, 699

Brandes G.R., Canter K.F., Horsky T.N., Lippel P.H. and Mills A.P.,
(1988) Rev. Sci. Instrum., **59**, 228

Brandt W. and Paulin R., (1968) Phys. Rev. Lett. **21**, 193
(1977) Phys. Rev, **B15**, 2511

Branscomb L.M. (1969) "Physics of One and Two Electron Atoms"
(Kleinpoppen H. and Bopp H., eds; North-Holland, Amsterdam) 694

Britton D.T., Huttunen P.A., Mäkinen J., Soininen E. and Vehanen A.,
(1989) Phys. Rev. Lett. **62**, 2413

Brown B.L., (1985) "Positron Annihilation" (Jain P.C.

Singru R.M. and Gopinathan K.P., eds; World
Scientific, Singapore), 328
(1986) "Proc. 3rd Int. Workshop on Positron (Electron) Gas
Scatt."(Kauppila W.E., Stein T.S. and Wadehra J.W., eds;
World Scientific, Singapore), 212
(1987) "Atomic Physics with Positrons" (Humberston J.W. and
Armour E.A.G., eds; Plenum, New York), 241

Brown C.J. and Humberston J.W., (1985) J. Phys. **B18**, L401

Buhring W. (1974) Proc. 4th ICAP (Kowalski J. and Weber H.G., eds;
Heidelberg Univ. Press) 417

Canter K.F., Coleman P.G., Griffith T.C., and Heyland G.R.,
(1972) J. Phys. **B5**, L167
(1974b) Appl. Phys. **3**, 249

Canter K.F., Brandes G.R., Horsky T.N., Lippel P.H. and
Mills A.P., (1987) "Atomic Physics with Positrons"
(Humberston J.W. and Armour E.A.G., eds; Plenum,
New York), 153

Canter K.F.. Mills A.P. and Berko S.,
(1974a) Phys. Rev. Lett. **33**, 7
(1975) Phys. Rev. Lett. **34**, 177

Caswell W.E. and Lepage G.P., (1979) Phys. Rev. **A20**, 36

Chang T-B., Li Y-Q., Wang Y-Y. and Tang X-W., (1982) "Positron
Annihilation" (Coleman P.G., Sharman S.C. and Diana L.M., eds;
North Holland, Amsterdam), 32

Chang Tianbao, Tang Hsiaowei and Li Yaoqing, (1985) "Positron
Annihilation" (Jain P.C., Singru R.M. and Gopinathan K.P.,eds;
World Scientific) 212

Charlton M., (1980) Ph.D. Thesis, University of London
(1985a) Rep. Prog. Phys. **48**, 737
(1985b) J. Phys. **B18**, L667
(1987) "Electronic and Atomic Collisions" (Gilbody H.B., Newell W.R.,
Read F.H. and Smith A.C.H., eds; Elsevier Science Publishers, B.V.)
(1988) "Positron Annihilation" (Dorikens-Vanpraet L.,
Dorikens M., and Segers D., eds; World Scientific, Singapore) 181

Charlton M., Andersen L.H., Brun-Nielsen L., Deutch B.I., Hvelplund P.,
Jacobsen F.M., Knudsen K., Laricchia G., Poulsen M.R., and

Pedersen, J.O., (1988) J. Phys. **B21**, L545

Charlton M., Brun-Nielsen L., Deutch B.I., Hvelplund P., Jacobsen F.M., Knudsen K., Laricchia G. and Poulsen M.R., (1989) J. Phys. **B22**, 2779

Charlton M., Clark G., Griffith T.C. and Heyland G.R., (1983b) J. Phys. **B16**, L465

Charlton M., Griffith T.C., Heyland G.R. and Wright G.L., (1983a) J. Phys. **B16**, 323

Charlton M., Laricchia G., Griffith T.C., Wright G.L. and Heyland G.R., (1984) J.Phys. **B17**, 4945

Chen D.M., Lynn K.G. Pareja R. and Nielsen B., (1985) Phys. Rev. **B31**, 4123

Cherry W., (1958) Ph.D. Thesis, Princeton University

Chevallier J., (1987) *private communication*

Chu S., Mills A.P. and Hall J.L, (1984) Phys. Rev. Lett **52**, 1689

Clark G. (1984) Ph.D Thesis, University of London

Coleman P.G. (1979) J. Phys. **E12**, 590

Coleman P.G., Griffith T.C. and Heyland G.R., (1973) Proc. Roy. Soc. Ser. **A331**, 561

Coleman P.G., Griffith T.C., Heyland G.R. and Killeen T.L., (1974) Appl. Phys. **3**, 271

(1974) Appl. Phys. **5**, 223

Coleman P.G. and Hutton J.T., (1980) Phys. Rev. Lett. **45**, 2017

Coleman P.G., Hutton J.T., Cook D.R. and Chandler C.A., (1982) Can. J. Phys. **60**, 584

Coleman P.G. and McNutt J.D., (1979) Phys. Rev. Lett. **42**, 1130

Costello D.G., Groce D.E., Herring D.F. and McGowan J.W., (1972a) Phys. Rev. **B5**, 1433

(1972b) Can. J. Phys. **50**, 23

Curry S. and Schawlow A.L. (1971) Phys. Lett. **37A**, 5

Dale J.M., Hulett L.D. and Pendayla S., (1980) Surf. Int. Anal. **2**, 199

Davies S.A. (1987) Ph.D. Thesis, University of London

DeBenedetti S., Cowan C.E. and Konneker W.R., (1949) Phys. Rev. **76**, 440

DeBenedetti S., Cowan C.E., Konneker W.R.and Primakoff,

(1950) Phys. Rev. **77**, 205

Deutch B.I., Jensen A.S., Miranda A. and Oades G.C.,
(1986) "Proc. Fermilab Workshop on Antimatter Physics at Low Energies" (Batavia Il: Fermi National Lab.) 371

Deutch B.I., Jacobsen L.H., Andersen L.H., Hvelplund P., Knudsen H., Holzscheiter M.H., Charlton M. and Laricchia G.
(1988) Physica Scripta **T22**, 248

Deutsch M., (1951a) Phys. Rev. **82**, 455
(1951b) Phys. Rev. **83**, 866
(1953) Prog. Nuc. Phys. **3**, 131

Dewangen D.P. and Walters H.R.J. (1977) J.Phys. **B10**, 637

Diana L.M., Coleman P.G., Brooks D.L., Pendleton P.K.
and Norman D.M., (1986a) Phys. Rev. **A34**, 2731

Diana L.M., Coleman P.G., Brooks D.L., Pendleton P.K. Norman D.M., Seay B.E. and Sharma S.C., (1986b) "Proc. 3rd Int. Workshop on Positron (Electron) Gas Scatt." (Kauppila W.E, Stein T.S. and Wadehra J.M., eds; World Scientific, Singapore), 296

Diana L.M., Fornari L.S., Sharma S.C. Pendleton P.K. and
Coleman P.G. (1985) "Positron Annihilation" (Jain P.C., Singru R.M. and Gopinathan K.P., eds; World Scientific, Singapore), 342

Diana L.M., Brooks D.L., Coleman P.G., Chaplin R.L. and Howell J.P,
(1988a) "Positron Annihilation" (Dorikens-Vanpraet L., Dorikens M., and Segers D., eds; World Scientific, Singapore) 308

Diana L.M., Brooks D.L., Coleman P.G., Chaplin R.L. and Howell J.P,
(1988b) "Positron Annihilation" (Dorikens-Vanpraet L., Dorikens M. and Segers D., eds; World Scientific, Singapore) 311

Dirac P.A.M., (1930a) Proc. Roy. Soc. **A126**, 360
(1930b) Proc. Camb. Phil. Soc. **26**, 361

Drachman R.J. (1968) Phys. Rev **173**, 190
(1979) Phys.Rev. **A19**,1900
(1982) Can. J. Phys. **60**,494

Drachman R.J. and Houston S.K., (1975) Phys. Rev. **A12**, 885
(1976) Phys. Rev. **A14**, 894

Drachman R.J., Omidvar K. and McGuire J,H.,
(1976) Phys Rev. **A14**, 100

DuBois R.D. and Kövèr A. (1989) Phys. Rev. **A40**, 3605

Dupasquier A. and Zecca A., (1985) Riv. Nuovo Cimento **8**, 3

Ellison D.C. and Kazanas D., (1983) Astron Astrophys **128**, 102

Ermolaev A.M., (1989) *private communication*

Ermolaev A.M., Bransden B.H. and Mandal C.R.,
(1989) J. Phys. **B22**, 3717

Fischer D.A., (1984) Ph.D. Thesis, University of Michigan

Fischer D.A., Lynn K.G. and Frieze W.E.,
(1983) Phys. Rev. Lett. **50**, 1149

Fischer D.A., Lynn K.G. and Gidley D.W, (1986) Phys. Rev. **B33**, 4479

Floeder K., Fromme D., Raith W., Schwab A. and Sinapius G.
(1985) J. Phys. **B18**, 3347

Fornari L.S., Dianna L.M. and Coleman P.G.,
(1983) Phys. Rev. Lett. **51**, 2276

Fraser P.A., (1961) Proc. Phys. Soc. **78**, 329
(1962) Proc. Phys. Soc. **79**, 721
(1968) J. Phys. **B1**, 1006

Fraser P.A. and Kraidy M., (1966) Proc. Phys. Soc. **89**, 533

Frenkel J., (1928) Z. Physik **51**, 232

Frieze W.E., Gildley D.W. and Lynn K.G., (1985) Phys. Rev. **B31**, 5628

Fromme D., Kruse G., Raith W. and Sinapius G.,
(1986) Phys. Rev. Lett. **57**, 3031
(1987) "Atomic Physics with Positrons" (Humberston J.W. and
Armour E.A.G., eds; Plenum, New York) 407

Fulton T. and Martin P.C. (1954) Phys. Rev. **95**, 811

Gabrielse G., Rolston S.L., Haarsma L. and Kells W.
(1988) Phys. Letts. **A129**, 38

Gertler F.H., Snodgrass H.B. and Spruch L. (1968) Phys. Rev. **172**, 110

Gemmell D.S., (1974) Rev. Mod. Phys. **46**, 129

Ghosh A.S., Majumdar P.S. and Basu M, (1985) Can. J. Phys **63**, 621

Gidley D.W., Köymen A.R. and Capeheart T.W.,
(1982) Phys. Rev. Lett. **49**, 1779
(1988) Phys. Rev. **B37**, 2465

Gidley D.W., Mayer R., Frieze W.E. and Lynn K.G.,
(1987) Phys. Rev. Lett. **58**, 595

Gidley D.W., Rich A., Sweetman E. and West D.,
(1982) Phys. Rev. Lett. **49**, 525

Gidley D.W., Rich A., Zitzewitz P.W. and Paul D.A.L.,
(1978) Phys. Rev. Lett. **40**, 737

Gidley D.W. and Zitzewitz P.W.,
(1978) Phys. Lett. **A69**, 97

Glashow S.L., (1986) Phys. Lett. **B167**, 35

Gol'danskii V.I., (1968) Atomic Energy Rev. **6**, 3

Gramsch E., Throwe J. and Lynn K.G. (1987) Appl. Phys. lett. **51**, 1862

Griffith T.C. (1984) "Positron Scattering in Gases" (Humberston J.W. and McDowell M.R.C., eds; Plenum, New York), 53
(1986) Adv. At. Mol. Phys. **22**, 37

Griffith T.C., Charlton M., Clark G., Heyland G.R. and Wright G.L.,
(1982) Positron Annihilation" (Coleman P.G., Sharma S.C.and Dianna L.M. eds; North Holland, Amsterdam), 61

Griffith T.C., Heyland G.R., Lines K.S. and Twomey T.R.,
(1978) Phys. Lett., **69**, 169
(1979) J. Phys. **B12**, L747

Groce D.E., Costello D.G., McGowan J.W. and Herring W.F.,
(1968) Bull. Am. Phys. Soc. **13**, 1397
(1969) 6th ICPEAC Abstr., 757

Gryziński M., (1965) Phys. Rev. **138**, 305 A (Part I), 322 A (Part II) and 336 A (Part III)

Guha S. and Saha B.C. (1980) Phys. Rev. **A21**, 564

Gullikson E.M. and Mills A.P., (1986) Phys Rev. Lett. **57**, 376

Gullikson E.M., Mills A.P. Crane W.S. and Brown B.L.,
(1985) Phys. Rev. **B32**, 5484

Gullikson E.M., Mills A.P. and Murray C.A.,
(1988) Phys. Rev. **B38**, 1705

Haftel M.I. and Mandelzweig V.B. (1989) Phys. Rev. **A39**, 2813

Haghgooie M., Mader J.J. and Berko S., (1978) Phys. Lett. **A69**, 293

Hansen H.E. and Ingerslev-Jensen U., (1983) J.Phys. **D16**, 1353

Hansen H.E., Linderoth and Petersen K., (1982) Appl. Phys. **A29**, 99

Hara S. and Fraser P.A., (1975a) J. Phys. **B8**, 219
(1975b) J. Phys. **B8**, L472

Harris I. and Brown L., (1957) Phys. Rev. **105**, 1656

Hartley H.M. and Walters H.R.J., (1987) J. Phys. **B20**, 1983

Hasegawa M., He Y.J., Hoffman K.R., Lee R.R. Berko S.

and Takeyama T. (1985) "Positron Annihilation" (Jain P.C., Singru R.M. and Gopinathan K.P., eds; World Scientific, Singapore), 260

Held A. and Kahana S., (1964) Can J. Phys. **42**, 1908

Heyland G.R., Charlton M., Griffith T.C. and Clark G., (1985) Chem. Phys. **95**, 157

Hildum E.A., Boesl U., McIntyre D.H., Beausoliel R.G. and Hansch T.W., (1986) Phys. Rev. Lett. **52**, 1689

Hill J., Geddes J. and Gilbody H.B. (1979) J. Phys. **B12**, 2341

Ho Y.K., (1978) Phys. Rev. **A17**, 1675

Hodges C.H. (1970) Phys. Rev. Lett. **25**, 284

Hodges C.H. and Stott M.J., (1973a) Solid State Comm. **12**, 1153
(1973b) Phys. Rev. **B7**, 73

Hughes R.H. and Choe S.S. (1972a) Phys. Rev. **A5**, 656
(1972b) Phys. Rev. **A5**, 1758

Howell R.H., Rosenberg I.J. and Fluss M.J., (1986) Phys. Rev. **B34**, 3069

Humberston J.W., (1979) Adv. At. Mol. Phys. **15**, 101
(1984) J. Phys. **B17**, 2353

Humberston J.W., Charlton M., Jacobsen F.M. and Deutch B.I., (1987) J. Phys. **B20**, L25

Hutchins S.M., Coleman P.G., Stone R.J. and West R.N. (1986) J. Phys **E19**, 282

Hyder G.M.A., Dababneh M.S., Hseih Y-F, Kauppila W.E., Kwan C.K., Mahdavi-Hezaveh M. and Stein T.S., (1986) Phys. Rev. Lett. **57**, 2252

Jacobs S. (1951) Phys. Rev **84**, 877

Jacobsen F.M. (1984) "Positron Scattering in Gases" (Humberston J.W. and McDowell M.R.C., eds; Plenum, New York), 85
(1986) Chem. Phys. **109**, 455

Joachain C.J., Vanderpoorten R., Winters K.H. and Byron F.W., (1977) J. Phys. **B10**, 227

Jones G.O., Charlton M., Laricchia G. and Griffith T.C. (1989) *private communication*

Jorch H.H. Lynn K.G. and McMullen T. (1984) Phys. Rev. **B30**, 93

Kahana S. (1960) Phys. Rev. **117**, 123

Karl M.W., Nakanishi H. and Schrader D.M.,
(1984) Phys. Rev. **A30**, 1624

Katayama Y., Sueoka O. and Mori S. (1987) J. Phys. **B20**, 1645

Kauppila W.E., Stein T.S. and Jeison G.,
(1976) Phys. Rev. Lett. **36**, 580

Kauppila W.E., Stein T.S., Smart J.H., Dababneh M.S.,
Ho Y.K., Downing J.P. and Pol V.,
(1981) Phys. Rev. **A21**, 725

Keever W.C., Jaduszliwer B. and Paul D.A. (1972) "Atomic
Physics" (Smith S.J. and Walters G.K., eds; Plenem
New York) 561

Khan P. and Ghosh A.S., (1983) Phys. Rev. **A28**, 2181

Khan P., Mazumdar P.S. and Ghosh A.S. (1984) J. Phys. **B17**, 4785
(1985) Phys. Rev. **A3**, 1405

Kimura M. and Lane N.F., (1988) Phys. Rev. **A37**, 2900

Klemperer O. (1934) Proc. Camb. Philos. Soc. **30**, 347

Konopinski E.J. (1966) "The Theroy of Beta Radioactivity"
(Oxford University Press, London)

Köymen A.R., Gidley D.W. and Capeheart T.W.
(1987) Phys. Rev. **B35**, 1034

Kuzminikh V.A. and Vorobiev S.A.,
(1979) Nucl. Instrum and Meth. **167**, 483

Lang N.D. and Kohn W., (1971) Phys. Rev. **B3**, 1215

Laricchia G. Charlton M., Clark G. and Griffith T.C.
(1985) Phys. Lett. **109A**, 97

Laricchia G., Charlton M., Davies S.A., Beling C.D. and Griffith T.C.,
(1987) J. Phys. **B20**, L99

Laricchia G., Charlton M., and Griffith T.C. (1988a) J. Phys. **B21**, L227

Laricchia G., Charlton M., Griffith T.C., and Jacobson F.M.,
(1986a) "Proc. 3rd Int. Workshop on Positron (Electron) Gas Scatt."
(Kauppila W.E., Stein T.S. and Wadehra J.M., eds; World
Scientific, Singapore), 303

Laricchia G., Davies S.A., Charlton M., Beling C.D. and Griffith T.C.,
(1986b) Proc. 2nd Int. Conf. on Positrons at Surfaces,
UEA, Norwich, (unpublished)

Laricchia G., Davies S.A., Charlton M. and Griffith T.C.,

(1988b) J. Phys. **E21**, 886

Laricchia G., (1989) *private communication*

Leung C.Y. and Paul D.A.L., (1969) J. Phys. **B2**, 1278

Lovelace R.V.E. and Ruchti C.B., (1983) "Positron Electron Pairs in Astrophysics" (Burns M.L., Harding A.K. and Ramaty R, eds; Am. Inst. Phys, New York), 314

Lowy D.N. and Jackson A.D., (1975) Phys. Rev. **B12**, 1689

Lubell M.S., (1987) "Atomic Physics with Positrons" (Humberston J.W. and Armour E.A.G. eds; Plenum, New York), 287

Lucas C.B., (1979) J. Phys. **B12**, 1549

Lynn K.G., (1980) *Unpublished, taken from Schultz and Lynn, 1988*

Lynn K.G., Gramsch E., Usmar S.G. and Sferlazzo P., (1989) Appl. Phys. Lett. **55**, 87

Lynn K.G. and Lutz H., (1980) Rev. Sci. Instrum. **51**, 977

Lynn K.G., Nielsen B. and Quateman J.H., (1985) Appl. Phys. Lett. **47**, 239

Lynn K.G., Schultz P.J. and MacKenzie I.K. (1981) Solid State Commun. **38**, 473

Lynn K.G. and Welch D.O., (1980) Phys. Rev. **B22**, 99

Mackenzie I.K., Khoo T.L., McDonald A.B. and McKee B.T.A., (1967) Phys. Rev. Lett. **19**, 946

Mackenzie I.K., Shulte C.W., Jackman J. and Campbell J.C., (1973) Phys. Rev. **A7**, 135

Madey J.M.J. (1969) Phys. Rev. Lett. **22**, 784

Makhov A.F., (1960) Fiz. Tverd. Tela (Leningrad) **2**, 2161 [Sov. Phys. Solid State **2**, 1934 (1960)]

Makhov A.F., (1960) Fiz. Tverd. Tela (Leningrad) **2**, 2172 [Sov. Phys. Solid State **2**, 1942 (1960)]

Makhov A.F., (1960) Fiz. Tverd. Tela (Leningrad) **2**, 2176 [Sov. Phys. Solid State **2**, 1945 (1960)]

Mandansky L. and Rasetti F., (1950) Phys. Rev. **79**, 397

Mandal P., Guha S. and Sil N.C., (1975) J.Phys. **B8**, 2377

(1979) J. Phys. **B12**, 2913

(1980) Phys. Rev. **A22**, 2623

Malter L. (1936) Phys. Rev. **50**, 48

Manuel A.A., (1981) in POS81, 581

Mapleton R.A. (1965) Proc. Phys. Soc. **85**, 841

Massey H.S.W. and Gilbody H.B., (1974) "Electronic and Ionic Impact Phenomena, Vol. 4" (Clarendon, Oxford)

Massey H.S.W. and Mohr C.B.O., (1954) Proc. Phys. Soc. **67**, 695

Massoumi G.R., Schultz P.J., Lennard W.N. and Ociepa J., (1988) Nucl. Instrum. Methods **B30**, 592

Mazumdar P.S. and Gosh A.S., (1986) Phys. Rev. **A34**, 4433

McClure G.W., (1968) Phys. Rev. **148**, 47

McEachran R.P. and Stauffer A.D. (1986) "Positron (Electron)-Gas Scattering" (Kauppila W.E., Stein T.S. and Wadhera J.M., eds; World Scientific, Singapore) 122

McNeal R.J., Clark D.C. and Klingberg R.A., (1970) Phys. Rev. **A2**, 131

Mertler G., Rey M. and Reichelt K., (1982) Nucl. Instrum. and Meth. **192**, 535

Mills A.P., (1978) Phys. Rev. Lett. **41**, 1828

(1979a) Appl. Phys. Lett. **35**, 427

(1979b) Solid State Commun. **31**, 623

(1980a) Appl. Phys. **23**, 189

(1980b) Appl. Phys. Lett. **37**, 667

(1981a) "Positron Solid-state Physics", Proc. S.I.F., Course LXXXIII (Brandt W. and Dupasquier A., eds; North-Holland, Amsterdam), 432

(1981b) Phys. Rev. Lett **46**, 717

(1983) Phys. Rev. Lett **50**, 671

Mills A.P., Berko S. and Canter K.F. (1975) Phys. Rev. Lett. **34**, 1541

Mills A.P. and Crane W.S., (1985) Phys. Rev. **A31**, 593

Mills A.P. and Gullikson E.M., (1986) Appl. Phys. Lett. **49**, 1121

Mills A.P. and Murray C.A., (1980a) Appl.Phys. **21**, 323

(1980b) Bull. Am. Phys. Soc. **25**, 392

Mills A.P. and Pfeiffer L., (1976) Phys. Rev. Lett. **36**, 1389

(1979) Phys. Rev. Lett. **43**, 1961

(1985) Phys. Rev. **B32**, 53

Mills A.P. Pfeiffer L. and Platzman P.M., (1983) Phys. Rev. Lett. **51**, 1085

Mills A.P., Platzman P.M. and Brown B.L., (1978) Phys. Rev. Lett. **41**, 1076

Mills A.P., Shaw E.D., Chichester R.J. and Zuckerman D.M.,
(1989) Phys. Rev. **B40**, 2045

Mills A.P. and Wilson R., (1982) Phys. Rev. **A26**, 490

Mogensen O.E. (1974) J. Chem. Phys. **60**, 998
(1975) Appl. Phys. **6**, 315
(1982) "Positron Annihilation" (Coleman P.G., Sharma S.C. and
Diana L.M., eds; North Holland, Amsterdam), 763

Mohorovic S., (1934) Astron. Nachr. **235**, 94

Moores D.L. (1976) "Electron and Photon Interactions with Atoms"
(Kleinpoppen H. and McDowell M.R.C., eds; Plenum, New York) 109

Mori S., Katayama Y. and Sueoka O. (1985)
Atomic Collisions Res. Jpn. **11**, 19

Mourino M., Löbl H. and Paulin R., (1979) Phys. Lett **71A**, 106

Murray C.A. and Mills A.P., (1980) Solid State Comm. **34**, 789

Nahar S.N. and Wadehra J.M., (1986) "Proc 3rd Int. Workshop on
Positron (Electron) Gas Scatt." (Kauppila W.E., Stein T.S.and
Wadehra J.M., eds; World Scientific, Singapore), 289
(1987) Phys. Rev **A35**, 4533

Nakanishi H. and Schrader D.M., (1986) Phys. Rev **A34**, 1810

Neumann R., Poth H., Winnacker A. and Wolf A.,
(1983) Z. Phys. **A313**, 253

Neilson D., Nieminen R.M. and Szymanski J., (1986)
Phys. Rev. **B33**, 1567

Nielsen B., Lynn K.G. and Chen Y-C, (1986) Phys. Rev. Lett. **57**, 1789

Nieminen R.M. and Hodges C.H., (1976) Solid State Commun. **18**, 1115
(1978) Phys. Rev. **B18**, 2568

Nieminen R.M. and Oliva J., (1980) Phys. Rev. **B22**, 2226

Norlander P. and Ronay M., (1987) Phys. Rev. **B36**, 4982

Oliva J., (1980) Phys. Rev. **B21**, 4909

Orbeli H.L., Andreev E.P., Ankudinov V.A. and Dukelski V.M.,
(1969) Zh. Eskp. Teor. Fiz. **57**, 108
[(1970) Sov. Phys. - JETP **30**, 63]

Ore A., (1949) Univ. of Bergen Arbok **9**
(1951) Phys. Rev. **83**, 665

Ore A. and Powell J.L., (1949) Phys. Rev. **75**, 1696

Pages L., Bertel E., Joffre H. and Sklavenitis L.

(1972) Atomic Data **4**, 1

Paulin R. and Ambrosino G. (1968) J.Phys (Paris) **29**, 263

Paulin R., Ripon R. and Brandt W., (1974) Appl. Phys. **4**, 343

Peach G., (1984) "Positron Scattering in Gases", Humberston J.W. and McDowell M.C.R., eds; Plenum, New York)

Pendyala S., Bartell D., Girouard F.E. and McGowan J.W. (1974) Phys. Rev Lett. **33**, 1031

Pendyala S., Bartell D., Girouard F.E. and McGowan J.W. (1976) Can. J. Phys. **54**, 1527

Pendyala S., Zitzewitz P.W., McGowan J.W.and Orth P.H.R. (1973) Phys. Letts. **A43**, 298

Perkins A. and Carbotte J.P., (1970) Phys. Rev. **B1**, 101

Pirenne J., (1946) Arc. Sci. Phys. Nat. **28**, 233

(1947) Arc. Sci. Phys. Nat. **29**, 121, 207, 265

Poth H. (1987) Appl. Phys. **A43**, 287

Poulsen M.R., Charlton M., Chevalier J., Deutch B.I., Jacobsen F.M. and Laricchia G., (1988) "Positron Annihilation", (Dorikens-Vanpraet L., Dorikens M. and Segers D., eds; World Scientific, Singapore) 597

Raith W., Olsson B., Sinapius G., Sperber W. and Spicher G.,(1989) presented at the International Conference on Gases and Galaxies, Washington

Riegler G.R, Ling J.C., Mahoney W.A, Wheaton W.A. and Jacobsen A.S. (1983) Proc "Positron-Electron Pairs in Astrophysics" (Burns M.L., Harding A.K. and Ramaty R., eds; American Institute of Physics, New York)

Rohrlich F. and Carlson B.C., (1954) Phys. Rev. **93**, 38

Rosenberg I.J., Howell R.H. and Fluss M.J., (1987) Phys. Rev. **B35**, 2083

Ruark A.E. (1945) Phys. Rev. **68**, 278

Ruzic D.N. and Cohen S.A. (1985) J. Chem Phys. **83**, 5527

Sauers I. and Thomas E.W. (1974) Phys. Rev. **A10**, 882

Schultz P.J., Gullikson E.M. and Mills A.P., (1986) Phys. Rev. **B34**, 442

Schultz P.J. and Lynn K.G., (1982) Phys. Rev **B26**, 2390

Schultz P.J. and Lynn K.G., (1988) Rev. Mod. Phys. **60**, 701

Schultz P.J., Lynn K.G., Frieze W.E. and Vehanen A., (1983) Phys. Rev. **B27**, 6626

Schwab A., Honër P, Raith W and Sinapius G (1987) "Atomic Physics with Positrons" (Humberston J.W. and Armour E.A.G. eds; Plenum, New York), 429

Sferlazzo P., (1985) Appl. Phys. **A36**, 93

Share G.H., Chupp E.L., Forrest, D.J. and Rieger E., (1983) Proc "Positron-Electron Pairs in Astrophysics" (Burns M.L, Harding A.K. and Ramaty R., eds; American Institute of Physics, New York)

Shah M.B., Elliott D.S. and Gilbody H.B., (1987) J. Phys. **B20**, 3501

Sharma S.C., McNutt J.D., Eftekhari A and Ataiiyan Y.J. (1982) Can. J. Phys. **60**, 616

Shearer J.W. and Deutsch M., (1949) Phys. Rev. **76**, 462

Simpson R.I., (1987) *private communication*

Simpson R.I., Stewart M.G., Beling C.D. and Charlton M (1989) J. Phys.: Condens Matter **1**, 7251

Sinapius G., Fromme D. and Raith W., (1986) "Proc 3rd Int. Workshop on Positron (Electron) Gas Scatt." (Kauppila W.E., Stein T.S. and Wadehra J.M., eds; World Scientific, Singapore), 61

Smith S.J., Hyder G.M.A. Kauppila W.E., Kwan C.K., Mahdavi-Hezaveh M. and Stein T.S., (1987) 15th ICPEAC Abstr., 404

Solov'ev E.S., Il'il R.N., Oparin V.A. and Fedorenko N.V. (1962) JETP **15**, 459

Stein T.S., Dubabneh M.S., Kauppila W.E., Kwan C.K. and Wan Y.J. (1987) "Atomic Physics with Positrons" (Humberston J.W. and Armour E.A.G. eds; Plenum, New York),251

Stein T.S. Gomez R.D., Hseih Y-F, Kauppila W.E., Kwan C.K. and Wan Y.J., (1985) Phys. Rev. Lett. **55**, 488

Stein T.S. and Kauppila W.E. (1982) Adv. At. Mol. Phys. **18**, 53

Stein T.S., Kauppila W.E., Pol V., Smart J.H. and Jeison G., (1978) Phys. Rev. **A17**, 1600

Stein T.S. Kauppila W.E. and Roellig L.O., (1974) Rev. Sci. Inst. **45**, 951

Stier P.M. and Barnett C.F., (1956) Phys. Rev. **103**, 896

Sueoka O., (1982) J. Phys. Soc. Jpn. **51**, 3757

Sueoka O., (1987) "Atomic Physics with Positrons" (Humberston J.W.

and Armour E.A.G. eds; Plenum, New York),41

Sueoka O., (1989) J. Phys. **B21**, L631

Sueoka O., Mori S. and Katayama Y. (1986) J. Phys. **B19**, L373

Sueoka O., Mori S. and Katayama Y. (1987) J. Phys. **B20**, 3237

Tong B.Y., (1972) Phys. Rev. **B5**, 1436

Valkealathi S. and Nieminen R.M., (1983) Appl. Phys. **A32**, 95

(1984) Appl. Phys. **A35**, 51

Van House J., Rich A. and Zitzewitz P.W.,

(1984) Origins of Life **14**, 413

Van Zyl B., Neumann H., Rothwell H.L. and Amme R.C.

(1980) Phys. Rev. **A21**, 716

Van Zyl B., Le T.Q. and Amme R.C. (1981) J. Chem. Phys. **74**, 314

Vehanen A., Lynn K.G., Schultz P.J., Cartier E., Gütherodt H.H. and Parkin D.M.

(1984) Phys. Rev. **B29**, 2371

Vehanen A., Lynn K.G., Schultz P.J. and Eldrup M.,

(1983) Appl. Phys. **A32**, 163

Vehanen A. and Mäkinen J., (1985) Appl. Phys. **A36**, 97

Vehanen A., Saarinen K., Hautojärvi P. and Huomo H.,

(1987) Phys. Rev. **B35**, 4606

Wadehra J.M., Stein T.S. and Kauppila W.E.,

(1984) Phys. Rev **A29**, 2912

Walters H.R.J. (1984) Physics Report **116**, 1

Ward S.J., Humberston J.W. and McDowell M.R.C.,

(1987) J. Phys. **B20**, 127

Weber M., Berko S., Brown B.L. Canter K.F., Lynn K.G., MIlls A.P.,

Roellig L.O. Tang S. and Viescas A., (1988) "Positron Annihilation"

(Dorikens-Vanpraet L., Dorikens M., and Segers D, eds;

World Scientific, Singapore) 28

West R.N. (1985) "Positron Annihilation" (Jain P.C., Singru R.M. and

Gopinathan K.P., eds; World Scientific, Singapore) 11

Westbrook C.I., Gidley D.W., Conti R.S. and Rich A.,

(1987) Phys. Rev. Lett. **58**, 1328

Weyl H., (1931) "Gruppentheorie und Quantenmechanick" 2nd ed., p234

Wheeler J.A., (1946) Ann. N. Y. Acad. Sci. **48**, 219

Williams J.F., (1967) Phys. Rev. **153**, 116

Wilson R.J. (1983) Phys. Rev. **B27**, 6974

Wilson R.J. and Mills A.P., (1983a) Phys. Rev. **B27**, 3949
(1983b) Surf. Sci. **128**, 70

Wiza J.L., (1979) Nucl. Inst. Meths. **162**, 587

Wonnacott D., (1987) *private communication*

Yang C.N., (1950) Phys. Rev. **77**, 242

Yoshimori M., Watanabe H., Okudaira K., Hirasima Y.
and Murakami H., (1979) Aust. J. Phys. **32**, 375

Zafar N., Chevallier J., Jacobsen F.M., Charlton M. and Laricchia G.,
(1988) Appl. Phys. **A47**, 409

Zafar N., Chevallier J., Laricchia G. and Charlton M.,
(1989) J. Phys. **D22**, 868

Ziock K.P., Dermer C.D., Howell R.H., Magnotta F. and Jones K.M.
(1990) J. Phys. **B23**, 329